Distribution Agreement

In presenting this thesis or dissertation as a partial fulfillment of the requirements for an advanced degree from Emory University, I hereby grant to Emory University and its agents the non-exclusive license to archive, make accessible, and display my thesis or dissertation in whole or in part in all forms of media, now or hereafter known, including display on the world wide web. I understand that I may select some access restrictions as part of the online submission of this thesis or dissertation. I retain all ownership rights to the copyright of the thesis or dissertation. I also retain the right to use in future works (such as articles or books) all or part of this thesis or dissertation.

Signature:

_____   _____

Ming-fai Fong   Date

The role of excitatory neurotransmission in the induction of homeostatic synaptic plasticity

by

Ming-fai Fong
Doctor of Philosophy

Graduate Division of Biological and Biomedical Sciences
Program in Neuroscience

_____
Steve M. Potter, PhD
Advisor

_____
Peter Wenner, PhD
Advisor

_____
Shawn Hochman, PhD
Committee Member

_____
Astrid A. Prinz, PhD
Committee Member

_____
Garrett B. Stanley, PhD
Committee Member

Accepted:

_____
Lisa A. Tedesco, PhD
Dean of the James T. Laney School of Graduate Studies

_____
Date

The role of excitatory neurotransmission in the induction of homeostatic synaptic plasticity

by

Ming-fai Fong

B.S., Massachusetts Institute of Technology, 2005

Advisors

Peter Wenner, PhD, and Steve M. Potter, PhD

An abstract of a dissertation submitted to the Faculty of the
James T. Laney School of Graduate Studies of Emory University
in partial fulfillment of the requirements for the degree of
Doctor of Philosophy

Graduate Division of Biological and Biomedical Sciences
Program in Neuroscience

2014

Abstract

The role of excitatory neurotransmission in the induction of homeostatic synaptic plasticity

by Ming-fai Fong

Homeostatic plasticity encompasses a family of compensatory mechanisms that help maintain stability within neural circuits. Synaptic scaling is a form of homeostatic plasticity characterized by a coordinated strengthening or weakening of all synaptic inputs onto a neuron by a common factor as a compensatory response to altered activity. While synaptic scaling has been widely observed both *in vitro* and *in vivo*, how neural circuits sense altered activity in order to trigger the scaling process remains unclear. Because prolonged blockade of spiking robustly leads to upward scaling, a leading hypothesis is that neurons monitor their own firing rates to induce scaling. However, chronic blockade of AMPA-type glutamate receptors (AMPARs) also leads to upward scaling, suggesting that reduced excitatory neurotransmission triggers the scaling process. Spiking and excitatory transmission are highly correlated at the circuit level, so distinguishing between reductions in firing rate and reductions in transmission as triggers for scaling presents a unique challenge.

In this dissertation, we systematically investigated the independent roles of reduced firing rate versus reduced AMPAergic transmission in the induction of homeostatic synaptic scaling. To test the importance of firing rate in scaling, we used multi-electrode recordings to continuously monitor spiking activity in cultured cortical networks during perturbations that trigger upward scaling. While each perturbation reduced spiking activity to some degree, there was no correlation between the severity of the reduction in firing rate and the degree of scaling observed. Next, we independently manipulated firing rate and AMPAergic transmission using two complementary strategies. First, we blocked AMPARs while restoring normal levels of spiking using closed-loop optogenetic stimulation. Second, we blocked spiking while partially restoring AMPAergic transmission using a pharmacological AMPAR modulator. In both cases, we found that the induction of upward scaling was driven by reductions in AMPAergic transmission, rather than reductions in firing rate. These results provide strong evidence that excitatory neurotransmission is the activity signal sensed by neural circuits in order to trigger homeostatic synaptic scaling. Our findings highlight the role of synaptic activity in the maintenance of circuit stability and raise important questions about the role of scaling in learning, development, and disease.

The role of excitatory neurotransmission in the induction of homeostatic synaptic plasticity

by

Ming-fai Fong

B.S., Massachusetts Institute of Technology, 2005

Advisors

Peter Wenner, PhD, and Steve M. Potter, PhD

A dissertation submitted to the Faculty of the
James T. Laney School of Graduate Studies of Emory University
in partial fulfillment of the requirements for the degree of
Doctor of Philosophy

Graduate Division of Biological and Biomedical Sciences
Program in Neuroscience

2014

interests gave rise to a productive and synergistic collaboration. His involvement in my dissertation work, through design of hardware and software, and through critical scientific discussions, has greatly enhanced this research. Jon is the first person with whom I share the excitement of a new finding or the disappointment of an experimental failure. The camaraderie we've developed through the years has been an invaluable part of my graduate experience.

I've been fortunate to have several other excellent colleagues and collaborators. In this regard, I'd like to acknowledge the former and current members of my two labs: Carlos, Miguel, Casie, Chad, Michelle, Nathan, Sharanya, Riley, and Alex. Each of them has given me important feedback on my research and many have taught me new skills. In addition, JT Shoemaker and Jack Tung have been especially helpful in tissue harvests and virus production, respectively, and Andrew Shaw has been a fantastic asset in learning confocal microscopy. Some very talented undergraduates— Candace, Marc, and Amanda—have also helped me over the years and I'm thankful for their contributions. Finally, several faculty in the GT-Emory Neurolab have been especially supportive. Dr. Lena Ting has been a great advocate and role model, and she has helped me with several fellowship applications. Dr. Michelle LaPlaca lent me a microscope for patch clamp experiments, which are used throughout the dissertation. Dr. Rob Butera has been supportive throughout this research, and has been particularly helpful in supervising me during Steve's sabbatical.

Being a student in the Emory Neuroscience Graduate Program has been a true privilege. I am particularly grateful to Dr. Yoland Smith, Sonia Hayden Perez, and Gary Longstreet for their tireless efforts and fantastic attitudes that have elevated the quality of our program's student experience. I'm also thankful to have received funding for my graduate studies through the NSF Integrative Graduate Education and Research Traineeship (DGE-0333411), the NSF Graduate Research Fellowship (09-630) and the Emory Scholars Program in Interdisciplinary Neuroscience Research

Pre-doctoral Fellowship. In addition, I've had the pleasure of working with several mentoring programs including SIRE-HHMI, LINCR, and Petit Scholars. While living in Atlanta, I have been lucky to have some fantastic friends and classmates who've supported me during my time here (in roughly chronological order): Megan, Meag, Damon, Dave, Chris, Katie, Karen, Katy, Lani, Callie, Monica, Laura Mar., Christina, Jeff, Seyed, Jon N., Dustin, Ash, Jason, Joanne, Becca, Mallory, Eric, Stephen, Frank, Lily, Vanessa, Jon E., Laura Mas., Craig, Amanda, Erin, Stef, Jeenah, Mak, Owen, Chase, Marc, and the other fantastic climbers of the Burrito Cup. You are amazing humans.

Finally, I would like to thank my family. My older sister, Hiu-fai (my "gajeh"), has been my role model and mentor since I was a child, and I still look to her for advice on anything that is stumping me (including how to begin my thesis!). My little sister, Wen-fai, has motivated me to try to be a role model/mentor figure, though in truth I often find myself looking to her for wisdom instead, especially when it comes to battling my indecisiveness. My dad instilled in me a love for science and engineering from a young age, and some of my fondest memories from childhood are from him and me woodworking together. My mom is the most patient and hardworking person I know, and I have leaned on her to re-energize on countless occasions throughout my life. I love you all very much, and I thank you for filling the past thirty years of my life with love, inspiration, and happy memories!

CONTENTS

LIST OF TABLES

LIST OF FIGURES

LIST OF ABBREVIATIONS

I_{Ca} calcium current

I_h hyperpolarization-activated current

I_K potassium current

I_{Na} sodium current

p_r probability of release

$[K^+]_o$ extracellular potassium concentration

AAV   adenoassociated virus

ACh   acetylcholine

AChR   acetylcholine receptor

AIS   axon initial segment

AMPA α-amino-3-hydroxy-5-methyl-4-isoxazolepropionic acid

AMPAR   AMPA-type glutamate receptor

APV   D(-)-2-amino-5-phosphonopentanoic acid

BDNF   brain-derived neurotrophic factor

bic   bicuculline

Ca_V voltage-gated calcium channel

ChR2 channelrhodopsin-2

CNQX 6-cyano-7-nitroquinoxaline-2,3-dione

CTZ cyclothiazide

DIV days *in vitro*

DMSO dimethyl sulfoxide

DNQX 6,7-dinitroquinoxaline-2-3-dione

EPSC excitatory postsynaptic current

GABA γ-aminobutyric acid

$GABA_A$R $GABA_A$ receptor

hChR2 H134R variant of the channelrhodopsin-2

IPSC inhibitory postsynaptic current

K_{ir}2.1 inwardly-rectifying potassium channel 2.1

LED light-emitting diode

MEA microelectrode array

mEPPs miniature endplate potentials

mEPSC miniature excitatory postsynaptic current

mGluR metabotropic glutamate receptor

mIPSC miniature inhibitory postsynaptic current

mPSC miniature postsynaptic current

Na_V voltage-gated sodium channel

NMDA N-methyl-D-aspartate

NMDAR NMDA-type glutamate receptor

NMJ   neuromuscular junction

PSC   postsynaptic current

RMS   root mean square

STG   stomatogastric ganglion

TARP transmembrane AMPAR regulatory protein

TTX   tetrodotoxin

INTRODUCTION

The nervous system is endowed with a remarkable capacity for change. In the human cortex, tens of billions of neurons form hundreds of trillions of synaptic connections during the first few years of life (Shepherd, 2004). This period of rapid synaptogenesis is accompanied by the development of an incredible repertoire of behaviors. During this time, children learn to walk, talk, and solve simple puzzles, and they gain the ability to express emotions and empathize with others (CDC) This development of language, motor, cognitive, and social skills continues through adolescent and adulthood as cells grow larger and synapses are refined. Even the mature nervous system remains incredibly plastic, endowed with the ability to encode and store information through Hebbian plasticity mechanisms, and recall these memories with high fidelity.

Perhaps equally remarkable is the fact that neural circuits can maintain stable activity patterns through a lifetime of these seemingly overwhelming changes. How is this achieved? In engineering, negative feedback can be used to stabilize the behavior of an otherwise unstable system. Neural circuits use a similar strategy to maintain activity in a healthy, functional range. Conceptually, this means that neural circuits can (1) measure and integrate activity over time, (2) compute deviations between actual and target activity levels, and (3) compensate for these deviations to restore a target activity level. In practice, we are still learning how these concepts are implemented in biology, though considerable progress has been made. Experimental

research has made it clear that neural stability is maintained, at least in part, through an array of compensatory plasticity mechanisms operating at the level of cells and synapses (Turrigiano, 2011; Davis, 2013). This set of compensatory mechanisms has collectively been referred to as homeostatic plasticity.

In this introductory chapter, I begin by briefly discussing evidence that the overall activity in neural circuits is homeostatically regulated. Next, I present a perspective on cellular and synaptic mechanisms that likely contribute to circuit-level homeostasis. I then discuss some of the fundamental challenges facing current research in homeostatic plasticity. I conclude with a presentation of my thesis objectives.

1.1 Activity homeostasis in neural circuits

The nervous system's ability to encode information and execute behaviors relies on proper levels and patterns of activity. However, the "proper" activity for each neural circuit may vary depending on the special functional role that it plays within the nervous system. In this section, I provide examples of three neural circuits, each of which play distinct functional roles within the organism. In spite of the different activity patterns displayed by each circuit, all three retain the capacity to homeostatically control their activity to restore normal output.

The first example comes from a small, well-defined neural circuit. The pyloric network is a rhythmically-active circuit containing 14 identified neurons in the crustacean stomatogastric ganglion (STG). This circuit controls muscles in the animal's stomach by generating a tri-phasic pyloric rhythm, which is driven by neuromodulatory inputs. When these modulatory inputs were severed, pyloric neurons stopped spiking (Thoby-Brisson and Simmers, 1998). However, over the course of a few days, spiking began to recover and eventually pyloric-like bursting emerged (Thoby-Brisson and Simmers, 1998). This finding demonstrated the capacity for neural circuits to

homeostatically recover from loss of afferent input to achieve physiologically-relevant firing patterns.

The next example comes from the chick spinal cord, which during embryonic development exhibits bursts of spontaneous activity that drive fetal kicking behavior. These bursts appear to be intrinsically generated, as they persist even when the spinal cord is isolated from the animal (Landmesser and O'Donovan, 1984). When glutamatergic transmission was pharmacologically blocked in the isolated cord, the network fell silent (Chub and O'Donovan, 1998). However, over the course of a few hours, rhythmic activity gradually recovered and the rate of spontaneous bursts returned to normal levels despite the sustained glutamatergic blockade (Chub and O'Donovan, 1998). Similarly, in the living chick embryo, pharmacological blockade of glutamatergic transmission produced an immediate loss of fetal kicking, but these movements also recovered and reached normal levels within 10 hours (Wilhelm and Wenner, 2008). These studies provide evidence for homeostatic regulation of spontaneous network activity and motor output within a heterogeneous neural network.

The third and final example is based on work in the rodent primary visual cortex (V1). Ongoing activity patterns in V1 are admittedly less well defined than the regular tri-phasic activity of the pyloric network or the spontaneous network activity of the developing spinal cord. However, it is generally agreed that in sensory cortex, average spontaneous firing rates are low, and activity patterns contain both temporally-structured and stochastic components (Destexhe and Contreras, 2006; Barth and Poulet, 2012). In a recent study, firing rates of regularly-spiking (RS) units in V1 were recorded before and during monocular deprivation (Hengen et al., 2013). This caused a dramatic reduction in the firing rates of RS units after the first day, but after a few days the overall ensemble firing rate recovered. Likewise, another study performed calcium imaging in V1 neurons and showed that binocular deprivation rapidly reduced firing rates, but within two days mean spiking levels had

recovered. Together, these findings suggest that the overall population firing rate can be homeostatically regulated in sensory cortex.

Despite the different roles of the pyloric circuit, the developing spinal cord, and the rodent visual cortex in generating behavior or encoding information, all three networks are capable of recovering functional output in spite of disruptions to activity. What types of changes in constituent neurons and synapses drive recovery of population activity? In the next few sections, I discuss some of the expression mechanisms that have been observed in various neural preparations that could contribute to the maintenance of functional network behavior.

1.2 Homeostatic regulation of intrinsic neuronal excitability

In order to maintain appropriate levels of activity, neural circuits must have the ability to manipulate activity when it deviates from an optimal range. One strategy for manipulating activity levels in a neural circuit is to change in the intrinsic excitability of constituent neurons. For instance, if activity levels are too low, one compensatory strategy could be to increase the expression of ion channels that flux current into the cell. Another possibility could be to reduce the number of ion channels that produce outward currents. Both of these options would increase a neuron's excitability and thus make it easier for that cell to fire action potentials and restore activity levels. Conversely, if activity levels are too high, inward currents could be downregulated or outward currents could be upregulated, both of which would homeostatically reduce excitability. However, changes in intrinsic excitability are not limited to changes in ion channel expression. Other possibilities include changes in channel distributions, unitary channel conductances, or current gating mechanisms. In this section, I discuss experimental evidence for homeostatic changes in intrinsic excitability, as well as current views on what might be triggering these processes. For reference, the

general properties of various ionic currents and channels discussed in this section are summarized in Table 1.1.

1.2.1 Evidence for intrinsic homeostasis

Early investigation on the consequences of long-term depolarization in heterologous expression systems showed that chronic increases in membrane potential led to a compensatory decrease in the number voltage-gated calcium (Ca_V) channels in the membrane (Delorme et al., 1986; DeLorme et al., 1988). Similarly, work in primary cultures of myenteric neurons showed that chronic depolarization triggered a gradual reduction in inward calcium currents (I_{Ca}), likely due to reduced calcium channel densities (Franklin et al., 1992). These studies suggested that calcium channel expression could be homeostatically regulated in response to elevation of membrane potential. In addition, exogenous expression of voltage-gated sodium (Na_V) channels in frog myocytes produced a compensatory increase in the expression of potassium currents (I_K) (Linsdell and Moody, 1994), revealing that ionic currents besides I_{Ca} could be homeostatically manipulated to regulate excitability. Lending support to the idea that changes in neuronal excitability might contribute to circuit function were findings in cortical cultures showing that chronic blockade of Na_V channels led to elevated spiking and bursting upon removal of the blockade (Ramakers et al., 1990).

A set of studies on neurons from the crustacean STG have provided particularly convincing evidence of homeostatic intrinsic plasticity. As previously mentioned, the pyloric circuit produces a tri-phasic rhythm, but relies on modulatory input to generate this activity pattern. In one set of experiments, individual STG neurons were excised from the animal and grown in culture. These synaptically-isolated neurons were unable to spike on the first day in culture, even when provided with depolarizing stimuli. However, over the course of a few days, neurons regained the ability to tonically spike, and eventually regained the ability to endogenously burst (Panchin et al.,

1993; Turrigiano and Marder, 1993). This finding suggested that neurons could increase their total inward conductances in order to compensate for the loss of synaptic and modulatory input. Indeed, subsequent experimental and modeling work showed that the gradual recovery of phasic bursting in isolated STG neurons was mediated by an increase in several different inward currents and a decrease in several different outward currents (Turrigiano et al., 1995). These studies suggested that individual neurons were capable of intrinsically recovering many aspects of normal spiking activity. Together with the observation that intact STG circuits, isolated from modulatory input, could recover pyloric-like rhythms (Thoby-Brisson and Simmers, 1998; Khorkova and Golowasch, 2007), this suggested that intrinsic changes in individual neurons contributed to recovery of circuit-level activity.

Since these early findings, a growing number of studies have highlighted the diversity in ionic currents involved in homeostatic regulation of intrinsic excitability. For example, reducing spiking activity by blocking spiking activity using tetrodotoxin (TTX) produces several compensatory changes in excitability. These include increases in I_{Na} (Desai et al., 1999a; Aptowicz et al., 2004), redistribution of Na_V channels (Aptowicz et al., 2004), and reductions in several types of I_K (Desai et al., 1999a), sometimes accompanied by co-regulation of the hyperpolarization-activated current (I_h) (Gibson et al., 2006). Likewise, increasing activity through electrical stimulation or elevated extracellular potassium ($[K^+]_o$) has led to compensatory reductions in intrinsic excitability, expressed through decreases in I_{Na} (O'Leary et al., 2010) and I_{Ca} (Hong and Lnenicka, 1995; O'Leary et al., 2010), as well as increases in I_K (Borde et al., 1995; O'Leary et al., 2010) and I_h (Fan et al., 2005). Homeostatic increases in I_K or I_h were also observed through indirect forms of activity elevation, such as enhancement of glutamatergic activity using pharmacological agonists (van Welie et al., 2004; Misonou et al., 2004) or relief from tonic inhibition by knocking out extrasynaptic $GABA_A$ receptors (Brickley et al., 2001a). Interestingly, some activ-

Table 1.1: Ion channels and currents

Symbol	Full Name	Function
Na_V	voltage-gated sodium channel	inward, voltage-gated channel
Ca_V	voltage-gated calcium channel	inward, voltage-gated channel
I_{Na}	sodium current	inward current
I_{Ca}	calcium current	inward current
I_K	potassium current	outward current
I_h	hyperpolarization-activated current	mixed cation current

ity elevation experiments triggered decreased excitability within an hour (Hong and Lnenicka, 1995; van Welie et al., 2004; Fan et al., 2005) or even within seconds (Borde et al., 1995), indicating that homeostatic regulation of hyperexcitability may occur on a faster timescale (although Nelson et al., 2003 provides evidence that inhibition can drive rapid increases in excitability). Needless to say, studies have identified many different ionic currents that seem to be involved in expressing homeostatic intrinsic plasticity. This diversity is likely explained by evidence that many different combinations of membrane conductances can accommodate similar activity patterns (Liu et al., 1998; Marder and Prinz, 2002; Prinz et al., 2004; Schulz et al., 2006).

In addition, more nuanced expression mechanisms supporting intrinsic plasticity have been revealed. Some examples include shifts in functional inhibition (Karmarkar and Buonomano, 2006) and co-regulation of related voltage-gated channels (MacLean et al., 2003; Mee et al., 2004; Etheredge et al., 2007; Bergquist et al., 2010). Recently, Grubb and Burrone identified the axon initial segment (AIS), a sodium channel-rich zone responsible for initiating action potentials, as a locus for homeostatically regulating excitability. After chronically depolarizing cells by elevating extracellular potassium levels, the authors observed a shift in the AIS away from the soma, which reduced excitability by decreasing the probability of action potential firing

Table 1.2: Common perturbations used to elicit homeostatic plasticity

Treatment	Symbol	Direct Action	Function
tetrodotoxin	TTX	voltage-gated sodium channel antagonist	blocks spiking
elevated extracellular potassium	$[K^+]_o$	increases K^+ reversal potential	depolarizes membrane
inwardly-rectifying potassium channel 2.1	$K_{ir}2.1$	increases outward I_K (for V_{mem} >-85-95 mV)	hyperpolarizes membrane
6-cyano-7-nitroquinoxaline-2,3-dione	CNQX	AMPA/kainate receptor antagonist	blocks AMPAergic transmission
D(-)-2-amino-5-phosphonopentanoic acid	APV	NMDA receptor antagonist	blocks NMDAergic transmission

(Grubb and Burrone, 2010). The authors further demonstrated that the reduction in excitability was cell-autonomous, as optogenetically-mediated depolarization of individual cells was sufficient to produce the AIS plasticity (Grubb and Burrone, 2010). These creative strategies for manipulating neuronal excitability highlight the diversity of expression mechanisms for achieving target levels of activity.

1.2.2 Potential triggers for intrinsic homeostasis

How do cells or circuits sense altered activity levels in order to trigger changes in cellular excitability? Early modeling studies showed that intracellular calcium could act as a sensor to trigger compensatory changes in ionic conductances (LeMasson et al., 1993), a suggestion that fit nicely with contemporary experimental findings. Previous studies had shown that changes in membrane potential, spiking activity, or synaptic/modulatory input could each elicit homeostatic intrinsic plasticity, and these variables were all positively correlated with intracellular calcium. Indeed, in the isolated STG neurons that homeostatically recovered bursting, the observed changes

Table 1.3: Ligand-gated neurotransmitter receptors

Name	Ligand	Permeant Ion(s)	Action
AMPA[*] receptor	glutamate	Na^+, K^+, sometimes Ca^{2+}	excitatory
NMDA[†] receptor	glutamate	Na^+, K^+, Ca^{2+}	excitatory
$GABA_A$ [§] receptor	GABA	Cl^-	inhibitory[§]

[*]α-amino-3-hydroxy-5-methyl-4-isoxazolepropionic acid; [†] N-methyl-D-aspartate;
[‡]γ-aminobutyric acid; [§]excitatory during early development

in intrinsic excitability could be reversed by re-introducing rhythmic activity, but only if intracellular calcium dynamics were unperturbed (Turrigiano et al., 1994). Interestingly, when the entire STG circuit was isolated (rather than individual neurons), rhythmic bursting in standard medium was observed even if elevated $[K^+]_o$ or TTX were applied during the recovery phase, suggesting that neither spiking nor membrane potential influenced this recovery (Thoby-Brisson and Simmers, 1998). Therefore, if calcium mediates this recovery, then the signaling is local and tied to dendritic excitability or neurotransmission, rather than spiking activity (Frick and Johnston, 2005; Siegel et al., 1994). Alternatively, there also is evidence supporting the idea that altering the signaling molecules (Desai et al., 1999b; Steinert et al., 2011), synaptic or neuromodulatory input (Khorkova and Golowasch, 2007; Wilhelm et al., 2009; Temporal et al., 2012; Driscoll et al., 2013) or sensory experience (Aizenman et al., 2003; Breton and Stuart, 2009) can also influence intrinsic plasticity. Given the breadth of timescales and expression mechanisms for maintaining cellular excitability, it is perhaps unsurprising that there may also be different activity sensors that trigger different plasticities, but converge upon the same functional output.

1.3 Homeostatic regulation of neurotransmitter release

Another strategy for tuning the balance of excitation and inhibition within a neural circuit is to manipulate the total amount of neurotransmitter released. This also represents a way for individual cells to tune their own influence on the rest of the network. For example, if activity levels are too low, increasing the probability of release (p_r) at excitatory synapses could increase excitatory drive within a circuit. Similarly, decreasing p_r at inhibitory synapses could lessen the effects of inhibitory drive, thus producing the same functional goal of shifting the balance toward excitation. Other ways to change overall levels of neurotransmitter release are through changes in the total number of release sites, the number of docked vesicles, or the amount/type of neurotransmitter packed into vesicles. In this section, I describe evidence for homeostatic regulation of both presynaptic release properties and vesicle content. For reference, the names of commonly-referenced synaptic receptors are listed in Table 1.3.

1.3.1 Evidence for transmitter release homeostasis

An early account of homeostatic regulation of presynaptic function was identified by Plomp et al. at the rat neuromuscular junction (NMJ). The authors showed that after a few weeks of blocking of muscle-type acetylcholine (ACh) receptors, there was a compensatory increase in the frequency of miniature endplate potentials (mEPPs), as well as an increase in quantal content[1] (Plomp et al., 1992). Like the recovery of bursting in STG neurons, these compensations could not be seen during the first few hours, but gradually manifested over the course of several days. This finding revealed a homeostatic mechanism for increasing motor neuron release properties in response to blocked postsynaptic transmission.

---

[1] quantal content refers to the average number of vesicles released due to a single presynaptic stimulus

Subsequently, adaptation of presynaptic release properties was observed at the larval fly NMJ (Stewart et al., 1996; Petersen et al., 1997; Davis and Goodman, 1998; Davis et al., 1998; DiAntonio et al., 1999; Paradis et al., 2001). This particular synapse has served as an excellent model for characterization of presynaptic homeostatic mechanisms due to its amenability to genetic manipulations. One study showed that a genetically-induced increase in transmission onto the muscle led to a compensatory decrease in probability of release (p_r) from presynaptic motor terminals (Davis and Goodman, 1998). Paradoxically, decreased muscle innervation led to a decrease in quantal content (implying reduced p_r), though it produced a homeostatic increase in quantal size [2] (Davis and Goodman, 1998). This result differs from other reports showing that chronically reducing synaptic transmission or muscle activity elicited compensatory increases in quantal content (Stewart et al., 1996; Petersen et al., 1997; Davis et al., 1998; Paradis et al., 2001), and likely reveals special properties in how different genetically-manipulated proteins effect the expression of plasticity. Overall, these studies provided clear evidence that presynaptic efficacy can be adjusted to compensate for altered postsynaptic activity, implying one or more retrograde signals contribute to the maintenance of stable synapses.

Studies of presynaptic homeostasis at the NMJ have been complemented by work in primary cultures of mammalian neurons. Imaging of vesicles loaded with the styryl dye, FM1-43, revealed that chronically blocking spiking or AMPA-type glutamatergic activity (for days) elicited a compensatory increase in the p_r as well as the number of vesicles docked at each release site (Murthy et al., 2001). Meanwhile, mild depolarization led to a pronounced decrease in the number of release sites Moulder et al. (2006), an effect that could be seen within hours (Moulder et al., 2004). Although there were no changes in synapse number or p_r at remaining release sites, the decrease in the number of these sites effectively reduced the overall pool of docked vesicles (Moulder

---

[2] quantal size refers to the postsynaptic response due to a single vesicle of neurotransmitter being released

et al., 2004, 2006). Over the years, homeostatic adjustments in vesicle pools following heightened or reduced activity have also been reported by several other groups (Liu and Tsien, 1995; Burrone et al., 2002; Thiagarajan et al., 2005; Branco et al., 2008; Kim and Ryan, 2010; Zhao et al., 2011; Lazarevic et al., 2011). Concurrently, innumerable proteins have been identified as mediators for homeostatic regulation of vesicles pools and p_r. Generally speaking, these proteins can be categorized as interacting with scaffolding/release machinery (Bacci et al., 2001; Thiagarajan et al., 2005; Dickman and Davis, 2009; Dickman et al., 2012; Weyhersmüller et al., 2011; Lazarevic et al., 2011; Müller et al., 2012), or mediating calcium channels/influx into the presynaptic terminal (Frank et al., 2009; Zhao et al., 2011; Lazarevic et al., 2011; Müller and Davis, 2012; Kim and Ryan, 2013). The vast number of molecules involved in this process underscore the complexity of expressing presynaptic homeostasis.

There is also evidence that the amount of transmitter released can be homeostatically regulated by changing the degree of vesicular filling. Vesicular transporters aid with the re-uptake of neurotransmitter and filling of vesicles, and thus can influence quantal size. For instance, increased transporter expression increases the amount of transmitter packed into a vesicle, which in turn increases the amount of transmitter released and produces a larger postsynaptic current (Wilson et al., 2005). Compensatory increases in the vesicular glutamate transporter, VGLUT1, were observed following glutamatergic blockade, and reductions in VGLUT1 were shown following GABAergic blockade in hippocampal cultures (Wilson et al., 2005). In addition, differential regulation of vesicular glutamate and GABA transporters, VGLUT and VGAT was reported following chronic blockade or elevation of spiking activity in cortical cultures (De Gois et al., 2005). Compensatory upregulation of VGLUT1 and downregulation of VGAT was observed following activity blockade, while the opposite effects were observed following activity elevation (De Gois et al., 2005). Interestingly VGLUT2 expression was "anti-homeostatic", which could reflect greater expression

of VGLUT2 at synapses onto inhibitory cells versus greater expression of VGLUT1 at synapses onto excitatory cells (De Gois et al., 2005). However, the upregulation of VGLUT1 stands in contrast to another study that showed no change following activity blockade (Hartman et al., 2006). On the other hand, the idea that vesicular packing of GABA can be homeostatically modulated has been corroborated for both activity reductions (Hartman et al., 2006) and elevations (Hartmann et al., 2008).

A final strategy for altering neurotransmitter release is by manipulating neurotransmitter production. This could be achieved either through subtle changes in the rate of production or more dramatic changes in the type of transmitter produced. A recent study showed decreases in the production of glutamic acid decarboxylase (GAD, enzyme required for GABA synthesis) following activity blockade, and compensatory increases in GAD production following activity elevations (Lau and Murthy, 2012). These alterations in GAD production changed the rate of GABA synthesis, which functionally changed the amplitude of mIPSCs (Lau and Murthy, 2012). In addition to changes in the rate of neurotransmitter production, there is emerging evidence that a cell's neurotransmitter phenotype can be homeostatically regulated (Spitzer, 2012; Borodinsky et al., 2014). A key study in the developing frog spinal cord revealed that neurotransmitter phenotype could be altered by chronic activity perturbations (Borodinsky et al., 2004). Reduced activity led to a decrease in the proportion of neurons that synthesized excitatory transmitters and an increase in neurons synthesizing inhibitory transmitters; the opposite changes were seen following activity elevations (Borodinsky et al., 2004). Subsequently, another study demonstrated that chronic elevations in excitatory transmission in mature hippocampal circuits could induce some glutamatergic cells to begin producing GABA to compensate for lack of inhibitory drive (Gómez-Lira et al., 2005). Similarly, chronic electrical stimulation of cortical cultures was shown to increase the proportion of GABAergic cells, and corresponded to a compensatory decrease in synchronous burst activity (Madhavan,

2007). There have also been accounts of homeostatic respecification of neurotransmitter phenotype that alter expression of dopaminergic (Dulcis and Spitzer, 2008; Dulcis et al., 2013) or serotonergic cells (Demarque and Spitzer, 2010) in the mature nervous system.

1.3.2 Potential triggers for transmitter release homeostasis

What aspect of activity might be sensed to trigger homeostatic changes in neurotransmitter release? In the case of changes in presynaptic properties, it appears that presynaptic calcium influx is a critical component (Frank et al., 2006, 2009; Zhao et al., 2011; Lazarevic et al., 2011; Müller and Davis, 2012; Kim and Ryan, 2013). Given that most homeostatic changes in presynaptic release appear to be synapse-specific and dependent on postsynaptic activity (Davis and Goodman, 1998; Paradis et al., 2001; Frank et al., 2006; Branco et al., 2008), there is an obvious need for a local retrograde signal. Synaptic retrograde signals could take the form of altered electric fields, interactions between synaptic or perisynaptic proteins, or release of signaling molecules. A recent study has provided evidence that local synthesis and secretion of brain-derived neurotrophic factor (BDNF) serves as a retrograde signal in response to synaptic blockade at specific glutamatergic synapses. Subsequently, a related study suggested that the retrograde BDNF signal facilitating presynaptic homeostasis also required concurrent AMPAR activation and postsynaptic calcium signaling (Lindskog and Li, 2010). Meanwhile, at GABAergic synapses, endocannabinoids have been identified as critical signaling molecules in the homeostatic regulation of presynaptic release (Kim and Alger, 2010; Gonzalez-Islas et al., 2012).

Triggers for homeostatic changes in neurotransmitter packing are less clear. Hartman et al. demonstrated that homeostatic reductions in vesicular GABA content occurred with a network-wide activity blockade, but did not occur when activity was reduced in individual presynaptic or postsynaptic cells. The absence of altered GABA

content after reducing postsynaptic activity suggests that presynaptic neurons do not monitor postsynaptic activity levels when homeostatically regulating vesicle filling. The absence of altered GABA content after reducing presynaptic activity suggests that presynaptic neurons gauge neither their own level of activity, nor postsynaptic receptor activation, to induce changes in vesicular filling. Whereas presynaptic changes in vesicle pools or probability of release are often synapse-specific and dependent on changes in postsynaptic activity, homeostatic regulation of transmitter packing seems to be neither of these. However, it is important to note that these results were specific to GABAergic synapses, so it will be important for future studies to gauge whether these results are representative of a general principle governing all synapse types.

1.4 Homeostatic regulation of postsynaptic response

Another means for stabilizing neural circuit activity is to manipulate the postsynaptic response to neurotransmitter. This represents a way for a cell to tune its own sensitivity to incoming synaptic inputs. For example, if activity is too low, an upregulation of excitatory synaptic receptors and/or a downregulation of inhibitory synaptic receptors could achieve the functional goal of shifting the balance toward excitation. Conversely, elevated activity could induce decreases in excitatory receptors and/or increases in inhibitory receptors at postsynaptic sites. In addition to changes in postsynaptic receptor number, an increase in the postsynaptic response to a fixed amount of neurotransmitter could be the result of changes in receptor distribution, receptor conductance, or receptor kinetics. In this section, I present evidence for different mechanisms of postsynaptic homeostasis, and discuss potential triggers for these mechanisms. As previously stated, the names of commonly-referenced synaptic receptors are listed in Table 1.3.

1.4.1 Evidence for postsynaptic homeostasis

Early accounts of homeostatic changes in postsynaptic receptors were the result of studies examining the long-term consequences of denervation. Chronic muscle paralysis or denervation led to an increase in muscle sensitivity due to accumulation and clustering of acetylcholine receptors (Berg and Hall, 1975). This principle of postsynaptic receptor accumulation following loss of synaptic activity was later found to hold for other ionotropic receptors. Blockade of NMDA-type glutamate receptors (NMDARs) produced a compensatory increase in the number of NMDARs (McDonald et al., 1990; Williams et al., 1992), as well as upregulation of mRNA and polypeptides for several NMDAR subunits (Follesa and Ticku, 1996). Notably, upregulation of NMDAR subunit mRNA and polypeptides could be reversed by co-treatment with NMDA, and did not occur with chronic AMPAR blockade, suggesting that reductions in NMDAR activation were required to produce the plasticity. Importantly, work by Rao and Craig, 1997 showed that chronic (1-week) blockade of NMDARs not only produced compensatory increases in NMDA receptors, but also increased clustering specifically at synaptic sites. Blocking spiking also elicited the increase in NMDARs, but this effect was mostly reversed by pairing the spiking blockade with chronic NMDA application (Rao and Craig, 1997). These findings suggested that chronic loss of NMDAR activation could directly trigger increases in NMDAR expression and synaptic localization to compensate for lost synaptic efficacy. Notably, there were no observed changes in AMPA receptor (AMPAR) expression following blockade of NMDARs or spiking as assessed through abundance of the GluA1 subunit, suggesting the effect was specific to NMDA receptors. In addition, a 4-hour blockade of NMDARs did not trigger the changes in receptor abundance or clustering, suggesting that the plasticity required days (Rao and Craig, 1997).

Subsequently, a series of studies in neuronal cultures provided evidence that AMPARs could also be homeostatically regulated (Turrigiano et al., 1998; Lissin

et al., 1998; O'Brien et al., 1998). Chronic blockade of AMPAergic transmission or spiking activity produced compensatory increases in abundance of synaptic AMPARs (O'Brien et al., 1998) and a concomitant increase in the amplitude of AMPAR-mediated miniature excitatory postsynaptic currents (mEPSCs) (Turrigiano et al., 1998). Importantly, blocking NMDAR receptors had no effect on either AMPAR abundance or mEPSC amplitude. Meanwhile, chronic blockade of inhibitory GABA$_A$ergic transmission produced a compensatory decrease in AMPARs (Lissin et al., 1998) and a concomitant decrease in AMPAergic mEPSC amplitude (Turrigiano et al., 1998; O'Brien et al., 1998). The disinhibition-induced decrease in AMPARs could be reversed by concurrently blocking spiking activity (Lissin et al., 1998), though interestingly was not heightened as would be expected if spiking activity alone was blocked (O'Brien et al., 1998). In contrast to (though not in conflict with) the increase in synaptic NMDARs that was previously seen in activity blockade conditions (Rao and Craig, 1997), elevations in activity did not seem to affect NMDAR expression (Lissin et al., 1998). Together, these studies laid the foundation for AMPARs as a central expression locus for homeostatic changes in synaptic strength.

A key observation in Turrigiano et al., 1998 was that the distribution of mEPSC amplitudes from activity-blocked cultures was proportionally increased above the control distribution, while the mEPSC amplitudes from chronically disinhibited cultures were proportionally decreased. This phenomenon, called synaptic scaling[3], provides a means for regulating neuronal excitability without disrupting relative synaptic strengths imposed by Hebbian processes (Oja, 1982; Miller and MacKay, 1994; Abbott and Nelson, 2000).

---

[3] In current literature, the term "synaptic scaling" has been used to encompass several forms of homeostatic plasticity. For the purposes of this thesis we use the term, synaptic scaling, as presented in its initial experimental description (Turrigiano et al., 1998): a cell-wide increase or decrease in quantal amplitudes by a common multiplicative factor as a compensatory response to altered activity.

Since its initial description, synaptic scaling has emerged as a widely-studied form of homeostatic plasticity. While there are differences in how different groups have characterized the sensing and expression mechanisms involved in scaling, there are features of scaling that are widely-accepted. First, scaling of excitatory synapses onto excitatory cells (the most commonly-observed form of scaling) is expressed through a change in the total excitatory receptor conductance. This could result from either insertion/removal of receptors at the synapse (O'Brien et al., 1998; Wierenga et al., 2005), replacement of low-conductance receptors with higher-conductance receptors (He et al., 2012; Garcia-Bereguiain et al., 2013), and/or shifts in the reversal potential of a receptor's permeant ions (Gonzalez-Islas et al., 2010). Secondly, while synaptic scaling can occur bidirectionally (Turrigiano et al., 1998), upward and downward synaptic scaling are mediated, at least in part, by distinct mechanisms. This is highlighted by the array of molecules that are critical for upscaling or downscaling, but not required for both (Rutherford et al., 1998; Leslie et al., 2001; Shepherd et al., 2006; Stellwagen and Malenka, 2006; Anggono et al., 2011; Sun and Turrigiano, 2011; Tatavarty et al., 2013). Third, scaling can influence both excitation and inhibition. While scaling has primarily been studied for excitatory inputs onto excitatory cells (Turrigiano, 2008), multiplicative compensatory changes in synaptic strength also occur at inhibitory synapses (Turrigiano et al., 1998; Hartman et al., 2006; Swanwick et al., 2006) and in inhibitory cells (Chang et al., 2010). Finally, synaptic scaling can occur *in vivo*. Scaling has primarily been induced in culture preparations, but *in vivo* perturbations to activity have revealed multiplicative increases in quantal amplitude in both sensory cortex (Desai et al., 2002; Goel and Lee, 2007) and the spinal cord (Gonzalez-Islas and Wenner, 2006; Knogler et al., 2010).

Importantly, there are several instances where homeostatic changes in receptor number occur throughout a cell, but do not follow a uniform scaling rule. For instance, blocking spiking activity in the hippocampus of juvenile rats for 2 days led

to an increase in average mEPSC amplitude in CA1 pyramidal cells, but the distribution of activity blocked amplitudes was not multiplicatively related to controls (Echegoyen et al., 2007). There are several possibilities for why the mEPSC amplitude distribution may shift non-uniformly. First, the increase in mEPSC amplitude was accompanied by changes in intrinsic excitability, presynaptic release, and inhibitory synaptic strength (Echegoyen et al., 2007), and together these may represent one of many solutions for supporting homeostatic recovery of activity (Marder and Prinz, 2002; Marder and Goaillard, 2006). Secondly, there could be preferential enlargement of already large synapses and elimination of already small synapses, thus increasing average mEPSC amplitude without achieving multiplicative scaling (Thiagarajan et al., 2005) A third possibility is that distal versus proximal inputs are differentially regulated, either because of distance-dependent dendritic filtering (Andrasfalvy and Magee, 2001) or layer-specific regulation of postsynaptic inputs (Vlachos et al., 2012); these effects seen in structured hippocampal slices could be lost in dissociated cultures, where scaling is robustly observed. Finally, subsets of postsynaptic inputs may be subject to different forms of homeostatic regulation depending on which hippocampal subfield the presynaptic cell is located in (Kim and Tsien, 2008). This possibility seems especially plausible in light of recent evidence showing that tadpole tectal neurons, which receive converging multi-modal sensory input, homeostatically regulate synaptic inputs from the visual pathway independently of synaptic inputs from the mechanosensory pathway (Deeg and Aizenman, 2011). Other non-multiplicative changes in mEPSC amplitude could also be explained by developmental differences. For example, chronic visual deprivation led to scaling in the primary visual cortex of juvenile rats, but non-uniform increases in mEPSC amplitude in primary visual cortex of adult rats (Goel and Lee, 2007). This suggests that scaling may be a form of plasticity primarily relevant in the developing nervous system (Turrigiano and Nelson, 2004). Indeed, other *in vivo* studies have shown dif-

ferences in homeostatic changes in mEPSC amplitude depending on the animal's age (Desai et al., 2002; Echegoyen et al., 2007).

In addition, there is growing evidence that homeostatic changes in postsynaptic AMPARs can occur at individual synapses or dendritic regions. This was first illustrated by Sutton et al.. During a network-wide spiking blockade, local perfusion of an NMDAR antagonist onto a small dendritic region triggered increases in GluA1 within a few hours, but only in the NMDAR-blocked region (Sutton et al., 2006). Meanwhile, a network-wide or local spiking blockade alone over the same timescale produced no change in GluA1 surface expression (Sutton et al., 2006). This suggested that a local synaptic blockade could produce increases in AMPARs. Similarly, Ibata et al. found that local spiking blockade in a portion of the dendrite did not produce any changes in synaptic GluA2 in that blocked region for several hours. However, this study also found that local glutamatergic blockade with CNQX and APV produced no change in GluA2 fluorescence, suggesting that local synaptic blockade was not sufficient to produce increases in AMPARs (Ibata et al., 2008). Important differences between these two studies are that Sutton et al. used TTX and APV to produce local changes in GluA1, while Ibata et al. used TTX or CNQX and APV, and failed to see local changes in GluA2. This suggests either an important role for the combined blockade of spiking and NMDAergic transmission in producing increases in mEPSC amplitude, or it suggests a special role for GluA1 in the expression of rapid dendrite-specific homeostasis.

Subsequently, Hou et al. and Béïque et al. demonstrated compensatory synapse-specific increases in synaptic AMPARs by chronically reducing glutamate release from individual presynaptic inputs in an otherwise intact culture system. They then examined how AMPAR accumulation at postsynaptic sites that experienced chronically reduced synaptic activity compared to neighboring sites experiencing normal activity (Hou et al., 2008; Béïque et al., 2011). They observed increases in synaptic AMPAR

expression only at synapses experiencing reduced activity (Hou et al., 2008; Béïque et al., 2011) which were correlated to increased EPSC amplitude in response to local glutamate uncaging (Béïque et al., 2011). These results indicated that individual synapses could homeostatically adjust their sensitivity to incoming input to compensate for reduced presynaptic drive. Importantly, the increase in AMPARs was due to insertions of GluA1 homomers. The importance of GluA1 receptors in the expression of synapse-specific plasticity suggests that dendrite-specific plasticity is probably due, at least in part, to insertion of GluA1 homomeric AMPARs (Sutton et al., 2006) and not GluA2-containing AMPARs (Ibata et al., 2008). Further, increasing glutamatergic release from individual presynaptic inputs produced a reduction in postsynaptic AMPARs only at synapses experiencing heightened activity (Hou et al., 2011), indicating that this synapse-specific form of homeostatic plasticity is bidirectional.

1.4.2 Potential triggers for postsynaptic homeostasis

What type of activity is sensed to trigger homeostatic changes in postsynaptic receptors? For synapse-specific and pathway-specific plasticity, altered synaptic activity appears to be paramount (Sutton et al., 2006; Hou et al., 2008; Kim and Tsien, 2008; Deeg and Aizenman, 2011; Béïque et al., 2011; Hou et al., 2011). Notably, most of these experiments do not distinguish between altered presynaptic release and postsynaptic receptor activation as triggers for changes in mEPSC amplitude, although Sutton et al. suggests that reductions in miniature NMDAergic events produce the dendrite-specific plasticity. In addition, these studies have all examined excitatory inputs to excitatory cells, so it will be important to see whether these principles translate to other cell-synapse combinations.

For synaptic scaling, several different groups have worked toward identifying a common trigger for this plasticity. An early hypothesis based on initial experiments was that changes in postsynaptic firing rate trigger bidirectional scaling (Abbott and

Nelson, 2000; Turrigiano and Nelson, 2004), and a recent study has provided strong support for the idea that a single neuron can autonomously regulate postsynaptic AMPARs based on its own firing rate (Ibata et al., 2008). However, other work complicates the firing rate model of synaptic scaling. Under this model, reductions in spiking activity would lead to upward scaling of quantal amplitude while elevations in spiking activity would lead to downward scaling. However, two groups have shown that reducing postsynaptic spiking through overexpression of the inwardly-rectifying potassium channel, $K_{ir}2.1$, does not lead to changes in mEPSC amplitude (Paradis et al., 2001; Burrone et al., 2002). In addition, two other groups have shown that downscaling can be achieved by depolarizing neurons with high $[K^+]_o$ (Leslie et al., 2001) or optogenetic stimulation (Goold and Nicoll, 2010) even when spiking is blocked. Even if changes in firing rate do not directly trigger scaling, other potential activity sensors that are typically correlated with spiking could explain the above results.

For upward scaling, it is possible that changes in synaptic transmission trigger scaling, as is the case with synapse- and pathway-specific changes in quantal amplitude. In this case, lack of scaling observed by Paradis et al. and Burrone et al. could be explained by the fact that transmission onto the cells was relatively normal. Notably, this possibility is in conflict with Ibata et al., 2008, which showed that perfusion of TTX onto the soma produced increases in AMPARs within a few hours, but perfusion of synaptic blockers had no effect. However, this study used changes in GluA2 fluorescence to assess scaling (rather than using mEPSC amplitude), and previous work has shown that TTX-induced scaling cannot be achieved within a few hours (Turrigiano et al., 1998; Sutton et al., 2006). Therefore, it will be important for future studies to validate these findings using direct measurements of quantal amplitude over timescales consistent with TTX-induced scaling. Further, with the diverse combinations of parameters that can achieve similar functional goals (Marder and

Prinz, 2002), it is perfectly plausible that changes in either spiking or transmission could produce scaling, and the tendency toward one or the other could be cell-type- or state-dependent.

For downward scaling, it is possible that changes in intracellular calcium trigger scaling, as with some forms of intrinsic and presynaptic homeostasis. In this case, the presence of downscaling observed by Leslie et al. and Goold and Nicoll in the absence of spiking could be explained by the fact that chronic membrane depolarization raises intracellular calcium levels, initiating the signaling cascade that produces removal of postsynaptic AMPARs. In agreement with this possibility, (Goold and Nicoll, 2010) showed that reductions in evoked EPSC amplitude that had been observed after chronic depolarization could not be achieved if L-type Ca_V channels were blocked.

Finally, there is evidence that other signaling molecules can trigger changes in postsynaptic strength. For example, it has been shown that glia can sense reduced levels of ambient glutamate, and release TNF-α, which in turn facilitates insertion of postsynaptic AMPARs (Stellwagen and Malenka, 2006). This model is particularly attractive because it does not localize plasticity to an individual neuron or synapse, but instead reflects a way to democratically survey population activity.

1.5 Challenges for studying homeostatic plasticity

Currently, our understanding of homeostatic plasticity is primarily based on observations of expression mechanisms (e.g. changes in intrinsic or synaptic properties). While these accounts help enrich our understanding of what strategies the neural circuits may exploit in the living system, an important goal of current and future research is to identify what specific features of activity are monitored to induce different forms of plasticity. Neuronal firing rate, intracellular calcium, and neurotransmission have all been identified as possible activity features that are sensed to trigger homeostatic plasticity, but these parameters are highly intertwined. Further, these parameters

have been difficult to monitor during the induction and expression of homeostatic plasticity. However, new tools in neuroscience research are making it possible to address some of these challenges.

1.6 Thesis Goals and Organization

Synaptic scaling is the most widely-observed form of homeostatic plasticity across different model systems (Turrigiano, 2008). There is little dispute that scaling is expressed in some form in the nervous system, but how synaptic scaling is triggered remains unclear. Rather than to identify a single molecule that disrupts or promotes scaling, I seek to disentangle the overarching system parameters that drive this special form of plasticity. As chronic blockade of spiking or excitatory synaptic transmission are the two most common experimental strategies for producing synaptic scaling, I focus my dissertation on these two parameters.

Conceptually, blocking AMPAergic transmission would be expected to dramatically reduce spiking at the network level due to loss of overall excitatory drive. Surprisingly, there is little information on how an AMPAergic blockade influences network-wide spiking over the time course that scaling occurs. In Chapter 2, I continuously monitor spiking activity from hundreds of neurons embedded in cultured cortical networks and examine how firing rates (at the network-wide and individual neuron level) change throughout the course of a chronic AMPAergic transmission blockade. In addition, spiking and AMPAergic transmission are highly-coupled system parameters, so understanding their independent roles in inducing synaptic scaling requires a strategy for decoupling these parameters at the network level. In Chapter 3, I present an approach for maintaining network spiking levels during a chronic AMPAR blockade, and test whether reduced transmission can independently trigger synaptic scaling. Conversely, in Chapter 4, I partially re-introduce AMPAergic transmission during a chronic spiking blockade, and evaluate the capacity for reduced spiking to

independently trigger scaling. Finally, I conclude the dissertation with a general discussion (Chapter 5) of these results in the context of previous research and provide an outlook for future studies. Following the main text, I provide a characterization of our spiking sorting approaches (Appendix A) and a brief investigation of plasticity in other neurotransmitters systems during AMPAergic blockade (Appendix B).

CHARACTERIZATION OF SPIKING ACTIVITY DURING CHRONIC AMPA RECEPTOR BLOCKADE

AMPA-type glutamate receptors (AMPARs) mediate fast excitatory synaptic transmission in the adult nervous system. Several forms of activity-dependent plasticity are triggered by chronic loss of AMPAergic transmission. However, relatively little is known about the temporal trajectory of activity that accompanies an AMPAergic transmission blockade. In this chapter we used micro-electrode array recordings to monitor how chronically blocking AMPARs impacts firing rates in dissociated cortical cultures over the course of 24 hours. We found that blocking AMPARs reduced firing rate by approximately 50%, primarily due to a reduction in the frequency of synchronous network-wide bursts. We also observed great variability in the effect of AMPAR blockade between different cultures and amongst individual cells, though spiking and bursting persisted to some degree in all cultures. Finally, we related the observed changes in firing rate to homeostatic synaptic scaling, a form of plasticity that has been widely shown to follow chronic AMPAR blockade. Surprisingly, we found no correlation between the magnitude of the reduction in firing rate and the subsequent degree of scaling. These findings demonstrate that spiking and bursting activity persist in the absence of AMPAergic transmission, and call into question the activity dependence of homeostatic synaptic scaling.

2.1 Introduction

2.1.1 Background

A balance of excitatory and inhibitory inputs is required for proper neural function. Indeed, chronic loss of either glutamatergic or GABAergic transmission has been shown to drive homeostatic mechanisms that compensate for the loss of synaptic input. For instance, when glutamatergic activity was chronically blocked in neuronal cultures, relief from the blockade led to seizure-like barrages of action potentials (Furshpan and Potter, 1989) and dramatically heightened levels of intracellular calcium (Van den Pol et al., 1996). This suggested that the absence of glutamatergic drive led to plasticity that homeostatically increased network excitability. Since then, numerous forms of plasticity have been described following chronic glutamatergic blockade, including alterations in expression of intrinsic excitability (Shin and Chetkovich, 2007; Driscoll et al., 2013) and synaptic strength (Turrigiano et al., 1998; O'Brien et al., 1998; Thiagarajan et al., 2005; Mateos et al., 2007). While many of these compensatory mechanisms are thought to be activity-dependent, relatively little is known about the profile of activity that drives the expression of homeostatic plasticity. How is spiking activity affected by loss of excitatory transmission? How do activity features change over the course of a sustained transmission blockade?

The most comprehensive studies to date on how chronic synaptic receptor blockade affects spiking activity have been performed by Michael Corner, Robert Baker, and Jaap van Pelt at the Netherlands Institute for Neuroscience (Corner et al., 2002, 2005, 2006, 2008). Collectively, these studies have provided an extensive survey of how spiking changes in cortical slice cultures following acute or chronic blockade of glutamatergic or GABAergic transmission at different developmental stages. In one set of experiments, cultures were grown in the AMPAR antagonist, 6,7-dinitroquinoxaline-2-3-dione (DNQX) for 1 or 2 weeks. At one week *in vitro*, cultures grown in DNQX

exhibited firing rates that were slightly reduced compared to controls; however, after two weeks *in vitro*, firing rates were slightly above control levels (Corner et al., 2005). This result suggests that the second week *in vitro* is a critical period during which cultures can homeostatically tune their excitability to compensate, or even overcompensate, for chronic loss in AMPAergic transmission. While these studies have provided an excellent database for assessing the consequences of blocking various synaptic receptors on spiking activity, it is still unclear how spiking activity is influenced over time *during* these week-long perturbations because recordings only lasted 15 minutes. In addition, the experiments were performed using a single extracellular electrode, such that culture-wide activity was approximated by 1-3 neurons. These limitations make it difficult to identify how changes in activity levels and patterns contribute to subsequent plasticity, or how different subsets of neurons may be differentially affected by synaptic blockade.

2.1.2 Micro-electrode arrays

In-vitro neuronal networks grown on substrate-integrated micro-electrode arrays (MEAs; Figs. 2.1 and 2.2) provide an excellent testbed for examining the network and single-cell activity patterns that drive plasticity (Liu et al., 2012). MEAs were first used to record from cardiac tissue (Thomas et al., 1972) and subsequently introduced for extracellular recording from neurons (Gross et al., 1977; Gross, 1979). Pioneering work by Pine used intracellular stimulation to depolarize individual neurons while simultaneously using an MEA to record extracellular action potentials from the stimulated cell. Remarkably, extracellular action potentials could be detected even in neurons located tens of microns away from the recording electrode (Pine, 1980). Since the development of these tools, academic research and commercial ventures have collectively improved the quality and accessibility of

Figure 2.1: Substrate-integrated microelectrode arrays. Micro-electrode array (MEA) is embedded in a glass dish. Shadows on hand reveal leads radiating from micro-electrodes. In additional to providing multichannel electrophysiological measurements, this system provides excellent pharmacological, genetic, and optical accessibility. Image source: Potter, 1998.

substrate-integrated MEAs, and they are becoming a common tool for many labs (Taketani and Baudry, 2006).

Among the advantages of modern-day MEAs is their capacity to provide stable recordings from many neurons over long periods of time. This has allowed for an excellent of characterization spiking activity in dissociated neuronal cultures (Van Pelt et al., 2004; Wagenaar et al., 2006a,b; Chiappalone et al., 2006; Minerbi et al., 2009), one of the most widely-used preparations in basic neuroscience research. In a stereotypical dissociated culture, neurons are fairly silent during the first few days after plating dissociated cells. Over time, neurons begin to form synaptic connections and spiking can be detected on electrodes at ∼4 days *in vitro* (DIV) (Figure 2.3). Action potentials become increasingly correlated by end of the first week, eventually producing bursts of action potentials that are synchronized across many electrodes (Figures 2.3 and 2.4). These network-wide bursts are the most prominent feature of spiking activity in dissociated cultures (Kamioka et al., 1996; Gross and Kowalski, 1999). The emergence of bursting shortly after synapse formation in dissociated cultures is reminiscent of spontaneous network activity that occurs in many other
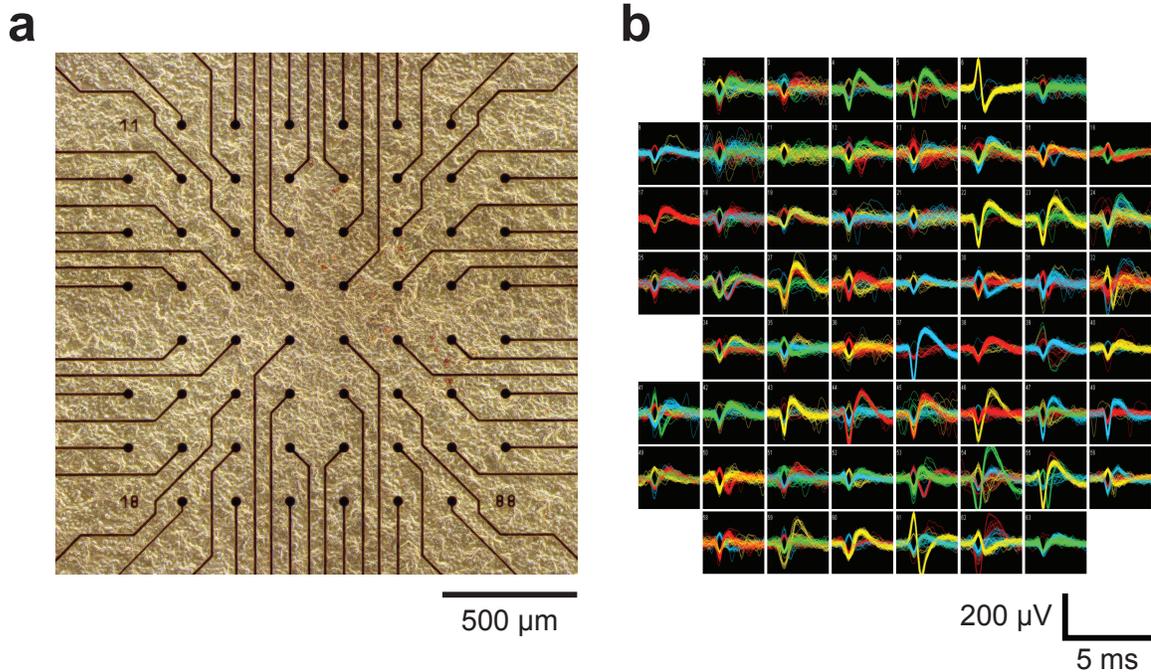
Figure 2.2: Dissociated cortical cultures grown on micro-electrode arrays. **(a)** Phase-contrast micrograph of dissociated cortical culture grown on a planar MEA. **(b)** Extracellular spike waveforms recorded on each microelectrode shown in (a). For each electrode, colors denote different sorted units.

developing neural circuits (Feller, 1999; Khazipov and Luhmann, 2006; Spitzer, 2006; Blankenship and Feller, 2010), although the persistence of synchronized bursting as cultures mature has led to comparisons with epileptiform activity (Wagenaar et al., 2005b; Wagenaar, 2006). Regardless, the vast majority of spiking occurs during bursts (Figure 2.4), so their presence dictates a culture's overall firing rate.

While MEA technology has provided us with a good sense of common activity themes exhibited in developing neural circuits, far less is known about how this activity is affected by perturbations that lead to plasticity (but see Minerbi et al., 2009). For instance, chronic blockade of AMPAergic transmission has been shown to induce homeostatic synaptic scaling after several hours, yet little is known about what activity looks like during the induction of this plasticity. Our goal is to characterize the
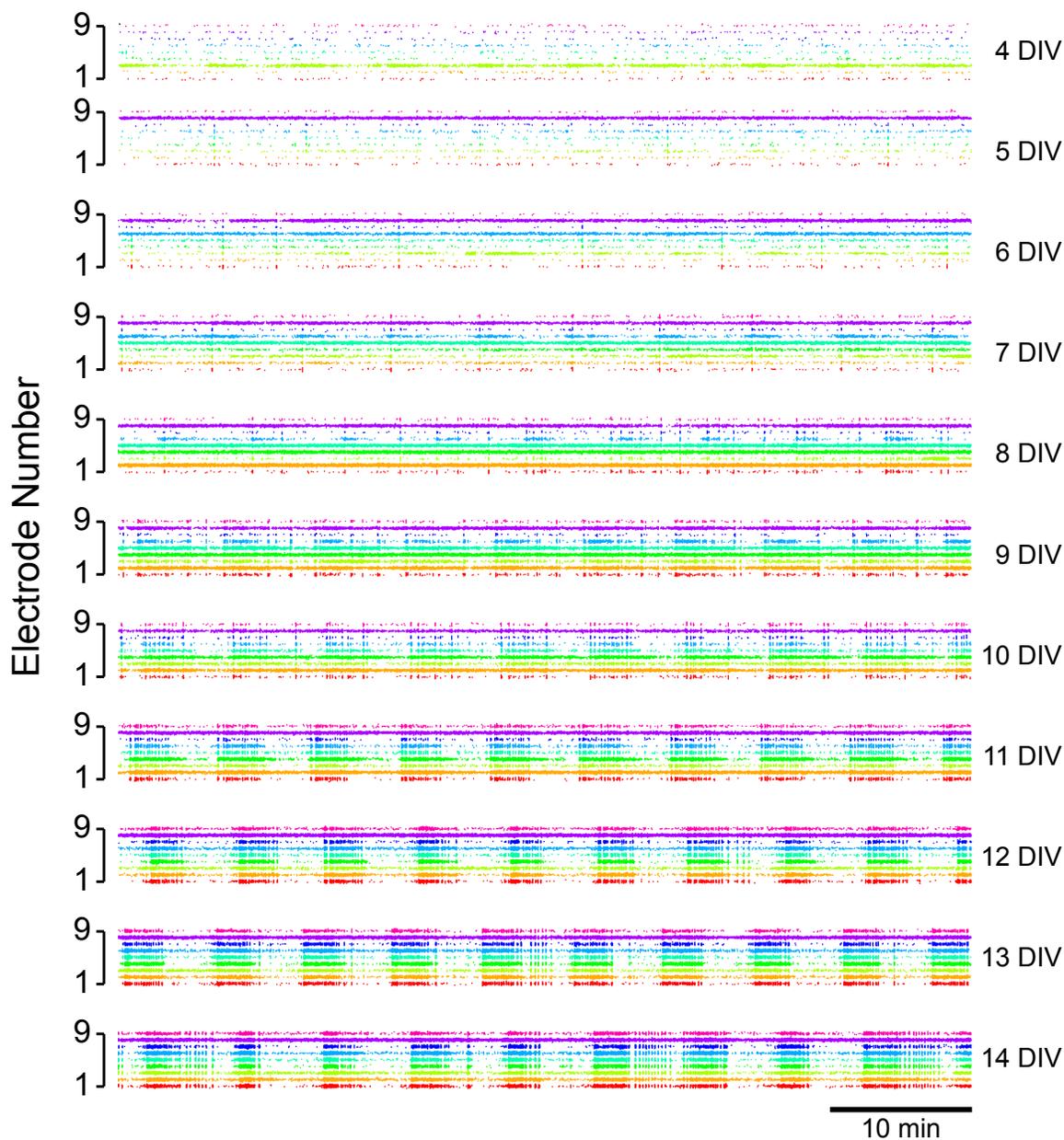
Figure 2.3: Development of spiking activity in cultured cortical networks. Spiking activity in a dissociated cortical culture was continuously recorded on 9 micro-electrodes for the first two weeks *in vitro*. The rastergrams show one hour from each day (centered at the 12th hour of each day) beginning at 4 DIV when spikes were first detected. Due to the large number of spikes, the points were vertically-jittered to make the data easier to view, and colors are used to denote different electrodes.
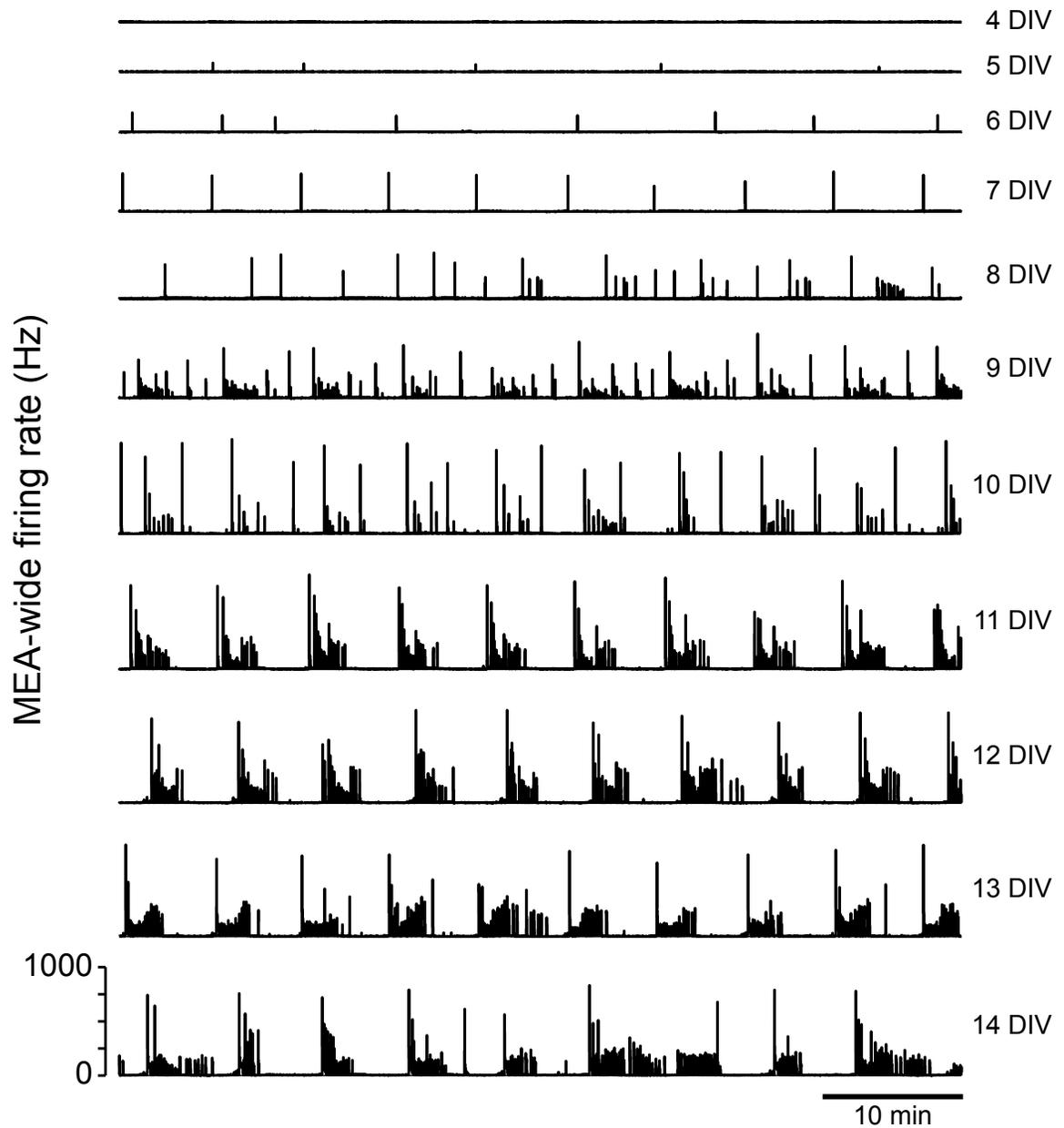
Figure 2.4: Development of spontaneous bursting in cultured cortical networks. Time histograms of spiking activity from same culture and time windows shown in Figure 2.3. The plots reveal the emergence of synchronized bursting activity by the end of the first week *in vitro*, and the development of patterned bursting during the second week *in vitro*. Bin size, 1 sec.

activity features that are altered during an AMPAergic transmission blockade, and directly relate these changes in activity to homeostatic changes in synaptic strength.

2.1.3 Chapter summary

In this chapter, we used chronic MEA recordings to track spiking activity in hundreds of neurons during a chronic blockade of AMPAergic transmission. We found that spiking was reduced by approximately 50%. While there was variability in the degree to which AMPAergic blockade reduced activity among cells and between cultures, every neuron continued to fire in some capacity, and all cultures still exhibited network-wide bursting. We next examined the effects of moderate reductions in spiking (induced by AMPAR blockade) versus complete elimination of spiking (induced by voltage-gated sodium channel blockade) on activity-dependent synaptic scaling. Surprisingly, we found that there was no difference in the degree of scaling in cultures that had experienced moderate versus complete reductions in spiking. Further, we observed no correlation between changes in synaptic strength and the preceding reductions in firing rate or burst rate. These findings suggest that firing rate may not be the only activity signal monitored to trigger scaling, and that another activity feature such as synaptic transmission, might also act as a sensor that triggers homeostatic plasticity.

2.2 Methods

2.2.1 Cell culture

2.2.1.1 Plating

Sterilized MEAs[1] and glass bottom dishes[2] (GBDs) were coated first with polyethyleneimine[3] to make the surface hydrophilic and then with laminin[4] to

---

[1] Multichannel Systems (Reutlingen, Germany), 60MEA200/30iR-Ti-pr or 60-6wellMEA200
[2] MatTek Corporation (Ashland, MA, USA), P35G-1.5-10-C
[3] Sigma-Aldrich (St. Louis, MO, USA), P-3143
[4] Sigma-Aldrich (St. Louis, MO, USA), L-2020

provide a substrate for adhesion and growth. Neocortical hemispheres were isolated from embryonic day 18 (E18) rats or equivalent tissue was purchased as isolated hemispheres[5]. Tissue was enzymatically dissociated using 20 $U \cdot mL^{-1}$ activated papain[6] at 36.5 °C and mechanically dissociated by trituration. The dissociated cells were then gravity filtered at 40 μm to remove large clumps, and centrifuged for 6 minutes at 200·g through 5% w/v bovine serum albumin to remove small particles. The resulting cell suspension was stained to assess viability using Trypan Blue[7] and diluted to 2,500 live cells·μL^{-1}. A drop of 35,000 cells was plated as a 2 mm diameter circle at the center of the grid of MEA electrodes or the GBD culturing surface. After 20-30 minutes in the incubator, dishes were flooded with growth medium modified from Jimbo et al., 1999 containing: 90% high-glucose DMEM, 10% horse serum, 0.5 mM GlutaMAX, 1 mM sodium pyruvate, 2.5 $\mu g \cdot mL^{-1}$ insulin (pH 7.2, adjusted to 315 mOsm). No antibiotics or antimycotics were used. The total volume of medium in each dish was 1.5 mL for standard MEAs and glass bottom dishes, and 0.5 mL for each well in a multi-well MEA. Medium was fully exchanged at 1 day in vitro (DIV), and half the medium was exchanged every 3 days thereafter. Growth medium was always warmed to 35 °C prior to flooding or exchanging media. MEAs and GBDs were sealed with fluorinated ethylene-propylene (Potter and Demarse, 2001) or polydimethylsiloxane (Blau et al., 2009) membranes to provide sterility and humidity control. Cultures were maintained in an incubator regulated at 35 °C, 5% CO_2, and 65% relative humidity. Further details of our culturing procedures are described in Hales et al., 2010. All procedures were in compliance with the National Research Council's Guide for the care and use of laboratory animals using a protocol approved by the Georgia Tech Institutional Animal Care and Use Committee.

---

[5]   BrainBits, LLC (Springfield, IL, USA), cx
[6]   Roche Applied Science (Indianapolis, IN, USA), 10108014001
[7]   Life Technologies (Grand Island, NY, USA), 15250

2.2.1.2 MEA Cleaning

Following the conclusion of an experiment, MEAs were cleaned for re-use. Old cultures were removed by pipetting culturing media toward the center of the dish using a P-1000 pipette positioned at a 30° angle from the culturing plane. All culturing media and debris were removed via aspiration and the dishes were rinsed with phosphate-buffered saline[8]. Subsequently, 1 mL of warm 0.25% trypsin[9] was added to the culturing well. A tightly-fitting lid was placed on the MEA, and the dish was left for 20 minutes at 35-37 °C, with gentle rocking when possible. The MEA was then washed with de-ionized water. If debris remained, the dish was re-incubated with trypsin for another 20 minutes and re-rinsed with water. MEAs exposed to TTX were decontaminated by autoclaving for 30 minutes at 121 °C. MEAs were stored in sterile water at 4 °C.

2.2.1.3 MEA Sterilization

All sterilization procedures were performed inside a biosafety cabinet. MEA dishes were submerged in 70% ethanol for 10 minutes. After removal, the bottom and sides of each dish were dried with a light-duty tissue wiper (e.g. Kimwipe). A vacuum aspirator was used to remove residual ethanol from the culturing surface. MEAs were left in the biosafety cabinet for 2-12 hours with the overhead UV light on before beginning the plating procedure.

2.2.2 Chronic treatments

Chronic treatments began during the second week *in vitro* (either 10, 11, or 12DIV) and lasted for 24 hours. In each case, MEA activity was recorded for at least 6 hours before adding the drug. The baseline pre-treatment condition was defined as the 3-

---

[8] Life Technologies (Grand Island, NY, USA), 10010-031
[9] Life Technologies (Grand Island, NY, USA), 25200-056

Table 2.1: Pharmacological agents

Drug	Concentration	Function
CNQX[1]	40 μM	AMPA/kainate receptor antagonist
TTX[2]	1 μM	voltage-gated sodium channel antagonist
APV[3]	50 μM	NMDA receptor antagonist
bicuculline[4]	20 μM	$GABA_A$ receptor antagonist
cyclothiazide[5]	20 μM	AMPA receptor positive allosteric modulator

Sigma-Aldrich (St. Louis, MO, USA): [1]C127, [2]T5651, [3]A8054, [4]14343
Enzo Life Sciences (Farmingdale, NY, USA): [5]ALX-550-338

hour period preceding drug or vehicle application, and the treatment condition was defined as the 24-hour period after drug or vehicle application. The concentrations and purpose of all drugs used in this thesis are summarized in Table 2.1. The vehicle used for control cultures was either standard growth medium, water, or dimethyl sulfoxide (DMSO). Concentrated TTX and CNQX aliquots were dissolved in water and DMSO, respectively. Therefore, in experiments involving pairs of sister cultures, water was used as the vehicle treatment in TTX experiments, and DMSO was used as vehicle for CNQX experiments. For experiments requiring patch clamp recordings from sister cultures, treatments were staggered by 4 hours so that they could be recorded from serially on the same patch clamp rig. Solid and liquid waste that came into contact with TTX-containing liquids were decontaminated through incubation in 2.5% sodium hypochlorite for at least 20 minutes.

2.2.3 Microelectrode array electrophysiology

We used two types of MEAs for our experiments. Standard MEAs contained 59 electrodes on an 8x8 grid, with 200 μm between adjacent electrodes (Figure 2.2). We also used multi-well dishes containing six isolated 9-electrode MEAs on a 3x3 grid, allowing for simultaneous recording for six sister cultures at the expense of lower

channel count. There was no difference in the standard and multi-well MEAs in terms of culturing procedure, plating densities, recording equipment, or analysis.

2.2.3.1 Recordings

MEA recordings were performed in standard growth medium in a cell culture incubator (35 °C, 5% CO_2, and 65% relative humidity). Voltages recorded through micro-electrodes were amplified 1200X and bandpass filtered between 10 Hz and 10 kHz using a 60-channel analog amplifier[10] and digitized at 25 kHz using the Neurorighter acquisition system[11] (Newman et al., 2013; Rolston et al., 2009). Voltages were digitally filtered with a 3rd order Butterworth bandpass at 300-5000Hz. Putative action potentials were detected at threshold of ± 5 times V_k^{RMS}, where V_k^{RMS} is defined as the average of lowest 10% of root mean square (RMS) values calculated from a group of 100 millisecond data windows of voltage values taken from channel k. This method prevents overestimates of V_k^{RMS} by excluding windows with large amounts of spiking activity from the RMS calculation (Wagenaar et al., 2005a). To adjust for fluctuations in channel noise levels, we calculated V_k^{RMS} adaptively using a sliding 10-second window. Two milliseconds of the raw voltage data around each spike time was saved so that action potential waveforms could be sorted post-hoc (Section 2.2.3.2 and Appendix A). In some experiments, we also recorded a few minutes of raw data before and during each treatment.

2.2.3.2 Extracellular unit analysis

We used the SqueakySpk[12] MATLAB class to validate and sort spike waveforms into extracellular units. Each unique waveform is thought to represent spiking activity from a unique neuron. For one culture, we manually sorted the putative spike data

---

[10] Multichannel Systems (Reutlingen, Germany), MEA60-Up
[11] Neurorighter codebase: https://sites.google.com/site/neurorighter/
[12] SqueakySpk codebase: code.google.com/p/squeakyspk

using the `LineSort`, a method for manually classifying each waveform as part of an extracellular unit available through the SqueakySpk[13] MATLAB class. Because manually sorting a single 48-hour, 59-channel data set took 1 month, we elected to use an unsupervised approach for the remainder of the data, using this manually sorted data set for validation (Appendix A). We selected an unsupervised strategy for sorting spikes, which used superparamagnetic clustering to classify time-frequency representations of spiking data (Quiroga et al., 2004). Notably, using this approach, we only felt comfortable comparing normalized changes in firing rate (rather than raw firing rates), as we found that raw firing rates were vulnerable to errors when compared to our manually-sorted data set (Appendix A).

2.2.3.3 Firing rate analysis

Offline analysis of recorded spike data was performed in MATLAB[14]. For analysis of multiple cultures, MEA-wide firing rate was normalized to the 3-hour pre-treatment period. Unless otherwise indicated, MEA-wide firing rate for a particular condition was taken from the 24-hour treatment period and normalized to the 3-hour pre-treatment period. For single-unit analysis, each unit was normalized to its own pre-treatment firing rate. Normality in all data sets was assessed using a Lilliefors test. For comparing the array-wide analysis of the three treatment groups, statistical significance was assessed using a Kruskal-Wallis test followed by Wilcoxon rank-sum tests with Bonferroni correction for multiple comparisons. For single-unit analysis of the two treatment groups, statistical significance was assessed using a Wilcoxon rank-sum test and a Kolmogorov-Smirnov test. Outliers were defined as being greater than the first quartile plus 1.5 times the interquartile range, or being less than the third quartile plus 1.5 times the interquartile range. Excluding outliers in our data sets did

---

[13] SqueakySpk codebase: `code.google.com/p/squeakyspk`
[14] The Mathworks (Natick, MA, USA)

not significantly alter the results, so values reported here are based on inclusion of all data.

2.2.3.4 Bursting analysis[15]

Groups of temporally-correlated action potentials that were spatially-distributed among electrodes were called 'bursts'. The time points when bursts occurred were detected post-hoc using a simple thresholding approach. First, the MEA-wide firing rate histogram was calculated for 10-ms bins. Any bin that exceeded 100 times the overall pre-treatment firing rate was initially counted as a candidate burst. Because a single burst typically spans several bins, candidate bursts from consecutive bins were combined into a single burst. Because bursts sometimes show reverberating activity toward their ends, candidate bursts detected within 1 second of a previous burst were discarded. The burst rate was calculated based on number of bursts occurring within a given time. The interburst firing rate was calculated from portions of the MEA-wide firing rate histogram that occurred at least 2 seconds before and 8 seconds after a burst occurred to eliminate the possibility that any buildup or residual activity contributed to this value. For both burst rate and interburst firing rate, any activity was assessed by normalizing the 24-hour treatment period to the 3-hour pre-treatment period. Statistical significance was determined using a Kruskal-Wallis test followed by Wilcoxon rank-sum tests with Bonferroni correction for multiple comparisons.

---

[15] While our lab has previously identified a 'superbursting' activity pattern that develops in some cultures during their second week *in vitro* (Wagenaar et al., 2006b), we did not find any evidence of superbursting in the cultures used for these experiments. In this work, we consistently maintained cultures at 35°C and ambient oxygen levels, but have made the anecdotal observation that sister cultures grown at higher temperatures (36.5-37°C) or at reduced oxygen levels (9%) were more likely to develop superbursting activity. For example, the culture shown in Figs. 2.3 and 2.4 remained at 36.5°C and developed superburst-like activity.

2.2.4 Patch clamp electrophysiology

2.2.4.1 mEPSC recordings

Patch pipettes were made from borosilicate capillaries[16] using a micropipette puller[17]. Tip diameters were ∼2-2.5 μm, and pipette resistances ranged from 2-8 MΩ. A silver electrode was soaked in sodium hypochlorite for 20 minutes prior to recording, and the electrode was re-chlorinated between experiments. A cylindrical Ag-AgCl pellet[18] was used for the bath electrode. An upright microscope[19] was used to identify pyramidal-shaped cells for recording. A digital micromanipulator[20] was used to position the patch pipette. Internal solution contained (in mM): 100 K-gluconate, 30 KCl, 10 HEPES, 2 MgSO4, 0.5 EGTA, 3 ATP (adjusted to pH 7.4 and 290 mOsm). mEPSCs were recorded using a HEKA amplifier and acquisition system[21]. Miniature excitatory postsynaptic currents (mEPSCs) were recorded from pyramidal-shaped neurons in a continuous perfusion of artificial cerebrospinal fluid containing (in mM): 126 NaCl, 3 KCl, 2 $CaCl_2$, 1.5 $MgSO_4$, 1 NaH_2PO_4, 25 $NaHCO_3$, and 25 D-glucose, and saturated with 95% O_2 and 5% CO_2 (pH 7.4, adjusted to 315 mOsm). To isolate AMPAergic mEPSCs, the external solution was supplemented with 1 μM TTX and 20 μM bicuculline. The solution temperature was regulated at 35 °C using an inline heater[22].

---

[16] Sutter Instruments (Novato, CA, USA), BF150-110-10
[17] Sutter Instruments (Novato, CA, USA), P-97 Flaming/Brown
[18] Harvard Apparatus (Holliston, MA, USA), 641309
[19] Nikon (Tokyo, Japan), Eclipse E600FN
[20] Sutter Instruments (Novato, CA, USA), MP-285
[21] HEKA Elektronik (Ludwigshafen am Rhein, Germany), EPC-8 amplifier with LIH1600 and Patchmaster software
[22] Warner Instruments (Hamden, CT, USA), 64-0102

2.2.4.2 mEPSC analysis

MiniAnalysis[23] was used post-hoc to visualize recorded current traces and identify mEPSCs. Analysis for each cell was performed blind to the treatment condition, and cells within an experimental cohort were analyzed in random order. Approximate mEPSC times were marked manually, and precise times were detected in software based on the fast rise time and peak amplitude criteria. Events with amplitudes less than 5 pA were excluded from analysis. mEPSC event times, amplitudes, charges, decay times, and average waveforms were computed in software. The data was exported to MATLAB and cells were re-sorted into their treatment groups for batch analysis. Normality in all data sets was assessed using a Lilliefors test. Statistical significance between groups was determined using a 1-way analysis of variance followed by t-tests with Bonferroni correction for multiple comparisons. Relationships between drug- and vehicle-treated mEPSC amplitude distributions were determined using simple linear regression, and least squares estimators were used to determine the scaling factor between two distributions. mEPSC amplitude distributions were compared using the Kolmogorov-Smirnov test. Relationships between mEPSC amplitudes and MEA-recorded firing rate data were determined using simple linear regression.

2.3 Results

2.3.1 Network-wide spiking activity persists during AMPAergic transmission blockade

Previous work has shown that chronic blockade of AMPA receptors triggers homeostatic synaptic scaling. It has been hypothesized that CNQX treatment elicits scaling because it indirectly abolishes spiking, and the reduction in spiking activity leads to scaling (Turrigiano et al., 1998; Turrigiano and Nelson, 2000). We tested the hypothe-

---

[23] Synaptosoft (Decatur, GA)

sis that CNQX eliminates spiking activity by continuously recording action potentials from dissociated cortical cultures before and during treatment with CNQX. We found that although CNQX dramatically reduced the firing rate, it did not abolish spiking. During the first three hours after CNQX treatment, MEA-wide firing rate was reduced to 38.7±19.1% of the pre-drug firing rate. There was a slight recovery in firing rate over time, and the overall firing rate was 46.2±4.1 % of pre-treatment firing rate (Fig. 2.5). Notably, treating control cultures with a vehicle caused a slight depression in firing rate, though the effect was not nearly as dramatic as CNQX in terms of magnitude or duration. Examination of the firing rates expressed in different cultures revealed a large variability in the degree to which both vehicle and CNQX affected spiking (Fig. 2.6). However, CNQX invariably reduced spiking for the entire duration in all cultures, while vehicle-treated cultures showed both moderate increases and decreases.

Because we were interested in activity patterns that accompany synaptic scaling, we compared the effects of CNQX with those of chronic TTX treatment, a common perturbation used to trigger scaling in cultured networks. TTX is a voltage-gated sodium channel antagonist, and therefore would be expected to block spiking activity. In contrast to our CNQX results, TTX effectively eliminated spiking (MEA-wide firing rate: 1.1±0.5% of the pre-treatment value), and this effect was sustained for the entire 24-hour treatment. Notably, there was a small fraction of low-amplitude spikes detected during TTX, a phenomenon that has previously been observed (Minerbi et al., 2009). We suspect that they probably reflect a combination of intrinsic noise in the recording system and true biological depolarizations, perhaps due to calcium spiking or TTX-insensitive channels. Such events may be more easily detected as spikes during TTX treatment because the RMS noise (used to determine our spike detection threshold) is low. In addition, there is occasionally higher noise that appears on a single electrode due to a poor contact. While this can cause false spikes to be

a

b
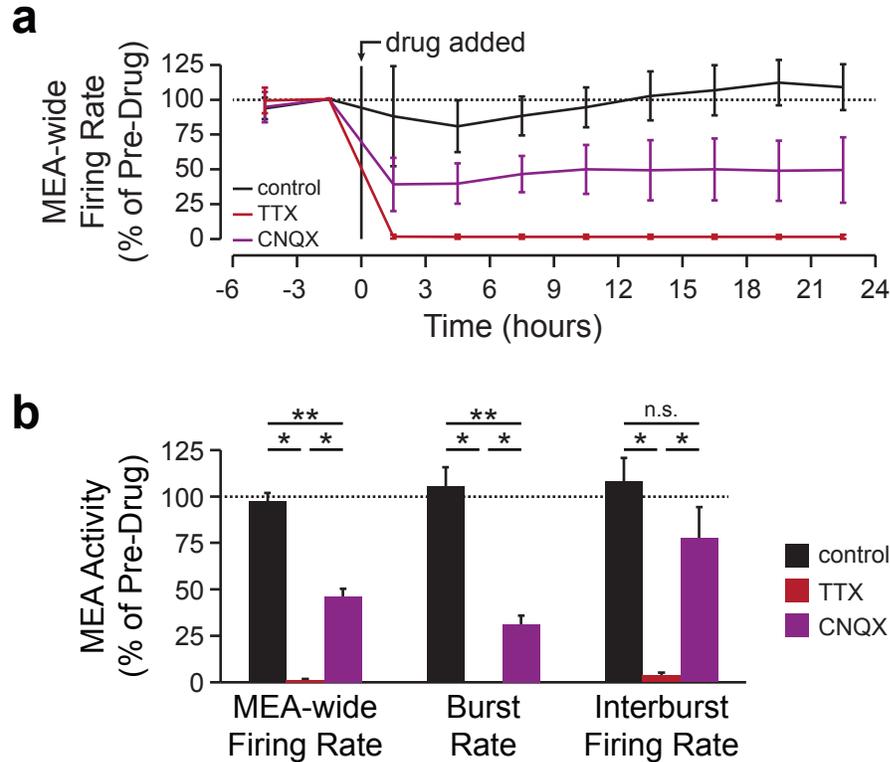
Figure 2.5: Spiking and bursting persist during AMPAergic transmission blockade.
(a) Mean MEA-wide firing rate over time in different conditions (vehicle-treated controls, $n = 12$ cultures; TTX, $n = 8$ cultures; CNQX, $n = 13$ cultures). Values are normalized to firing rate during 3 hour window before drug/vehicle application. Bin size, 3 h. Error bars, s.d. (c) Mean MEA-wide firing rate (control, 97.3±4.6%; TTX, 1.1±0.5%; CNQX, 46.2±4.1%; $p < 10^{-6}$), burst rate (control, 105.8±10.0%; TTX, 0%; CNQX, 31.2±4.8%; $p < 10^{-6}$), and interburst firing rate (control, 108.1±12.7%; TTX, 3.6±1.5%; CNQX, 77.4±16.8%; $p < 10^{-4}$) over the entire 24-hour treatment window, normalized to pre-drug values. Non-significant differences denoted by n.s. Significant differences denoted by $^*p < 10^{-3}$, $^{**}p < 10^{-4}$. Error bars, s.e.m. Averages and statistical significance are summarized in Tables 2.2 and 2.3.

detected, our spike detection threshold is based on an adaptive calculation of RMS noise (Section 2.2.3.1), so any false spikes are only counted for a few seconds. However, these events are rare in the context of a day-long recording and are not unique to TTX treatment. In all treatment conditions, every event detected as a spike was included in our analysis of network-wide activity features unless a recording artifact was time-locked to an identified source.

Although CNQX does not eliminate spiking activity, it is possible that some other feature of network activity is abolished to elicit synaptic scaling. The most obvious
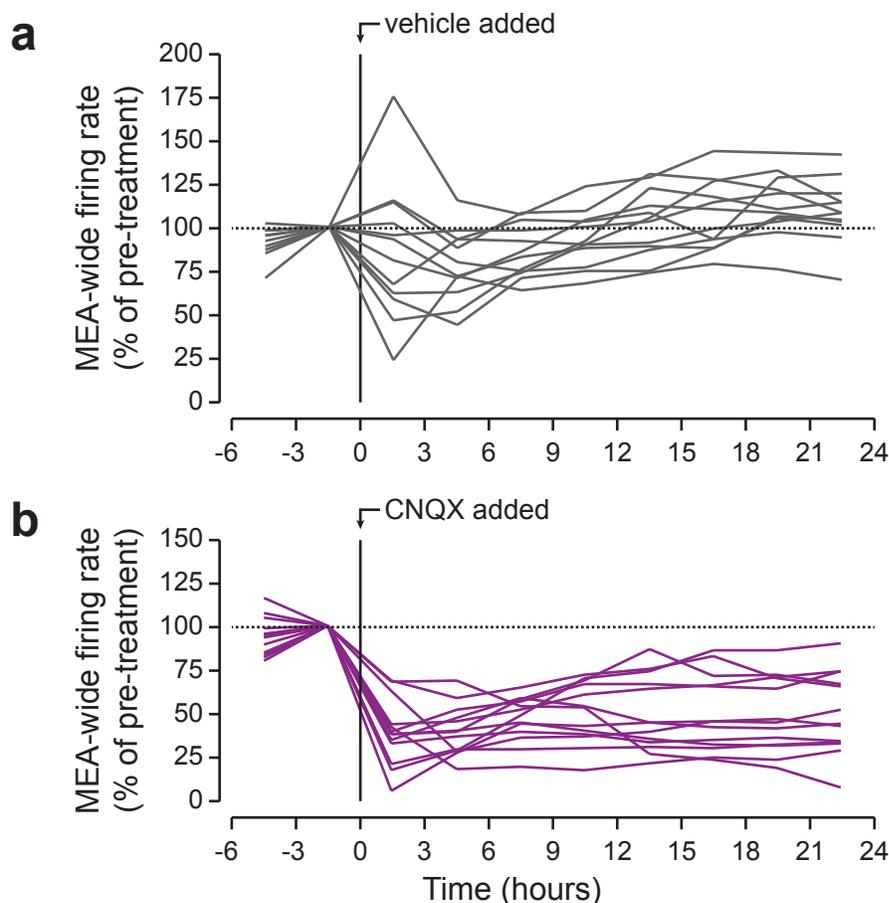
Figure 2.6: Culture-to-culture variability in response to CNQX. (a) Changes in overall firing rate over time for individual vehicle-treated cultures. The greatest variability is present during the first 3 hours. Subsequently, firing rates settle in a similar, albeit wide, range close to 100%. Most cultures show a mild increase in firing rate by the end of the 24-hour vehicle treatment. **(b)** Changes in overall firing rate over time for individual CNQX-treated cultures. CNQX invariability reduces firing rate for the entire 24-hour period. However, there is great variability in the magnitude and trajectories of reductions from culture to culture.

feature of network activity during the second week *in vitro* is synchronized bursting, where hundreds of spikes recorded on each microelectrode are coordinated with hundreds of spikes on other microelectrodes. These bursts typically account for >90% of all spikes, and blockade of ionotropic glutamate receptors eliminates bursting for days (Corner et al., 2002). Because CNQX blocks AMPA receptors, and NMDA receptors are thought to require coincident depolarization to be active, a possibility is that bursting is abolished during CNQX treatment due to a lack of excitatory neurotransmission. However, analysis of bursting revealed that like overall firing rate, bursting
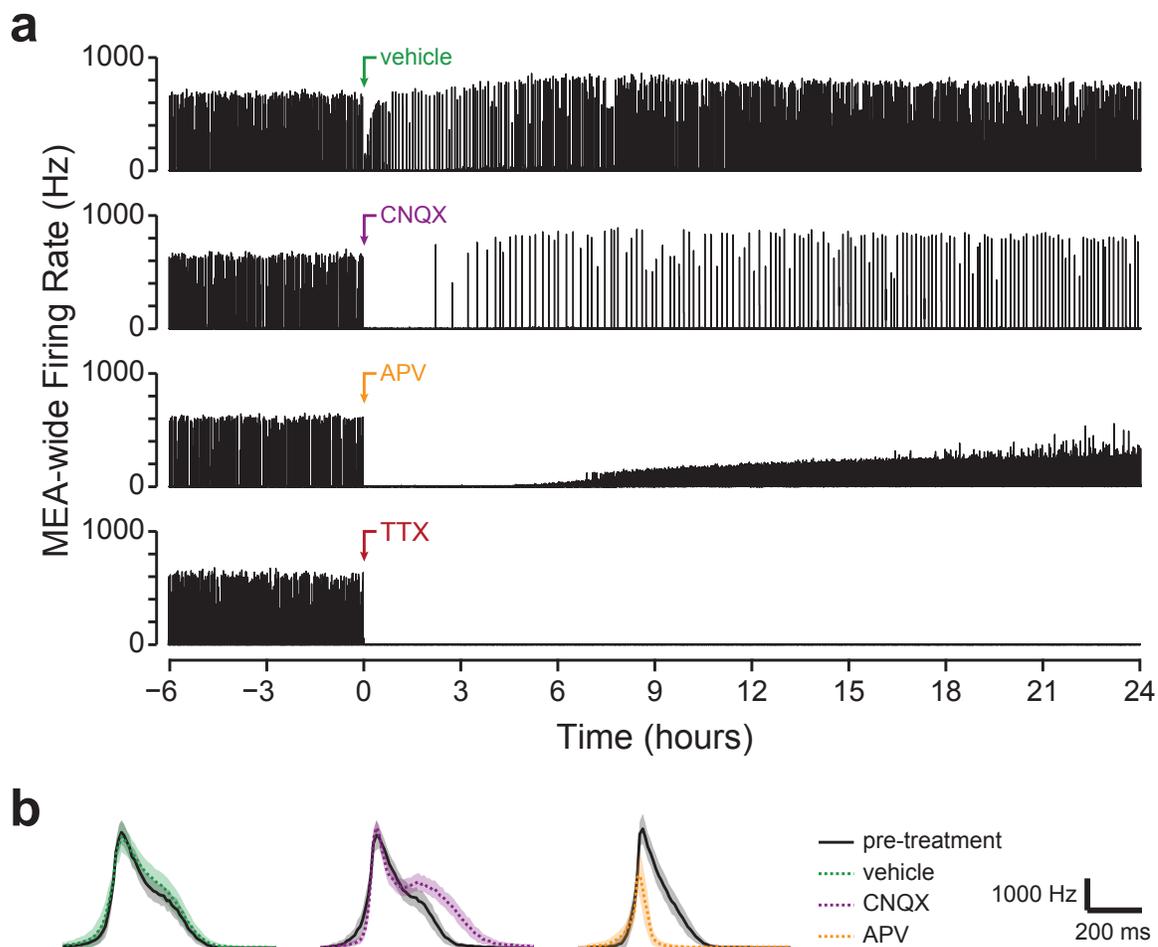
Figure 2.7: Distinct forms of bursting recover during blockade of AMPA-type versus NMDA-type glutamate receptors.(a) MEA-wide firing rate of 4 sister cultures treated with vehicle, CNQX, APV, or TTX. Bursting recovers in both AMPAergic and NMDAergic blockade. When AMPAergic transmission is blocked, burst amplitude recovers (and may overshoot the pre-drug condition), but burst frequency is reduced. When NMDAergic transmission is blocked, burst frequency recovers (and may overshoots the pre-drug condition), but burst amplitude is reduced. TTX eliminates bursting completely. Vehicle induces a slight reduction in burst frequency during the first few hours. Bin size, 1 s. **(b)** Average burst waveform before (black solid lines) and after (colored dotted lines) treatment with vehicle, CNQX, or APV. TTX is excluded because no bursts were detected following treatment. When AMPAergic transmission is blocked, there is a pronounced increase in burst duration. When NMDAergic transmission is blocked, burst duration is significantly reduced. Vehicle does not qualitatively alter burst shape. Shading denotes s.d. Bin size, 10 ms.

Table 2.2: Average network activity features for chronic CNQX or TTX treatments

| | Treatment | | | p-value[†] |
	vehicle	TTX	CNQX	
Sample size				
number of cultures	12	8	13	
Feature				
MEA-wide firing rate	97.3±4.6%	1.1±0.5%	46.2±4.1%	$< 10^{-6}$
Burst rate	105.8±10.0%	0%	31.2±4.8%	$< 10^{-6}$
Interburst firing rate	108.1±12.7%	3.6±1.5%	77.4±16.8%	$< 10^{-4}$

[†]Kruskal-Wallis test, α=0.05

was reduced but not eliminated, during CNQX treatment (Fig. 2.5b). The persistance of bursting in the absence of AMPAergic transmission was somewhat surprising, and we discuss possible mechanisms mediating this recovery in Appendix B.

Interestingly, bursts that occurred during CNQX treatment typically showed a larger number of spikes per burst, suggesting that a homeostatic mechanism might be compensating for the overall loss of spiking. Although the recovery of bursting and synaptic scaling both occur on the timescale of hours to days, the sustained blockade of AMPARs meant that any increase in AMPAergic synaptic strength could not be contributing to increased burst amplitude. We suspect that the augmented bursts may be partially due to compensation in the NMDAergic system. Blocking NMDARs produces a dramatic decrease the number of spikes per burst (Fig. 2.7), suggesting that synaptic transmission through NMDARs may facilitate the late phase of each burst. Therefore, augmented bursts may reflect a compensatory plasticity in the NMDAergic transmitter system that extends bursts to compensate for reduced overall or synchronous activity. In addition, studies in hippocampal cultures have suggested that chronic AMPAR blockade produces an increase in the size of vesicle

Table 2.3: Post-hoc tests: network activity features for chronic CNQX or TTX treatments

Post-Hoc Tests	Significance[†]	p-value
MEA-wide firing rate		
vehicle vs. TTX	$*$	$< 10^{-3}$
vehicle vs. CNQX	$*$	$< 10^{-4}$
TTX vs. CNQX	$*$	$< 10^{-3}$
Burst rate		
vehicle vs. TTX	$*$	$< 10^{-3}$
vehicle vs. CNQX	$*$	$< 10^{-4}$
TTX vs. CNQX	$*$	$< 10^{-3}$
Interburst firing rate		
vehicle vs. TTX	$*$	$< 10^{-3}$
vehicle vs. CNQX	n.s.	0.021
TTX vs. CNQX	$*$	$< 10^{-3}$

[†]Wilcoxon rank-sum test, α=0.017 (Bonferroni adjusted)
$*$ denotes significant differences; n.s. denotes non-significant differences

pools at glutamatergic synapses, so this could also contribute to the increased burst amplitude (Murthy et al., 2001; Thiagarajan et al., 2005).

As compared to pre-treatment rates, CNQX reduced bursting to $31.2 \pm 4.8\%$ ($n = 13$ cultures). In contrast, no bursts were observed during TTX treatment ($n = 8$ cultures). Bursting remained intact in vehicle-treated controls ($105.8 \pm 10.0\%$, $n = 12$ cultures), and all three treatment conditions were significantly different (control, $105.8 \pm 10.0\%$; TTX, 0%; CNQX, $31.2 \pm 4.8\%$; $p < 10^{-6}$).

While the vast majority of spikes occur in bursts, most cells still exhibit endogenous spiking activity that occurs between bursts. To examine whether blockade of AMPAergic transmission might reduce tonic spiking activity, we calculated how firing rate between bursts was affected by CNQX treatment. The interburst firing rate was reduced to $77.4 \pm 16.8\%$ after CNQX application, but this reduction was not signif-

icant. Meanwhile vehicle had little effect on interburst firing rates. Unsurprisingly, TTX eliminated nearly all spiking between bursts ($3.6 \pm 1.5\%$), though again, these remaining spikes may reflect a combination of recording noise and biology. The results of these analyses are summarized in Tables 2.2 and 2.3.

2.3.2 Firing of individual extracellular units persists during AMPAergic blockade

In the previous section, we observed a persistance of $\sim$50% of spiking and bursting activity during CNQX treatment at the network level. However, the distribution of changes in firing rate was non-normal, so it is possible that the $\sim$50% reduction in network-wide firing is not representative of the entire population; rather, spiking might be silenced in a subpopulation of cells during CNQX treatment while another subpopulation of cells might show little change in firing rate. To test this possibility, we sorted spikes into unique extracellular units (which presumably come from different neurons). Using a manual sorting approach, we identified nearly 400 units in a single culture and tracked firing rate before and during CNQX treatment. We found that the vast majority of units initially showed a dramatic reduction in firing rate, but this reduction attenuated over the course of hours (Fig. 2.8). A small fraction of cells showed no change or increased firing during CNQX treatment. However, of the 400 units identified, spiking was not completely eliminated in any of these cells.

We next used an unsupervised spike sorting strategy to identify units across all CNQX-treated cultures. We computed each unit's firing rate normalized to its own pre-treatment firing rate. CNQX application induced a leftward shift in the overall distribution of unit firing rates compared to vehicle (Fig. 2.9a). On average, CNQX reduced firing rates of individual units by $\sim$50%. We arbitrarily labeled units that remained within $\pm$10% of their pre-treatment firing rate as units that showed no change. A unit's firing rate was defined as slower if it fell below 90% of pre-treatment
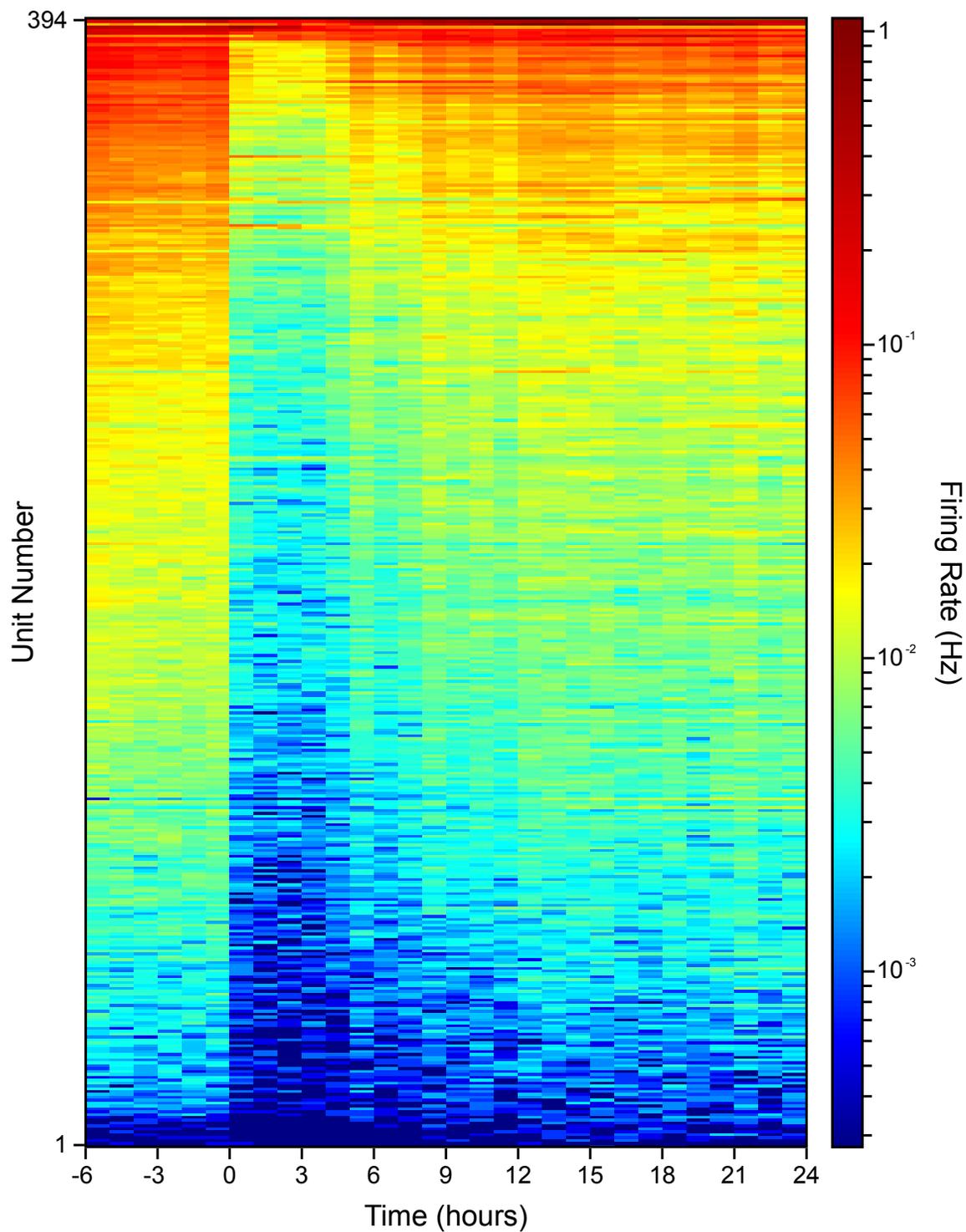
Figure 2.8: Firing rate of individual extracellular units during CNQX treatment in a single culture. Example of hundreds of unit firing rates in a single CNQX-treated culture tracked over time. CNQX was added at 0 hours. Units were sorted manually and are ordered from lowest (1) to highest (394) firing rates.

rates, while any units with firing rates above 110% of pre-treatment rates were considered faster. Using this terminology, ~87% of units showed slower firing rates after CNQX was added. Interestingly, ~8% of units had faster firing rates. These could be the result of disinhibition due to blockade of AMPARs on GABAergic neurons, or compensatory increases in intrinsic excitability in endogenously-active cells. Importantly, all of the 750 units that we sampled continued spiking (albeit, mostly at a slower rate) after CNQX application, suggesting that CNQX does not completely block spiking activity in any cells. These data are summarized in Table 2.4.

We then examined firing rate during 3 hour intervals over the 24-hour treatment, and similar to network-wide firing rate results, there was a dramatic reduction in firing rate during the first 3 hours after treatment (~35% of pre-treatment firing rate). Firing rate recovered slightly and reached ~50% of the pre-treatment firing rate by 6 hours, and remained at this level for the remainder of the treatment period (Fig. 2.9b, Fig. 2.10). Notably, vehicle treatment also reduced the median unit firing rates during the first 3 hours (~80% of pre-vehicle), though this recovered to the pre-treatment distribution thereafter.

2.3.3 Relationship between reductions in spiking and homeostatic changes in synaptic strength

Upward scaling of quantal amplitudes has been observed following chronic AMPA receptor blockade or spiking blockade (Turrigiano et al., 1998). It has been hypothesized that upward scaling of quantal amplitudes is a direct result of reductions in firing rate. We next asked whether there was a difference in the amount of synaptic scaling elicited by complete elimination of spiking (using TTX) versus ~50% reduction (using CNQX). To this end, we treated cultures with either CNQX or TTX for 24 hours, and subsequently assessed synaptic strength using whole-cell voltage clamp recordings of miniature excitatory postsynaptic currents (mEPSCs, Fig. 2.11a-b).

Table 2.4: Firing rates of individual units during 24-hour vehicle or CNQX treatment

Feature	Control	CNQX
Number of units	552[†]	750[§]
Median firing rate (% of pre-treatment)	107.0%	47.4%
Interquartile range (IQR)	51.7%	33.9%
Outliers less than Q1-1.5*IQR	0	0
Outliers greater than Q3+1.5*IQR	3.6% (20)	7.5% (56)
Units that drop below 90% of pre-treatment firing rate	31.0% (171)	87.3% (655)
Units that rise above 110% of pre-treatment firing rate	46.2% (255)	8.4% (63)
Units that stop spiking	0	0
Units that begin spiking	1.4% (8)	0.008% (6)

[†]12 cultures total (five 59-electrode MEAs, seven 9-electrode MEAs)

[§]13 cultures (six 59-electrode MEAs, seven 9-electrode MEAs)
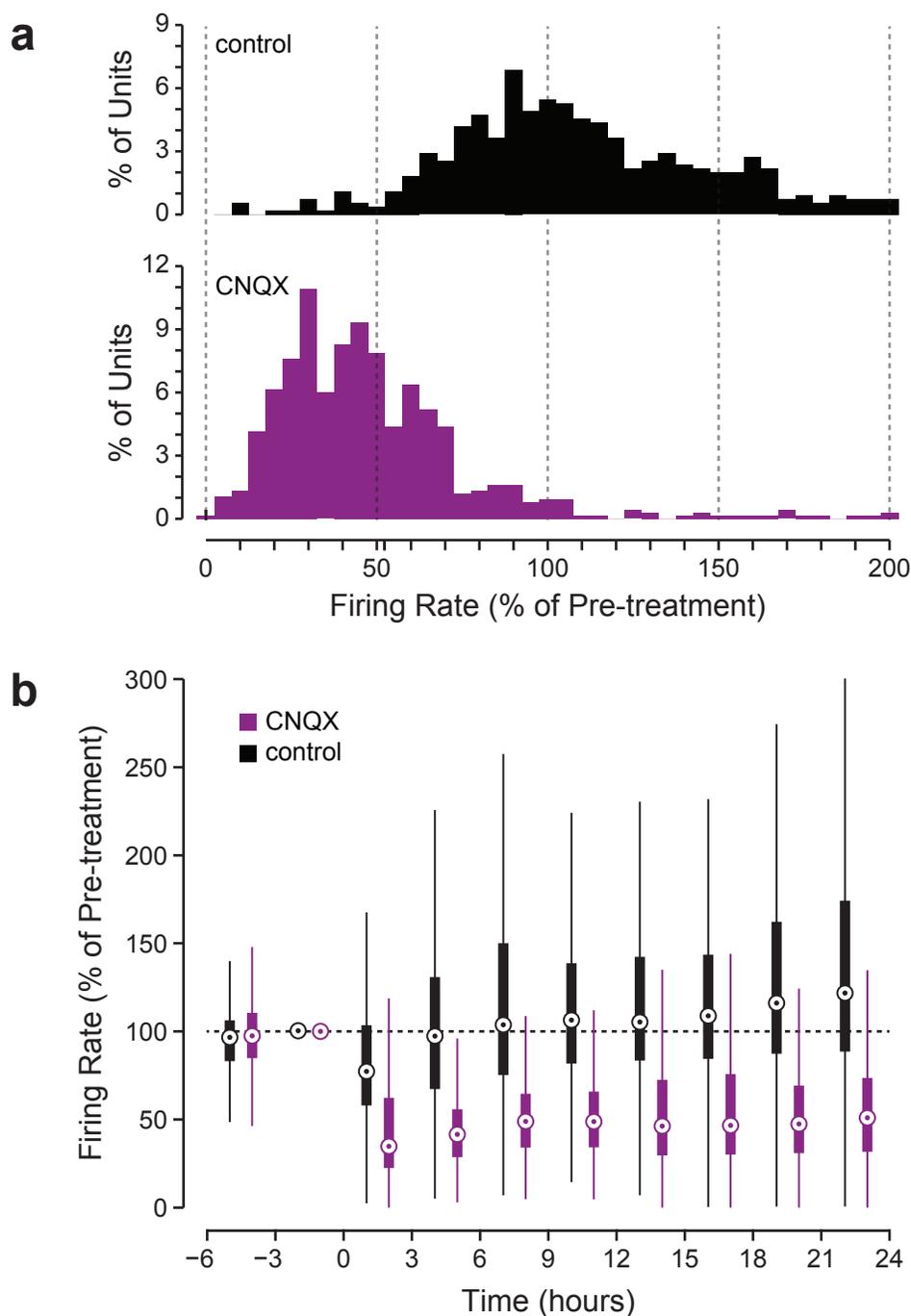
Figure 2.9: Firing rate distributions of CNQX-treated units. **(a)** Histograms showing the changes in firing rate experienced by the entire distribution of vehicle- or CNQX-treated units as a percentage of each unit's pre-treatment firing rate (100% denotes no change). CNQX significantly reduces the distribution of unit firing rates (control, median, 107.02%; $n = 552$ cells from 12 cultures; CNQX, median, 47.37%; $n = 750$ cells from 13 cultures; Wilcoxon rank-sum test, $p < 10^{-112}$; Kolmogorov-Smirnov, $p < 10^{-127}$). Additional features of this distribution are summarized in Table 2.4. **(b)** Median firing rate over time. Thick lines denote the interquartile range and thin lines denote the limits for outliers. Note that all units are normalized to their own pre-treatment firing rate.
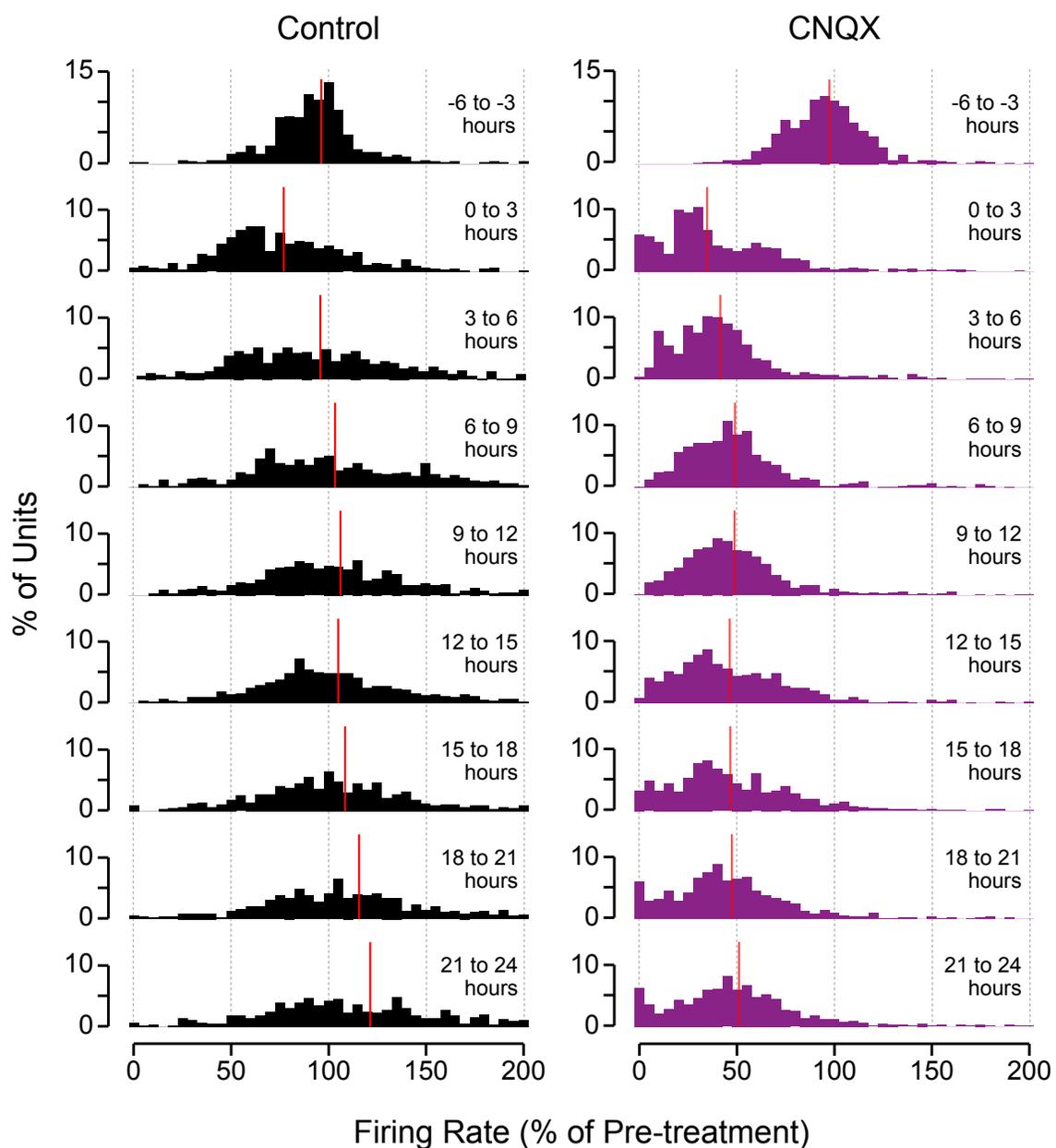
Figure 2.10: Firing rate distributions of CNQX-treated units over time. Distribution of unit firing rates for 3-hour bins before and during vehicle or CNQX treatment. All unit firing rates were normalized to their own firing rates during the pre-treatment (-3 to 0 hours) bin. The red vertical lines denote the median for each distribution. In both cases, treatment elicits a leftward shift in the distribution, though it is much more pronounced in the CNQX condition compared to control. The average vehicle-treated unit recovers pre-treatment firing rates after a few hours, while the average CNQX-treated unit only partially recovers and remains near 50% of pre-treatment firing rates for most of the perturbation. For both conditions, there is a notable broadening of the unit firing rate distributions over time.

Consistent with previous findings, chronic TTX and CNQX treatments both elicited increases in the mean and distribution of mEPSC amplitudes compared to vehicle-treated sister control cultures (Fig. 2.11b, c-d, f-g) without producing changes in mEPSC frequency (Fig. 2.12). The mEPSC amplitude distribution of CNQX-treated cultures was increased over the control distribution by a common multiplicative factor (Fig. 2.11d-e, g-h), consistent with synaptic scaling. However, both TTX and CNQX lead to similar increases in mean mEPSC amplitude (TTX, 146.8±8.0% of control; CNQX, 142.9±4.5% of control), indicating that changes in firing rate might not be a sensitive predictor of how much synaptic strength changes.

We noticed a larger variability in the percent increase in average mEPSC amplitudes between different TTX- and CNQX-treated cultures (∼110-180% of controls). Given that there is also variability in the degree to which CNQX reduces firing rate in each culture (Fig. 2.6), we asked whether changes in firing rate could be used to predict the degree of synaptic scaling on a culture-by-culture basis. For each culture we computed the correlation between the change in network-wide firing rate (over the pre-treatment level) and the change in mEPSC amplitude (over a vehicle-treated sister control). However, there was no correlation in the magnitude of these changes in firing rate versus the increase in mEPSC amplitude (Fig. 2.13a), indicating the change in firing rate was a poor predictor of changes in mEPSC amplitude. We further assessed whether changes in burst rate or interburst rate were correlated to the magnitude of the mEPSC amplitude increase, but again found no relationship (Fig. 2.13b-c). Overall, these results suggest the homeostatic changes in mEPSC amplitude are not adjusted proportionally with overall changes in spiking activity.

2.4 Discussion

In this chapter, we aimed to characterize the changes in firing rate triggered by chronic blockade of AMPAergic transmission and to assess the relationship between these
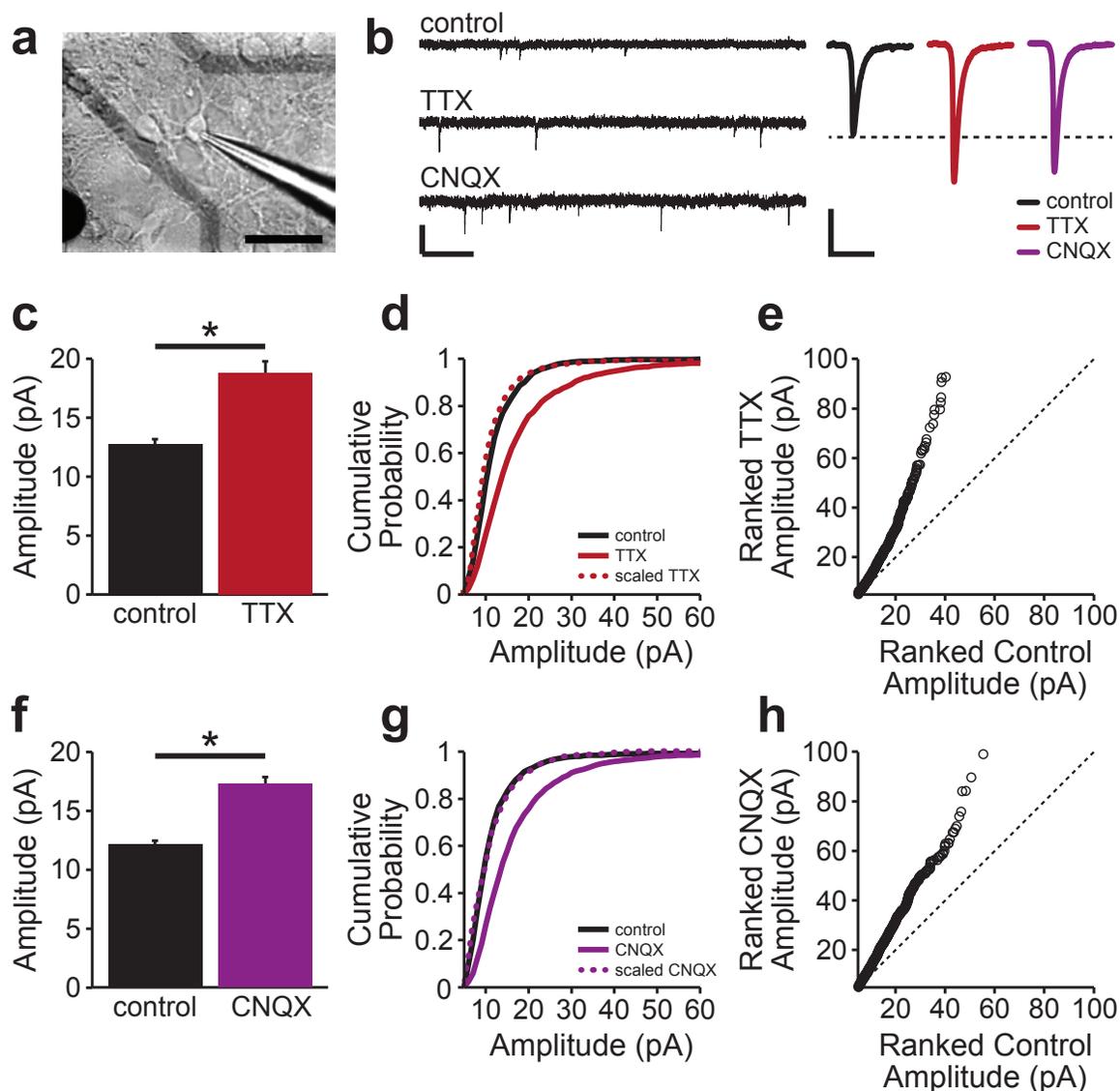
Figure 2.11: TTX and CNQX treatments lead to same degree of synaptic scaling. (a) Pyramidal cell during whole-cell recording. Scale bar, 50 μm. **(b)** Left, sample mEPSC recordings following 24-hour treatment with vehicle, TTX, or CNQX. Scale bars, 25 pA, 200 ms. Right, average mEPSC waveforms. Scale bars, 5 pA, 20 ms. **(c)** Mean mEPSC amplitude from 6 sister culture pairs (control: 12.8$\pm$0.4 pA, $n = 47$ cells; TTX: 18.8$\pm$1.0 pA, $n = 58$ cells; $p < 10^{-5}$). Error bars, s.e.m **(d)** Cumulative distribution of mEPSC amplitudes following TTX or vehicle treatment. The multiplicatively scaled TTX distribution matches control ($p > 0.6$). **(e)** Ranked TTX mEPSC amplitudes plotted against ranked control amplitudes (linear fit, R^2=0.975). Dotted line denotes the line of identity. **(f)** Mean mEPSC amplitude for 10 sister culture pairs (control: 12.1$\pm$0.3 pA, $n = 89$ cells; CNQX, 17.3$\pm$0.5 pA, $n = 94$ cells; $p < 10^{-12}$). **(g)** Cumulative distribution of mEPSC amplitudes following CNQX or vehicle treatment. The multiplicatively scaled CNQX distribution matches control ($p > 0.9$). **(h)** Ranked CNQX mEPSC amplitudes plotted against ranked control amplitudes (linear fit, R^2=0.996)

changes and AMPAergic scaling of quantal amplitude. First, we continuously monitored spiking activity across cultured networks with 30-hour micro-electrode array (MEA) recordings. Contrary to previous predictions where activity was only recorded briefly (Opitz et al., 2002; Wagenaar, 2006), we found that blockade of AMPAergic transmission with CNQX does not abolish spiking and in fact, ~50% of spiking remains. We also showed that while individual extracellular units were differentially affected by CNQX application, there were no units that completely stopped spiking. Finally, we showed that reductions in spiking did not correlate with the magnitude of upscaling. Together, these results complicate the simple hypothesis that reductions in spiking directly lead to corresponding increases in mEPSC amplitude.

Previous reports on the effects of acute AMPAR blockade varied. Modern studies typically claim that acute blockade of AMPA receptors also blocks spiking activity (Turrigiano et al., 1998; Turrigiano and Nelson, 2000), but data to support this claim is not typically shown. Studies that have provided data on the effects of acute AMPAR blockade have been mixed, with some claiming dramatically reduced firing and elimination of synchronous activity (Opitz et al., 2002; Wagenaar, 2006), and others claiming no obvious effect (Kamioka et al., 1996), though in all cases the data presented is still limited to sample traces. In contrast, our survey of 13 cultures and 750 units over 24 hours provides a comprehensive assessment of the range over which AMPAergic blockade may impact both firing and burst rate. During the first 3 hours after treatment we observed great variability in the effects of CNQX on spiking activity, both between cultures (ranging from 4.4 to 68.5% of pre-treatment; Fig. 2.6) and amongst cells (Fig. 2.10). Burst rate was also highly variable during the first 3 hours of CNQX treatment (ranging from 2% to 70.8% of pre-treatment). These broad firing and burst rate distributions could explain some of the disparate reports from previous groups based on single trials or qualitative observations.
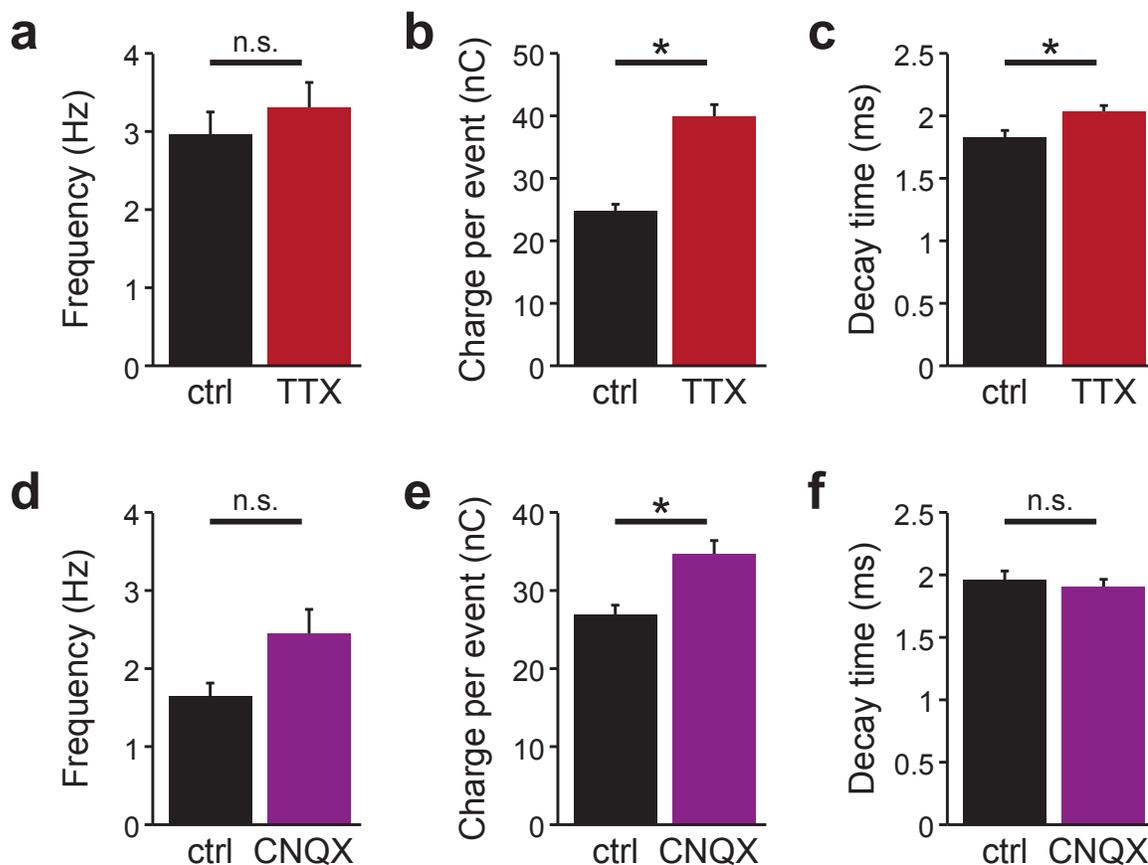
Figure 2.12: Changes in mEPSC features associated with chronic TTX and CNQX treatments. Mean frequency, charge, or decay time for mEPSCs following treatment with TTX (a, b, c) or CNQX (d, e, f) compared to controls. Non-significant differences denoted by n.s. Significant differences denoted by $*p < 0.05$. Error bars, s.e.m.

The variability in spiking activity observed with AMPAR blockade continued for the entire 24-hr treatment. We hypothesized that this variability might be predictive of the homeostatic increase in mEPSC amplitude observed following relief from the treatment. However, we found no correlation between the changes in any obvious feature of spiking activity and the percent increase in mEPSC amplitude. There are several reasons why changes in synaptic strength might be poorly correlated with changes in spiking activity. One possibility is that any reduction in spiking activity beyond a certain threshold triggers the same scaling response. The most mild reduction in spiking activity ($\sim$30% reduction after CNQX) still led to scaling. Another possibility is that postsynaptic spiking is not the activity signal being monitored to
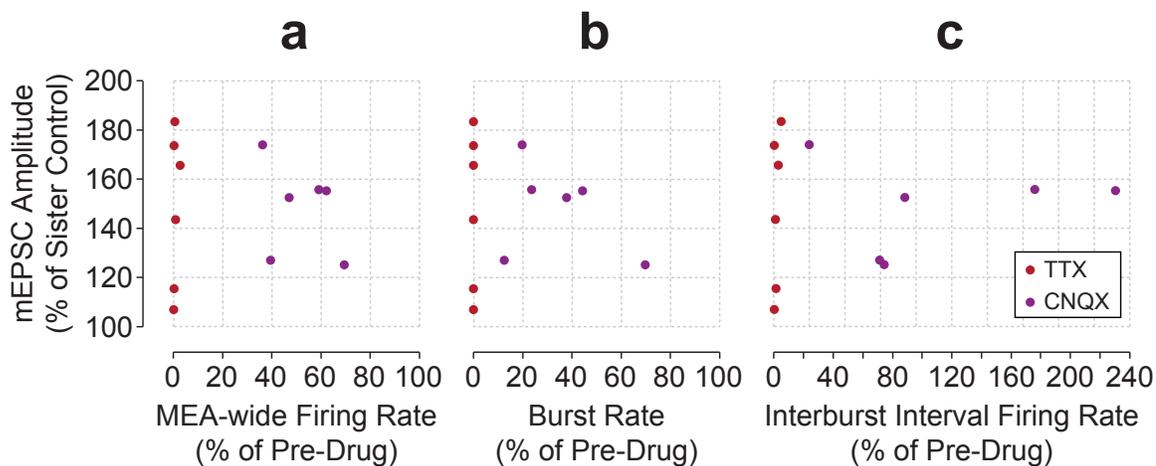
Figure 2.13: No correlation between changes in firing rate and degree of synaptic scaling. (a) Mean mEPSC amplitude for individual cultures plotted against the firing rate they exhibited during TTX or CNQX treatment. mEPSC amplitudes are normalized to corresponding sister control cultures, and MEA-recorded activity is normalized to pre-drug levels (linear fit, r=-0.047). **(b, c)** Mean mEPSC amplitude plotted against burst rate and interburst firing rate (linear fits: burst rate, r=-0.114, interburst firing rate, r=0.044).

trigger scaling, and that reductions in AMPAR activation might directly trigger scaling. These possibilities of a neurotransmission-dependent trigger for scaling will be explored further in Chapters 3 and 4.

Another scenario could be that TTX and CNQX are triggering two different forms of plasticity, both of which lead to scaling. Indeed, there is evidence from other labs suggesting that blockade of spiking versus AMPAergic transmission leads to different homeostatic changes in terms of protein expression (O'Brien et al., 1998; Wilson et al., 2005; Ibata et al., 2008), signaling molecules (Jakawich et al., 2010; Wang et al., 2011), and quantal amplitude (Jakawich et al., 2010). In our analysis, we observed a slight but significant increase in the decay time constant of mEPSCs from TTX-treated, but not CNQX-treated, cultures (Fig. 2.12). This may reflect a difference in subunit composition of AMPARs that have been inserted to mediate the increased mEPSC amplitude observed for both treatment conditions. While most AMPARs in cortical circuits are GluA1/GluA2 heteromers (Lu et al., 2009), several labs have identified a role for GluA1 homomers in the expression of homeostatic

synaptic plasticity (Ju et al., 2004; Thiagarajan et al., 2005; Sutton et al., 2006; Shepherd et al., 2006; Aoto et al., 2008; Hou et al., 2008; Jakawich et al., 2010; Béïque et al., 2011; Garcia-Bereguiain et al., 2013). For example, a 3-hour blockade of AMPAergic transmission was shown to increase mEPSC amplitude via insertion of GluA1, but not GluA2, an effect that was absent for a 3-hour spiking blockade (Jakawich et al., 2010). Another study also found no changes in GluA2 expression after a 3-hour glutamatergic blockade, but did observe increased GluA2 expression after a 3-hour spiking blockade (Ibata et al., 2008). By 48-72 hours, however, both AMPAergic and spiking blockade produce equivalent increases in both GluA1 and GluA2 (O'Brien et al., 1998; Wierenga et al., 2005; Anggono et al., 2011) and no differences in decay kinetics (Turrigiano et al., 1998). Together, these results suggest differential regulation of GluA1 and GluA2 during the first few hours of TTX- versus CNQX-induced scaling, followed by normalization of receptor subunits after a few days. Our study disrupted spiking or AMPAergic transmission for 24 hours, an intermediate time point amongst previous results, which might explain the small but significant difference we see in decay kinetics in mEPSCs from TTX- versus CNQX-treated cultures. This explanation, however, is speculative and would require a careful assessment of AMPAR subunits over time. Notably, TTX-induced synaptic scaling has been observed in cultures from both GluA1 and GluA2 knockout mice (Altimimi and Stellwagen, 2013), arguing against the idea that one subunit is required for scaling. Regardless, the possibility that TTX and CNQX may be triggering scaling in different ways in wildtype cultures might explain why studies that employ different strategies for blocking "activity" could identify different molecules that are "critical" for the expression of scaling.

Regardless of how scaling is triggered, it is clear that there is large variability in the degree of scaling expressed from culture to culture (Fig. 2.13). Admittedly, this could result from a sampling error or experimental limitations, but also could

be a result of variability in factors that mediate induction of scaling. For example, if changes in somatic calcium levels trigger scaling, variability in calcium conductances may contribute to the varied degree of scaling. In addition to variability in the sensors for scaling, there could also be variability in the molecules mediating the expression of scaling. For example, each culture could have an upper limit on the rate of insertion of AMPA receptors, such that further increases in quantal amplitude are not possible during the 24 hour treatment period. Understanding how diversity in the induction and expression mechanisms contribute to the varied degrees of scaling will be important in future studies. Indeed, the realization that multiple expression mechanisms can can produce the same functional output has revolutionized the study of homeostatic plasticity in small neural circuits (Prinz et al., 2004), these principles of variability may even be more pronounced in increasingly complex networks (Marder and Goaillard, 2006).

An unexpected observation was the reduction in network-wide and unit firing rates during the first few hours after vehicle application. Previously, Wagenaar et al. observed that cortical cultures were more likely to fire bursts of action potentials (though with preserved overall firing rates) during the first 5 minutes of recording. This observation was made by opening the incubator door, raising and resetting the culture, and then beginning a recording. The authors attributed this effect to the cultures' sensitivity to movement (Wagenaar et al., 2006b), though it could also be the result of briefly altering the ambient CO_2 content while opening the incubator door (thus altering pH). While we also observed heightened burst frequency during the first few minutes following vehicle treatment, the more overwhelming effect, which has not been previously described, was the reduction in firing rate that lasted for at least an hour. We suspect that the reduced firing rate results from a combination of factors. First, removing the culture from the incubator changes the ambient temperature and CO_2 content during the 30-second period while drug or vehicle is being added and

mixed. In addition, exchanging media changes nutrient content and osmolarity of the surroundings. Finally, mechanical perturbation (both due to moving the culture as in Wagenaar et al., 2006b, and due to pipetting during the mixing process) leads to the dispersion of small molecules that typically reside in a microenvironment near the cells, and disturbance of these molecules might disrupt spiking activity or synaptic transmission. Although we cannot rule out the possibility that vehicle treatment (water or DMSO) contributes to the reduction in spiking activity, we have observed similar reductions in spiking when simply removing the culture from the incubator, gently pipetting culture media up and down once, and returning the culture to the incubator. While it is plausible these various factors could acutely reduce firing rates, the slow rate of recovery of firing rate was surprising. This observation underscores the necessity for vehicle-treated control cultures in any experiments where comparisons are made with pharmacologically manipulated cultures. In addition, this period of reduced activity following vehicle treatment will be an important consideration for electrophysiologists planning experiments that closely follow a medium change or wash. Such effects could be eliminated by employing a perfusion system that provides slow, continuous exchange of culturing medium (Gross and Schwalm, 1994; Blau and Ziegler, 2001; Biffi et al., 2012).

Our observation that spiking recovered during CNQX treatment raised the obvious concern about whether the concentration of CNQX used was sufficient to chronically block AMPAergic transmission. In fact, we began these studies only using 20 μM CNQX as had been previously reported to abolish spiking and trigger scaling in dissociated cortical cultures (Turrigiano et al., 1998). Based on our initial observation that bursting recovered during treatment with 20 μM CNQX, we performed a series of voltage clamp experiments where we progressively stepped the concentration of CNQX from 1 μM to 1 mM (data not shown). We found that a small population of AMPAergic currents still remained in 20 μM CNQX, and we excluded data collected

in 20 μM CNQX from our analyses since AMPAergic transmission was not completely blocked in those experiments. Instead, we chose to use 40 μM CNQX for subsequent experiments as it eliminated AMPAergic currents, and had been shown in other literature to be an effective concentration for reducing action potential firing (Martinoia et al., 2005). To address the concern that CNQX might degrade or be metabolized over the 24-hour period, we pre-treated cultures with CNQX for 24-hours and then did one of three things: (1) replenished the CNQX (which required replacing the media) (Fig. B.1), (2) pipetted the media up an down twice, or (3) mixed in a second treatment. All three approaches produced a slight dip in firing rate for the first few hours (as is typical of vehicle treatment), but then recovered the firing levels observed at the end of the first 24-hour period. In addition, for cultures that had received no 24-hour pre-treatment, we either delivered a fresh treatment of CNQX, or pipetted the removed CNQX-containing medium (from a previous removal) into different cultures. We actually observed a more mild reduction in firing rate for cultures treated with "new" CNQX, but this could be accounted for in the inherent variability between cultures.

An interesting finding from our individual unit analysis is that the firing rate of a 8.4% of neurons showed increased firing rate following CNQX treatment (with 4.3% showing no change beyond $\pm 10\%$ of the pre-treatment firing rate). There are several potential reasons for this increase in firing rate during AMPAergic blockade. First, reduced AMPAergic transmission onto GABAergic cells could lead to reduced firing of inhibitory neurons. This in turn would reduce spike-evoked release of GABA, allowing for disinhibition of postsynaptic targets. Another possibility is that homeostatic mechanisms, such as changes in ionic conductances or presynaptic release, are engaged in a subset of cells in response to overall loss of fast excitatory transmission. Finally, an intriguing possibility is that CNQX might not but a pure antagonist in our cultures. Previous reports have shown CNQX can act as a partial agonist in specific

inhibitory cell populations in the hippocampus (McBain et al., 1992; Maccaferri and Dingledine, 2002), cerebellum (Brickley et al., 2001b; Menuz et al., 2007), and thalamus (Lee et al., 2010). Transmembrane AMPAR regulatory proteins (TARPs) are a family of proteins that facilitate AMPAR trafficking and modulate channel properties, and the partial agonist effects of CNQX have been attributed to the presence of particular TARP subtypes (Menuz et al., 2007; Lee et al., 2010). Because the excitatory effects of CNQX have been isolated to inhibitory cell types (unless a positive AMPAR modulator is co-applied with CNQX, Menuz et al., 2007), and the presumed proportion of inhibitory cells in our cortical cultures are $\sim$10%, it is possible that CNQX may be acting as a partial agonist in inhibitory cells in our cultures to account for the 8.4% of cells that display increased firing rates. Importantly, as a partial agonist, CNQX still blocks glutamate from binding, and glutamate has far greater excitatory actions than a partial agonist. Therefore, it is likely that other mechanisms would need to act in concert with any agonist effects of CNQX in order to raise firing rate above levels where glutamatergic transmission is normal. Alternatively, incorporation of the TARP γ-2 subtype (which is required for the transition of CNQX from an antagonist to an agonist, Menuz et al., 2007) could be a homeostatic effect that contributes to the recovery of spiking and bursting activity during CNQX treatment.

Finally, the persistence of bursting during CNQX treatment was somewhat puzzling. Although presynaptic and intrinsic plasticity mechanisms could facilitate overall increases in release probability and neuronal excitability, the synchronous nature of bursting suggests a network-wide postsynaptic target. Because CNQX blocks both AMPA and kainate receptors, the only remaining ionotropic glutamatergic receptors are NMDARs. It is likely that NMDARs, at least in part, mediate bursting that occurs during CNQX treatment, as concurrent AMPAR and NMDAR blockade eliminates bursting for days (Corner et al., 2002). However, NMDARs are traditionally thought to require concurrent depolarization (to remove the magnesium block) in

addition to ligand-binding in order to be active. Therefore, what could be providing this depolarization? There are several possibilities. First, it is possible that NMDARs from cultures at this age *in vitro* do not require depolarization. Previously, Ben-Ari et al. showed that NMDAR-mediated currents could be produced at membrane potentials as low as -60 mV. Subsequently, Kleckner and Dingledine showed that NMDARs from rats during their second postnatal week showed less sensitivity to magnesium block compared to NMDARs from older or younger animals. Although it is difficult to compare *in vitro* and *in vivo* ages, our use of tissue from E18 rats and experimentation during the second week *in vitro* seems well-aligned to the *in vivo* developmental window of reduced NMDAR depolarization sensitivity. Another possibility is that depolarization could be mediated by GABAergic transmission. While GABA is traditionally thought of as an inhibitory neurotransmitter, it acts as an excitatory transmitter during development and after injury when intracellular chloride levels are high (Ben-Ari et al., 2007; Wenner, 2011). Because second week *in vitro* is still fairly young, and because loss of AMPAergic transmission could trigger compensation in the GABAergic system, it is plausible that $GABA_A$Rs could be mediating excitatory transmission. We explore the possibilities of contributions from the NMDAergic and GABAergic transmitter systems in the recovery of bursting further in Appendix B. Two other possible sources of excitatory drive could be electrical coupling through gap junctions or signaling through metabotropic glutamate receptors (mGluRs). Gap junctions have recently been identified as mediators of local high-frequency oscillations in cortical cultures (Hales et al., 2012), and could potentially mediate other forms of neuronal excitation. Meanwhile, mGluRs, which have also been found in cortical cultures (Janssens and Lesage, 2001), can mediate both slow depolarizations McCormick and von Krosigk (1992) or potentiation of NMDAergic currents (Awad et al., 2000). Further, it was recently shown that a chronic spiking blockade leads to the compensatory shifts in astrocytic mGluR signaling (Xie et al.,

2012). Given the potential for contributions from both chemical and electrical signaling, as well as targets on both neurons and glia, perhaps it is no surprise that bursting can persist in the absence of AMPAergic transmission.

REDUCTIONS IN AMPAERGIC TRANSMISSION DIRECTLY TRIGGER HOMEOSTATIC SYNAPTIC SCALING

Synaptic scaling is a form of homeostatic plasticity characterized by a coordinated increase or decrease in synaptic strength as compensatory response to altered activity. A special feature of synaptic scaling is that the strengths of all synaptic inputs onto a cell are adjusted by a common multiplicative factor. This is particularly important because it ensures that the relative distribution of all synaptic strengths, widely believed to be a substrate for memory, can be preserved during the homeostatic process. Synaptic scaling has been robustly exhibited in many different neural preparations following chronic blockade of spiking. This has led to the hypothesis that a neuron monitors its own firing rate, and reductions in firing rate trigger a coordinated, cell-wide increase in synaptic strength. However, scaling has also been widely observed following chronic blockade of AMPARs, suggesting that reductions in AMPAergic transmission might be the activity signal monitored to trigger scaling. Notably, spiking and AMPAergic transmission are highly correlated within a neural circuit, so identifying their independent contributions to the scaling process is particularly difficult. To overcome this technical challenge, we developed a method for precisely controlling population firing rate in cortical cultures using closed-loop optogenetic stimulation. Using this tool, we restored normal levels and patterns of

spiking during a chronic AMPAR blockade. Finally, we assessed whether synaptic scaling typically elicited by AMPAR blockade was prevented by the restoration of firing rate. We found that restoring spiking activity had no effect on the capacity of cultures to express scaling following a chronic AMPAR blockade. This result demonstrates that reductions in AMPAergic transmission can independently trigger synaptic scaling without changes in firing rate, and suggests that synaptic activity can be directly monitored to induce scaling. Our findings have important implications for other forms of transmission-dependent plasticity, including long-term potentiation, long-term depression, and synapse-specific homeostatic plasticity.

3.1 Introduction

3.1.1 Background

Synapses undergo rapid modifications during learning and development that can cause neural circuits to become unstable (Abbott and Nelson, 2000). Homeostatic plasticity encompasses a set of mechanisms that are thought to stabilize neural circuits by maintaining activity levels within functional bounds. The synapse is a hotbed for the expression of homeostatic plasticity. For instance, chronic blockade of network-wide spiking activity leads to compensatory increases in excitatory synaptic inputs (Turrigiano et al., 1998; O'Brien et al., 1998; Burrone et al., 2002; Gonzalez-Islas and Wenner, 2006; Stellwagen and Malenka, 2006; Keck et al., 2013) and decreases in inhibitory synaptic strength (Kilman et al., 2002; Hartman et al., 2006; Swanwick et al., 2006) onto excitatory pyramidal cells. Conversely, when network activity is chronically elevated, there are compensatory increases in inhibitory synaptic strength (Hartmann et al., 2008; Peng et al., 2010; Rannals and Kapur, 2011) and decreases in excitatory synaptic strength (Turrigiano et al., 1998; Leslie et al., 2001). In many cases, homeostatic changes in synaptic strength occur in a coordinated fashion, where

the weights of all synaptic inputs onto a cell are increased or decreased by a common multiplicative factor. This form of homeostatic synaptic plasticity, called synaptic scaling, has the special property of preserving the distribution of relative synaptic weights, presumably imposed by Hebbian mechanisms and widely believed to underlie memory storage in the brain.

Synaptic scaling has been observed across many reduced preparations, and there is a general consensus that scaling occurs in the living nervous system. However, a subject of greater debate has been what sensor or sensors directly trigger scaling. The most widely-observed form of synaptic scaling has been multiplicative increases in AMPAergic quantal amplitudes following network-wide blockade of spiking activity (Turrigiano et al., 1998; Burrone et al., 2002; Gonzalez-Islas and Wenner, 2006; Stellwagen and Malenka, 2006; Knogler et al., 2010), leading to the hypothesis that neurons sense their own firing rates in order to trigger scaling. Blockade of AMPARs has also produced upward scaling (Turrigiano et al., 1998; Thiagarajan et al., 2002; Knogler et al., 2010; Jakawich et al., 2010), and it has been assumed that this was because blocking AMPAergic transmission would effectively abolish spiking activity. However, we found that blocking AMPARs only reduced spiking by 50%, while blocking voltage-gated sodium channels completely eliminated spiking (Chapter 2). Although there was variability in the degree to which AMPAR blockade reduced spiking activity, this variability was not predictive of the increases in quantal amplitude.

The lack of correlation between reductions in spiking and subsequent increases in quantal amplitude suggests several alternative possibilities. First, it is possible that reductions in spiking trigger scaling, but that there is a threshold either in the induction or expression mechanism. For instance, a threshold in the induction mechanism could mean that any drop in firing rate beyond, say ∼30%, is sufficient to trigger a pre-determined level of scaling. An example of a threshold in the expression mechanism could mean that greater reductions in firing rate do trigger a greater

degree of scaling, the insertion of AMPARs is rate-limited and we cannot see this manifest within a single day.

Another explanation for the lack of correlation between spiking and scaling could be that changes in spiking do not actually produce synaptic scaling. Given that chronic network-wide blockade of AMPARs robustly produces upward synaptic scaling (upscaling), one possibility is that reductions in AMPAergic transmission, rather than reductions in spiking, directly trigger upscaling. However, it has been difficult to distinguish between the isolated effects of spiking and AMPAergic transmission on synaptic scaling. Blockade of AMPAergic transmission using CNQX eliminates depolarization of cells via excitatory currents through AMPARs, and thus decreases postsynaptic spiking. Conversely, blockade of spiking using TTX eliminates evoked neurotransmitter release, and thus reduces the amount of glutamate that can activate AMPARs. Therefore, TTX and CNQX each reduce spiking and AMPAergic transmission, either directly or indirectly. Because of this, identifying the independent effects of reduced spiking versus reduced transmission on the scaling process has proven challenging.

A few studies have circumvented this difficulty by manipulating spiking activity in individual neurons while leaving neurotransmission intact (Burrone et al., 2002; Ibata et al., 2008; Goold and Nicoll, 2010), but have produced mixed results. Burrone et al. found that reducing postsynaptic spiking had no effect on quantal amplitude of incoming synaptic inputs, suggesting that reduced spiking does not trigger upscaling. Subsequently, Ibata et al. found that blocking postsynaptic spiking multiplicatively increased GluA2 expression, suggesting that reduced spiking *does* trigger upscaling. Finally, Goold and Nicoll showed that elevating postsynaptic spiking lead to multiplicative decreases in quantal amplitude, suggesting that elevated spiking triggers downward synaptic scaling. All these studies elegantly separated the effects of spiking from neurotransmission in individual cells, and the different outcomes likely reflect

subtleties in the different strategies for manipulating activity, and the readout for scaling.

There are also studies that have manipulated neurotransmission onto a cells while leaving spiking activity relatively intact (Sutton et al., 2006; Hou et al., 2008; Béïque et al., 2011; Deeg and Aizenman, 2011; Hou et al., 2011). These studies have revealed that synapse-specific compensatory changes in EPSC amplitude or GluA1 accumulation can occur following local perfusion of a receptor antagonist (Sutton et al., 2006), manipulation of presynaptic release (Hou et al., 2008; Béïque et al., 2011; Hou et al., 2011), or alteration of sensory input *in vivo* (Deeg and Aizenman, 2011). These studies suggest that local reductions in neurotransmission trigger homeostatic increases in AMPAergic quantal amplitude, though importantly, synapse-specific increases in GluA2 have not been observed (Ibata et al., 2008). Regardless, synapse-specific forms of homeostatic plasticity do not produce multiplicative changes in quantal amplitude, and thus have been discussed as distinct from cell-wide synaptic scaling (Turrigiano, 2008, 2012; Lee, 2012; Queenan et al., 2012; Lee et al., 2014; but see Rabinowitch and Segev, 2008; Vitureira et al., 2012). Experiments that have identified these synapse-specific forms of homeostatic plasticity all used clever strategies to manipulate synaptic activity without affecting spiking.

To summarize, several studies have examined homeostatic changes in synaptic strength after independently manipulating spiking or neurotransmission. A few studies have manipulated cell-wide spiking while leaving neurotransmission intact (Burrone et al., 2002; Ibata et al., 2008; Goold and Nicoll, 2010), and others have manipulated transmission at specific synaptic inputs while leaving cell-wide spiking intact (Sutton et al., 2006; Hou et al., 2008; Ibata et al., 2008; Béïque et al., 2011; Deeg and Aizenman, 2011; Hou et al., 2011). However, to date, no studies have manipulated cell-wide neurotransmission while leaving spiking intact and subsequently examined the effects on homeostatic synaptic plasticity. The goal of our present study is to fill
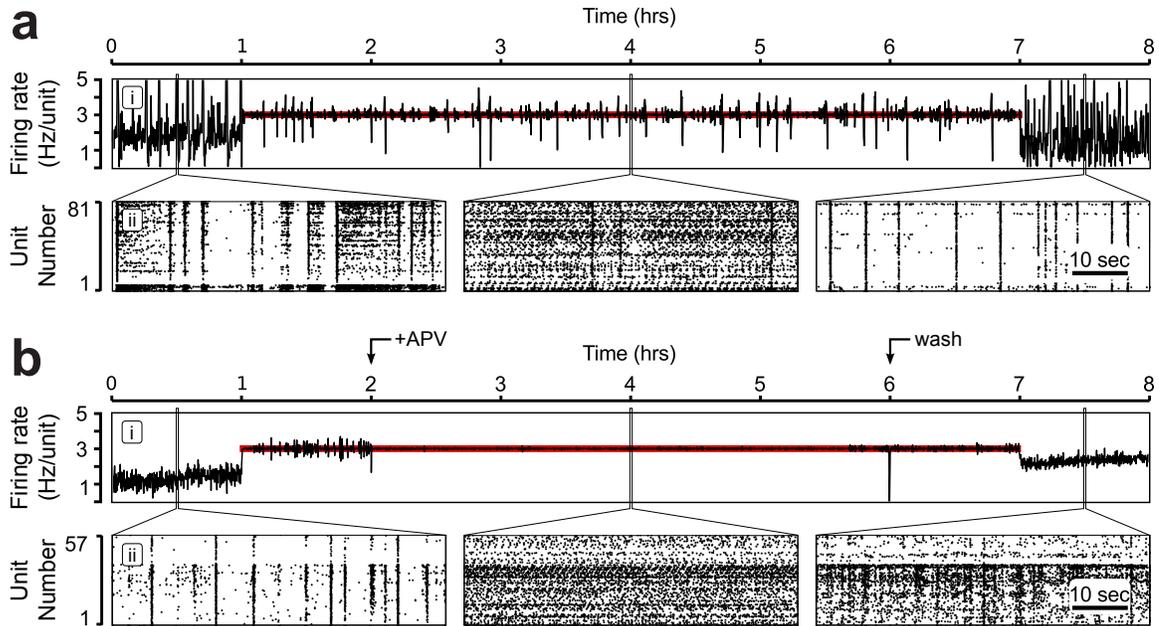
Figure 3.1: Closed-loop electrical stimulation for controlling network firing rate over long timescales. Modified from Newman et al., 2013. A dissociated cortical culture was plated on a micro-electrode array, and distributed closed-loop stimulation was used to clamp neuronal firing rate at an elevated setpoint for 6 hours. The controller was also able to maintain the elevated target rate even when NMDAergic transmission was blocked using APV. **(a)** (i) The neuronal firing rate (black) compared to the target rate (red line). (ii) Zoomed rastergrams showing short time scale network spiking before, during, and after the controller was engaged. **(b)** Same as (a) except that APV was added 1 h after the start of the closed-loop controller and removed 4 h later. This is indicated by the arrows at the top of the figure.

in this gap in knowledge. This presents a considerable technical challenge. How can one globally manipulate transmission without disrupting spiking activity? Because spiking and neurotransmission are highly coupled at the network level, to achieve our goal we must develop a strategy for precisely controlling network-wide spiking activity while concurrently manipulating network-wide neurotransmission. In addition, we must be able to sustain this control of spiking activity for the timescales relevant to synaptic scaling (hours to days). As with the problem of maintaining stability in the nervous system, maintaining spiking activity over long timescales relies critically on feedback control.

3.1.2 Feedback control of neural activity

Perhaps the best-known form of feedback control in modern neuroscience research is voltage clamp. In this case, a feedback circuit is used to compensate for deviations in membrane potential from a user-defined setpoint using intracellular current injections. While voltage clamp uses feedback to control membrane potential of individual cells, the same principles have now been applied to control network-level activity parameters (Potter et al., 2006; Arsiero et al., 2007). For example, network firing rate and spike timing have been precisely controlled in cortical cultures by recording activity using a substrate-integrated MEA, and delivering electrical stimulation contingent on MEA-recorded activity (Wagenaar et al., 2005b; Wallach et al., 2011; Newman et al., 2013). This approach provides a strategy for diverse research questions, including the role of network synchrony in the dynamics of constituent neurons (Wallach and Marom, 2012) or directing the behavior of an embodied neural network (Demarse et al., 2001; Bakkum et al., 2008). A particularly relevant finding to our present study is that closed-loop stimulation can precisely control neuronal firing rates over many hours even during blockade of NMDA-type glutamatergic transmission (Fig. 3.1; Newman et al., 2013). In each of these studies, network-wide activity was "clamped" to a user-defined setpoint using multisite electrical recording to monitor neural activity and multisite electrical stimulation to manipulate activity.

In recent years, optical strategies for monitoring and manipulating activity in neural circuits have emerged as powerful tools in modern neuroscience research (Miesenböck and Kevrekidis, 2005; Fenno et al., 2011; Bernstein and Boyden, 2011; Knöpfel, 2012). Light-sensitive proteins that can be exogenously expressed in neural tissue have been of particular interest because they can be used to monitor or manipulate activity in genetically-defined cell types. The term, optogenetics, refers to the subset of these proteins that, upon activation with a specific wavelength of light, can be used to manipulate cellular activity. The first optogenetic protein that gained

widespread use was channelrhodopsin-2 (ChR2), a light-gated non-specific cation channel derived from green algae (Nagel et al., 2003). When ChR2 was overexpressed in neurons, brief stimulation with blue light allowed for rapid depolarization that was sufficient to trigger action potentials with high fidelity on a millisecond-timescale (Boyden et al., 2005; Li et al., 2005). Further, optical stimulation of ChR2 expressed in the spinal cord (Li et al., 2005) or muscles (Nagel et al., 2005) could direct motor patterns *in vivo*. Since these original experiments using ChR2, newly-identified microbial opsins and their variants have continued to expand the toolset for manipulating neuronal activity. Optogenetic proteins can now be used to depolarize cells, hyperpolarize cells, direct biochemical signaling, or alter gene expression, all with a diversity of options in terms of kinetics, permeant ions, and wavelength of activating light (Fenno et al., 2011; Miesenböck, 2011).

As a strategy for manipulating neural activity, optogenetic stimulation has several distinct advantages over electrical stimulation. Some of these advantages include the elimination of electrical stimulation artifacts, genetic control over cell types receiving stimulation, and the capacity to excite or inhibit cells (instead of just excite). As such, several labs have begun to incorporate optogenetic tools into closed-loop control systems *in vivo*. For example, closed-loop optogenetic stimulation has been used to control sensory input (O'Connor et al., 2013) or motor output (Stirman et al., 2011; Leifer et al., 2011) in healthy animals, or to suppress seizures in epileptic animals (Paz et al., 2013; Krook-Magnuson et al., 2013). While optogenetic feedback control provides an excellent way to study behavior or therapeutic strategies *in vivo*, there has been surprisingly little work using closed-loop optogenetic stimulation *in vitro* to study basic scientific questions.

3.1.3 Chapter summary

In this chapter, we sought to determine the role of reduced AMPAergic neurotransmission, independent of changes in spiking activity, in the induction of homeostatic synaptic scaling. To accomplish this goal, we performed three primary tasks. First, we developed an optogenetic feedback system for controlling network-wide firing rates in dissociated cortical cultures over long timescales. We found that an on-off control architecture provided robust control of firing rates for a range of setpoints over many hours. Secondly, we chronically blocked AMPAergic transmission using CNQX, and used our optogenetic feedback system to restore normal firing rates. We found that our controller easily restored network-wide firing rates to pre-CNQX levels, in addition to preserving burst rate, burst shape, channel-to-channel correlations, and the distribution of individual unit firing rates. Finally, we assessed changes in mEPSC amplitude in cultures following this global reduction of AMPAergic transmission paired with intact network-wide spiking. We found that mEPSC amplitudes from cultures treated with CNQX and closed-loop stimulation were significantly scaled up compared to sister control cultures, but were no different than cultures treated with CNQX alone. These results indicate that reduced AMPAergic transmission can directly induce synaptic scaling, and that changes in spiking are not required for cell-wide scaling. Our findings suggest that synaptic scaling might not function to homeostatically regulate neuronal firing rates, but instead acts to stabilize excitatory synaptic strength.

3.2 Methods

Culturing, MEA electrophysiology, and patch clamp electrophysiology were carried out as described in Section 2.2.
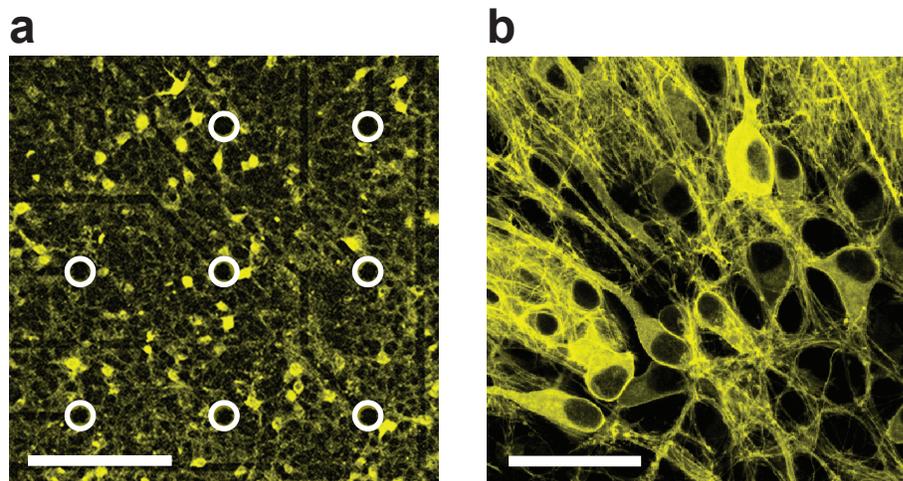
Figure 3.2: Expression of channelrhodopsin-2 in a dissociated cortical culture. A dissociated cortical culture grown on an MEA was infected with AAV9-hSynapsin-ChR2(H134R)-eYFP. Confocal micrographs reveal expression of the eYFP reporter protein at 8 DIV (7 days post-infection), indicative of ChR2 expression. **(a)** Image shows density of ChR2-eYFP-expression relative to micro-electrode positions (circled in white). Scale bar, 200 μm. **(b)** Zoomed image shows ChR2-eYFP expression in somas and processes of neurons. Dark circles at center of each neuron denote nucleus locations, and dark circles between neurons are likely to be be glial cells. Scale bar, 50 μm.

3.2.1 Transfections

The H134R variant of the channelrhodopsin-2 (hChR2) gene was delivered to neurons using an adenoassociated virus (AAV). For most experiments, expression was driven by the human synapsin 1 promoter (hSyn) for neuronal expression, and the AAV9 serotype was used due to its rapid expression time *in vitro*[1]. For some experiments in Section 3.3.1, expression was driven by the calcium-calmodulin-dependent protein kinase IIα promoter (CaMKIIα) for excitatory pyramidal cell expression, and the AAV2 serotype was used. Unless otherwise noted, all data presented in this chapter (including control data) were obtained from cultures infected with the AAV9-hSynapsin-hChR2-eYFP construct[2]. For some early experiments, we used AAV2-CaMKIIα-hChR2-mCherry construct[3], and these instances are noted in the figure captions. We

---

[1] based on correspondence with Dr. Charu Ramakrishnan
[2] University of Pennsylvania Vector Core, AV-9-26973P (Addgene 26973)
[3] University of North Carolina Vector Core, AAV2-CaMKIIα-hChR2-mCherry, (Addgene 26975)

stored all viruses at -80 °C and defrosted them on ice for at least 30 minutes before handling. We added the virus at a genomic titer of 1×10^{13} c.f.u.·mL^{-1} at 1 DIV during the first medium exchange. Solid and liquid waste that came into contact with virus-containing liquids (e.g. from media exchanges) were decontaminated through incubation in 1% sodium hypochlorite for at least 20 minutes. Reusable equipment that came into contact with virus-containing liquids (e.g. MEAs) were decontaminated by autoclaving for 1 hour at 121 °C. Expression of the eYFP reporter protein was verified during the second week *in vitro* using a confocal microscope[4] (Fig. 3.2). All procedures were in compliance with the National Institutes of Health Guidelines for Research Involving Recombinant or Synthetic Nucleic Acid Molecules using a protocol approved by the Georgia Tech Institutional Biosafety Committee.

3.2.2 Chronic treatments

Chronic drug treatments were performed as described in Section 2.2.2, with a few exceptions. First, for proof-of-concept experiments presented in Section 3.3.1, cultures ranged from 10 to 40 DIV. Secondly, experiments in Sections 3.3.2 and 3.3.3 were performed exclusively in triplicate sister cultures, where cultures were treated with either CNQX, CNQX and stimulation (CNQX+stimulation), or vehicle. Finally, for the CNQX+stimulation condition, CNQX was allowed 5 minutes to take effect before beginning a 24-hour closed-loop optical stimulation protocol (Section 3.2.3). Therefore, all treatment periods were extended to 24 hours and 5 minutes, rather than 24 hours alone.

---

[4] Zeiss (Oberkochen, Germany), LSM 700

3.2.3 Optical stimulation

To deliver optical stimuli, we used the Cyclops LED driver[5], a custom current source built around an N-channel enhancement mode MOSFET, to deliver current to blue LED (465±11 nm, full width at half maximum)[6] with high precision. The LED was butt-coupled to a randomized fiber bundle[7], which fed light to a custom Köhler illumination train mounted beneath the MEA amplifier, creating uniformly-distributed illumination in the plane of the culture (Fig. 3.3).

The average network firing rate was calculated every $dt = 10$ ms according to

$$f[t] = \alpha r[t] + (1 - \alpha)f[t - dt] \tag{3.1}$$

where

$$\alpha = \frac{2}{\tau/_{2 \cdot dt} + 1} \tag{3.2}$$

defines a first-order averaging filter with a time constant, $\tau = 2.5$ seconds, and instantaneous firing of $r[t]$ = number of detected spikes/dt. The target rate, f^*, was defined as $f[t]$ over a 3 hour period prior to CNQX application. Five minutes following the application of CNQX to the culturing medium, an error signal was generated between the target and measured firing rate according to

$$e_f[t] = f^* - f[t] \tag{3.3}$$

Finally, an on-off controller was used to determine stimulus application according to

---

[5] Designed by Dr. Jonathan P. Newman
   Hardware and software: https://potterlab.gatech.edu/main/newman/wiki
   Design repository: https://github.com/jonnew/Cyclops-LED-Driver
[6] LEDEngin (San Jose, CA, USA), LZ4-00B200
[7] Schott AG (Mainz, Germany), A21045
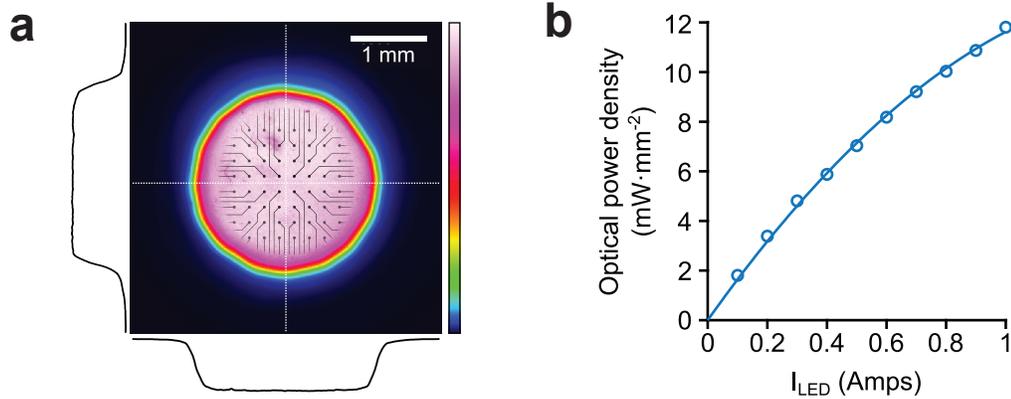
Figure 3.3: Optical light distribution and power. (a) Colormap indicating uniform spatial light intensity profile projected onto the cell layer using a Köhler illuminator. Cross-sectional intensity profiles (black lines) are shown for the horizontal and vertical centers (white dotted lines) of the illuminated region. An image of the MEA is superimposed on the profile to provide an indication of scale. (b) Optical power density as a function of forward diode current for a single 465 nm LED.

$$\text{if } \sum_{k=0}^{t} e_f[k] > 0, \text{apply the 10 ms light pulse.} \tag{3.4}$$

Each stimulus pulse resulted in uniformly distributed 10.1 mW·mm^{-2} light onto the plane of the culture. The rise and fall times of each LED pulse were ∼10 μs. The maximum possible stimulation frequency was set at 10 Hz for early experiments described in Section 3.3.1, and at 2 Hz for concurrent CNQX+stimulation experiments described in Section 3.3.2. A general schematic of the closed-loop optical stimulation system is shown in Fig. 3.4, and a full description and characterization of the system is given in Newman et al., Under review; Newman, 2013.
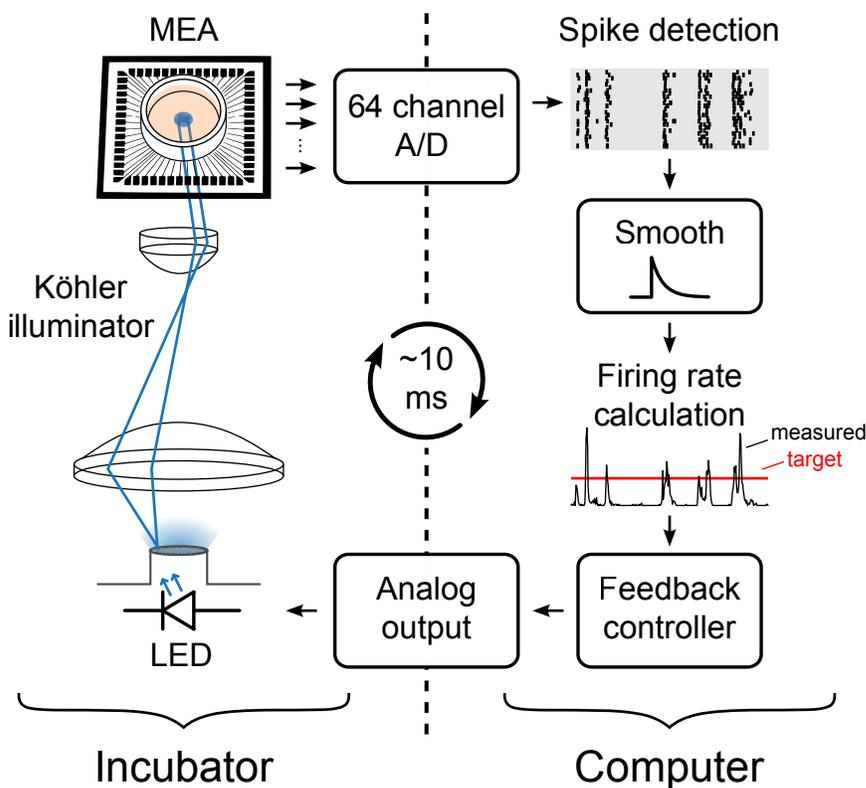
Figure 3.4: Schematic of closed-loop optical stimulation system. Spiking activity is recorded through the MEA. When the integrated error between the target and measured MEA-wide firing rate becomes positive, a 10-ms current pulse is delivered to a blue LED. A Köhler illuminator is used to produce uniformly bright illumination at the cell layer (Fig. 3.3).

3.3 Results

3.3.1 Optogenetic feedback system for controlling firing rates[8]

Our first goal was to develop a closed-loop optogenetic stimulation system for controlling firing rates over long timescales. The following paragraphs describe the steps we took toward achieving this goal. In this section, some experiments were done using cultures transfected with the AAV2-CaMKIIα-hChR2-mCherry, while others

---

[8] The work described in Section 3.3.1 was part of a collaboration with Dr. Jonathan P. Newman. Contributions: J.P.N. created the hardware and software. J.P.N. and M.F. designed experiments, and collected and analyzed the data. J.P.N. created Figs. 3.3, 3.6 and 3.8. J.P.N. and M.F. co-created Fig. 3.4. M.F. created all other figures and tables.
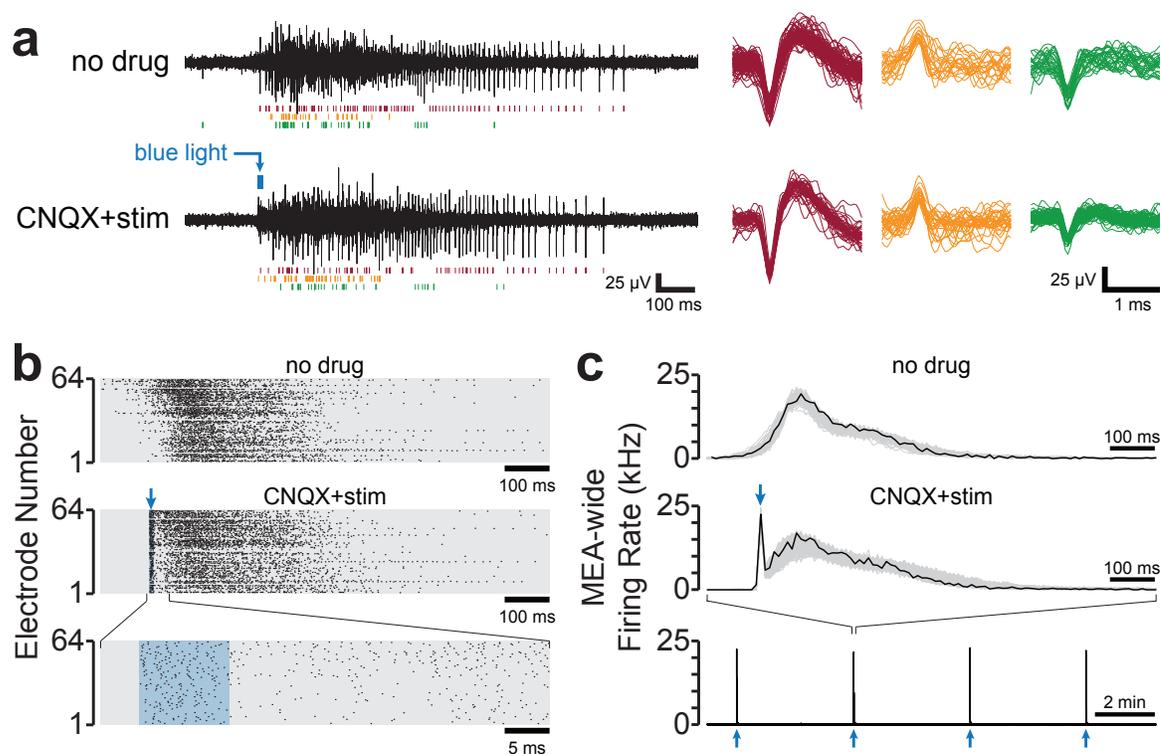
Figure 3.5: Brief pulse of blue light reliably produces spontaneous-like bursts. In this experiment, spontaneous activity was recorded for several hours. Then CNQX was added, and 10-ms pulses of blue light were used to drive bursts every few minutes. **a** *Left*, voltage trace recorded from a single micro-electrode during a spontaneous burst in the absence of any drug (top) and during an optically-evoked burst after addition of CNQX (bottom). The blue arrow denotes the timing of the stimulus, and the width of the blue rectangle indicates the duration of the light pulse (10 ms), which is brief compared to the total burst duration. The rastergrams (colored vertical bars) below each voltage trace denote the spike times of 3 different extracellular units captured on the electrode. The pattern of recruitment of units is qualitatively similar between the two conditions. *Right*, expanded voltage traces showing all spikes detected during burst, separate units are displayed in different colors. Colors correspond to spike times at left. The similarity between the spike waveforms across the two conditions indicate that they are likely from the same neurons. **b** Rastergram showing spike times recorded across all electrodes during a spontaneous burst (top) and an optically-evoked burst after addition of CNQX (middle). The recruitment of spikes across the entire MEA is qualitatively similar between the two conditions. The blue arrow denotes the timing of the light pulse. An expanded rastergram shows spikes occurring at burst onset (bottom) and blue shading denotes when light is on. **c** MEA-wide firing rate computed during the bursts shown in **(b)**, denoted by black lines. Other bursts occurring during the pre-CNQX (top) and CNQX+stimulation (middle) recording sessions are plotted in grey. Zooming out in time (bottom) shows that each stimulus reliably evokes a burst. Blue arrows denote timing of the light pulse. Bin size, 10 ms.

were performed using cultures transfected with AAV9-hSyn-hChR2-eYFP, and this information is specified in individual figure captions.

3.3.1.1 Stimulus selection

Because the eventual purpose of this controller would be to reproduce spontaneous-like activity patterns during CNQX treatment, our first goal was to select a stimulus that met this need. Because the reductions in firing rate that accompany CNQX application were primarily due to reductions in network-wide bursts (Fig. 2.5b), we sought a stimulation strategy that could reinstate bursts even when AMPARs were blocked. We found that a 10-ms pulse of blue light at 10.1 mW·mm^{-2} reliably evoked bursts in ChR2-expressing neurons, even during CNQX treatment (Fig. 3.5). These bursts were characterized by some short-latency spikes that resulted directly from ChR2 activation, followed by a longer-latency barrage of action potentials, which occurred tens to hundreds of milliseconds after the blue light pulse had terminated. These longer-latency barrages closely resembled spontaneously-occurring bursts in terms of time course and profile of network recruitment. Further, units participating in spontaneous bursts also participated in bursts evoked by blue light stimulation during CNQX treatment. Because the late phase of a burst is eliminated during NMDAR blockade (Fig. 2.7), we suspect that the ability for stimulation to produce spontaneous-like bursts relied on intact NMDAergic transmission (discussed further in Section 3.4).

3.3.1.2 Clamping firing rate

We next developed a closed-loop strategy for clamping network-wide spiking activity, and found that an on-off control strategy using the short, high-power stimuli (as described above) could robustly control firing rates over many hours (Newman, 2013; Newman et al., Under review).

These proof-of-concept experiments were performed in cultures of different ages and from different platings, and using MEAs with varying quality in terms of electrode impedances. These factors introduce variability in the total number of active units and thus influence the total MEA-wide firing rate. Thus, we used two strategies for normalizing for these factors in order to make data comparable across cultures. In some instances, the network firing rate was assessed by calculating the average per unit firing rate. This specifically accounts for differences in the total number of units detected, and allows us assess whether the average neuron can spike at a particular setpoint. In other instances, the network firing rate calculation was not normalized to the number of units, but the setpoint was determined as a multiple of the MEA-wide spontaneous firing rate. This has similar benefits in making cultures comparable even if they have different spontaneous firing rates, and has the unique advantage of accounting for the culture's initial state. Both strategies have different strengths, and our closed-loop system accommodates either depending on the experimenter's preference.

To demonstrate that closed-loop optical stimulation could be used to introduce precise levels of spiking into a neural circuit, we first used this controller to maintain network firing rates at different elevated setpoints. Within a single culture, we were able to maintain firing rate at six different setpoints for 12-hour periods (Fig. 3.6a). We set the maximum possible stimulation frequency at 10 Hz. At the most ambitious setpoint the controller saturated at this 10 Hz value, and was considered a control failure. Importantly, the stimulation frequency required to maintain each target firing rate did not always correspond to the setpoint value (Fig. 3.6b-c); some of the mid-range setpoints required more stimulation, and some higher setpoints required less stimulation. This indicates that the culture's state may influence the difficulty of the task and suggests that an open-loop controller would not be able to maintain a target rate under these conditions. Notably, at lower stimulation frequencies, the unimodal
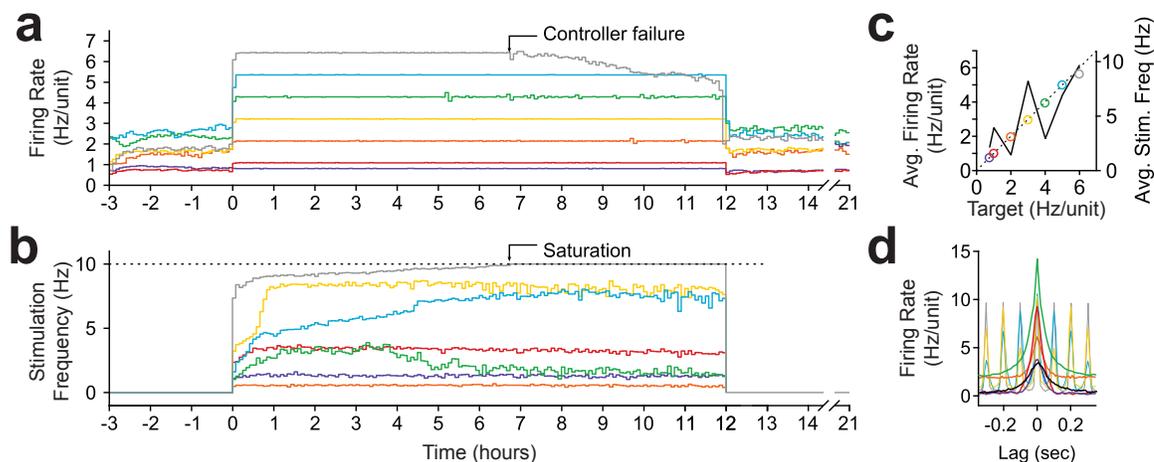
Figure 3.6: Closed-loop optogenetic controller clamps population firing rate for 12 hour epochs at different setpoints. (a) Network firing rate during each control epoch. In these experiments, spikes were sorted online and the network firing rate measurement was based on the MEA-wide firing rate using only units that were active before the clamp began. The firing rate was normalized to the total number of detected units. Colors denote different experiments performed for different target firing rates ranging from 0.75 Hz/unit to 6 Hz/unit. At the highest setpoint, the controller failed. Bin size, 5 min. **(b)** Closed-loop stimulation frequency over the course of the 12-hour clamp. Colors correspond to the different target rates shown in **(a)**. For a target rate of 6 Hz/unit, the controller saturated at the maximal frequency of 10 Hz at around 7 hours into the control epoch, and target tracking failed as a result. **(c)** Time- and unit-averaged ring rates (colors, left axis) and control signal (black, right axis) across each 12-hour clamping period. The dotted line is identity. **(d)**The average cross-correlation function between 30 randomly selected units during on-off control is plotted for each target rate. The correlation function for spontaneous activity is shown in black. When low stimulation frequencies were required, the unimodal correlation structure of spontaneous activity was preserved using on-off control. All data presented in this figure were obtained from a single culture transfected with AAV2-CaMKIIα-hChR2-mCherry. Data was collected over the course of 2 weeks.

cross correlation structure characteristic of spontaneous activity could be reproduced (Fig. 3.6d).

We next attempted to control network-wide firing rates for a 24-hour period, the time course over which we had previously performed AMPAergic blockade experiments and observed scaling. We were able to double the network-wide firing rate for the entire 24 hours (Fig. 3.7a), and this was primarily due to our ability to produce synchronous bursts with each light pulse (Fig. 3.7b). Although firing rate doubled, burst rate increased by almost six-fold, indicating that the number of spikes per burst and/or spiking during the interburst interval had decreased.
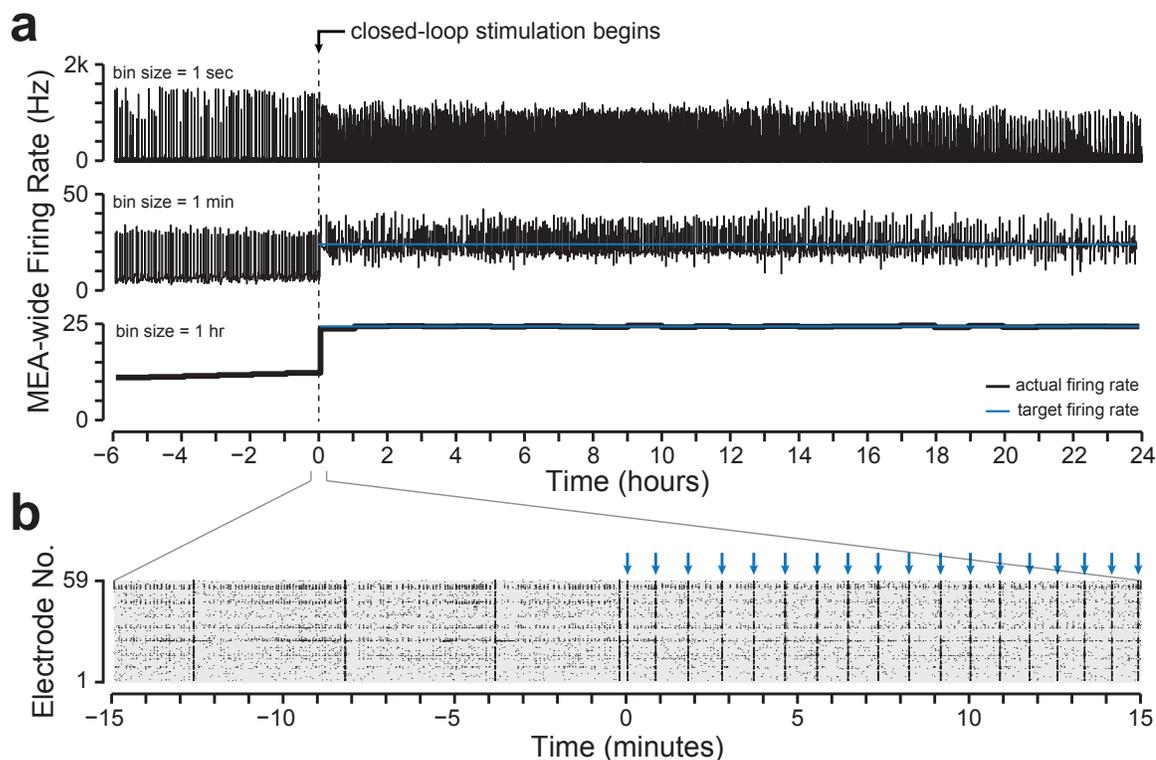
Figure 3.7: Closed-loop optogenetic controller doubles population firing rate for 24 hours (a) MEA-wide firing rates for a culture that had its firing rate doubled for 24 hours. Each plot represents that same data, but at different bin sizes to allow observation of bursting (top) and successful maintenance of the target firing rate (bottom). **(b)** Rastergram showing a half hour of spike data surrounding the onset of closed-loop control. Bursts of activity appear both before and after the clamp epoch begins. Blue arrows denote the times when the controller delivered a 10-ms pulse of blue light. Every pulse of blue light reliably produces a burst.

3.3.1.3 Compensating for glutamatergic blockade

Finally, we used our optogenetic feedback controller to compensate for disruption of excitatory synaptic transmission. Chronic blockade of either AMPAergic or NMDAergic transmission both reduce network firing rates either by changing burst number or structure (Fig. 2.7), and we wanted to assess our controller's capacity to restore normal firing rates during these perturbations. To this end, we applied either CNQX or APV to a culture, in each case using the pre-treatment firing rate as the setpoint for closed-loop control.
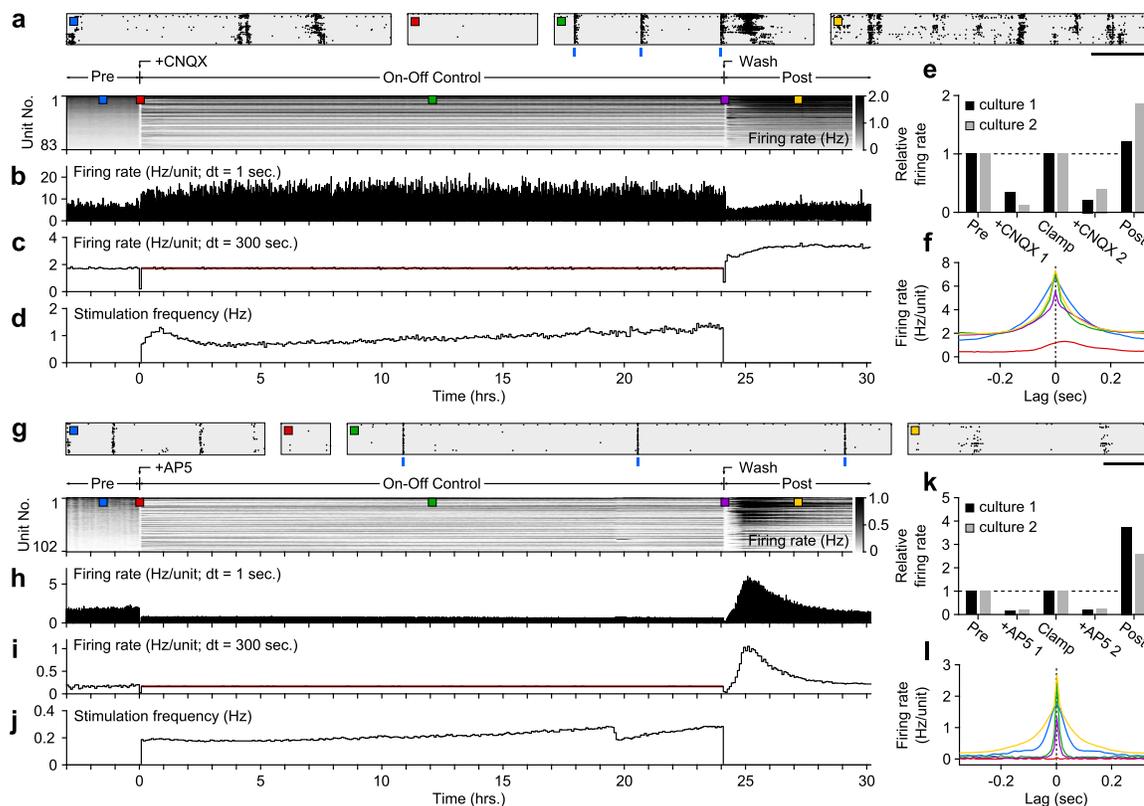
Figure 3.8: Decoupling spiking and glutamatergic neurotransmission. **(a)** Summary of unit spiking activity over the course of the protocol. *Top*, rastergrams show zoomed portions of spiking activity taken from discrete epochs during the experiment. Blue bars indicate stimulus times. Horizontal scale bar, 1 s. *Bottom*, firing rate histogram for the duration of the 33-hour recording for each unit, using 5-minute bins. Firing levels are indicated by the grey-scale to the right. CNQX was added at time 0 and removed 24 hours and 10 minutes later. Closed-loop stimulation began 5 minutes after CNQX addition and lasted 24 hours. Colored boxes indicate the location of the zoomed rastergrams. **(b)** The average unit firing rate using 1-second bins and **(c)** 5-minute bins. The red line indicates the target rate. **(d)** Closed-loop stimulation frequency. **(e)** Time- and unit-averaged firing rates for each epoch, normalized to the pre-drug firing level. **(f)** The average unit-unit cross-correlation function for each epoch (50 units). **(g-l)** Same as **(a-f)** but using APV to perturb network activity instead of CNQX. In these experiments, spikes were sorted online and the network firing rate measurement was based on the MEA-wide firing rate using only units that were active before the clamp began. The firing rate was normalized to the total number of detected units. All data presented in this figure were obtained from cultures transfected with AAV2-CaMKIIα-hChR2-mCherry.

For both AMPAergic and NMDAergic blockade, closed-loop optical stimulation effectively restored pre-treatment firing rates for 24 hours without saturating the controller (Fig. 3.8). Stimulation frequency remained below 2 Hz for the entire duration (Fig. 3.8d). Spiking was restored primarily by optically evoking network-wide bursts (Fig. 3.8a,g). Following the 24-hour treatments, we washed out the CNQX or APV and continued recording spontaneous spiking activity. Interestingly, we found a dramatic increase in overall network firing rate following the washes, suggesting that homeostatic mechanisms had increased network excitability to compensate for the reduced glutamatergic activity, even though firing rates had been restored to normal levels. For CNQX, the post-wash spiking activity was characterized by a moderate but sustained increase in firing and burst rate that lasted for hours (Fig. 3.8a-c,e). Meanwhile, for APV, post-wash spiking was characterized by a dramatic increase that gradually attenuated over the course of a few hours (Fig. 3.8g-i,k). While these data represent only a few examples, they may provide insight into different activity-independent homeostatic mechanisms triggered by loss of AMPAergic versus NMDAergic transmission.

3.3.2 Closed-loop stimulation restores spiking activity during an AMPAergic transmission blockade

The overall goal of our study was to test whether reductions in AMPAergic transmission are sufficient to trigger synaptic scaling even when firing rate is unchanged. Having developed an optogenetic feedback controller capable of compensating for the effects of glutamatergic blockade, we next sought to conduct a carefully controlled set of experiments where we blocked AMPAergic transmission and restored pre-treatment firing rates. To this end, we transfected cultures with AAV9-hSyn-hChR2-eYFP to express ChR2 in neurons. At 10-12 DIV, we recorded spontaneous firing rates for 12-24 hours, and used the final 3 hours to generate a firing rate setpoint. We then added

Table 3.1: Average network activity features for chronic CNQX+stimulation treatment

	Treatment			
	vehicle[†]	CNQX[†]	CNQX+stim	p-value[§]
Sample size				
number of cultures	12	13	5	
Feature				
MEA-wide firing rate	97.3±4.6%	46.2±4.1%	100.2±0.2%	$< 10^{-4}$
Burst rate	105.8±10.0%	31.2±4.8%	97.7±14.3%	$< 10^{-4}$
Interburst firing rate	108.1±12.7%	77.4±16.8%	96.2±11.1%	0.045

[†]reproduced from Table 2.2 from comparison; [§]Kruskal-Wallis test, α=0.05

CNQX to the culture, allowed 5 minutes for the drug to take effect, and then began closed-loop optogenetic stimulation to restore the pre-treatment firing rate setpoint. This protocol was carried out on 5 cultures, and the results are summarized below.

3.3.2.1 Network-wide spiking activity

Closed-loop stimulation effectively restored MEA-wide firing rate to 100% of the pre-CNQX level for the entire 24-hour treatment period (Table 3.1 and Fig. 3.10a). Firing rate did not dip during the first few hours following treatment (as was previously observed in vehicle-treated control cultures), but remained locked at the pre-treatment firing rate. Typically, pulses of stimulation were delivered once every 3 to 5 minutes, and each stimulus invariably produced a network-wide burst. For all cultures, the average stimulation frequency was below 0.008 Hz.

While our optogenetic feedback system was designed to restore MEA-wide firing rate, we wanted to determine how well it could preserve activity features that were not directly controlled. To this end, we first computed the burst rate and interburst firing rate and compared these values to those observed in vehicle- and CNQX-treated cultures in Section 2.3.1. We found that burst rate was significantly elevated above CNQX-treated cultures, and statistically indistinguishable from vehicle-treated con-

Table 3.2: Post-hoc tests: network activity features for chronic CNQX+stimulation treatment

Post-Hoc Tests	Significance[§]	p-value
MEA-wide firing rate		
vehicle vs. CNQX[†]	$*$	$< 10^{-4}$
vehicle vs. CNQX+stim	n.s.	> 0.6
CNQX vs. CNQX+stim	$*$	$< 10^{-3}$
Burst rate		
vehicle vs. CNQX[†]	$*$	$< 10^{-4}$
vehicle vs. CNQX+stim	n.s.	> 0.6
CNQX vs. CNQX+stim	$*$	$< 10^{-3}$
Interburst firing rate		
vehicle vs. CNQX[†]	n.s.	0.021
vehicle vs. CNQX+stim	n.s.	> 0.9
CNQX vs. CNQX+stim	$*$	0.012

[†]reproduced from Table 2.3 for comparison
[§]Wilcoxon rank-sum test, $\alpha=0.017$ (Bonferroni adjusted)
$*$ denotes significant differences; n.s. denotes non-significant differences

trols (Table 3.1 and Fig. 3.10b). Interburst firing rate was also unaffected by the CNQX+stimulation treatment. A summary of average firing rates, burst rates, and interburst firing rates for the three treatment conditions are provided in Tables 3.1 and 3.2.

3.3.2.2 Individual unit firing activity

We next examined firing rates of individual units experiencing concurrent CNQX and closed-loop stimulation. The median unit firing rate was maintained at 103.2% of pre-treatment value, with 36.1% of units firing more slowly and 44.9% of units firing more quickly (Table 3.3). In addition, the distribution of firing rates for CNQX+stimulation units matched the distribution of vehicle-treated, but not CNQX-treated, units (Wilcoxon rank-sum: control vs. CNQX+stimulation, $p > 0.3$; CNQX
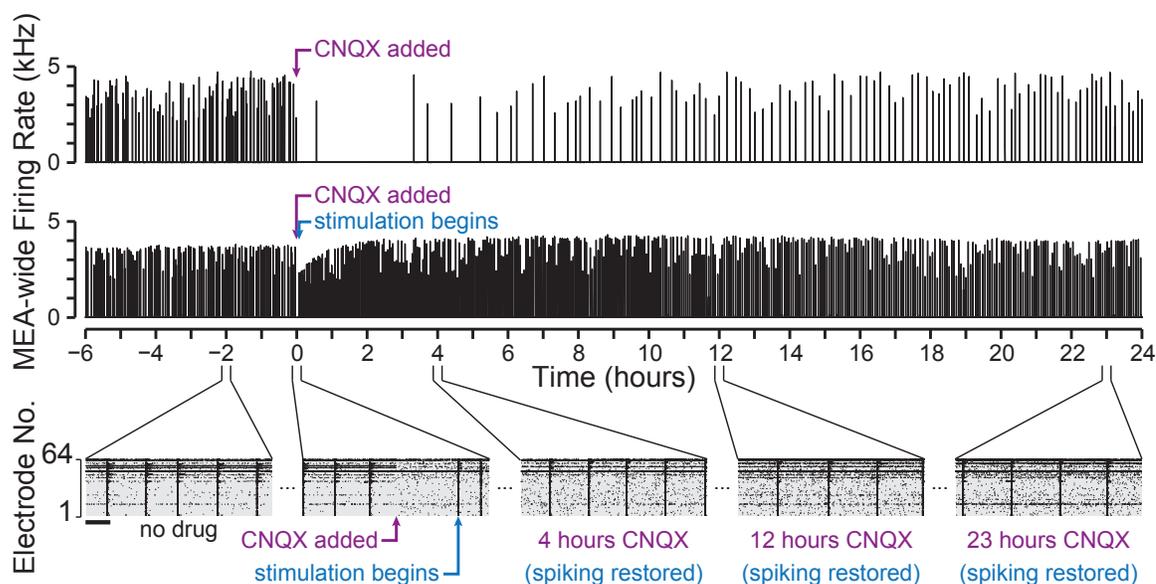
Figure 3.9: Closed-loop optical stimulation restores firing rate throughout chronic AM-PAergic transmission blockade. *Top*, MEA-wide firing rates from an example recording before and during application of CNQX. No stimulation is used. *Middle*, MEA-wide firing rates from a sister culture treated with CNQX, but with pre-CNQX firing rates restored using closed-loop photostimulation. The closed-loop controller begins 5 min after CNQX is added to verify that the drug has taken effect. Bin size, 1 s. *Bottom*, rastergrams show 15-minute segments of spiking activity at different time points throughout the recording. Neurons throughout the culture contribute to restored spiking activity during the entire 24-hour CNQX treatment. Scale bar, 2 min.

vs. CNQX+stimulation, $p < 10^{-106}$; Fig. 3.11a). In addition, there was an overall widening of the distribution of CNQX+stimulation units following the treatment, which closely-resembled the widening distribution previously observed in vehicle-treated controls (Fig. 3.12).

Importantly, there were a few differences between control and CNQX+stimulation distributions. During the initial hours after CNQX was added and stimulation began, there was a slight increase in the median firing rate (Fig. 3.11b). This is in contrast to vehicle-treated control cultures which exhibited a surprising reduction in firing rate during the first 3 hours (median, ∼80% of pre-treatment). Interestingly, there was also a slight reduction in the median CNQX+stimulation unit firing rate over time (Figs. 3.11b and 3.12). One explanation for this gradual decrease could be the emergence of new detectable units that contribute to the overall spike count used by
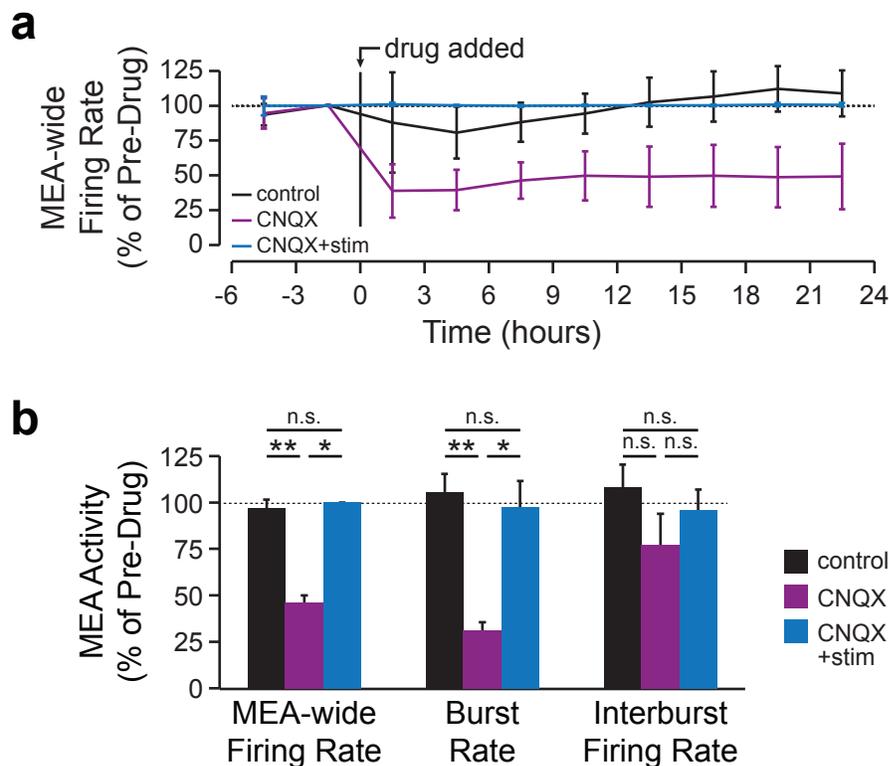
Figure 3.10: Closed-loop optical stimulation restores spiking activity features during chronic AMPAergic transmission blockade. (a) Mean MEA-wide firing rate over time for CNQX-treated cultures with restored spiking ($n = 5$ cultures). Control and CNQX values from Fig. 2.5 are shown for comparison. Closed-loop stimulation effectively locked firing rate to pre-CNQX levels. Bin size, 3 h. Error bars, s.d. **(b)** Mean MEA-wide firing rate, burst rate, and interburst firing rate for CNQX+photostimulation cultures over the 24-hour treatment window, with control and CNQX values from Fig. 2.5 shown for comparison. CNQX-treated cultures with restored spiking showed no differences in MEA activity compared to vehicle-treated controls. Non-significant differences denoted by n.s. Significant differences denoted by $^*p < 10^{-3}$, $^{**}p < 10^{-4}$. Averages and statistical significance are summarized in Tables 3.1 and 3.2. Error bars, s.e.m.

the controller to maintain firing rate. 3.0% of the total detected units emerged following treatment in the CNQX+stimulation condition, compared to 1.4% and 0.008% of units emerging in the vehicle- or CNQX-treated conditions, respectively. Because our control scheme was based on overall firing rate, the emergence of new units contributes to the total firing rate calculation, and these make it so other units can afford to fire at a slightly lower rate. Nonetheless, these differences between the control and CNQX+stimulation distributions were minor compared to differences observed when comparing to CNQX alone. Although our controller was not specifically designed

Table 3.3: Firing rates of individual units during CNQX+stimulation treatment

Feature	Value
Number of units	599[†]
Median firing rate (% of pre-treatment)	103.2%
Interquartile range (IQR)	55.6%
Outliers less than Q1-1.5*IQR	0
Outliers greater than Q3+1.5*IQR	9.0% (54)
Units that drop below 90% of pre-treatment firing rate	36.1% (217)
Units that rise above 110% of pre-treatment firing rate	44.9% (269)
Units that stop spiking	1.0% (6)
Units that being spiking	3.0% (18)

[†]5 cultures total (all plated on 59-electrode MEAs)

to maintain the distribution of unit firing rates, the outcome argues that precisely controlling overall firing rate indirectly maintains unit firing rates.

3.3.2.3 Activity patterns within bursts

The profiles of bursts can be quite diverse from culture-to-culture (Wagenaar et al., 2006b; Madhavan et al., 2007). Although our stimulation strategy effectively reproduced burst rate, we next questioned how closely burst structure matched the pre-treatment condition. As previously mentioned, a single pulse of stimulation generated two epochs of spiking. The first was composed of few spikes on each electrode that were time-locked to the blue light and dissimilar to spontaneous pre-treatment activity (Fig. 3.14b-c). The second epoch was a barrage of spikes, resulting from tens to hundreds of spikes per electrode. This longer-latency epoch was qualitatively similar to spontaneous pre-treatment voltage recordings on individual electrodes (Figs. 3.5 and 3.14a). Further, the CNQX+stimulation condition for each culture was well-
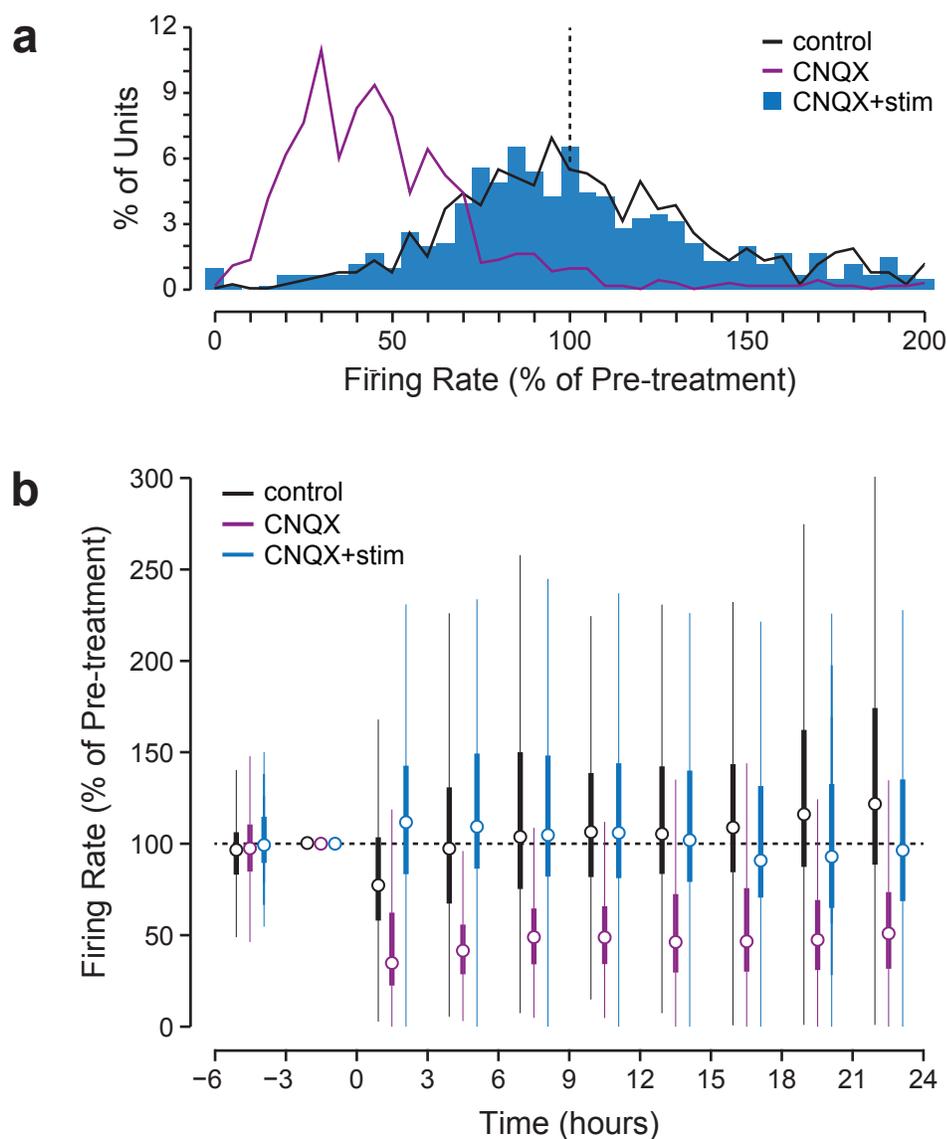
Figure 3.11: Firing rate distributions of CNQX-treated units with restored firing rate
(a) Histogram showing the change in firing rate experienced by the entire distribution of units from the CNQX+stimulation condition. CNQX- and vehicle-treated distributions from Fig. 2.9 are overlaid for comparison. Dotted line denotes no change. CNQX+stimulation maintains the pre-drug distribution of unit firing rates (median, 103.22%; $n = 599$ cells from 5 cultures). The CNQX+stimulation distribution is statistically indistinguishable from control (Wilcoxon rank-sum test, $p = 0.37$; Kolmogorov-Smirnov, $p = 0.22$), but significantly elevated above CNQX alone (Wilcoxon rank-sum test, $p < 10^{-106}$; Kolmogorov-Smirnov, $p < 10^{-126}$). Additional features of this distribution are summarized in Table 3.3. (b) Median firing rate over time. Thick lines denote the interquartile range and thin lines denote the limits for outliers. Note that all units are normalized to their own pre-treatment firing rate.
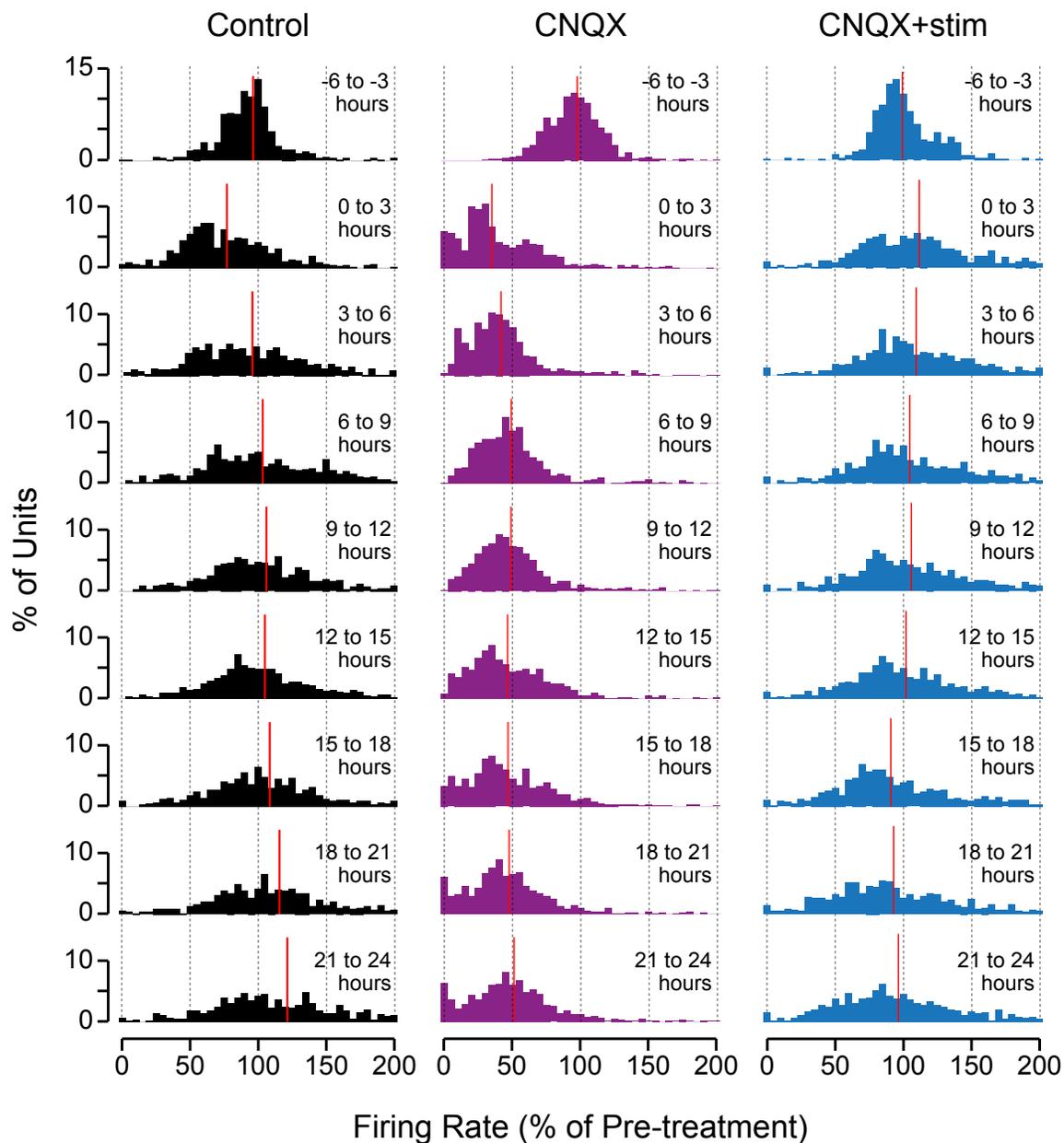
Figure 3.12: Firing rate distributions of CNQX-treated units with restored firing rate over time. Distribution of unit firing rates for 3-hour bins before and during CNQX+stimulation treatment. All unit firing rates were normalized to their own firing rates during the pre-treatment (-3 to 0 hours) bin. The red vertical lines denote the median. CNQX- and vehicle-treated distributions from Fig. 2.10 are overlaid for comparison. Initially, CNQX+stimulation elicits a slight rightward shift in the distribution, but over time the distribution broadens and there is a slight leftward shift.
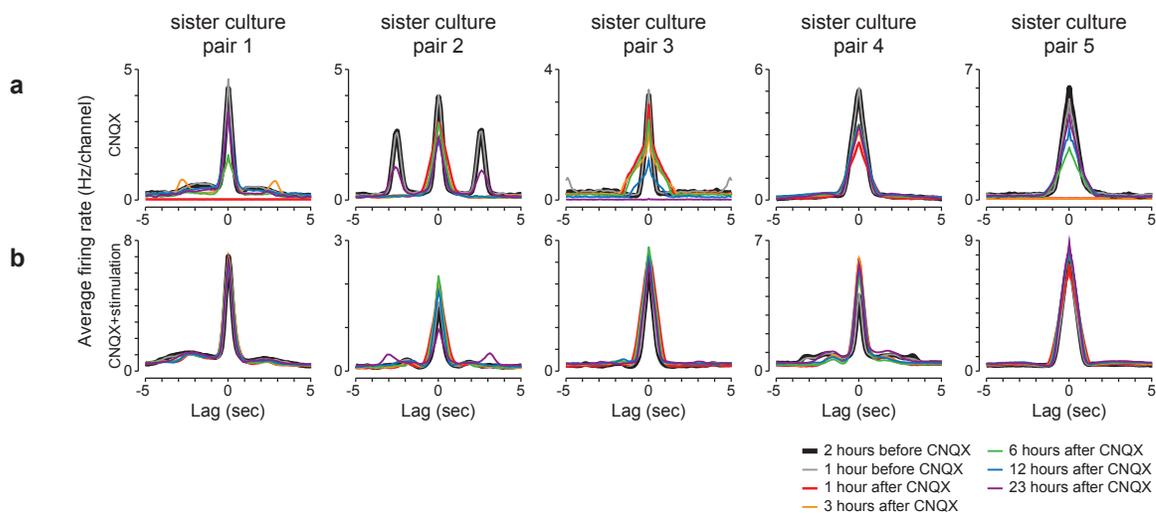
Figure 3.13: Closed-loop optogenetic stimulation during CNQX treatment reproduces channel-to-channel firing correlations. **(a)** Spike detection rate (bin size, 10 ms) cross-correlation was computed for each pair of channels, and averaged across all pairs, for five CNQX-treated cultures (no stimulation). This analysis was performed at several time points before and after CNQX was added, denoted by different colored lines. Spiking across channels became less correlated during first few hours after CNQX application, though spiking correlations generally increased over the 24-hour treatment. **(b)** Same as **(a)**, but for CNQX-treated cultures experiencing optically-restored spiking levels. Closed-loop stimulation maintained pre-drug channel-to-channel firing correlations immediately after CNQX treatment, and this effect was sustained over 24 hours.

matched to its own pre-treatment spontaneous bursting activity in terms of the pattern of recruitment (Fig. 3.14b) and and overall burst profile (Fig. 3.14c). In fact, spontaneous bursts (no drug) had profiles that, qualitatively, appeared more similar to stimulation-evoked bursts within the same cultures than to spontaneous bursts from other cultures (Fig. 3.14c).

To quantitatively assess the degree to which stimulation restored synchronized bursting, we computed firing cross-correlations between different channels at several time points before and during CNQX treatment. In most cultures, CNQX induced a significant reduction in the average channel-to-channel firing correlations, but recovered over time as bursting began to re-emerge in each culture (Fig. 3.13a). In sister cultures that were treated with both CNQX and closed-loop stimulation, there was no such drop in the channel-to-channel correlations.
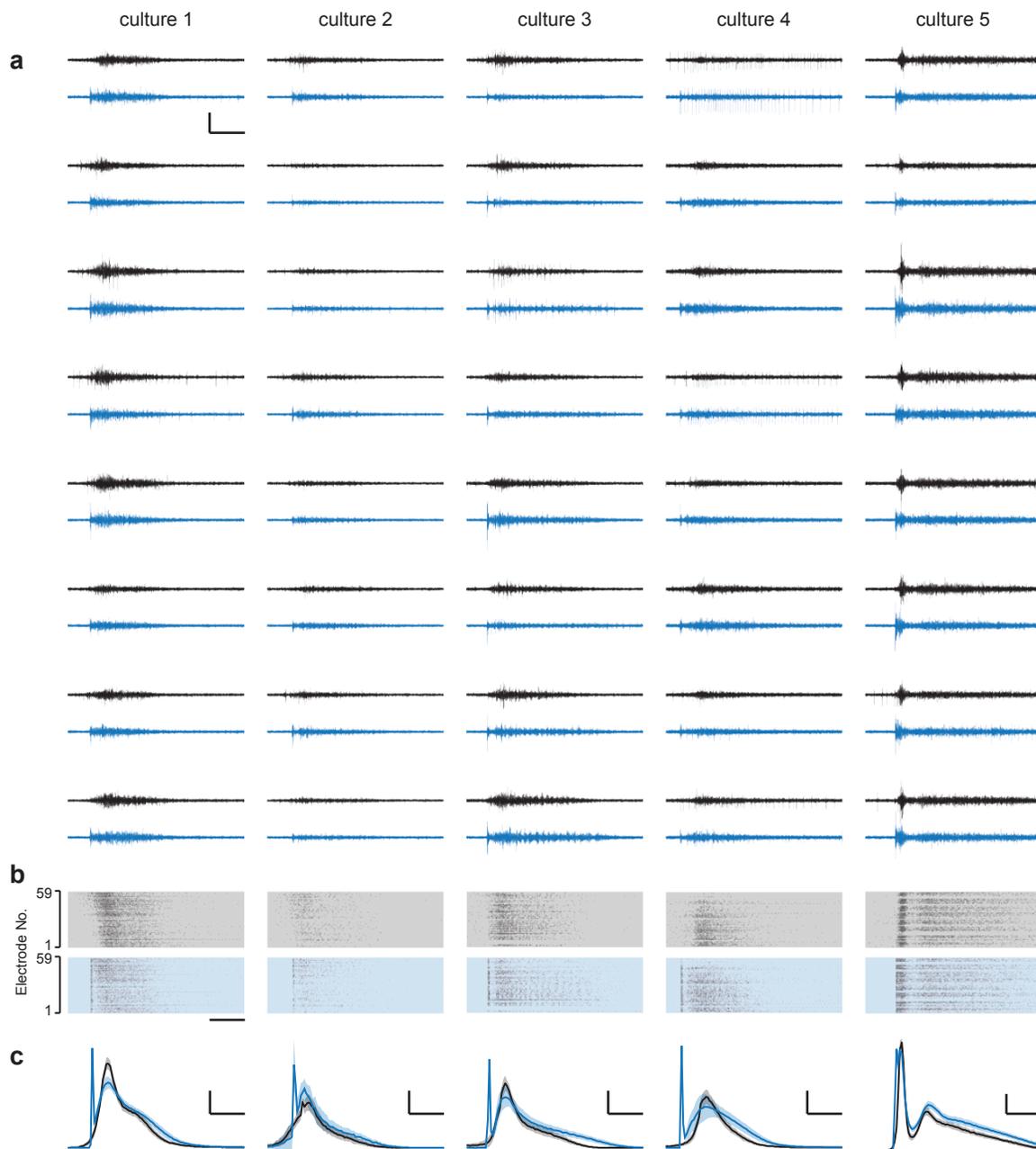
Figure 3.14: Optogenetic stimulation during CNQX treatment effectively mimics spontaneous bursts within individual cultures. **(a)** Raw voltage traces showing spiking activity on individual electrodes during a spontaneous burst before adding CNQX (black), or an optically-evoked burst after the addition of CNQX (blue). Data is shown from all 5 chronically-photostimulated cultures, and the 8 electrodes that were most active during the pre-drug period were selected for display. Scale bars, 100 μV, 200 ms. **(b)** Rastergrams showing spike times for all MEA electrodes corresponding to the bursts shown in (a). Grey background denotes spontaneous data, and blue background denotes condition with CNQX during an optically-evoked burst. Scale bar, 200 ms. **(c)** Average MEA-wide firing rate during a burst (spontaneously-occurring, black, 6 hours of burst data; optically-evoked during CNQX, blue, 24 hours of burst data). Shaded regions denote s.d. Bin size, 10 ms. Scale bars, 5 kHz (cultures 1, 3, 4, 5), 2 kHz (culture 2), 200 ms (all).

3.3.2.4 Summary

Closed-loop optogenetic stimulation restored many features of network-wide spiking activity. First, the controller perfectly restored pre-treatment firing rates in all cultures during CNQX treatment, as it was designed to do, maintaining low stimulation frequencies throughout the clamp. In addition, optogenetic feedback indirectly reproduced several other features of spiking activity including burst rate, burst shape, unit firing rates, and spiking correlations. Together, these experiments and analysis indicate that we have achieved our goal of reducing AMPAergic transmission while leaving spiking activity intact. This allowed us to next test the importance of AMPAergic transmission versus spiking in homeostatic synaptic scaling.

3.3.3 Reductions in AMPAergic transmission are sufficient to trigger synaptic scaling

Having reproduced pre-treatment spiking during an AMPAergic transmission blockade, we next examined whether this restored spiking activity would prevent upward synaptic scaling that typically follows chronic CNQX treatment. To this end, we performed a set of controlled experiments in triplicate sister cultures:

1. **Control**: vehicle-treated control cultures experiencing normal AMPAergic transmission and normal spiking activity

2. **CNQX**: CNQX-treated cultures experiencing blocked AMPAergic transmission and thus a $\sim$50% reduction in spiking

3. **CNQX+stimulation**: photostimulated CNQX-treated cultures experiencing blocked AMPAergic transmission but 100% restored spiking activity (described in Section 3.3.2)

All cultures were transfected with AAV9-hSyn-hChR2-eYFP, regardless of whether they were to be stimulated. We monitored spiking activity in cultures using
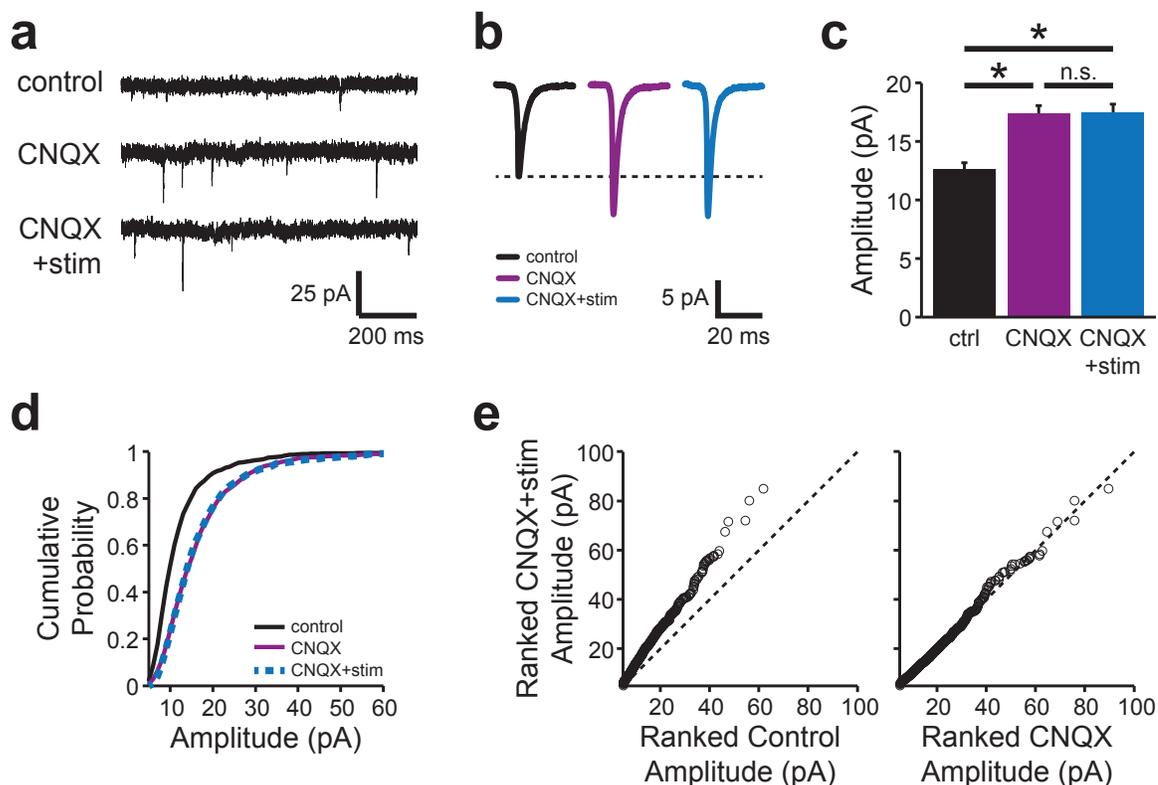
Figure 3.15: Reduced AMPAergic transmission directly triggers upward synaptic scaling. **(a)** Sample mEPSC recordings following 24-hour treatment with vehicle, CNQX, or CNQX+photostimulation. Scale bars, 25 pA, 200 ms. **(b)** Average mEPSC waveforms. Scale bars, 5 pA, 20 ms. **(c)** Mean mEPSC amplitude for 5 sister culture pairs from the 3 treatment conditions (control: 12.6±0.6 pA, n=44 cells; CNQX: 17.4±0.7 pA, n=51 cells; CNQX+photostimulation: 17.4±0.8 pA, n=46 cells; $p < 10^{-6}$). Non-significant differences denoted by n.s. Significant differences denoted by $^*p < 10^{-5}$. Error bars, s.e.m. **(d)** Cumulative distribution of mEPSC amplitudes following the 3 treatment conditions. Multiplicatively scaled CNQX and CNQX+photostimulation distributions matched control ($p > 0.9$ for both, Suppl. Fig. 5a), and there was no difference between the CNQX and CNQX+photostimulation distributions ($p > 0.9$). **(e)** Ranked CNQX+photostimulation mEPSC amplitudes plotted against ranked control or CNQX amplitudes (linear fits, $R^2 = 0.998$ and $R^2 = 0.995$, respectively). Dotted line denotes the line of identity.

MEA recording, in some cases used closed-loop optogenetic stimulation to control firing rate, and subsequently measured mEPSCs from all cultures using whole-cell recordings.

Consistent with previous results (Fig. 2.11), we observed that mEPSC amplitudes from cultures treated with CNQX only were increased compared to sister control cultures (Fig. 3.15a-c). Interestingly, we found that mEPSC amplitudes from CNQX-treated cultures experiencing restored spiking were also increased above controls, and

were no different than CNQX alone (adjusted t-test, $p > 0.9$). In fact, the distribution of mEPSC amplitudes from photostimulated CNQX-treated cultures was statistically indistinguishable from CNQX-treated cultures experiencing reduced activity (Fig. 3.15d-e; Kolmogorov-Smirnov, $p > 0.9$). Consistent with the increases in mEPSC amplitude representing cell-wide synaptic scaling, both distributions were increased over the control distribution by a common multiplicative factor. As expected, charge per event was increased for both CNQX-treated distributions, and there was no change in decay time. Interestingly, mEPSC frequency of the photostimulated CNQX-treated cells was increased over control values (Bonferroni adjusted t-test, $p = 0.002$; Fig. 3.16b).

Overall, these results show that restoring spiking activity had no effect on the capacity for CNQX to trigger synaptic scaling. This demonstrates that reductions in spiking are not required to trigger upward synaptic scaling. Instead, reduced AMPAergic transmission can directly and independently trigger upscaling even when spiking is restored.

3.4 Discussion

In this chapter, we aimed to determine the importance of spiking activity versus AMPAergic transmission in the induction of synaptic scaling. Our strategy was to block AMPAergic transmission throughout a cultured network while leaving network-wide firing rates intact, and subsequently assess homeostatic changes of synaptic strength. To this end, we first designed a closed-loop optogenetic stimulation system capable of clamping firing rates to specific user-defined setpoints. We showed that our control strategy could be used to control firing rate for many hours, even if glutamatergic transmission was pharmacologically disrupted. Secondly, we used this closed-loop system to restore firing rates in CNQX-treated cultures to their pre-CNQX levels. We found that our closed-loop control perfectly restored firing rates
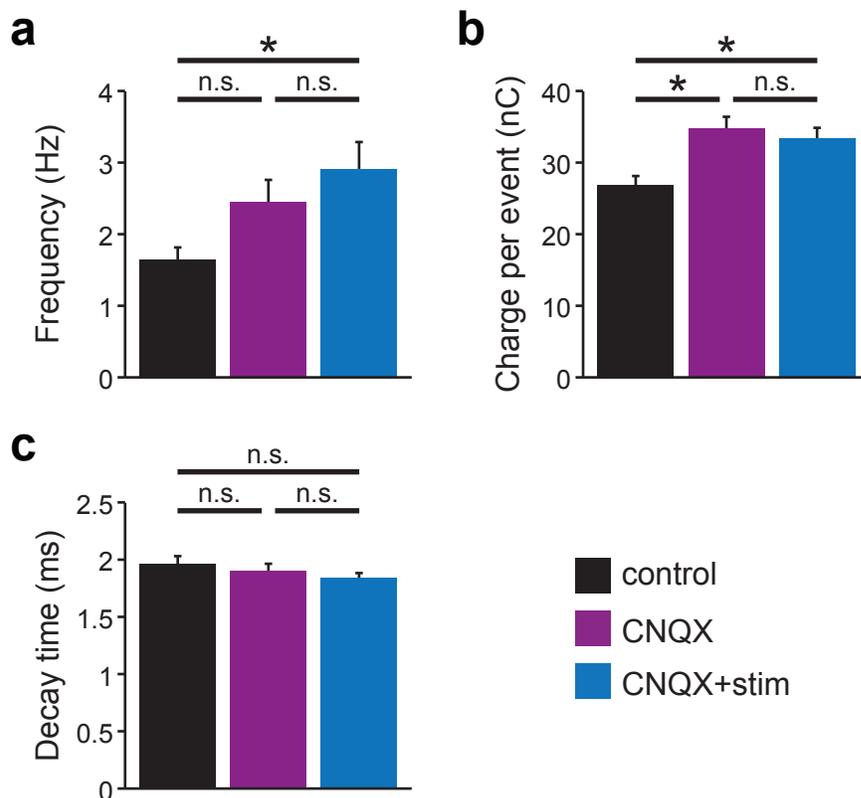
Figure 3.16: Changes in mEPSC features associated with chronic CNQX and CNQX+stimulation conditions. (a) Mean frequency (control, 1.6±0.2 pA, n=44 cells; CNQX, 2.3±0.3 pA, n=51 cells; CNQX+photostimulation, 2.6±0.3 pA, n=46 cells; $p < 0.02$). There is a significant difference between the control vs. CNQX+photostimulation conditions ($p < 10^{-2}$). **(b)** Mean charge per event (control, 27.0±1.2 fC; CNQX, 34.8±1.6 fC; CNQX+photostimulation, 33.5±1.4 fC; $p < 10^{-3}$). There are significant differences between control vs. both CNQX cases (control vs. CNQX, $p < 10^{-3}$; control vs. CNQX+photostimulation, $p < 10^{-3}$). **(c)** Decay time constant (control, 2.0±0.06 ms; CNQX, 1.9±0.06 ms; CNQX+photostimulation, 1.8±0.04; $p > 0.2$). All other post-hoc comparisons were insignificant at the Bonferroni adjusted $\alpha = 0.017$.

during CNQX treatment, while also indirectly restoring other features of bursting and individual unit firing activity. Finally, we examined changes in synaptic strength in cultures treated with vehicle, CNQX alone, or CNQX plus closed-loop stimulation. We found that there was no difference in the synaptic strength distributions from cultures treated with CNQX versus CNQX+stimulation, and both were scaled up compared to vehicle-treated control cultures. Together, these results demonstrate that changes in spiking are not required for synaptic scaling, and that reductions in AMPAergic transmission alone are sufficient to trigger the plasticity.
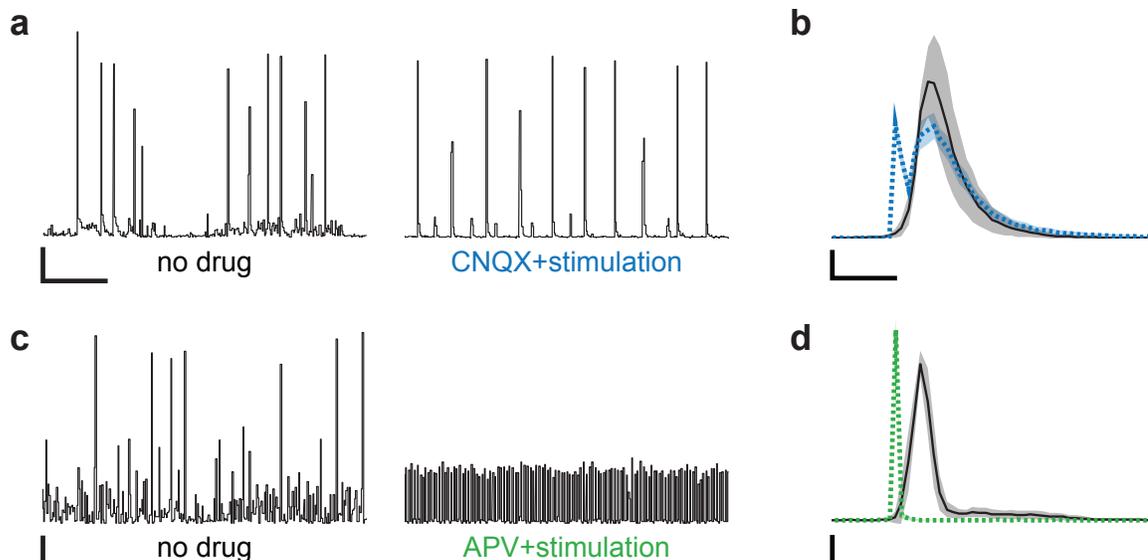
Figure 3.17: Closed-loop optical stimulation facilitates bursting during AMPAergic, but not NMDAergic, blockade. (a) MEA-wide firing rate for a culture before drug treatment (left), and during CNQX treatment with optogenetically-restored firing rate (right). Bin size, 1 s. Scale bars, 200 Hz, 1 min. **(b)** Average burst waveforms for the two conditions pre-drug (black) and CNQX+photostimulation (blue) conditions. Data used to generate averages was taken for an hour before and after traces shown in **(a)**. Bin size, 10 ms. Scale bar, 2 kHz, 100 ms. **(c)** MEA-wide firing rate for a culture before drug treatment (left), and during APV treatment with optically-restored firing rate (right). Bin size, 1 s. Scale bars, 200 Hz, 1 min. **(d)** Average burst waveforms for the pre-drug (black) and APV+stimulation (green) conditions. Data used to generate averages was taken for an hour before and after trace shown in **(c)**. Bin size, 10 ms. Scale bars, 800 Hz, 100 ms. Data shown in this figure was generated from cultures infected with AAV2-CaMKIIα::ChR2(H134R)-mCherry, and recordings were performed at 26 DIV **(a-b)** and 33 DIV **(c-d)**.

In designing our controller, we elected to clamp firing rate rather than another activity feature (e.g. burst rate or shape) because we felt this was the most appropriate variable to control for the purposes of our scientific question. Although we tried to select a stimulus that would promote bursts, the degree to which our stimulus could reproduce spontaneous-like bursts, despite the presence of CNQX, was quite remarkable. Because the vast majority of spikes that followed a blue light pulse occurred tens to hundreds of milliseconds after the light had turned off, we suspect that the capacity for stimulation to produce long-lasting bursts relied on NMDAergic transmission. This hypothesis is based on our previous observation that bursts occurring during NMDAR blockade terminate more quickly (Fig. 2.7). In addition, when we looked

more closely at our data from experiments on closed-loop control of firing rate during AMPAergic or NMDAergic blockade (Section 3.3.1.3 and Fig. 3.8), we observed very different firing patterns. Bursts produced by closed-loop stimulation during CNQX treatment were of similar amplitude and duration as spontaneous pre-CNQX bursts (Fig. 3.17a-b). Meanwhile, bursts produced by closed-loop stimulation during APV treatment were lower amplitude and much faster than spontaneous pre-APV bursts (Fig. 3.17c-d). This further supports that notion that NMDAergic transmission is required for the elongation of bursts, even when depolarization is provided by ChR2 activation. In this sense, our experimental need to block AMPARs, rather than another neurotransmitter receptor, was quite serendipitous because it allowed for us to reproduce spontaneous-like bursts as we were controlling overall firing rates.

Another consideration in designing our experiments was how to choose the controller's firing rate setpoint. Vehicle-treated cultures showed slightly reduced firing rates during the first few hours, and slightly increased firing rate during the final few hours (Fig. 2.5). However, they also showed extreme culture-to-culture variability in their overall firing rates (Fig. 2.6), and individual units were affected quite differently by vehicle treatment (Figs. 2.9 and 2.10). Given these different considerations, we elected to keep things simple and maintain spiking levels at their pre-CNQX firing rates. Although this did not capture the variability observed in the vehicle-treated controls, trying to make the setpoint follow a "typical" temporal trajectory or a yoked vehicle-treated culture seemed too arbitrary. Synaptic scaling had been thought of as a mechanism for maintaining firing rates within a neural circuit, so in deciding upon a control strategy, we chose to maintain pre-treatment firing rates within the network, rather than to use an external reference.

One consequence of choosing an on-off controller is that stimuli were delivered as soon as the integrated error between target and measured firing rates became positive. As a result, bursts were reliably triggered every few minutes for the entire 24-hour

perturbation. However, typically the timing of bursts is not quite as reliable in a spontaneously active culture. This is best illustrated by looking at the distribution of interburst intervals (IBIs; Fig. 3.18). While the average IBI is preserved between the pre-treatment condition and the CNQX+stimulation period, there is a narrowing of the distribution, indicating that bursts are occurring at more regular intervals than they would occur spontaneously. One strategy for reproducing the spontaneous pre-treatment IBI distribution might be to introduce random noise into the error calculation, or introduce random delays (positive or negative) into the pulse timing. These modifications seemed unnecessary for the purposes of our initial question, but we anticipate future experimental studies driven by other scientific questions may seek to control for differences in burst timing when using closed-loop stimulation. However, in the present study, we believe that this subtlety in burst timing is unlikely to affect the interpretation of our results, that changes in firing rate are not required to induce synaptic scaling.

It has been proposed that reductions in spiking trigger upward synaptic scaling by reducing the influx of somatic calcium, and subsequent calcium signaling then mediates the expression of cell-wide scaling (Ibata et al., 2008). Because we measured spiking activity, rather than somatic calcium levels, one possibility is that our stimulation strategy did not sufficiently restore intracellular calcium in cultures, and thus scaling was still expressed. We find this possibility unlikely for several reasons. First, concurrent MEA and calcium imaging studies have revealed that intracellular calcium is highly correlated with network-wide bursts (Murphy et al., 1992; Jimbo et al., 1993; Opitz et al., 2002; Minerbi et al., 2009). Because we restored network-wide burst rate (Fig. 3.10), we have restored the primary source of intracellular calcium. Further, because the shape of bursts and pattern of recruitment is well-preserved (Figs. 3.5, 3.13 and 3.14), many features of intracellular calcium dynamics that occur during a burst are likely preserved. Finally, depolarization via ChR2 activation has been
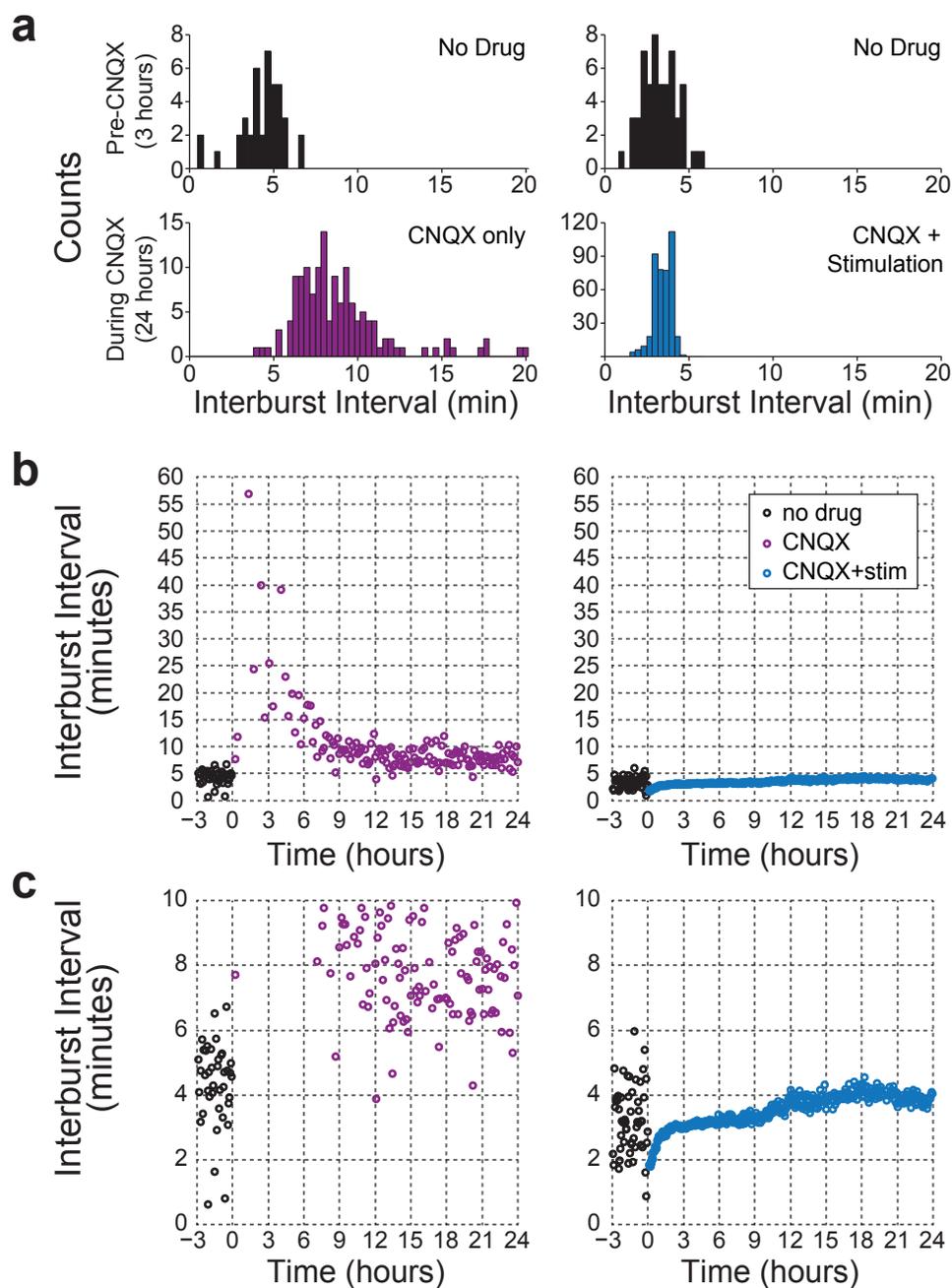
Figure 3.18: Closed-loop optical stimulation narrows the distribution of interburst intervals. (a) IBI histogram for pre-treatment period (top) compared to 24-hour treatment period (bottom), either for a culture treated with CNQX alone (left) or a sister culture treated with CNQX and closed-loop stimulation (right). Compared to the pre-treatment condition, CNQX induces a rightward shift in the distribution, while CNQX+stimulation narrows the distribution. **(b)** The distribution of IBIs over the duration of treatment, including 3 hours of pre-treatment data is for reference. **(c)** Same as **(b)**, but vertically zoomed on IBIs shorter than 10 minutes. For comparison purposes, this data is from the same pair of sister cultures shown in Fig. 3.9.

shown to open voltage-gated calcium channels, such that more calcium enters the cell that would normally occur during a spontaneous action potential (Zhang and Oertner, 2007). Since chronic ChR2 activation and elevated calcium levels are associated with downward scaling (Goold and Nicoll, 2010), it is perhaps even more surprising that we observed no attenuation of scaling in cultures treated with CNQX+stimulation. However, these experiments using ChR2 were not performed in CNQX, so it is difficult for us to speculate about the the effect this may have on intracellular calcium dynamics. For instance, it is plausible that blockade of AMPAergic transmission alters spike-triggered somatic calcium dynamics. In order to explore these possibilities, we are currently working on experiments to image the burst-associated calcium dynamics during CNQX+stimulation, as compared to CNQX or vehicle treatment.

One peculiarity in our results was the increase in mEPSC frequency for cultures treated with CNQX+stimulation compared to vehicle-treated sister controls (Fig. 3.16). Meanwhile, CNQX treatment revealed a mild increase in mEPSC frequency that was neither significantly different from control or CNQX+stimulation cultures. Changes in mEPSC frequency could result from a change in synapse number or change in presynaptic release properties. Previous work has shown that blockade of AMPAergic transmission, but not spiking, increases the probability of release (Murthy et al., 2001; Bacci et al., 2001). Although we did not observe a significant increase in mEPSC frequency with CNQX treatment alone, the aforementioned studies blocked transmission for several days (whereas our treatment was only 1 day), so it is possible that we might see increases in mEPSC frequency if we extended our treatment window. One possibility that could explain the increase in mEPSC frequency for cultures treated with CNQX+stimulation (as well as a slight but insignificant increase in mEPSC frequency for cultures treated with CNQX alone) would be that homeostatic increases in probability of release require a mismatch between neurotransmitter release and receptor activation. For instance, with CNQX treatment

alone, AMPARs are blocked, but because spiking is reduced, there is a reduction in spike-evoked glutamate release. Over the course of a few days, spiking activity and spike-evoked glutamate release gradually recover, but receptors are still blocked. This excess of unbound glutamate could be detected by extrasynaptic or metabotropic glutamate receptors which in turn trigger presynaptic changes. Meanwhile, with CNQX+stimulation treatment, AMPARs are blocked, but spiking and spike-evoked glutamate release is immediately restored. Therefore, the mismatch between glutamate release and AMPAR activation is apparent immediately, thus triggering faster changes in probability of release. While this possibility is speculative, it could provide an explanation for the disparity in mEPSC frequency between the different conditions.

Upward synaptic scaling is characterized by a coordinated increase in the strength of all synaptic inputs onto a neuron. In contrast, recent work has identified a local form of homeostatic plasticity that regulates the strength of individual synapses. In these studies, neurotransmission was reduced in subset of presynaptic inputs through local application of a receptor antagonist (Sutton et al., 2006; but see Ibata et al., 2008), reductions in presynaptic release (Hou et al., 2008; Béïque et al., 2011), or altering sensory input *in vivo* (Deeg and Aizenman, 2011). Reducing neurotransmission at specific postsynaptic sites (leaving postsynaptic spiking largely intact) resulted in compensatory strengthening of only those synapses. Our finding that cell-wide synaptic scaling can be directly triggered by reduced AMPAergic transmission without changes in firing rate suggests that synapse-specific compensatory plasticity may be more closely related to cell-wide scaling than previously thought. Specifically, both scaling and synapse-specific compensations can be engaged by altered synaptic transmission independent of changes in spiking. Given this similarity, it is possible that CNQX-induced synaptic scaling might be the result of global application of the drugs, which in turn reduce AMPAergic transmission at all synapses and trigger local synaptic compensations throughout the cell. Local strengthening of all synapses

onto a neuron would then resemble a cell-wide multiplicative increase in synaptic strength. While it seems reasonable that local and global reductions in AMPAergic transmission would both trigger increases in synaptic strength in similar ways, it is not clear that scaling that follows global blockade of spiking also requires reductions in AMPAergic transmission. In Chapter 4, we explore the importance of AMPAergic transmission in TTX-induced synaptic scaling.

Finally, while we observed that upward synaptic scaling does not require changes in spiking, changes in spiking have been shown to influence downscaling (Leslie et al., 2001; Goold and Nicoll, 2010). In this study, we only assessed the roles of spiking and AMPAergic transmission in upscaling. The expression of upward and downward scaling are mediated by different molecular mechanisms (Rutherford et al., 1998; Leslie et al., 2001; Shepherd et al., 2006; Stellwagen and Malenka, 2006; Anggono et al., 2011; Sun and Turrigiano, 2011; Tatavarty et al., 2013), so the idea that they may be triggered by different signals seems quite plausible. In some preliminary experiments where we doubled firing rate during CNQX treatment, we found that upscaling was prevented. These preliminary data are generally in agreement with previous literature that downscaling depends on spiking activity (Leslie et al., 2001; Goold and Nicoll, 2010), although more work will be required to fully interpret our results. Still, if downscaling is triggered by elevated spiking, and upscaling is triggered by reduced transmission, this suggests distinct functional goals for each phenomenon. Downscaling may be a compensatory mechanism that protects neural circuits against hyperexcitability and protects individual neurons against excitotoxicity. Meanwhile, upscaling may function to tune synaptic activity to promote information transmission between cells and within neural circuits.

REDUCTIONS IN AMPA RECEPTOR ACTIVATION ARE REQUIRED TO TRIGGER UPWARD SYNAPTIC SCALING

Chronic neuronal silencing robustly elicits upward scaling of excitatory quantal amplitudes. This has lead to the hypothesis that neurons monitor their own firing rates, and deviations from an internal firing rate setpoint can induce cell-wide scaling. However, in the previous chapter we observed that changes in firing rate were not required to achieve upward synaptic scaling, and that reductions in AMPAergic transmission alone were sufficient to trigger scaling. Because reduced AMPAergic transmission can directly trigger scaling, it is possible that chronic blockade of spiking activity leads to scaling by indirectly reducing AMPAergic transmission. Still, it is also possible that either reductions in spiking or reductions in AMPAergic transmission are sufficient to induce scaling. To distinguish between these possibilities, we first established a strategy for partially restoring AMPAR activation during a chronic spiking blockade. We then assessed whether synaptic scaling traditionally elicited by a spiking blockade was affected by the partial restoration of AMPAR activation. We found that partially restoring AMPAR activation significantly attenuated the capacity for cultures to express scaling following a chronic spiking blockade. This result demonstrates that blocking spiking elicits scaling, at least in part, by indirectly reducing AMPAR

activation. Our findings highlight the critical role for AMPAergic transmission in the induction of cell-wide synaptic scaling.

4.1 Introduction

4.1.1 Background

Chronic blockade of neuronal spiking has important consequences for neural development, and many of these consequences are expressed at the level of synapses. Before synapse formation, chronic blockade of action potentials can disrupt synaptogenesis both *in vitro* (Burrone et al., 2002) and *in vivo* (Riccio and Matthews, 1985a). In the visual system, intraocular injections of TTX lead to pathfinding errors during prenatal development (Shatz and Stryker, 1988) and disrupt spine formation during postnatal development (Riccio and Matthews, 1985b). After synapse formation, one of the most widely-observed consequences of a chronic spiking blockade is a compensatory increase in excitatory synaptic strength. This form of homeostatic plasticity has been observed both *in vitro* (Turrigiano et al., 1998; O'Brien et al., 1998; Burrone et al., 2002) and *in vivo* (Desai et al., 2002; Gonzalez-Islas and Wenner, 2006; Goel and Lee, 2007; Knogler et al., 2010). Often these compensatory increases occur in a coordinated fashion across the entire cell, such that the distribution of synaptic strengths is scaled up by a common multiplicative factor. This compensatory cell-wide change in synaptic strength is referred to as synaptic scaling (Turrigiano et al., 1998). By tuning the strength of all synapses in a coordinated manner, synaptic scaling can elegantly tune the overall excitability of a cell without disrupting the relative distribution of synaptic strengths.

While synaptic scaling has been widely observed following network-wide blockade of spiking, it not clear what triggers this process. A popular hypothesis is that neurons monitor their own firing rates, and can autonomously trigger cell-wide increases

in synaptic strength when firing rate falls below a setpoint. Two studies tested this hypothesis by reducing activity in individual neurons, but have lead to different conclusions (Burrone et al., 2002; Ibata et al., 2008). One study reduced spiking activity by overexpressing an inwardly-rectifying potassium channel, $K_{mir}2.1$, into individual neurons in a hippocampal culture (Burrone et al., 2002). This resulted in chronic hyperpolarization and reduced spiking in the few cells expressing $K_{mir}2.1$, but activity throughout the rest of the network was normal (Burrone et al., 2002). Despite the chronically reduced spiking activity, $K_{mir}2.1$-expressing cells showed no difference in mEPSC amplitude compared to non-transfected cells, suggesting that reductions in spiking are not required for upward scaling (Burrone et al., 2002). Another study reduced spiking in individual cells by perfusing TTX directly onto the soma of cells embedded in a cortical culture (Ibata et al., 2008). This study showed that the TTX perfusion caused rapid multiplicative accumulation of GluA2 (an AMPAR subunit) in the dendrites, suggesting that reductions in spiking can directly trigger scaling (Ibata et al., 2008). Importantly, these two studies used different neural preparations, different approaches for reducing activity, and different readouts for scaling. Therefore, the distinct conclusions reached by these studies may lie in some of these differences, and together these studies suggest that spiking plays an important but nuanced role in synaptic scaling.

Although some progress has been made in identifying the role of spiking in trigger scaling within individual cells, less is known about importance of network-wide spiking activity in synaptic scaling. However, we have begun to fill in some of these uncertainties. In Chapter 2, we showed that network-wide reductions in spiking activity were not correlated to the magnitude of subsequent increases in synaptic strength. In Chapter 3, we showed that reductions in AMPAergic transmission were sufficient to trigger scaling, even when network-wide spiking levels were maintained at nor-

mal levels. Together, these findings indicate that at the network level, reductions in spiking are not required to achieve upward synaptic scaling.

If reduced spiking is not required to induce synaptic scaling, why does a network-wide spiking blockade so consistently lead to scaling? One possibility is that chronic blockade of spiking activity leads to upscaling by preventing spike-dependent release of neurotransmitter. This leads to consequent reductions in AMPAergic transmission, which are sufficient to trigger upscaling. An alternative possibility is that reductions in either spiking or AMPAergic transmission could trigger scaling, perhaps through different signaling pathways, and both produce the same multiplicative increase in mEPSC amplitude. Distinguishing between these possibilities is challenging because spiking and neurotransmission are highly correlated at the network level. Therefore, we must develop a strategy for manipulating AMPAergic transmission during a chronic spiking blockade.

4.1.2 Chapter Summary

In this chapter, our goal was to determine whether reductions in spiking were sufficient to trigger upward synaptic scaling, or if reductions in AMPAergic transmission were required to induce the plasticity. To this end, we performed two primary tasks. First, we established a strategy for partially restoring AMPAR activation during a TTX-induced spiking blockade. We found that disrupting AMPAR desensitization using cyclothiazide (CTZ) increased the amplitude and frequency of the AMPAergic mEPSCs that remained during a TTX treatment. While this did not fully restore normal synaptic currents, it did partially restore AMPAR activation, and the effects lasted for hours without disrupting the efficacy of TTX to block spiking activity. Secondly, we assessed changes in synaptic strength in cultures following this partial restoration of AMPAR activation during a spiking blockade. We found that mEPSC amplitudes from cultures treated with TTX and CTZ were scaled up compared to control val-

ues, but significantly attenuated compared to mEPSCs from cultures treated with TTX alone. This attenuation in TTX-induced scaling following a partial restoration in AMPAR activation indicates that reductions in spiking alone were insufficient to trigger a full scaling response. Taken together with the results of Chapter 3, our findings show that reductions in AMPAR activation are both necessary and sufficient to induce upward synaptic scaling.

4.2 Methods

Culturing and MEA electrophysiology were carried out as described in Section 2.2.

4.2.1 Patch clamp electrophysiology

To assess the effect of CTZ treatments on AMPAergic mEPSCs, we performed whole-cell voltage clamp recordings from pyramidal-shaped cells at a holding potential of -70 mV. External and internal solutions were the same as described in Section 2.2.4.1. We added 1 μM TTX and 20 μM bicuculline to isolate events to AMPAergic mEPSCs, and recorded from 5 cells. While recording from the 5th cell, we added 100 μM cyclothiazide (CTZ). We recorded mEPSCs from additional cells for 3 to 11 hours. In assessments of the acute effects of CTZ on AMPAergic mEPSCs, only data from the first 3 hours after CTZ application were included. mEPSCs were analyzed as described in Section 2.2.4.2.

For assessing changes in synaptic strength following chronic treatments, mEPSC recordings and analysis were performed as described in Section 2.2.4.

4.2.2 Chronic treatments

Chronic drug treatments lasted for 24 hours and were performed as described in Section 2.2.2. In addition, experiments were performed exclusively in triplicate sister cultures, where cultures were treated with either TTX, TTX and CTZ, or vehicle.

Concentrated TTX and CTZ aliquots were dissolved in water and DMSO, respectively. Therefore, the TTX solution was supplemented with DMSO, the CTZ solution was supplemented with water, and the vehicle was a mixture of water and DMSO.

4.3 Results

4.3.1 Cyclothiazide partially restores AMPAR activation during a spiking blockade

To test the importance of reduced AMPAergic transmission on TTX-induced synaptic scaling, we sought to enhance the quantal AMPAergic currents that remained during a spike blockade. AMPARs mediate fast glutamatergic transmission and desensitize quickly after binding glutamate. In order to enhance AMPAergic mEPSCs we used cyclothiazide (CTZ), an a positive allosteric AMPAR modulator ($K_I = 60 \pm 6\mu M$ at 100 μM, Kovács et al., 2004 CTZ). CTZ disrupts desensitization and thus increases receptor open time (Partin et al., 1993; Yamada and Tang, 1993; Zorumski et al., 1993; Rammes et al., 1994), allowing more charge to flow across the AMPAR when glutamate is bound. CTZ has also been shown to enhance presynaptic release at glutamatergic synapses (Diamond and Jahr, 1995), providing another way to increase the total current flowing across AMPARs.

In our cultures, CTZ induced a ~1.6-fold increase in amplitude, ~3-fold increase in decay time, a ~4.5-fold increase in charge per event, and a ~4.5-fold increase in frequency of AMPAergic mEPSCs compared to TTX treatment alone. (Fig. 4.1). These values are similar to values that have been reported in previous characterizations (Mennerick and Zorumski, 1995; Diamond and Jahr, 1995). Notably, synaptic currents recorded in the drug-free condition were still significantly larger than the augmented mEPSCs recorded in TTX and CTZ (Fig. 4.1). Therefore, CTZ treatment during a spiking blockade represented only a partial restoration of AMPAergic
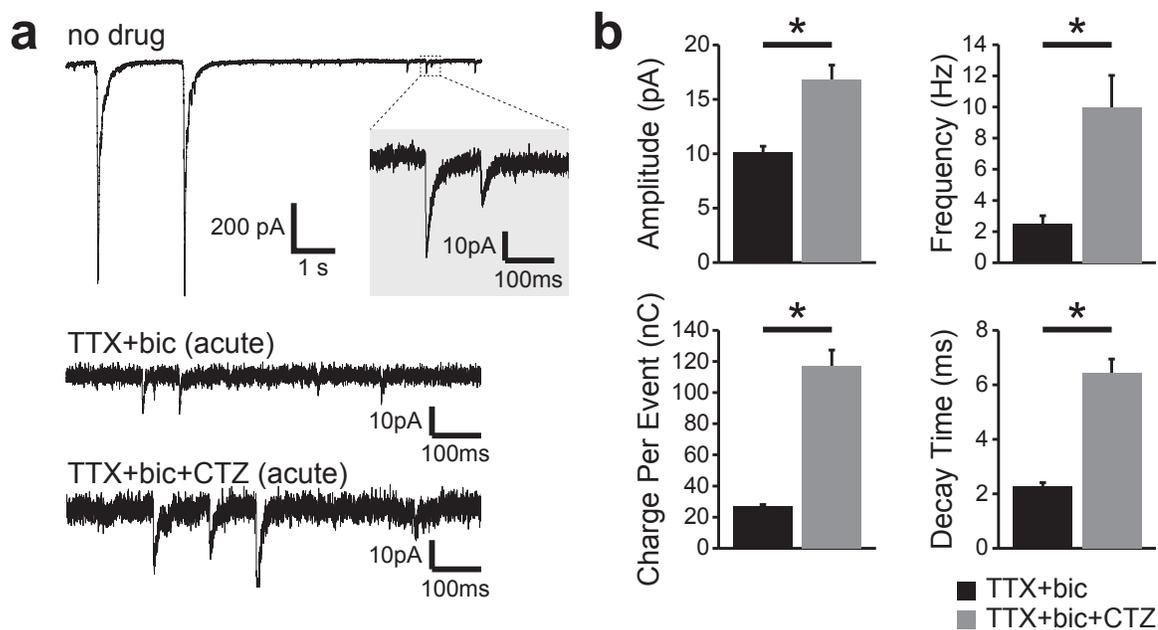
Figure 4.1: Cyclothiazide increases charge fluxed by AMPAergic mEPSCs. (a) *Top*, sample post-synaptic currents recorded before any drugs are added. The shaded inset shows a zoomed trace of some lower-amplitude events. *Middle and bottom*, sample AMPAergic mEPSCs recorded before (middle) and after (bottom) addition of CTZ. **(b)** Mean amplitude ($p < 10^{-3}$), frequency ($p < 10^{-2}$), charge per event ($p < 10^{-7}$), and decay time constant ($p < 10^{-6}$) of AMPAergic mEPSCs before and during acute application of CTZ (before, n=10 cells; during, n=11 cells).

transmission. Still, compared to TTX treatment alone, CTZ produced approximately a 20-fold increase the total current.

Because previous literature had not provided evidence of CTZ-modulated currents over long timescales, we were concerned that CTZ might lose its efficacy over the duration of our 24-hour treatment. To address this concern, we recorded AMPAergic mEPSCs from several different cells over the course of an 11-hour CTZ treatment. We found that the increases in mEPSC amplitude, frequency, charge per event, and decay time persisted over the course of 11 hours (Fig. 4.2). Although one might argue that an increase in mEPSC amplitude could be due to the sustained TTX treatment (which on its own leads to increases in quantal amplitude), a good indication that CTZ is still effective is the sustained increase in the decay time constant (Fig. 4.2, bottom), indicative of a sustained disruption of AMPAR desensitization. By comparison, this
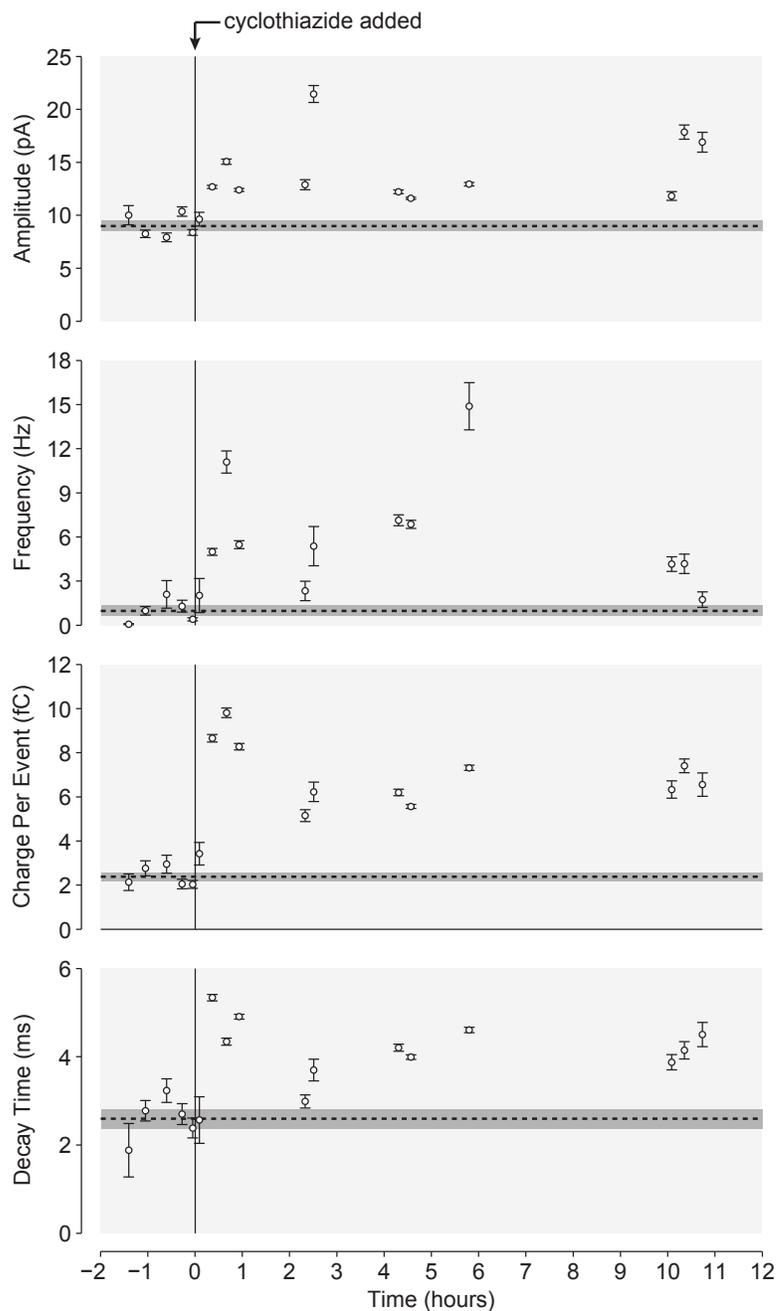
Figure 4.2: Cyclothiazide is effective for enhancing quantal AMPAR activation for at least 11 hours. mEPSCs were recorded from 4 different cells, using TTX and bicuculline to isolate AMPAergic events. After CTZ was added, mEPSCs were recorded from 11 additional cells at various time points over the course of 11 hours. Mean mEPSC amplitude, frequency, charge per event, and decay time constant is shown for all 15 cells. Points just before and after CTZ application represent the same cell.

Table 4.1: Average network activity features for chronic TTX+cyclothiazide treatment

	Treatment			
	vehicle[†]	TTX[†]	TTX+CTZ	p-value[§]
Sample size				
number of cultures	12	13	5	
Feature				
MEA-wide firing rate	97.3±4.6%	1.1±0.5%	1.1±0.002%	$< 10^{-6}$
Burst rate	105.8±10.0%	0%	0%	$< 10^{-6}$
Interburst firing rate	108.1±12.7%	3.6±1.5%	4.26±1.91%	$< 10^{-4}$

[†]reproduced from Table 2.2 from comparison; [§]Kruskal-Wallis test, α=0.05

elevated decay time is approximately double the value observed in mEPSCs from cultures chronically treated with TTX alone (Fig. 2.12)

4.3.2 Partially restoring AMPAR activation attenuates TTX-induced synaptic scaling

In order to test how partially restoring AMPAergic transmission affected TTX-induced scaling, we treated sister cultures with either TTX, TTX and CTZ, or vehicle. As with previous experiments, we recorded spiking activity through the MEA during the 24-hour treatment period. Like TTX alone, application of TTX and CTZ completely eliminated spiking and burst activity for the entire treatment period (Fig. 4.3).

Having partially restored AMPAergic transmission during a spiking blockade, we next examined whether this restored activation of AMPARs would prevent upward synaptic scaling. To this end, we recorded mEPSCs from triplicate sister cultures:

1. **control**: vehicle-treated control cultures experiencing normal spiking activity and normal AMPAergic transmission
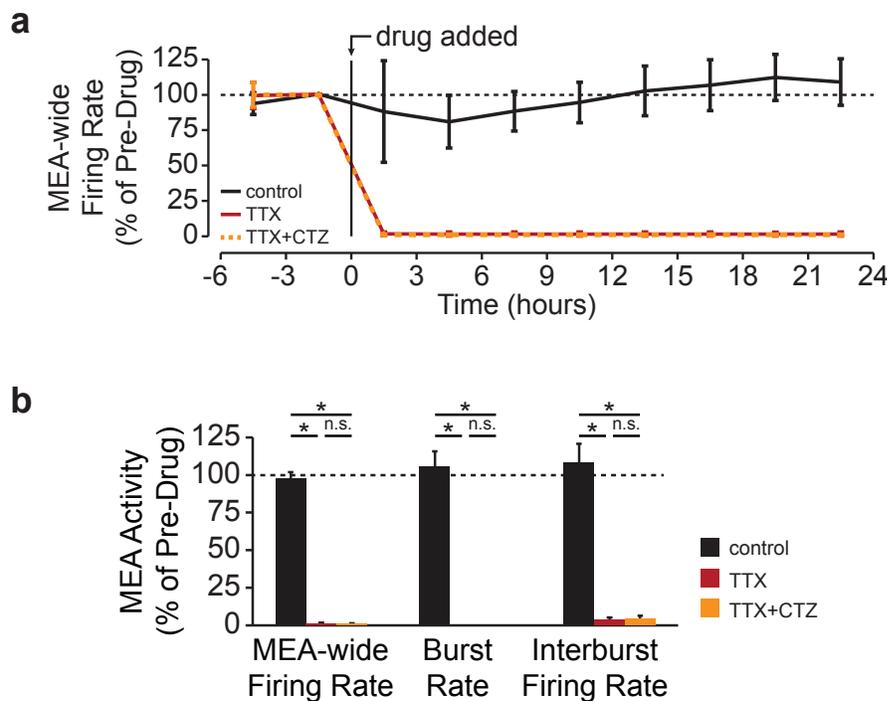
Figure 4.3: Cyclothiazide does not change effects of TTX on spiking activity. (a) Mean MEA-wide firing rate over time for cultures co-treated with TTX and CTZ (n=5 cultures). Control and TTX values from Fig. 2.5 are shown for comparison. All TTX-treated cultures eliminate spiking, regardless of whether CTZ is present. Bin size, 3 h. Error bars, s.d. **(b)** Mean MEA-wide firing rate, burst rate, and interburst firing rate for the TTX+CTZ condition during the 24-hour treatment window, with control and TTX values from Fig. 2.5 shown for comparison. TTX+CTZ completely abolished spiking and bursting, and the effect on MEA activity is no different than TTX alone. Averages and statistical significance are summarized in Tables 4.1 and 4.2. Error bars, s.e.m.

2. **TTX**: TTX-treated cultures experiencing no spiking and dramatically reduced AMPAergic transmission

3. **TTX+CTZ**: TTX- and CTZ-treated cultures experiencing no spiking and moderately reduced AMPAergic transmission

All mEPSC recordings were performed after washing out the drug or vehicle, before perfusing them with external recording solution. As shown previously (Fig. 2.11), mEPSC amplitudes from cultures treated with TTX only were significantly increased compared to vehicle-treated sister control cultures (Fig. 4.4a-c). Interestingly, we found that mEPSC amplitudes from cultures co-treated with TTX and CTZ were significantly reduced compared to sister cultures treated with TTX alone (adjusted

Table 4.2: Post-hoc tests: network activity features for chronic TTX+cyclothiazide treatment

Post-Hoc Tests	Significance[§]	p-value
MEA-wide firing rate		
vehicle vs. TTX[†]	$*$	$< 10^{-3}$
vehicle vs. TTX+CTZ	$*$	$< 10^{-3}$
TTX vs. TTX+CTZ	n.s.	> 0.3
Burst rate		
vehicle vs. TTX[†]	$*$	$< 10^{-3}$
vehicle vs. TTX+CTZ	$*$	$< 10^{-3}$
TTX vs. TTX+CTZ	n.s.	1
Interburst firing rate		
vehicle vs. TTX[†]	$*$	$< 10^{-3}$
vehicle vs. TTX+CTZ	$*$	$< 10^{-3}$
TTX vs. TTX+CTZ	n.s.	> 0.4

[†]reproduced from Table 2.3 for comparison
[§]Wilcoxon rank-sum test, $\alpha=0.017$ (Bonferroni adjusted)
$*$ denotes significant differences; n.s. denotes non-significant differences

t-test, $p < 10^{-2}$). On the other hand, mEPSC amplitudes from cultures co-treated with TTX and CTZ were significantly increased compared to vehicle-treated controls (adjusted t-test, $p < 10^{-2}$). This intermediate increase in synaptic strength is likely because CTZ only increased quantal currents and did not fully restore normal postsynaptic currents observed in control cultures with intact spiking (Fig. 4.1a). The distribution of mEPSC amplitude for both TTX and TTX+CTZ were increased over the control distribution by a common multiplicative factor, indicating that the increases in synaptic strength were consistent with synaptic scaling (Fig. 4.4d-e). Meanwhile, mEPSC frequency and decay time were no different for the TTX+CTZ condition when compared to either cultures treated with TTX only or vehicle-treated controls (Fig. 4.5).
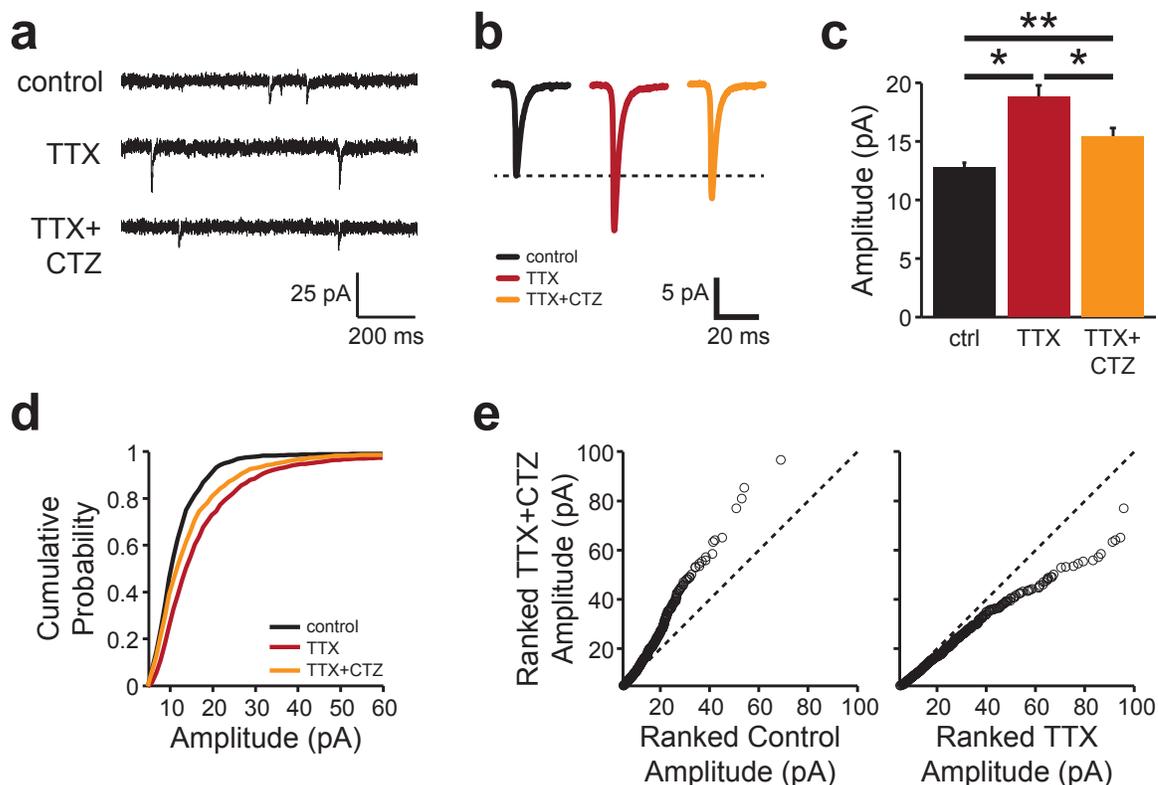
Figure 4.4: Synaptic scaling that follows chronic spiking blockade is mediated by reduced AMPAR activation. **(a)** Sample mEPSC recordings following 24-hour treatment with vehicle, TTX, or TTX+CTZ. Scale bars, 25 pA, 200 ms. **(b)** Average mEPSC waveforms. Scale bars, 5 pA, 20 ms. **(c)** Mean mEPSC amplitude for 6 sister culture pairs treated from the 3 treatment conditions (control and TTX cultures same as Fig. 2.11c; TTX+CTZ: 15.5±0.7 pA, $n = 50$ cells; $p < 10^{-5}$). Significant differences denoted by $^*p < 10^{-2}$ and $^{**}p < 10^{-5}$. Error bars, s.e.m. **(d)** Cumulative distribution of mEPSC amplitudes following the 3 treatment conditions (control and TTX cultures same as Fig. 2.11d). The distribution of mEPSC amplitudes is significantly different between the TTX and TTX+CTZ conditions ($p < 10^{-6}$). **(e)** Ranked TTX+CTZ mEPSC amplitudes plotted against ranked control or TTX amplitudes (linear fits, R^2=0.990 and R^2=0.989, respectively). Dotted line denotes the line of identity.

Overall, these results show that moderately restoring AMPAR activation during a spiking blockade can significantly attenuate TTX-induced synaptic scaling. While it has previously been hypothesized that the scaling that follows a spiking blockade is a direct result of reductions in firing rate, our result demonstrates the critical role for reduced AMPAergic transmission in the induction of upward synaptic scaling.
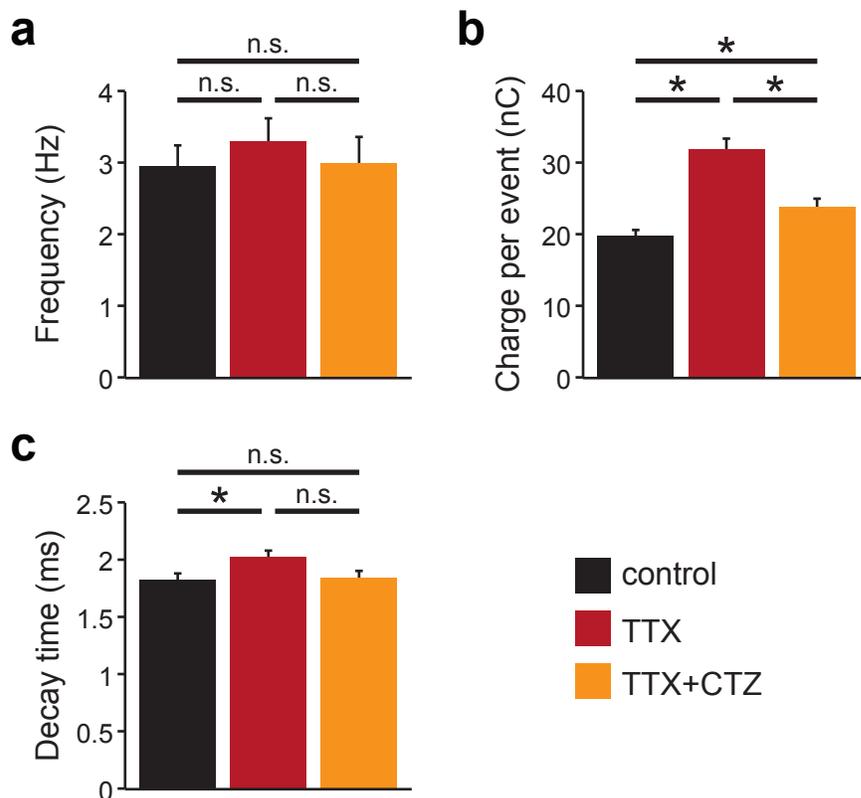
Figure 4.5: Changes in mEPSC features associated with chronic TTX and TTX+stimulation conditions. (a) Mean frequency (control, 3.0±0.3 Hz, n=47 cells; TTX, 3.3±0.4 Hz, n=58 cells; TTX+CTZ, 3.0±0.4 Hz, n=50 cells; $p > 0.6$). (b) Mean charge per event (control, 24.9±0.9 fC; TTX, 40.0±1.9 fC; TTX+CTZ, 29.9±1.4 fC; $p < 10^{-10}$). There are significant differences in charge between all conditions (control vs. TTX, $p < 10^{-8}$; control vs. TTX+CTZ, $p < 10^{-2}$; TTX vs. TTX+CTZ, $p < 10^{-4}$). (c) Decay time constant (control, 1.8±0.06 ms; TTX, 2.0±0.05 ms; CNQX+photostimulation, 1.9±0.06; $p < 0.02$). There was a significant difference in decay time constant for cultures treated with TTX (control vs. TTX, $p < 10^{-2}$). All other post-hoc comparisons were insignificant at the Bonferroni adjusted $\alpha = 0.017$. Control and TTX cultures same as Fig. 2.12a-b.

4.4 Discussion

In this chapter, we sought to determine whether reductions in AMPAergic transmission were necessary for TTX-induced synaptic scaling, or whether reductions in spiking alone could induce scaling. To achieve this goal, we developed a strategy for partially restoring AMPAergic transmission during a chronic spiking blockade. We found that CTZ enhanced the total AMPAergic current (charge per unit time) during concurrent TTX treatment by increasing the amplitude, decay time, and fre-

quency of mEPSCs. We then examined changes in synaptic strength in sister cultures treated with vehicle, TTX alone, or TTX+CTZ. We found that cultures treated with TTX+CTZ showed a moderate degree of scaling compared to controls, though significantly less scaling than cultures treated with TTX alone. This attenuation in TTX-induced scaling demonstrated that partially re-introducing AMPAR currents was sufficient to partially block the scaling response. These results suggest synaptic scaling that typically follows TTX treatment is not the result of reduced spiking. Instead, chronic TTX treatment indirectly reduces AMPAergic transmission which in turn triggers scaling.

On the surface, our observation that CTZ attenuated, but did not block, TTX-induced synaptic scaling may lead one to believe that reductions in AMPAergic transmission cannot fully account for synaptic scaling typically observed following a spiking blockade. Admittedly, we do not have evidence to rule out the possibility other factors, including reductions in spiking, might contribute to this process. However, it is important to note that we only partially restored AMPAergic transmission. At this developmental age, cultured neurons are subject to high levels of synaptic bombardment, and we frequently observe synaptic currents with amplitudes on the order of nanoamps ($V_{\text{hold}} = -70$ mV; Figs. 4.1a, 4.6). TTX treatment isolates these synaptic currents to infrequent miniature release events, producing mEPSCs with amplitudes primarily in the range of 5-20 pA. Meanwhile, TTX+CTZ treatment induces a 1.6-fold increase in mEPSC amplitude, and a 3-fold increase in mEPSC frequency, above TTX alone. This increase is significant, but in no way reproduces the typical synaptic currents observed in the absence of a spiking blockade (Fig. 4.6). Therefore, we hypothesize that the partially sustained scaling observed following TTX+CTZ treatment is likely due to this incomplete restoration of AMPAergic activity. In fact, in light of the relatively small AMPAergic currents produced by TTX+CTZ compared to normal synaptic activity, it seems remarkable that this perturbation even

TTX+bicuculline (acute)

TTX+bicuculline+ cyclothiazide (acute)

no drug

200pA

1s
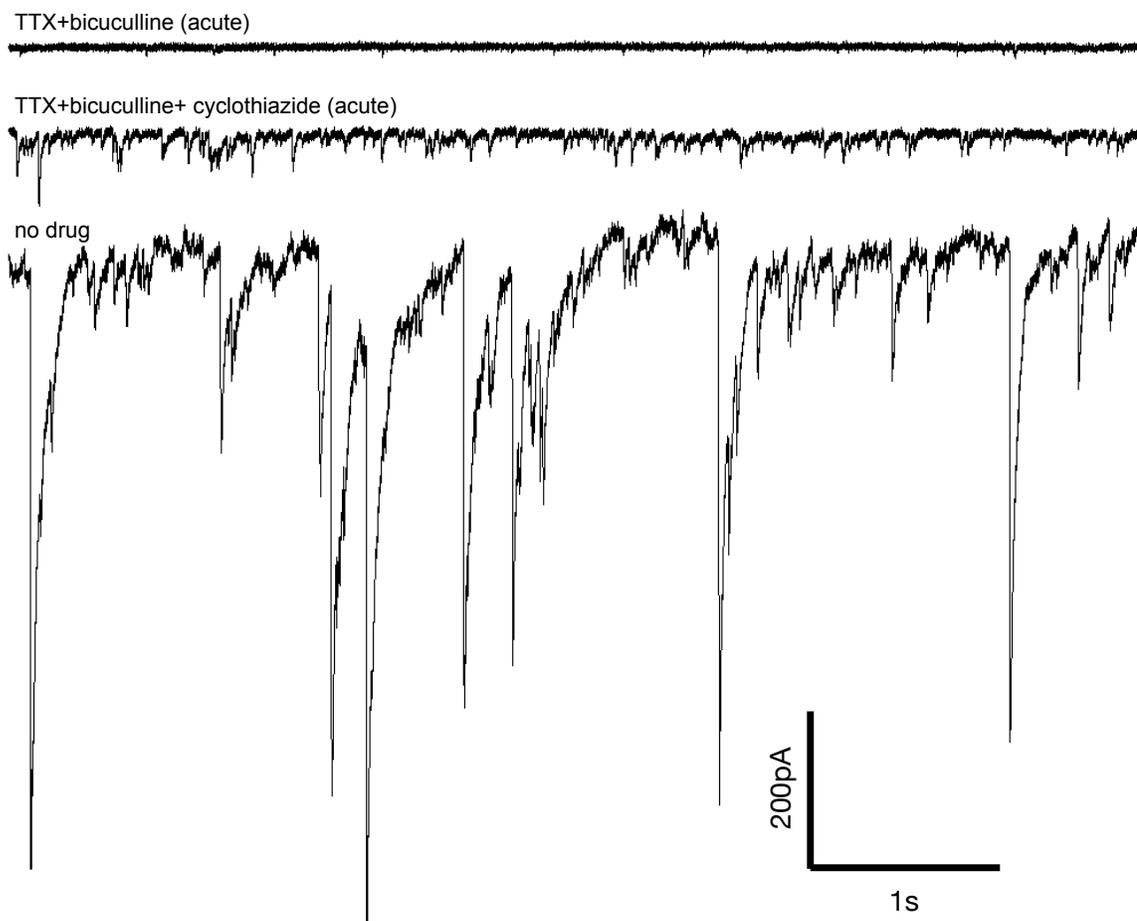
Figure 4.6: Cyclothiazide enhances AMPAergic mEPSCs, though cannot fully restore normal synaptic currents. *Top*, typical AMPAergic mEPSCs recorded in TTX and bicuculline. Miniature events are small downward deflections from baseline. *Middle*, CTZ-enhanced AMPAergic mEPSCs in a cell that showed particularly large and frequent currents, and are significantly increased in amplitude and frequency above typical mEPSCs shown in the top panel. *Bottom*, synaptic currents recorded from the same culture as the top and middle panels prior to adding any drugs. These currents are significantly larger than even one of the more active recordings of CTZ-enhanced mEPSCs, shown in the middle panel.

influenced scaling. However, miniature glutamatergic transmission has previously been reported as an important mechanism for triggering local homeostatic increases in mEPSC amplitude (Sutton et al., 2006), so there may be some commonality in mechanisms driving cell-wide scaling and local forms of homeostatic plasticity.

One weakness of this study was our inability to directly monitor levels of AMPAR activation throughout the 24-hour TTX treatment in the same way that we were able to directly monitor spiking activity in Chapters 2 and 3. While we did record

AMPAergic mEPSCs for 11 hours following CTZ application ($n = 11$ cells, Fig. 4.2), maintaining cell health on the patch rig beyond 12 hours was not possible. Since we wanted to examine the sustained effects of a single application of CTZ, we could not exchange the external recording solution during the experiment (although we did not observe significant shifts in pH or osmolarity). In addition, upon relief from a 24-hour treatment with TTX and CTZ, there is a slight increase in mEPSC amplitude (Fig. 4.4). Therefore, it is possible that the sustained mEPSC amplitude over first 11 hours (Fig. 4.2) is in part due to compensatory insertion of AMPARs in combination with CTZ-mediated modulation of those newly-inserted receptors. While our inability to precisely monitor AMPAR activation during TTX treatment makes it difficult to quantify exactly how much AMPAergic transmission we were able to restore using CTZ, it does not change our interpretation of the results. Based on our recordings of synaptic currents, we know that transmission was not close to being fully restored, even in cells showing the greatest enhancement of mEPSCs (Fig. 4.6). Beyond that, reinstating transmission by 5% versus 50% still represents a partial restoration of transmission, which in turn produced a partial, but not complete, block of TTX-induced scaling.

In our study, we found that reductions in AMPAR activation, rather than reductions in spiking, are responsible for TTX-induced synaptic scaling. This result stands in apparent contrast to previous work showing that local perfusion of TTX onto the soma was sufficient to trigger multiplicative accumulation of GluA2, despite leaving AMPAergic neurotransmission at the dendrites intact (Ibata et al., 2008). However, one explanation for this apparent discrepancy is work demonstrating the glial cells play an important role in TTX-induced scaling. Stellwagen and Malenka demonstrated that glia can sense reductions in ambient glutamate levels during TTX treatment, and respond by releasing the pro-inflammatory cytokine, TNF-α, which then leads to upward synaptic scaling. In our study, we manipulate AMPAR activa-

tion to demonstrate its importance in upscaling, but because we apply CTZ globally, the partial restoration in AMPAR activation applies not only to postsynaptic receptors, but also extrasynaptic, presynaptic, and glial AMPARs. In Ibata et al., 2008, the authors report that they were able to achieve significantly faster synaptic scaling than they had previously reported (Turrigiano et al., 1998) due to plating neurons with a glia. In our study, we also co-culture neurons with glia, and importantly, cultured astrocytes have previously been shown to express CTZ-sensitive AMPARs (Patneau et al., 1994; Gallo and Russell, 1995). One possibility is that glia sense glutamate levels through astrocytic AMPARs, and in turn release TNF-α to trigger scaling in nearby neurons. In this way, when spiking activity is blocked in a single pyramidal neuron (as in Ibata et al., 2008), spike-evoked release of neurotransmitter is also blocked, thus reducing ambient glutamate that can activate AMPARs on nearby glial cells. Conversely, when CTZ is used to partially restore AMPAR activation during a spiking blockade (as in our present study), glial AMPARs become partially re-activated, thus attenuating any TNF-α signaling that might normally lead to scaling. This possibility could be tested using a conditional knockout or short hairpin RNA knockdown of astrocytic AMPARs.

Our observation that CTZ treatment was sufficient to attenuate TTX-induced scaling demonstrated the critical role for AMPAR activation in upscaling. Naturally, this led us to wonder how CTZ might independently affect both spiking activity and synaptic strength. In some preliminary experiments, we have found that 24-hour treatment with CTZ leads to downscaling. However, we also have results supporting a role for elevated spiking levels in prevention of upscaling. The idea that different activity features may be monitored to trigger upward versus downward scaling is quite plausible given the diverse molecular mechanisms mediating only one or the other (Rutherford et al., 1998; Leslie et al., 2001; Shepherd et al., 2006; Stellwagen and Malenka, 2006; Anggono et al., 2011; Sun and Turrigiano, 2011; Tatavarty et al.,

2013), but this also opens the possibility of "mixed messages" that may lead to opposing changes in synaptic strength. Therefore, identifying the trigger for downward scaling will be important for studying the interaction between these two forms of homeostatic synaptic plasticity. Our work in Chapter 3 leveraged closed-loop optogenetic stimulation for decoupling CNQX-induced reductions in spiking from CNQX-induced blockade of AMPAergic transmission in the study of upward scaling. A goal of future work will be to use the same strategy to restore normal activity levels during perturbations that lead to downscaling (e.g. chronic bicuculline treatment), via stimulation of a hyperpolarizing optogenetic protein.

Fortunately, our picture of how neural circuits achieve upward scaling is becoming more clear. In Chapter 3, we demonstrated that reductions in spiking are not required for upward synaptic scaling, and that reductions in AMPAergic transmission can directly trigger scaling. In this chapter, we showed the reductions in AMPAergic transmission are required for TTX-induced upscaling, and suggest that reduced spiking only indirectly mediates scaling by reducing AMPAR activation. Taken together, these findings provide a compelling challenge to the widely-held view that cells monitor their own firing rates to trigger homeostatic synaptic scaling. Instead, our findings suggest that reductions in AMPAR activation directly and independently trigger upward scaling, even when reduced AMPAR activation is the indirect result of a spiking blockade. These findings have important implications for several other forms of transmission-dependent plasticity, including both Hebbian and homeostatic mechanisms.

Chapter 5

Discussion

In this dissertation, we have uncovered a critical role for AMPAergic neurotransmission in the induction of homeostatic synaptic scaling. Previously, cell-wide synaptic upscaling had been described as a phenomenon that was directly triggered by reductions in neuronal firing rate. However, we found that after chronic TTX or CNQX treatment, any reduction in spiking activity invariably led to upward synaptic scaling, without any apparent correlation between the severity of the reduction in spiking and the degree of scaling observed (Chapter 2). This suggested that spiking might not be triggering scaling, but instead was correlated to another variable that was directly triggering the plasticity. We then tested the hypothesis that AMPAergic transmission might be the activity signal monitored to induce upward synaptic scaling. To this end, we independently manipulated spiking and AMPAergic transmission in two ways. First, we blocked AMPARs while restoring normal levels or spiking using closed-loop optogenetic stimulation (Chapter 3). Secondly, we blocked spiking while partially restoring AMPAR activation using a pharmacological modulator of AMPARs (Chapter 4). In both cases, we found that reductions in AMPAergic transmission, rather than reductions in spiking activity, were directly driving the expression of upward synaptic scaling. While these findings challenge current models of cell-wide synaptic scaling based on spiking activity, they also provide new insight on potential interactions between scaling and other forms of transmission-dependent synaptic plasticity.

In this final chapter, I begin by discussing how a transmission-dependent model of synaptic scaling fits into the context of homeostatic and Hebbian plasticity. I then discuss how (and if) transmission-dependent synaptic scaling manifests in the living nervous system. Finally, I conclude with an outlook on how new tools for sensing and controlling various features of neural activity can help us understand the biological machinery that mediates different forms of plasticity in the nervous system.

5.1 Transmission-dependent synaptic scaling: relationships to other forms of synaptic plasticity

In our experiments, we used a highly-accessible culture system and global pharmacological perturbations to study synaptic scaling. This has allowed us to make a crucial discovery, that upward synaptic scaling is directly triggered by reduced AMPAR activation. However, synaptic scaling is only one of many plasticity mechanisms employed by neural circuits. In this section, we discuss relationships between transmission-dependent synaptic scaling and several other forms of plasticity.

5.1.1 Local homeostatic regulation of synaptic strength

An emerging theme in homeostatic plasticity is the idea that the strength of specific synaptic inputs can be regulated (reviewed in Vitureira et al., 2012; Lee et al., 2014). Like upward synaptic scaling, some forms of synapse-specific homeostatic plasticity are mediated by reduced neurotransmission and are expressed through an increase in synaptic AMPARs. For example, Hou et al. and Béïque et al. showed that chronic reductions in presynaptic release onto excitatory synapses caused a compensatory accumulation of GluA2-lacking AMPARs only at synapses experiencing reduced activation. Béïque et al. further showed that this synapse-specific increase in AMPAR content corresponded to greater AMPAergic currents as compared to neighboring

spines that had experienced normal synaptic activity. A similar increase in GluA2-lacking AMPARs was seen in specific dendritic regions perfused with an NMDAR antagonist during a global spiking blockade (Sutton et al., 2006). This insertion of GluA2-lacking receptors was mediated by local protein synthesis (Ju et al., 2004; Sutton et al., 2006), and could occur even if the dendrite was physically detached from the cell body (Ju et al., 2004), supporting the idea that somatic spiking activity was not involved in this plasticity.

There are several common features between synaptic scaling and synapse-specific AMPAR accumulation. First, both are triggered by reduced glutamatergic neurotransmission and do not require changes in postsynaptic spiking. Secondly, both are expressed through increases in AMPAergic synaptic strength mediated by accumulation of AMPARs (O'Brien et al., 1998; Ju et al., 2004; Hou et al., 2008; Béïque et al., 2011). Given these commonalities, we propose that upscaling could be a cell-wide manifestation of this synapse-specific plasticity. Therefore, upward synaptic scaling might be the result of network-wide application of pharmacological blockers. This would result in reduced AMPAergic transmission at all synapses and trigger synapse-specific AMPAR accumulation throughout the cell. This cell-wide accumulation of synaptic AMPARs would then take on the appearance of a global multiplicative increase in synaptic strength.

An additional link between synapse-specific AMPAR accumulation and cell-wide scaling is evidence that scaling also involves accumulation of GluA2-lacking AMPARs (Thiagarajan et al., 2002; Ju et al., 2004; Thiagarajan et al., 2005; Aoto et al., 2008; Groth et al., 2011; Lindskog and Li, 2010; Garcia-Bereguiain et al., 2013). Most cortical AMPARs contain the GluA2 subunit, and flux sodium and potassium ions upon ligand binding (Lu et al., 2009). However, AMPARs that lack the GluA2 subunit are also permeable to calcium. Therefore, the compensatory insertion of GluA2-lacking AMPARs suggests that local calcium signaling is also increased following

chronic reductions in transmission (Lee, 2012). Importantly, there is also evidence the scaling is also expressed through increases in GluA2-containing AMPARs (O'Brien et al., 1998; Wierenga et al., 2005; Cingolani et al., 2008). It has been suggested these differences may be due to the time course of expression of GluA2-lacking versus GluA2-containing receptors during homeostatic plasticity (Man, 2011). However, synaptic scaling has been observed in cultures from both GluA1 and GluA2 knockout mice (Altimimi and Stellwagen, 2013), suggesting that the requirement for a particular AMPAR subunit is flexible. It will be important to determine whether synapse-specific AMPAR accumulation can also occur in GluA1 and GluA2 knockout cultures, as this would shed light on how closely-related synaptic scaling is to this local form of homeostatic plasticity.

There are also homeostatic changes in AMPAergic synaptic strength that depend on presynaptic cell identity and are thus considered to be input-specific. Recent work in semi-mature hippocampal cultures (21^+ DIV) has highlighted this idea of segregated homeostatic mechanisms for different inputs (Kim and Tsien, 2008; Lee, 2012). In slice cultures, Kim and Tsien demonstrated differential regulation of different synapse types. In response to chronic treatment with TTX, Schaffer collateral synapses (CA3-CA1) showed homeostatic increases in mEPSC amplitude, while the mossy fiber synapses (dentate-CA3) showed homeostatic increases in mEPSC frequency. Meanwhile, recurrent synapses (CA3-CA3) showed no change in amplitude and a paradoxical decrease in mEPSC frequency (Kim and Tsien, 2008). In dissociated cultures, Lee et al. also observed differences in homeostatic regulation of synapses onto CA3 neurons and found spatially-segregated populations of inputs that express increases in synaptic strength. Specifically, only proximal inputs (primarily dentate-CA3 synapses) displayed increases in sucrose-evoked EPSC amplitude, but distal inputs (primarily CA3-CA3 synapses) showed no change (Lee et al., 2013b). Although the two studies suggest different expression mechanisms for reg-

ulating synapses onto CA3 neurons, the general framework is similar. Mossy fiber inputs exhibit clear homeostatic regulation of synaptic function, while recurrent CA3-CA3 synapses do not. In our dissociated cortical cultures, we also recorded excitatory inputs onto pyramidal cells. However, we did not distinguish between pyramidal cells from different layers, nor did we monitor the types of excitatory inputs that contribute to our mEPSC distribution. However, our observation that multiplicative synaptic scaling occurred suggests that all glutamatergic inputs onto the cells we recorded from were influenced in a uniform manner. A likely reason that we observed cell-wide scaling is because we conducted our experiments in younger cultures ($\sim$10-13 DIV). In fact, Lee et al. observed cell-wide increases synaptic strength for cultures during the second week *in vitro*, and only observed input-specific regulation during the fourth week and beyond. It would be interesting to see whether scaling could persist in our cultures at a more mature stage, perhaps using cells derived from a transgenic animal with layer-specific expression of a reporter protein (to assess inputs onto specific cell types) and/or layer-specific expression of ChR2 (to activate specific inputs onto a cell). However, a stronger approach would be to perform these experiments in neural preparations where the overall cytoarchitecture is better preserved. Indeed, recent studies have begun to address the importance of the how different inputs, cortical layers, and developmental ages affect the expression of scaling *in vivo* (discussed in Section 5.2).

Overall, there are many parallels between the synapse- and input-specific forms of plasticity discussed above and cell-wide synaptic scaling. The possibility that upscaling is equivalent to synapse-specific homeostatic plasticity raises questions about its relationship to Hebbian plasticity, where the strength of individual synapses are adjusted in a competition-based manner, widely believed to underlie memory encoding and storage. A cell-autonomous model of synaptic scaling provided a potential solution for stabilizing a neuron's activity levels without disrupting the relative synaptic

strengths established through Hebbian plasticity. Conversely, a synapse-autonomous model (where scaling emerges when activity at all synapses is similarly disrupted) suggests that information encoded by the relative weights of individual synapses is vulnerable to interference from homeostatic modifications. Importantly, our work shows that the AMPAR activation is monitored to induce upward scaling, but it does not distinguish between the possibilities of this signal being monitored through individual synapses or dendrites, an integrated measure of synaptic activity throughout the cell, or non-synaptic AMPARs on neurons and glia. Future work will need to dissect out these possibilities in order to better understand how AMPAR activation is sensed by synapses, neurons, and/or glia to produce cell-wide increases in synaptic strength.

5.1.2 Hebbian plasticity

An important feature of synaptic scaling is that synapses are stabilized in a coordinated fashion throughout a neuron, so as to preserve the relative distribution of synaptic strengths established by Hebbian mechanisms. This feature is particularly attractive as it suggests that homeostatic and Hebbian regulation of synaptic strength can operate independently without erasing changes imposed by one another. A model for scaling triggered by changes in neuronal firing rate was suggested as a computationally tractable way to coordinate compensatory cell-wide changes in synaptic strength (Turrigiano et al., 1998; Abbott and Nelson, 2000). However, our finding that upward synaptic scaling is directly triggered by reduced neurotransmission, and our suggestion that it could be a global manifestation of local homeostatic mechanisms, complicates that idea of a cell-wide coordinator for synaptic strength. While it has been argued that a transmission-dependent homeostatic regulation of synaptic strength might antagonize Hebbian learning (Turrigiano, 2012), alternative models of the synergistic coordination between homeostatic and Hebbian plasticity are gaining

traction (Rabinowitch and Segev, 2008; Vitureira and Goda, 2013). Although we focus our discussion here on synaptic mechanisms, it is important to note that modern views of memory storage encompass both synaptic and non-synaptic forms of information encoding (Daoudal and Debanne, 2003; Zhang and Linden, 2003; Mozzachiodi and Byrne, 2010).

AMPAergic transmission directly induces upward scaling, but where transmission is monitored is not clear. In discussing the relationship between Hebbian plasticity and synaptic scaling, we entertain the possibilities that AMPAergic transmission is monitored in a cell-wide, dendrite-wide, or synapse-specific manner.

5.1.2.1 Hebbian plasticity and cell-wide homeostasis

One interpretation of our finding that upward synaptic scaling is dependent on reduced AMPAR activation is that neurons have a mechanism for integrating total synaptic activity, and subsequently increasing synaptic strength to compensate for reductions in excitatory input. Therefore, if a subset of inputs underwent synaptic depression (and therefore experienced reduced AMPAR activation), this could trigger homeostatic increases in synaptic strength in the rest of the inputs. This phenomenon would be functionally similar to a previously reported form of plasticity where low-frequency stimulation was used to induce LTD at specific synapses, and concomitant heterosynaptic LTP was observed at unstimulated inputs onto the same cell (Royer and Paré, 2003; Wöhrl et al., 2007). Because this particular form of heterosynaptic LTP accompanies homosynaptic LTD, it takes on a compensatory role—by strengthening the unstimulated inputs, the total synaptic input onto the cell is theoretically preserved at a setpoint. Although synaptic scaling and heterosynaptic LTP differ significantly in terms of time course, their overlapping functional consequences and their dependence on reduced neurotransmission suggest redundancy in short-term and long-term mechanisms for stabilizing synapses following Hebbian plasticity.

5.1.2.2 Hebbian plasticity and dendrite-wide homeostasis

In addition to cell-wide monitoring of synaptic activity, it has been proposed that dendrites monitor total synaptic input and can homeostatically respond to LTP or LTD at individual synapses (Rabinowitch and Segev, 2008). For instance, activity at a single synapse undergoing Hebbian plasticity could be detected by neighboring synapses, which subsequently undergo compensatory changes in synaptic strength in order to maintain overall dendritic excitability (Rabinowitch and Segev, 2008). Supporting this hypothesis, a recent study showed that motor skill learning promoted the formation of an enlarged presynaptic input spanning pairs of dendritic spines onto cerebellar Purkinje cells; this change was accompanied by a shrinkage of spines at excitatory synapses on the same dendrite (Lee et al., 2013a). Because spine size is correlated with synaptic AMPAR content (Matsuzaki et al., 2004), this change is indicative of a reduction in synaptic strength, which could serve to counterbalance the increased synaptic activity at adjacent inputs in order to maintain overall excitatory input to the dendrite. This transmission-dependent compensatory plasticity is reminiscent of synaptic scaling, but operating in a dendrite-wide, rather than a cell-wide, manner. Additional work will need to be done to understand whether the temporal expression and electrophysiological signatures of synaptic scaling are similar to this compensatory dendritic plasticity that follows Hebbian learning. Still, a mechanism for maintaining overall synaptic strength within an individual dendrite complements the idea that memory engrams can be stored in groups of clustered synapses, rather than across all inputs onto a cell (Govindarajan et al., 2006; Larkum and Nevian, 2008; Winnubst and Lohmann, 2012). Importantly, the possibility of a coordinated homeostatic change in synaptic strength throughout a dendrite requires that total synaptic activity can somehow be monitored. However, given the rich literature on dendritic integration (Yuste and Tank, 1996; Magee, 2000; London and Häusser, 2005; Sprus-

ton, 2008), the idea that dendrites can monitor their total synaptic activity seems quite plausible.

5.1.2.3 Hebbian plasticity and synapse-specific homeostasis

Finally, rather than a cell-wide or dendrite-wide signal for triggering scaling, the simplest solution could be that synapses monitor and homeostatically regulate their own levels of neurotransmission, and that scaling is merely a cell-wide manifestation of a synapse-specific plasticity. Of note is that anti-Hebbian mechanisms for regulating synaptic strength have previously been proposed for maintaining synaptic efficacy between and within dendrites (Goldberg et al., 2002; Rumsey and Abbott, 2004). However, what distinguishes the synapse-specific forms of homeostatic plasticity that we have discussed from such anti-Hebbian mechanisms is their slow dynamics. Because of these dynamics, local homeostatic mechanisms are well-suited to provide a running-average of the history of an individual synapse. For instance, the synapse-specific accumulation of of GluA2-lacking AMPARs serve as a molecular tag for chronic reductions in synaptic activity. The calcium permeability of GluA2-lacking AMPARs also allows for local biochemical signal to mark the deprived synapse. These molecular and biochemical signatures could define a synapse's state. An innovative computational model of how information is encoded in neural circuits suggests that synapses can take on numerous different states ranging from highly plastic to highly static, and transitions between these synaptic states can help prolong memory storage (Fusi et al., 2005). In this sense, homeostatic mechanisms such as chronic reductions in glutamatergic activity facilitate transitions from one state to another. While neurotransmission has been suggested as a primary source of shifting between postsynaptic states (Coba et al., 2009), there are likely other players. For instance, sustained release of glial TNF-α, which has been shown to mediate cell-wide synaptic scaling (Stellwagen and Malenka, 2006), has also been suggested as a perturbation that can

shift synapses into highly plastic states (Steinmetz and Turrigiano, 2010). In this sense, homeostatic synaptic plasticity could serve as a form of metaplasticity, which helps to enhance or hinder Hebbian potentiation or depression.

5.1.3 Metaplasticity

Metaplasticity, in its original description, is a "persistant synaptic plasticity... induced by synaptic or cellular activity [and expressed] as a change in the ability to induce subsequent synaptic plasticity" (Abraham and Bear, 1996). The idea that homeostatic synaptic plasticity functions as form of metaplasticity is particularly intriguing. A historically popular instantiation of metaplasticity is the Bienenstock-Cooper-Munro (BCM) model of synaptic modification based on a sliding threshold for the induction of LTP and LTD (Bienenstock et al., 1982; Bear et al., 1987). Like early models of multiplicative synaptic scaling (Oja, 1982; Miller and MacKay, 1994), the BCM model was proposed as a way to stabilize synaptic weights during Hebbian learning (Cooper and Bear, 2012). An early example of the BCM model operating *in vivo* was presented in Kirkwood et al., 1996, which showed that visual experience could alter the capacity of layer 3 neurons in primary visual cortex to undergo LTP and LTD. Using a standard low-frequency stimulation protocol (1 Hz), the authors showed that dark-reared animals underwent significantly attenuated LTD compared to light-reared animals (Kirkwood et al., 1996). Meanwhile, high frequency stimulation (10 Hz) produced significantly enhanced LTP in dark-reared animals compared to light-reared animals (Kirkwood et al., 1996). These results suggested the that chronically reduced visual experience shifted the threshold for synaptic modification to favor the induction of LTP over LTD. This form of metaplasticity has a distinctly homeostatic flavor, as the shift toward a state favoring LTP might act to compensate for sensory deprivation. Importantly, chronic dark rearing has also been shown to trigger synaptic scaling in layer 2/3 of visual cortex (Desai et al., 2002; Goel et al., 2006), and is

characterized by accumulation of GluA2-lacking AMPARs (Goel et al., 2011). While the shift in the LTP/LTD stimulation rate threshold expressed through insertion of NMDARs (Quinlan et al., 1999; Philpot et al., 2003), it is not clear whether reduced AMPAR activation plays a role in triggering deprivation-induced metaplasticity as it does in upward scaling. While this question cannot be addressed in our simple culture system, recent studies *in vivo* are beginning to identify overlapping features of two forms of plasticity (Huang et al., 2012; Guo et al., 2012). It will be interesting to see whether upward scaling and deprivation-induced metaplasticity act in parallel, or are somehow coordinated, in their contributions to shifting in cortical excitability.

An interesting example of homeostatic synaptic plasticity functioning as a form of metaplasticity is evident in the formation of silent synapses. These synapses are described as silent because they only contain NMDARs, but not AMPARs, and thus are thought to be functionally silent due to lack of local AMPAR-mediated depolarization. Using mature hippocampal cultures, Nakayama et al. showed that chronic TTX treatment led to the formation of GluN2B-containing silent synapses. Upon relief from TTX treatment, which others have shown leads to synchronized bursting activity (Ramakers et al., 1990; Kamioka et al., 1996), AMPARs were rapidly incorporated into these newly-formed silent synapses (Nakayama et al., 2005). This rapid conversion of silent synapses to functional synapses suggests that a rapid form of plasticity, such as LTP invoked by highly-synchronized spiking activity, could have mediated AMPAR accumulation at silent synapses. In addition, the formation of silent synapses by GluN2B is particularly interesting, as this subunit is associated with improved synaptic potentiation and learning (Tang et al., 1999), as well as impaired synaptic depression (Liu et al., 2004). A recent study in hippocampal slice cultures has shed light on how synaptic scaling and the homeostatic formation of silent synapses contributes to Hebbian plasticity (Arendt et al., 2013). The authors first showed that LTP at Schaffer collateral synapses (CA3-CA1) was significantly

enhanced in cultures chronically pre-treated with TTX. Consistent with previous observations, the authors found that chronic TTX treatment led to AMPAergic scaling at existing synapses (e.g. Turrigiano et al., 1998) as well as the formation of silent synapses containing only NMDARs (Nakayama et al., 2005). Subsequent LTP led to the insertion of AMPARs, thus unsilencing the newly-formed synapses. Therefore, LTP in TTX-treated cultures both strengthened the scaled up synapses and converted silent synapses to functional synapses (Arendt et al., 2013). Meanwhile, LTP in untreated cultures only strengthened the existing unscaled synapses (Arendt et al., 2013). Together, these results provide evidence that synaptic scaling and other homeostatic mechanisms can tune the capacity for a synapse to undergo subsequent LTP. The findings support the idea of homeostatic synaptic plasticity can function as a form of metaplasticity to shift synapses into states that promote Hebbian learning.

5.2 Synaptic scaling in the living nervous system

An attractive feature of synaptic scaling is that all synapses onto a cell can be globally tuned to promote the proper balance of excitation and inhibition within a cell or circuit. However, in Section 5.1.1, we suggested that multiplicative synaptic scaling may be the consequence of local synaptic compensations occurring throughout a neuron due to global pharmacological perturbations. We also discussed how different homeostatic rules might regulate different synapse types, and how a global scaling rule could be insufficient to account for homeostatic changes in mature systems. In light of this, it seems prudent to ask whether synaptic scaling has any relevance beyond our simple cortical culture. In this section, we argue that synaptic scaling plays an important role in the living nervous system. We discuss some of the issues with multiplicative scaling in the context of input-specificity and developmental stage.

5.2.1 Sensory systems

Two groups have identified synaptic scaling *in vivo* in layer 2/3 (L2/3) of primary visual cortex (V1) following visual deprivation (Desai et al., 2002; Goel and Lee, 2007). The presumed mechanism has been that reducing sensory experience will eventually reduce spiking in sensory cortex, and thus trigger multiplicative changes in synaptic strength. This concept is complicated by the fact that perturbations used to reduce visual experience do not change spontaneous firing rates in the lateral geniculate nucleus (LGN) of the thalamus (Linden et al., 2009). In fact, monocular TTX injection, which was shown to induce scaling in V1 (Desai et al., 2002), actually increases the LGN bursting activity (Linden et al., 2009). These results are somewhat counterintuitive, as increased LGN bursting would imply synchronized output to V1, and thus produce an overall increase in firing rates. This in turn might be expected to produce downscaling, rather than upscaling, of excitatory inputs. Meanwhile, eyelid suture, which was shown to have no effect (He et al., 2012) or decrease (Maffei and Turrigiano, 2008) mEPSC amplitude, reduces LGN bursting (Linden et al., 2009). These results are similarly paradoxical and are reminiscent of a Hebbian-like plasticity. Our finding that synaptic scaling depends on AMPAergic transmission suggests that overall firing rates in V1 do not matter, but instead glutamatergic inputs onto L2/3 cells. These inputs are primarily inputs from layer 4 (L4) or recurrent connections from other L2/3 cells. New studies are beginning to monitor activity levels in V1 (Hengen et al., 2013; Keck et al., 2013), and suggest that spiking activity in L2-4 are reduced following monocular deprivation (Hengen et al., 2013). The reduced spiking in L2-4 cells suggests reduced glutamatergic output from these cells. This is consistent with our model that activity in presynaptic inputs from L2/3 and L4 cells would need to be uniformly reduced to trigger cell-wide multiplicative increases in synaptic strength in L2/3 cells. Although the reduced firing rate could in theory drive scaling, this would require knowledge of firing rates in L2/3 alone. However,

the authors only provide pooled data from layers L2-4 (Hengen et al., 2013), so it is not clear how these changes in firing rate are distributed among layers.

Importantly, there is evidence that the homeostatic response to visual deprivation depends on both development age and cortical layer. For example, deprivation-induced scaling was observed in L2/3 in young animals (P21), but in older animals (P90$^+$) the increase in mEPSC was no longer multiplicative (Goel and Lee, 2007). Meanwhile, very young animals (P16) showed scaling in L4 (Desai et al., 2002) and non-multiplicative increases in mEPSC amplitude in L6 (Petrus et al., 2011), but neither of those changes persisted beyond P21. Finally, L5 neurons showed changes in intrinsic excitability following deprivation in young animals (P19; Nataraj et al., 2010), but showed synaptic scaling in older animals (P40$^+$; Keck et al., 2013). These age- and layer-specific differences likely reflect the non-uniformity of input types onto each cell. Segregating between these different sets of glutamatergic inputs is challenging, but may help address whether a scaling-like rule can be applied to a group of inputs. One potential solution could be to use a transgenic animal expressing ChR2 only in specific layers. This would allow for comparison of evoked currents from different sets of presynaptic inputs.

Evidence that different inputs can be differentially regulated has been shown in the tadpole optic tectum, a region that integrates multi-modal sensory information (Deeg and Aizenman, 2011). Two days of dark exposure caused compensatory increases in evoked unitary EPSCs only from inputs in the visual pathway (Deeg and Aizenman, 2011). Meanwhile, providing a 2-day somatosensory vibration stimulus caused compensatory decreases in evoked unitary EPSCs only from inputs in the mechanosensory pathway (Deeg and Aizenman, 2011). This input-specific regulation of synaptic strength has some commonality with upscaling in that both are engaged by altered neurotransmission. Further, it is possible that a scaling-like rule oper-

ate within groups of presynaptic inputs, rather than across all inputs, as has been suggested by work in hippocampal slice cultures (Kim and Tsien, 2008).

5.2.2 Hippocampus

While there is evidence for scaling in sensory cortex following deprivation, there is no evidence for multiplicative increases in synaptic strength in the hippocampus *in vivo*. Still, there are indications of possible homeostatic mechanisms. Echegoyen et al., 2007 showed the chronic release of TTX into the hippocampus of juvenile rats led to increases in mEPSC and mIPSC amplitude, mEPSC frequency, and cellular excitability. With the exception of increases in mIPSC amplitude, all of these changes would be thought to restore excitability to the circuit through presynaptic, postsynaptic, and intrinsic changes. Meanwhile, the same perturbation in adults led to increases in mIPSC amplitude, mIPSC frequency, and cellular excitability (Echegoyen et al., 2007). These changes are more difficult to interpret as homeostatic. Notably, for TTX treatment in both juvenile and adult animals, Schaffer collateral synapses (CA3-CA1) showed enhanced potentiation (Echegoyen et al., 2007), suggesting a possible link to *in vitro* findings that silent synapse formation during TTX treatment mediated enhanced LTP following the perturbation (Arendt et al., 2013). Overall, however, these observations are difficult to relate to transmission-dependent synaptic scaling because they are not accompanied by multiplicative changes in mEPSC amplitude that have been seen in CA1 neurons in hippocampal cultures (Burrone et al., 2002; Kim and Tsien, 2008). Although additional studies will be necessary to verify these findings, the reduced presence of homeostatic regulation in the hippocampus could explain why is it a common epileptic seizure focus. Further, the differences in plasticity mechanisms observed in the hippocampus versus cortex may underlie their different functional roles in information encoding, consolidation, storage, and retrieval.

5.2.3 Motor systems

Although studying plasticity *in vivo* has its caveats, some of the cleanest experiments in homeostatic plasticity have been conducted in the spinal cord of living chick embryo. In this system, spontaneous network activity in the developing spinal cord drives bouts of embryonic limb movements. Because embryonic development is not affected by placing a small opening the egg shell, limb movements can be monitored throughout gestation as a proxy for activity in the spinal network. This feature allows for monitoring network activity during perturbations that trigger homeostatic plasticity. For instance, chronic blockade of spiking using the voltage-gated sodium channel antagonist, lidocaine, completely abolished limb movements and led to upward multiplicative scaling of both AMPAergic and GABAergic inputs onto motor neurons (Gonzalez-Islas and Wenner, 2006). Importantly, GABAergic transmission is excitatory at embryonic stages, so upward GABAergic scaling is homeostatic. Chronic blockade of excitatory GABA$_A$ receptors using gabazine produced the same scaling response as lidocaine (Wilhelm and Wenner, 2008). However, unlike lidocaine, gabazine initially blocked limb movements, but these movements began to recover within an hour and recovered control values by ∼12 hours (Wilhelm and Wenner, 2008).

The observation that both a spiking blockade and excitatory transmission blockade trigger the same amount of scaling, despite their differential effects on activity (limb movements), parallels what we have seen in cortical cultures following TTX and CNQX treatment (Chapter 2). This suggests that a transmission-dependent model of scaling could also operate *in vivo* to regulate excitatory synaptic strength (Wilhelm and Wenner, 2008). However, the capacity for blockade of GABAergic transmission to produce changes in AMPAergic synaptic strength suggests that a global integrated measure of GABAergic activity triggers scaling throughout the cell. Alternatively, AMPAergic scaling might not be triggered by reductions in GABAergic transmission, but may be indirectly triggered by the expression of GABAergic scaling. Because the

expression of GABAergic and AMPAergic scaling are mediated by different mechanisms (Gonzalez-Islas et al., 2010; Garcia-Bereguiain et al., 2013; Lindsly et al., 2014), the idea that they may have separate triggers seems likely. To dissect out the different possibilities, it will be important to see whether GABAergic scaling can be achieved in isolation from AMPAergic scaling, and vice versa. In all cell types discussed in previous sections, excitatory inputs were only glutamatergic, so teasing out the rules governing different subpopulations of excitatory inputs has been challenging. Because excitatory GABAergic and AMPAergic currents can be recorded simultaneously and easily separated based on mPSC kinetics, this system provides a unique opportunity to study differential regulation of two sets of excitatory inputs onto the same cell. This may help to shed light on input-specific rules employed in other cell types.

5.3 Future Outlook

In our study, we used substrate-integrated micro-electrode arrays to continuously monitor spiking activity throughout perturbations that trigger homeostatic plasticity. This allowed us to correlate the degree of scaling with changing in firing rate, create a controller that clamped spiking activity to specific target firing rates, and ultimately demonstrate the firing rate is not the activity signal monitored to trigger homeostatic synaptic scaling. Because of the large membrane depolarization and well-established dynamics of action potentials, they are particularly easy to measure and over long periods of time. However, as we have shown, neural circuits monitor other features of activity (e.g. AMPAR activation), and it will be important to have a readout for these variables to truly understand their role in triggering plasticity. In this section, I discuss new approaches in neuroscience research that have the potential to revolutionize the study of synaptic plasticity.

5.3.1 Monitoring and manipulating neurotransmission

In recent years there has been an explosion of genetically-targetable optical tools for monitoring and manipulating various aspects of neural activity. Of particular relevance to us are those relating to neurotransmission. Several studies in homeostatic plasticity have been particularly progressive in their use of chronic optical manipulations to dissect out sensing and expression mechanisms (Sutton et al., 2006; Ibata et al., 2008; Goold and Nicoll, 2010; Hou et al., 2011; Makino and Malinow, 2011; Lindsly et al., 2014). Because changes in AMPAR accumulation are a cornerstone in the expression of upward synaptic scaling, monitoring AMPARs is of critical importance. Recently, a set of genetically-engineered AMPAR subunits tagged with Super Ecliptic pHluorin (SEP), a pH-sensitive green fluorescent protein (GFP) were introduced (Makino and Malinow, 2011). The tagging of the GluA1, GluA2, and GluA3 subunits with SEP allows them to fluoresce when inserted into the membrane (Makino and Malinow, 2011), providing a powerful tool for tracking insertion and removal of AMPARs.

Another set of optical tools under development are fluorescent glutamate sensors. Several fluorescent glutamate indicators have been previously reported, but their use has been limited by the requirement for Förster resonance energy transfer (FRET)-based imaging (Okumoto et al., 2005; Hires et al., 2008). A single-wavelength high signal-to-noise glutamate sensor, iGluSnFR, has recently been published (Marvin et al., 2013). The ability to image on a single-wavelength is particularly attractive because it opens up spectral bandwidth for imaging or optically-activating other probes. The authors provide examples of concurrent calcium and glutamate imaging, and also correlate individual EPSP amplitudes with glutamate fluorescence measured locally at individual spines (Marvin et al., 2013). An exciting possibility is that iGluSnFR imaging could be combined with GluA1-SEP and/or GluA2-SEP imaging. This would allow for concurrent monitoring of glutamate release and subsequent receptor

trafficking, providing a powerful tool for quantifying how changes in neurotransmission trigger AMPAR accumulation during synaptic scaling or other forms of plasticity. In addition, concurrent glutamate and AMPAR imaging would allow monitoring of spillover glutamate onto extrasynaptic and glial AMPARs, which could be part of the sensing machinery that induces scaling. Further, combining this with closed-loop optogenetic stimulation to depolarize or hyperpolarize an individual of presynaptic input could provide another way to test the previously-discussed theory of homeostatic dendritic equalization. Currently iGluSnFR and GluA-SEP are both GFP-based and thus could not be imaged concurrently, but as the demand for multiplex imaging becomes greater, we anticipate that red-shifted sensors will become available.

Optical strategies for manipulating synaptic activity are also beginning to surface. We briefly mentioned the potential for optogenetic stimulation of presynaptic neurons as a way to influence neurotransmitter release. Specifically, depolarizing or hyperpolarizing opsins could be expressed in the cell body to manipulate spiking activity, in turn enhancing or inhibiting transmitter release (Schoenenberger et al., 2011). However, this requires coupling of presynaptic spiking with neurotransmitter release. Therefore, using somatic depolarization or hyperpolarization to manipulate transmitter release opens the door for other spike-dependent signals to influence subsequent plasticity. A new tool has been introduced to specifically inhibit neurotransmitter release by hijacking the SNARE machinery (Lin et al., 2013). While this tool has not been available long enough for extensive validation in the neuroscience literature, the the development of a strategy for manipulating transmitter release, independent of neuronal spiking, is a forward-thinking approach with great potential. For instance, combining this tool with glutamate imaging would allow the for closed-loop optical control of neurotransmitter release.

Because we have found that AMPAR activation is critical for synaptic scaling, an interesting possibility is that receptor activation could be directly manipulated

without requiring presynaptic release, and there is recent work suggesting that this has a promising future. Several years ago, the ligand-binding properties of the GluK2 subunit of the kainate receptor were engineered to include a "ball-and-chain" ligand that is bound upon activation with UV light, and is unbound upon exposure to green light (Volgraf et al., 2006). When expressed in neurons, this light-gated glutamate receptor (LiGluR) could be optically activated to produce reliable action potentials Szobota et al. (2007). Currently, LiGluR does not have mechanism for being localized to the synapse, so its use is limited to act as a cation channel that can be used to elevate neuronal activity. However, a hope for LiGluR and future light-gated gluta-mate receptor variants is that existing machinery that locates endogenous synaptic receptor subunits can be hijacked to localize LiGluRs. This could allow us to test the subtleties of neurotransmitter receptor binding in triggering synaptic scaling.

5.3.2 Monitoring and manipulating calcium

The primary conclusion of this dissertation has been that reductions in AMPAR acti-vation, rather than reductions in firing rate, trigger upward synaptic scaling. In each of our manipulations of spiking and AMPAergic transmission, the uncertainty about exactly how our manipulations impact calcium dynamics has been the "elephant in the room". By reinstating bursts during CNQX treatment using closed-loop optogenetic stimulation, we strongly suspect that somatic calcium dynamics are largely restored, as somatic calcium influx is tightly-correlated to network-wide bursts (Murphy et al., 1992; Jimbo et al., 1993; Opitz et al., 2002; Minerbi et al., 2009). Conversely, by blocking spiking activity with TTX, we believe that there is very little calcium influx at the soma, even when AMPAR activation is partially restored using CTZ. Although we have ideas about how calcium might be affected in the cell body, we have much less certainty about calcium dynamics in the dendrites or surrounding glia. While monitoring calcium during our manipulations may help correlate changes in calcium

to subsequent plasticity, we propose that true understanding of the role of somatic and dendritic calcium signaling in synaptic scaling requires tight control of calcium dynamics.

The toolset of calcium indicators and activators is rapidly expanding, and is significantly more developed than the aforementioned tools for sensing/manipulating neurotransmission. This presents an exciting possibility that calcium could be controlled using real-time feedback. For monitoring calcium levels, modern genetically-encoded calcium indicators (GECIs) provide high signal-to-noise readout of calcium in targeted cell populations (Akerboom et al., 2013). Manipulating calcium is somewhat less developed, but potential tools include CaTCh (Kleinlogel et al., 2011), a calcium-permeable variant of ChR2, or the aforementioned LiGluR, which has been shown to flux slightly more calcium than CaTCh (Li et al., 2012). Thus, stimulation of CaTch and LiGluR could be delivered contingent on GECI fluorescence in order to maintain a target level or pattern of calcium. This strategy could be used at the soma, or perhaps more powerfully in individual dendritic regions. Another possibility would be to restore normal calcium dynamics in astrocytes during a chronic TTX or CNQX treatment. Finally, combining closed-loop control of calcium with AMPAR imaging would enable direct measurements of how global and local calcium dynamics regulate AMPAR accumulation during scaling and other forms of synaptic plasticity.

5.3.3 Monitoring and manipulating activity in vivo

Ultimately, the relevance of synaptic scaling in the nervous system lies in how it is triggered and expressed in the living nervous system. Some of the optical tools we have suggested above might be impractical for *in vivo* experimentation, though the demand for delivering light and/or measuring optical activity in awake, behaving mammals continues to drive innovative solutions to these challenges (Alivisatos et al., 2013; Deisseroth and Schnitzer, 2013). These technologies will invariably be useful

for studying the activity patterns in thalamus, sensory cortex, and hippocampus that lead to homeostatic synaptic plasticity.

While optical sensors and activators provide an exciting new avenue for reading out neural activity, it is important to take a step back from these research trends and consider how they can best advance a scientific question. For example, the embryonic chick limb movements provide an excellent readout for spontaneous network activity. However, a strategy for driving limb movements using optogenetics would provide a useful tool for potential closed-loop regulation of network activity. Indeed, the the first report of neurons transfected with ChR2 *in vivo* were in the chick embryo spinal cord (Li et al., 2005), and subsequent work has shown that this can be used to drive embryonic limb movements at normal rates, even in the presence of excitatory $GABA_AR$ blockade (Kastanenka and Landmesser, 2010). Because we have shown in culture that reduced excitatory transmission triggers scaling even when spiking is restored, we would predict that reduced excitatory GABAergic transmission would trigger scaling in motor neurons even when network-driven limb movements were restored. This experiment is a natural extension of our work. Even if the results do not match our finding in cortical culture, this experiment would provide the first *in vivo* evidence of a direct trigger for synaptic scaling.

5.4 Concluding remarks

Synaptic plasticity is a field that has garnered sustained interest since the original description of LTP (Bliss and Lomo, 1973). Over the past 40 years the number of synaptic plasticity mechanisms have extended far beyond hippocampal LTP, to include a breadth of Hebbian, homeostatic, and metaplastic strategies distributed throughout the brain and spinal cord. This growth has been paralleled by the advancement of genetic, electrophysiological, computational, anatomical, pharmacological, and optical tools for studying these plasticity mechanisms. Both the challenge and promise of

future research lies in leveraging these approaches to maximize our understanding of the nervous system. In this dissertation, I have tried to hold true to these principles by using an array of modern neuroscience tools to answer a basic scientific question about how synapses are homeostatically regulated in neural circuits. From this work, I have identified a critical role for excitatory neurotransmission in stabilizing synaptic function. By advancing current knowledge on how stability is maintained through synaptic plasticity, I hope to contribute to the a broader understanding of how neural circuits respond to both traumatic injury and innocuous environmental influences to promote healthy function in the nervous system.

Appendices

SPIKE SORTING

One challenge we faced in this work was to find an appropriate strategy for sorting detected spikes into defined extracellular units. We began with a manual sorting strategy but found that it took nearly a month to sort 48 continuous hours of spiking data from 59 electrodes. We therefore tested two different sorting algorithms. Here we discuss the results of sorting manually versus using an unsupervised strategy. We conclude by summarizing how to use unsupervised spike sorting to make fair comparisons between our data sets.

A.1 Approach

In this analysis, we used a spiking data collected from one of our prototypical experiments where CNQX is added to a culture for 24 hours. The network firing rate for this recording is shown in Fig. 3.7 (top panel).

In this experiment, we began recording from the culture at 12DIV. CNQX was added to the culture at 13DIV (at zero hours), and we continued to record from the culture for 24 hours (until 14DIV). We first sorted the data using the `LineSort`, a method for manually classifying each waveform as part of an extracellular unit available through the SqueakySpk[1] MATLAB class. Given that the length of our recordings, there were hundreds of thousands of spikes per channel, and 59 channels,

---

[1] SqueakySpk codebase: `code.google.com/p/squeakyspk`

Table A.1: Post-hoc tests: comparing raw unit firing rates for difference spike sorting strategies

Post-Hoc Tests	p-value	
	Pre-treatment	CNQX
Medians of raw firing rates		
Overall[†]	$< 10^{-35}$	$< 10^{-39}$
Manual vs. Wavelet[‡]	$< 10^{-23}$	$< 10^{-22}$
Manual vs. PCA[‡]	$< 10^{-21}$	$< 10^{-25}$
Distributions of raw firing rates		
Manual vs. Wavelet[§]	$< 10^{-21}$	$< 10^{-21}$
Manual vs. PCA[§]	$< 10^{-24}$	$< 10^{-25}$
Wavelet vs. PCA[§]	0.9816	0.9321

[†]Kruskal-Wallis test, $\alpha=0.05$
[‡]Wilcoxon rank-sum test, $\alpha=0.017$ (adjusted)
[§]Kolmogorov-Smirnov test, $\alpha=0.05$

so manual sorting of all the data was not a viable option for every recording. Therefore, we next tried two unsupervised spike sorting strategies that were also available on SqueakySpk, and compared these to our manual approach. We used the `WaveClus` method in SqueakySpk to generate units using wavelet transform and principal component analysis (PCA) strategies. Our goal was to determine what features of unit spiking activity are not biased based on a sorting strategy.

A.2 Analysis

Following spike sorting using each strategy, we computed the firing rate of individual units before and during CNQX treatment. We assessed whether these firing rates were conserved between different sorting strategies, and compared the three distributions in 4 primary ways. First, we compared the median unit firing rates during the predrug and CNQX for the three distributions. Median firing rates were significantly different between manual and unsupervised methods. Secondary, we compared the

Table A.2: Post-hoc tests: comparing normalized unit firing rates for difference spike sorting strategies

Post-Hoc Tests	p-value
Medians of raw firing rates	
Overall[†]	0.4318
Manual vs. Wavelet[‡]	0.3642
Manual vs. PCA[‡]	0.2682
Distributions of raw firing rates	
Manual vs. Wavelet[§]	0.5768
Manual vs. PCA[§]	0.4872

[†]Kruskal-Wallis test, $\alpha=0.05$
[‡]Wilcoxon rank-sum test, $\alpha=0.017$ (adjusted)
[§]Kolmogorov-Smirnov test, $\alpha=0.05$

distribution of unit firing rates during pre-drug and during CNQX, and again found the unsupervised strategies failed to reproduce the manual distribution. These two sets of tests are summarized in Table A.1.

Because of the large disparity in the number of units detected by manual versus unsupervised methods, the raw firing rates may not be the best way to examine spiking data. We next normalized each unit's firing rate to its own pre-drug firing rate, and repeated the comparisons between manual and unsupervised methods. By normalizing the data, we now saw the the median and distribution of normalized unit firing rates were are statistically indistinguishable between manual and unsupervised strategies. These results are summarized in Table A.2.

A.3 Conclusion

We conclude that unsupervised strategies for sorting spikes may underestimate the total number of units, and thus skew the raw firing rate distribution. However, if firing rates are normalized to pre-treatment levels, unsupervised strategies can be

used to accurately measure changes in unit firing rate. Therefore, in Chapter 3, we only analyze individual unit firing rate following normalization of each unit to its own pre-treatment firing rate. We did not observe any significant difference between the Wavelet and PCA strategies for our test data set, suggesting that either could work well for our purposes.

Compensatory changes in NMDA and GABA synaptic currents help recover synchronous activity during chronic AMPAergic blockade

B.1 Motivation

In Chapter 2 we observed that network-wide bursting recovered during AMPAergic blockade. This was puzzling because NMDARs are thought require depolarization to be activated, and $GABA_A$Rs are thought to mediate inhibitory transmission. Although increases in intrinsic excitability were likely occurring, synchronous activity in the network suggests the persistence of synaptic coordination. Importantly, we do not believe that the recovery of bursting is due to our drug wearing off, as bursts continue when CNQX is replenished at 24 hours (Fig. B.1). Although most of our previous analysis was isolated to the second week *in vitro*, we have actually treated cultures of various ages with CNQX, ranging from 7-28 DIV, and all show some degree of recovery in bursting activity.
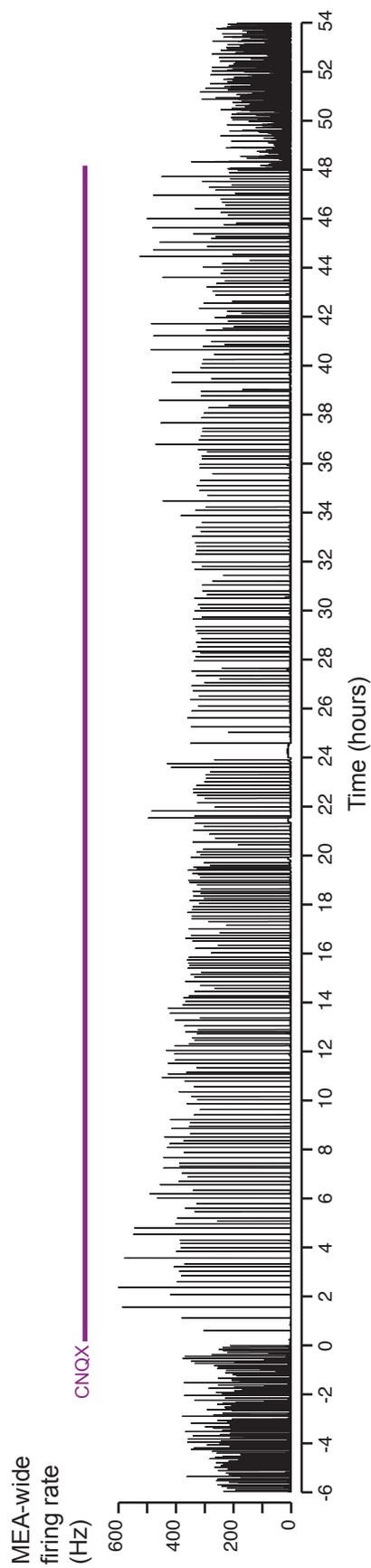
Figure B.1: MEA-wide firing rate during AMPAergic blockade from 14-16DIV. Array-wide firing rate histogram for culture treated with CNQX at time zero. The drug was replenished after 1 day and washed after 2 days. Bin size, 5s.

B.2 Results

B.2.1 Inward GABAergic currents emerge during AMPAergic blockade

We wanted to simultaneously assess population bursts and potential synaptic currents that could mediate the recovery of bursting. Because population bursts engage the entire network, we suspected the whole-cell recordings would provide a good way to measure both population bursts and synaptic currents. To verify that population bursts could be detected using whole cell recordings, we conducted a concurrent MEA and whole-cell recording in mature networks (>4 weeks *in vitro*) that exhibited frequent population bursts. We found that population bursts invariability drove inward currents near or above 1 nA (Fig. B.2), whereas other synaptic currents were on the order of 100 pA or less.

Having determined that whole-cell recordings could be used to monitor bursts, we next surveyed the profile of postsynaptic currents that persisted during CNQX treatment in cultures during their second *in vitro*. We found that CNQX dramatically reduced the total charge of postsynaptic currents, and none of the currents we recorded were characteristic of network-wide bursts (Fig. B.3). However, over the course of a few hours, postsynaptic currents gradually increased in amplitude until intracellular currents representative of network-wide bursts began to appear (Fig. B.3).

What neurotransmitter systems could be mediating these inward currents and bursts? Because cortical cultures are primarily composed of glutamatergic and GABAergic cells, we reasoned that bursts must be driven by either glutamate or GABA receptors. To dissect out these possibilities, we treated cultures during their second week *in vitro* with CNQX and APV to block all glutamatergic currents. During the first half hour after treatment, only miniature events were apparent. However, larger-amplitude currents gradually recovered (Fig. B.4a). An hour into glutamatergic blockade, synchronous bursting began to re-emerge. Bursting and
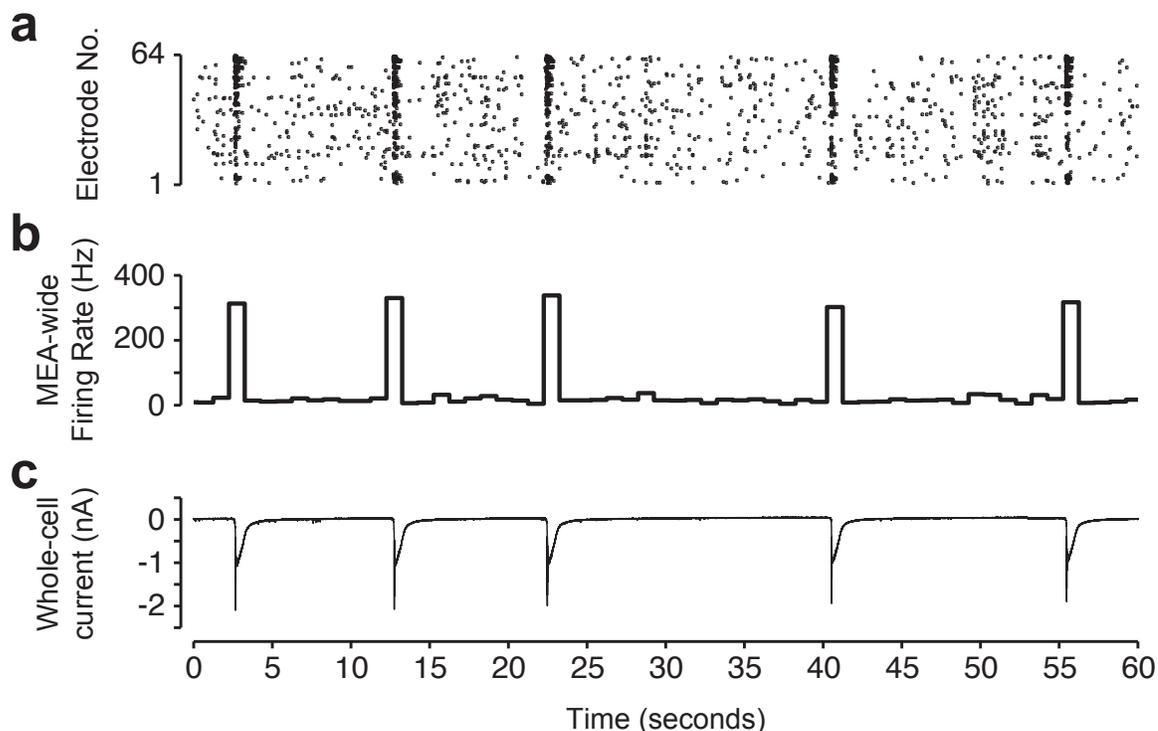
Figure B.2: Population bursts can be assessed using MEA or whole-cell recordings.
(a) Rastergram showing MEA-recorded spike times by electrode number. Five population bursts
are shown. **(b)** MEA-wide firing rate histogram of spike times in **(a)**, collapsed across the entire
MEA. Bin size, 1s. **(c)** Concurrent whole-cell recording showing intracellular currents elicited during
population bursts. V_{hold}, -70 mV.

inward currents were abolished by application of bicuculline, suggesting that that
GABAergic transmission mediated these inward currents. Further, the persistence
of population bursts suggested the these GABAergic currents were sufficiently de-
polarizing to produce network-wide activation. An anecdotal observation in doing
these recordings was that younger cultures (< 14 DIV) produced lower-amplitude
population bursts (< 1 nA currents; e.g. Fig. B.4a, top trace) while older cultures
(> 14 DIV) produced larger-amplitude population bursts (>1 nA currents; e.g.
Fig. B.4b, top trace).

The idea that GABAergic currents could mediate network-wide depolarizations
has a distinctly developmental flavor. Because intracellular chloride levels are high
during embryonic and early postnatal development, GABA can act as an excitatory
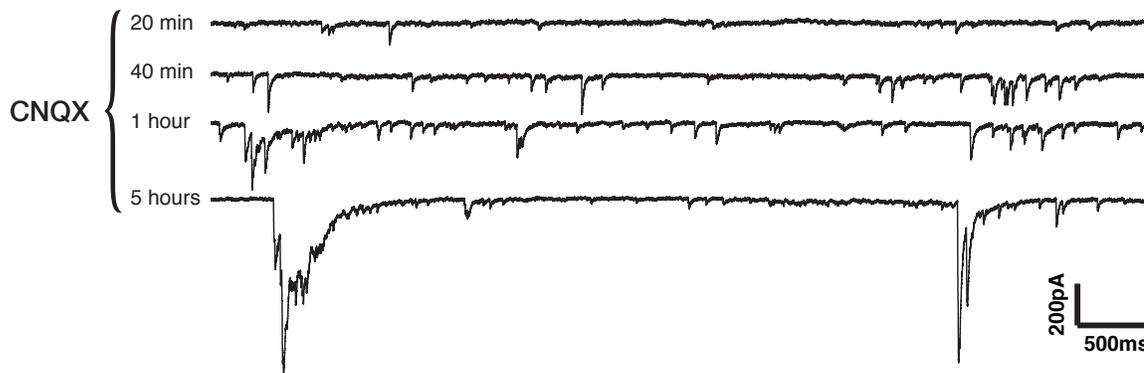
Figure B.3: Increased inward current amplitude during AMPAergic blockade. Representative postsynaptic currents recorded during CNQX treatment during the second week *in vitro*. The remaining currents increase with duration of treatment. V_{hold}, -70 mV.

neurotransmitter. However, as animals grow, chloride is extruded at an accelerated rate and the reversal potential for GABA becomes hyperpolarized. To examine whether the GABA-mediated recovery of bursting during glutamatergic blockade could be a developmental phenomenon, we recorded intracellular currents from cortical neurons following application of CNQX and APV during their third week *in vitro* (Fig. B.4b). Like younger cultures, CNQX and APV treatment isolated synaptic currents to miniature events during the first half hour, but larger currents slowly began to emerge. However, these currents never escalated to the magnitude of a population burst, suggesting that GABA mediates the recovery of bursting in younger, but not older cultures. Notably, the inward currents that did re-emerge during glutamatergic blockade were blocked by bicuculline, suggest that GABA could provide local depolarization, but it was insufficient to trigger bursting.

B.2.2 NMDAergic transmission drives population bursting

The differential recovery of GABAergic currents during the second versus third week *in vitro* suggested that during AMPAergic blockade, GABA might help recover bursting in at early developmental stages while NMDA might mediate the recovery at later
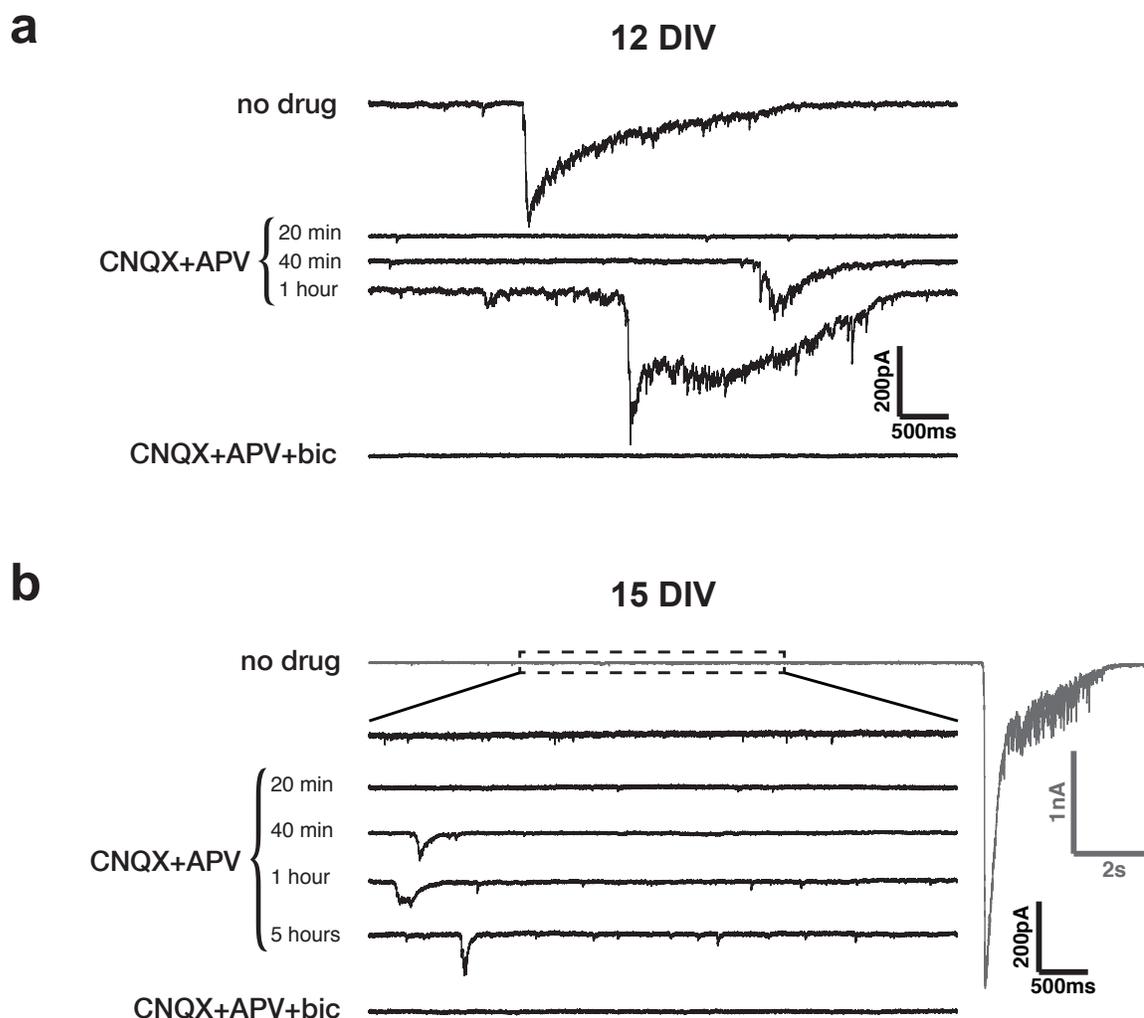
Figure B.4: GABAergic inward currents increase during glutamatergic blockade. Post-synaptic currents recorded during a treatment with CNQX and APV at **(a)** 12 or **(b)** 15 DIV. The remaining currents increase with duration of treatment and are presumed to be GABAergic since they are abolished by bicuculline. V_{hold}, -70 mV.

stages. To test these possibilities we conducted a series of MEA experiments using multi-well MEAs. Standard MEAs contain 59 electrodes, but multi-well MEAs contain six pharmacologically-isolated wells each with 9 electrodes (Fig. B.5), but use all the same recording hardware and software as standard MEAs. Because we were specifically interested in the recovery of bursting, and bursting involves culture-wide activation, having 9 electrodes was plenty to assess whether a burst occurred in a
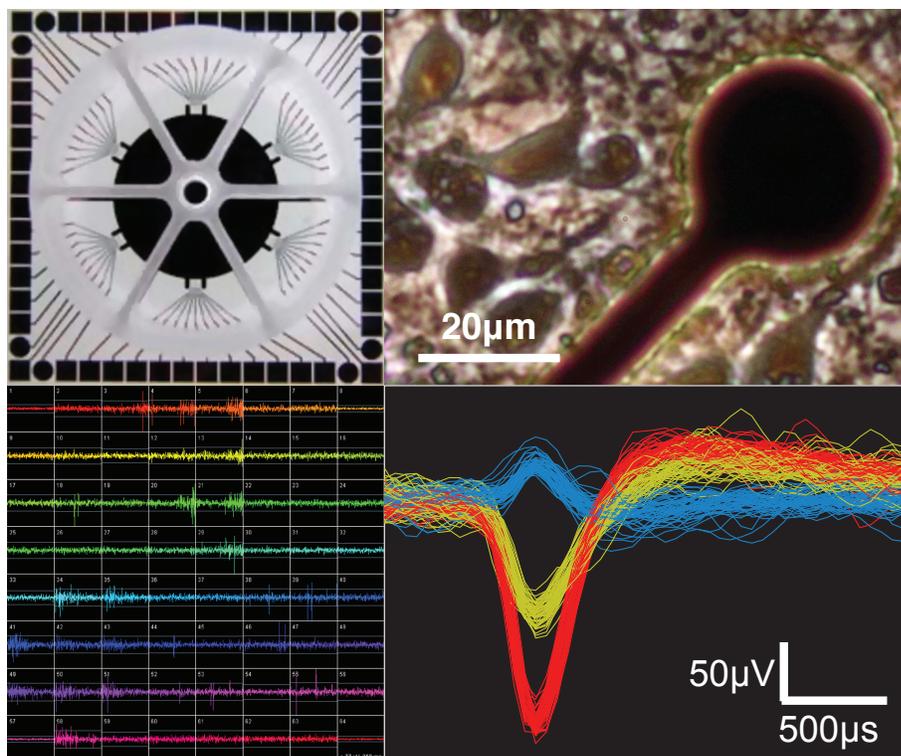
Figure B.5: Multi-well MEAs for recording bursting activity. *Top, left*: Multi-well MEA with six pharmacologically-isolated recording chambers. *Top, right*: Phase-contrast micrograph of neurons near an MEA electrode. *Bottom, left*: Voltage traces recorded on each electrode using the Neurorighter acquisition system. *Bottom, right*: Sorted spike waveforms recorded on single MEA electrode.

culture. Meanwhile, the six isolated 9-electrode MEAs allowed us to perform several perturbations on sister cultures.

The treatments we chose to perform were:

1. **48-hours bicuculline, replenishing the drugs after 24 hours.** We hoped this experiment would give us a sense of whether GABA was inhibitory or excitatory at the network level during these experiments. We hypothesized that we would observe significantly more bicuculline-mediated disinhibition in older than younger networks.

2. **48-hours CNQX, with bicuculline added after 24 hours.** We hoped this would distinguish between the possibilities of GABA being excitatory to begin

with, versus GABA homeostatically shifting toward an excitatory state. We hypothesized GABA was mediating the recovery of bursting in young cultures, so treatment with bicuculline following 24-hours CNQX would reduce burst frequency. We guessed that in older cultures the effect would be less dramatic.

3. **48-hours CNQX and APV, replenishing the drugs after 24 hours.** We hypothesized that bursting would recover with CNQX and APV in young, but not older cultures, as we observed in our intracellular assessments.

Some results from these experiments are shown in Figs. B.6 and B.7, and they were somewhat anti-climactic, though there are some interesting lessons to be drawn. Young cultures definitely showed less disinhibition after bicuculline treatment than older cultures. In fact, bicuculline had relatively little effect on the network-firing rate of these younger cultures, suggesting that bicuculline is neither excitatory nor inhibitory during the second week *in vitro*. Meanwhile, older cultures showed dramatically increased bursting with bicuculline treatment. Similarly, in younger cultures, bicuculline had little effect on bursting in cultures pre-treated with CNQX for 24 hours, but had a clear disinhibitory effect in older cultures. Finally, co-treatment with CNQX and APV completely eliminated bursting for the entire 48-hour treatment for cultures of both ages.

These results did not seem to agree with what we had found in our intracellular recordings, where GABAergic inward currents could drive network-wide depolarizations in younger cultures. The discrepancy might simply be a result of our low sample sizes for each experiment. Our results in older cultures, however, are consistent with our intracellular recordings. These experiments reveal an important role of NMDAergic transmission driving the recovery of bursting during AMPAergic blockade.

The complete blockade of bursting for the full 48 hours by CNQX and APV was rather surprising. We tested whether bursting could recover in conditions of complete glutamatergic blockade. We found that on the fourth day of glutamatergic blockade,

bursting began to recover (Fig. B.8). The rate of bursting gradually accelerated through the fifth day. On the sixth day, we added bicuculline and found that bursting was abolished, suggesting that excitatory GABA facilitated this recovery. Although the time course of this GABAergic homeostasis is significantly slower than we observed in our whole-cell recordings, it provides support to the idea that compensations in the GABAergic system can also can help recover bursting activity during glutamatergic blockade.

B.3 Summary

The emergence of synchronous bursts of action potentials is a hallmark of cultured neuronal networks during the first few weeks in vitro (Figs. 2.3 and 2.4; Van Pelt et al., 2004; Wagenaar et al., 2006b). While it has often been assumed that pharmacological blockade of AMPAergic transmission using CNQX eliminates population bursts, we have shown that this effect is transient, and when CNQX is applied chronically, bursting returns within hours (Chapter 2). Here, we sought to determine how population bursting homeostatically recovers in the absence of AMPAergic transmission and examined how other transmitter systems contributed to this recovery. Whole-cell voltage clamp recordings revealed an increase in the amplitude of inward synaptic currents within an hour of AMPAergic blockade. MEA recordings showed that NMDA mediates the recovery of population bursting during the first 48 hours of AMPAergic blockade, but that GABAergic transmission alone was sufficient to recover bursting during a more extended glutamatergic blockade. Together these results suggest that impaired AMPAergic transmission triggers compensatory changes in two other transmitter systems that help recover normal patterns of network activity. This form of plasticity offers a unique strategy for maintaining excitatory drive in cortical circuits when other avenues for excitation are chronically impaired.
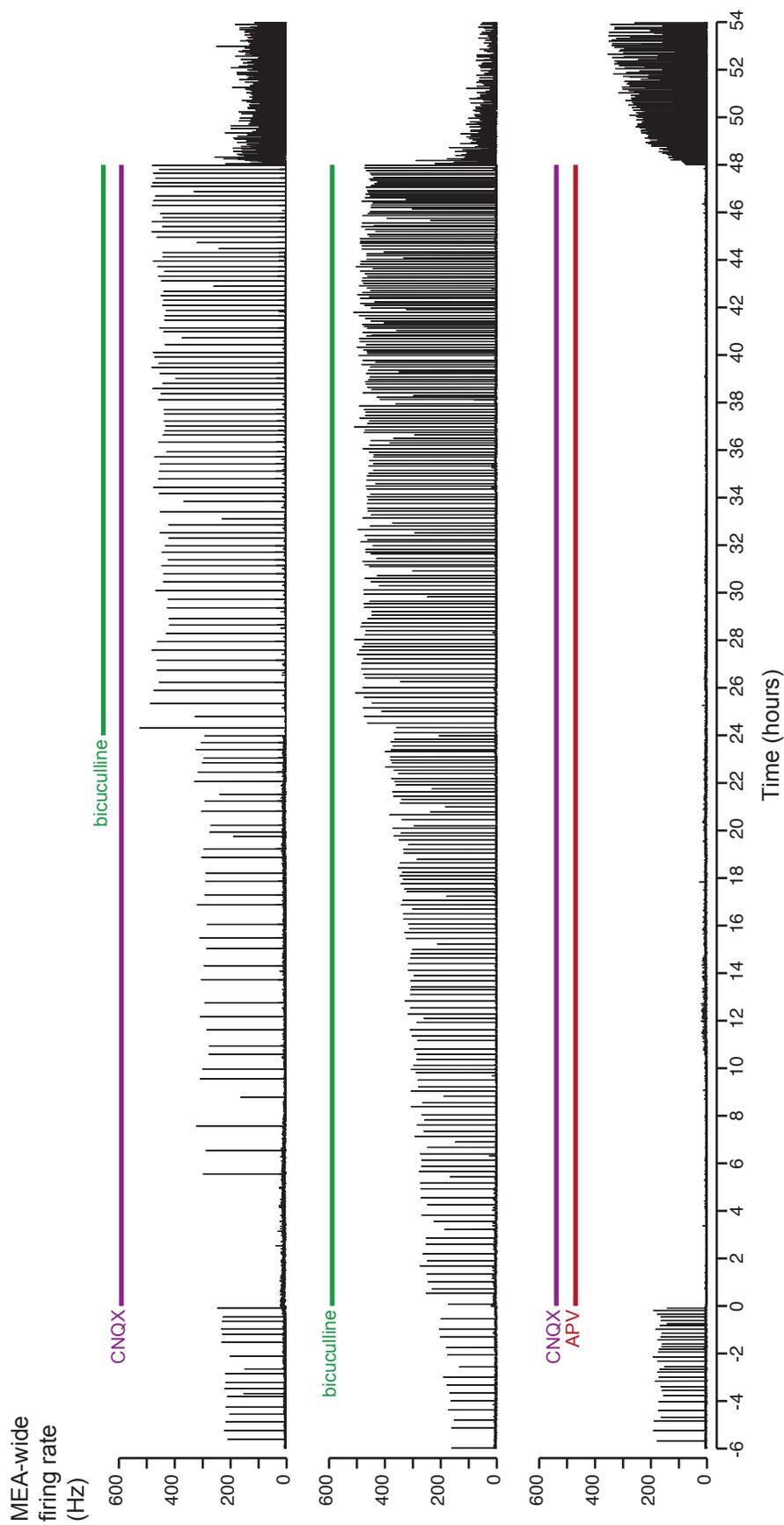
Figure B.6: NMDAergic transmission can recover population bursting in younger cultures. *Top*, MEA-wide spike histogram for culture treated with CNQX at 12 DIV, and bicuculline 1 day later. *Middle*, MEA-wide spike histogram for culture treated with bicuculline for 2 days. *Bottom*, MEA-wide spike histogram for culture treated with CNQX and APV at 12 DIV. In all cases, drugs were washed at 14 DIV. For 2-day treatments, drugs were replenished after 24 hours.
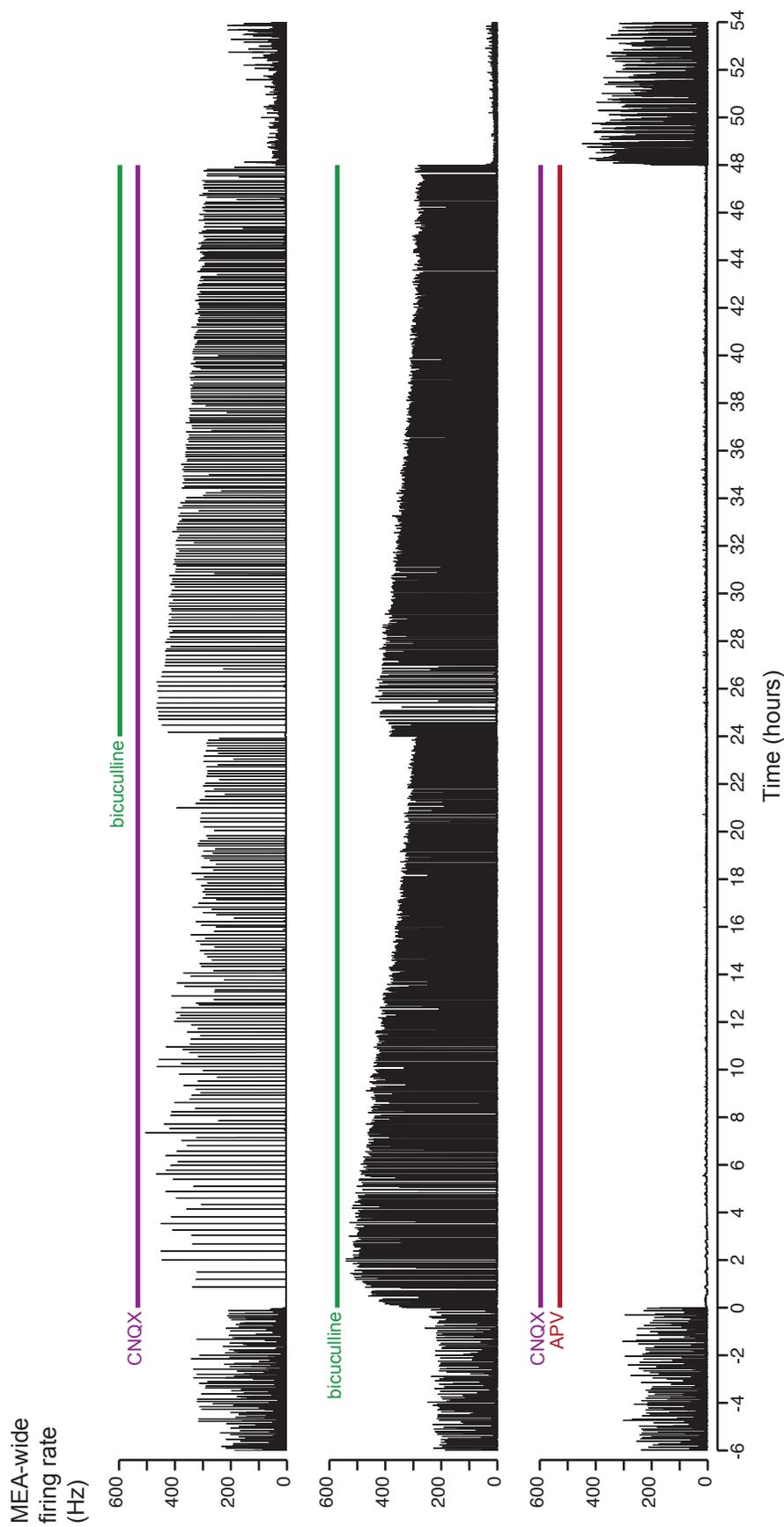
Figure B.7: NMDAergic transmission can recover population bursting in older cultures. *Top,* MEA-wide spike histogram for culture treated with CNQX at 15 DIV, and bicuculline 1 day later. *Middle,* MEA-wide spike histogram for culture treated with bicuculline for 2 days. *Bottom,* MEA-wide spike histogram for culture treated with CNQX and APV at 15 DIV. In all cases, drugs were washed at 17 DIV. For 2-day treatments, drugs were replenished after 24 hours.
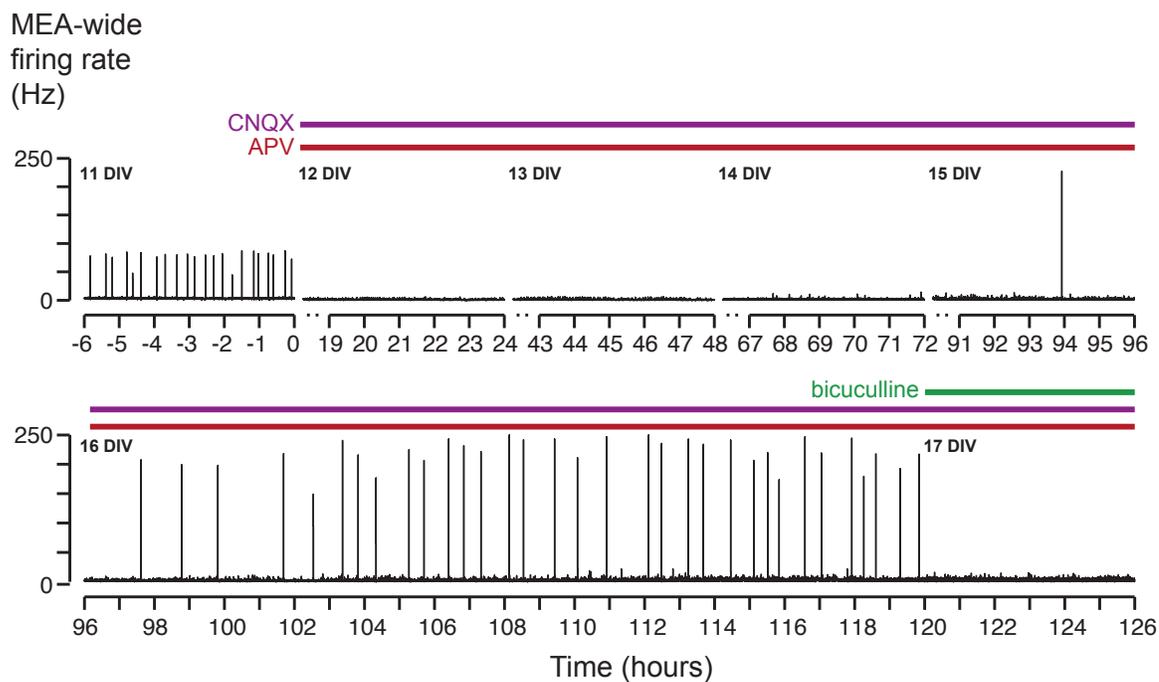
Figure B.8: Sustained glutamatergic transmission blockade elicits GABA-mediated bursting. Array-wide spike histogram showing firing rate during a 5-day treatment using CNQX and APV. Drugs were replenished every 24 hours. Bursting returns at the end of the 4 days, and is abolished by bicuculline. Bin, 5s.

Bibliography

Abbott, L. F. and Nelson, S. B. Synaptic plasticity: taming the beast. *Nature Neuroscience*, 3:1178–83, Nov. 2000.

Abraham, W. and Bear, M. F. Metaplasticity: the plasticity of synaptic plasticity. *Trends in Neurosciences*, 19(4):126–130, 1996.

Aizenman, C. D., Akerman, C. J., Jensen, K. R., Cline, H. T., Brook, S., and York, N. Visually driven regulation of intrinsic neuronal excitability improves stimulus detection in vivo. *Neuron*, 39:831–842, 2003.

Akerboom, J., Carreras Calderón, N., Tian, L., Wabnig, S., Prigge, M., Tolö, J., Gordus, A., Orger, M. B., Severi, K. E., Macklin, J. J., Patel, R., Pulver, S. R., Wardill, T. J., Fischer, E., Schüler, C., Chen, T.-W., Sarkisyan, K. S., Marvin, J. S., Bargmann, C. I., Kim, D. S., Kügler, S., Lagnado, L., Hegemann, P., Gottschalk, A., Schreiter, E. R., and Looger, L. L. Genetically encoded calcium indicators for multi-color neural activity imaging and combination with optogenetics. *Frontiers in Molecular Neuroscience*, 6(March):2, Jan. 2013.

Alivisatos, a. P., Andrews, A. M., Boyden, E. S., Chun, M., Church, G. M., Deisseroth, K., Donoghue, J. P., Fraser, S. E., Lippincott-Schwartz, J., Looger, L. L., Masmanidis, S., McEuen, P. L., Nurmikko, A. V., Park, H., Peterka, D. S., Reid, C., Roukes, M. L., Scherer, A., Schnitzer, M., Sejnowski, T. J., Shepard, K. L., Tsao, D., Turrigiano, G., Weiss, P. S., Xu, C., Yuste, R., and Zhuang, X. Nanotools for neuroscience and brain activity mapping. *ACS Nano*, 7(3):1850–66, Mar. 2013.

Altimimi, H. F. and Stellwagen, D. Persistent synaptic scaling independent of AMPA receptor subunit composition. *The Journal of Neuroscience*, 33(29):11763–7, July 2013.

Andrasfalvy, B. K. and Magee, J. C. Distance-dependent increase in AMPA receptor number in the dendrites of adult hippocampal CA1 pyramidal neurons. *The Journal of Neuroscience*, 21:9151–9159, 2001.

Anggono, V., Clem, R. L., and Huganir, R. L. PICK1 loss of function occludes homeostatic synaptic scaling. *The Journal of Neuroscience*, 31(6):2188–96, Feb. 2011.

Aoto, J., Nam, C. I., Poon, M. M., Ting, P., and Chen, L. Synaptic signaling by all-trans retinoic acid in homeostatic synaptic plasticity. *Neuron*, 60(2):308–20, Oct. 2008.

Aptowicz, C. O., Kunkler, P. E., and Kraig, R. P. Homeostatic plasticity in hippocampal slice cultures involves changes in voltage-gated Na+ channel expression. *Brain Research*, 998:155–163, 2004.

Arendt, K. L., Sarti, F., and Chen, L. Chronic inactivation of a neural circuit enhances LTP by inducing silent synapse formation. *The Journal of Neuroscience*, 33(5): 2087–96, Jan. 2013.

Arsiero, M., Lüscher, H.-R., and Giugliano, M. Real-time closed-loop electrophysiology: towards new frontiers in in vitro investigations in the neurosciences. *Archives italiennes de biologie*, 145:193–209, 2007.

Awad, H., Hubert, G. W., Smith, Y., Levey, a. I., and Conn, P. J. Activation of metabotropic glutamate receptor 5 has direct excitatory effects and potentiates NMDA receptor currents in neurons of the subthalamic nucleus. *The Journal of Neuroscience*, 20(21):7871–9, Nov. 2000.

Bacci, A., Coco, S., Pravettoni, E., Schenk, U., Armano, S., Frassoni, C., Verderio, C., De Camilli, P., and Matteoli, M. Chronic blockade of glutamate receptors enhances presynaptic release and downregulates the interaction between synaptophysin-synaptobrevin-vesicle-associated membrane protein 2. *The Journal of Neuroscience*, 21:6588–6596, 2001.

Bakkum, D. J., Chao, Z. C., and Potter, S. M. Spatio-temporal electrical stimuli shape behavior of an embodied cortical network in a goal-directed learning task. *Journal of Neural Engineering*, 5(3):310–323, 2008.

Barth, A. L. and Poulet, J. F. a. Experimental evidence for sparse firing in the neocortex. *Trends in Neurosciences*, 35(6):345–55, June 2012.

Bear, M. F., Cooper, L. N., and Ebner, F. F. A physiological basis for a theory of synapse modification. *Science*, 237(4810):42–8, July 1987.

Béïque, J.-C., Na, Y., Kuhl, D., Worley, P. F., and Huganir, R. L. Arc-dependent synapse-specific homeostatic plasticity. *Proceedings of the National Academy of Sciences of the United States of America*, 108(2):816–821, Dec. 2011.

Ben-Ari, Y., Cherubini, E., and Krnjevic, K. Changes in voltage dependence of NMDA currents during development. *Neuroscience Letters*, 94(1-2):88–92, Nov. 1988.

Ben-Ari, Y., Gaiarsa, J.-L., Tyzio, R., and Khazipov, R. GABA: a pioneer transmitter that excites immature neurons and generates primitive oscillations. *Physiological Reviews*, 87(4):1215–84, 2007.

Berg, D. K. and Hall, Z. W. Increased extrajunctional acetylcholine sensitivity produced by chronic acetylcholine sensitivity produced by chronic post-synaptic neuromuscular blockade. *The Journal of Physiology*, 244:659–676, 1975.

Bergquist, S., Dickman, D. K., and Davis, G. W. A hierarchy of cell intrinsic and target-derived homeostatic signaling. *Neuron*, 66(2):220–34, Apr. 2010.

Bernstein, J. G. and Boyden, E. S. Optogenetic tools for analyzing the neural circuits of behavior. *Trends in Cognitive Sciences*, 15(12):592–600, Dec. 2011.

Bienenstock, E. L., Cooper, L. N., and Munro, P. W. Theory for the development of neuron selectivity: orientation specificity and binocular interaction in visual cortex. *The Journal of Neuroscience*, 2(1):32–48, Jan. 1982.

Biffi, E., Regalia, G., Ghezzi, D., De Ceglia, R., Menegon, a., Ferrigno, G., Fiore, G. B., and Pedrocchi, a. A novel environmental chamber for neuronal network multisite recordings. *Biotechnology and Bioengineering*, 109:2553–66, 2012.

Blankenship, A. G. and Feller, M. B. Mechanisms underlying spontaneous patterned activity in developing neural circuits. *Nature Reviews Neuroscience*, 11(1):18–29, 2010.

Blau, A., Neumann, T., Ziegler, C., and Benfenati, F. Replica-moulded polydimethylsiloxane culture vessel lids attenuate osmotic drift in long-term cell cultures. *Journal of biosciences*, 34(1):59–69, Mar. 2009.

Blau, A. W. and Ziegler, C. M. Prototype of a novel autonomous perfusion chamber for long-term culturing and in situ investigation of various cell types. *Journal of Biochemical and Biophysical Methods*, 50:15–27, 2001.

Bliss, T. V. P. and Lomo, T. Long-lasting potentiation of synaptic transmission in the dentate area of the anaesthetized rabbit following stimulation of the preforant path. *The Journal of Physiology*, 232:331–356, 1973.

Borde, M., Cazalets, J. R., and Buño, W. Activity-dependent response depression in rat hippocampal CA1 pyramidal neurons in vitro. *Journal of Neurophysiology*, 74:1714–29, 1995.

Borodinsky, L. N., Root, C. M., Cronin, J. a., Sann, S. B., Gu, X., and Spitzer, N. C. Activity-dependent homeostatic specification of transmitter expression in embryonic neurons. *Nature*, 429(6991):523–30, June 2004.

Borodinsky, L. N., Belgacem, Y. H., Swapna, I., and Sequerra, E. B. Dynamic regulation of neurotransmitter specification: relevance to nervous system homeostasis. *Neuropharmacology*, 78:75–80, Mar. 2014.

Boyden, E. S., Zhang, F., Bamberg, E., Nagel, G., and Deisseroth, K. Millisecond-timescale, genetically targeted optical control of neural activity. *Nature Neuroscience*, 8(9):1263–8, 2005.

Branco, T., Staras, K., Darcy, K. J., and Goda, Y. Local dendritic activity sets release probability at hippocampal synapses. *Neuron*, 59(3):475–85, Aug. 2008.

Breton, J.-D. and Stuart, G. J. Loss of sensory input increases the intrinsic excitability of layer 5 pyramidal neurons in rat barrel cortex. *The Journal of Physiology*, 587 (Pt 21):5107–19, Nov. 2009.

Brickley, S., Revilla, V., Cull-Candy, S., Wisden, W., and Farrant, M. Adaptive regulation of neuronal excitability by a voltage-independent potassium conductance. *Nature*, 409(6816):88–92, 2001a.

Brickley, S. G., Farrant, M., Swanson, G. T., and Cull-Candy, S. G. CNQX increases GABA-mediated synaptic transmission in the cerebellum by an AMPA/kainate receptor-independent mechanism. *Neuropharmacology*, 41:730–736, 2001b.

Burrone, J., O'Byrne, M., and Murthy, V. Multiple forms of synaptic plasticity triggered by selective suppression of activity in individual neurons. *Nature*, 420 (6914):414–418, 2002.

CDC. Developmental milestones, *Center for Disease Control and Prevention*. URL www.cdc.gov/ncbddd/actearly/milestones/. Accessed March 27, 2014.

Chang, M. C., Park, J. M., Pelkey, K. a., Grabenstatter, H. L., Xu, D., Linden, D. J., Sutula, T. P., McBain, C. J., and Worley, P. F. Narp regulates homeostatic scaling of excitatory synapses on parvalbumin-expressing interneurons. *Nature Neuroscience*, 13(9):1090–7, Sept. 2010.

Chiappalone, M., Bove, M., Vato, A., Tedesco, M., and Martinoia, S. Dissociated cortical networks show spontaneously correlated activity patterns during in vitro development. *Brain Research*, 1093(1):41–53, June 2006.

Chub, N. and O'Donovan, M. J. Blockade and recovery of spontaneous rhythmic activity after application of neurotransmitter antagonists to spinal networks of the chick embryo. *The Journal of Neuroscience*, 18(1):294–306, Jan. 1998.

Cingolani, L. a., Thalhammer, A., Yu, L. M. Y., Catalano, M., Ramos, T., Colicos, M. a., and Goda, Y. Activity-dependent regulation of synaptic AMPA receptor composition and abundance by beta3 integrins. *Neuron*, 58(5):749–62, 2008.

Coba, M. P., Pocklington, A. J., Collins, M. O., Kopanitsa, M. V., Uren, R. T., Swamy, S., Croning, M. D. R., Choudhary, J. S., and Grant, S. G. N. Neurotransmitters drive combinatorial multistate postsynaptic density networks. *Science Signaling*, 2(68):ra19, Jan. 2009.

Cooper, L. N. and Bear, M. F. The BCM theory of synapse modification at 30: interaction of theory with experiment. *Nature Reviews Neuroscience*, 13(11):798–810, Nov. 2012.

Corner, M. A., van Pelt, J., Wolters, P., Baker, R., and Nuytinck, R. Physiological effects of sustained blockade of excitatory synaptic transmission on spontaneously active developing neuronal networks–an inquiry into the reciprocal linkage between intrinsic biorhythms and neuroplasticity in early ontogeny. *Neuroscience and Biobehavioral reviews*, 26:127–85, Mar. 2002.

Corner, M. A., Baker, R. E., van Pelt, J., and Wolters, P. S. Compensatory physiological responses to chronic blockade of amino acid receptors during early development in spontaneously active organotypic cerebral cortex explants cultured in vitro. *Progress in Brain Research*, 147(04):231–48, Jan. 2005.

Corner, M. A., Baker, R. E., and van Pelt, J. Homeostatically regulated spontaneous neuronal discharges protect developing cerebral cortex networks from becoming hyperactive following prolonged blockade of excitatory synaptic receptors. *Brain Research*, 1106(1):40–5, Aug. 2006.

Corner, M. A., Baker, R. E., and van Pelt, J. Physiological consequences of selective suppression of synaptic transmission in developing cerebral cortical networks in vitro: differential effects on intrinsically generated bioelectric discharges in a living 'model' system for slow-wave sleep activity. *Neuroscience and Biobehavioral reviews*, 32(8):1569–600, Oct. 2008.

Daoudal, G. and Debanne, D. Long-term plasticity of intrinsic excitability: learning rules and mechanisms. *Learning and Memory*, 10(6):456–65, 2003.

Davis, G. W. Homeostatic signaling and the stabilization of neural function. *Neuron*, 80(3):718–28, Oct. 2013.

Davis, G. W. and Goodman, C. S. Synapse-specific control of synaptic efficacy at the terminals of a single neuron. *Nature*, 392(6671):82–6, Mar. 1998.

Davis, G. W., DiAntonio, A., Petersen, S. A., and Goodman, C. S. Postsynaptic PKA controls quantal size and reveals a retrograde signal that regulates presynaptic transmitter release in Drosophila. *Neuron*, 20:305–315, 1998.

De Gois, S., Schäfer, M. K.-H., Defamie, N., Chen, C., Ricci, A., Weihe, E., Varoqui, H., and Erickson, J. D. Homeostatic scaling of vesicular glutamate and GABA transporter expression in rat neocortical circuits. *The Journal of Neuroscience*, 25 (31):7121–33, 2005.

Deeg, K. E. and Aizenman, C. D. Sensory modality-specific homeostatic plasticity in the developing optic tectum. *Nature Neuroscience*, 14(5):548–50, May 2011.

Deisseroth, K. and Schnitzer, M. J. Engineering approaches to illuminating brain structure and dynamics. *Neuron*, 80:568–577, 2013.

DeLorme, E., Rabe, C., and McGee Jr., R. Regulation of the number of functional voltage-sensitive Ca channels on PC12 cells by chronic changes in membrane potential. *Journal of Pharmacology and Experimental Therapeutics*, 244(3):838–843, 1988.

Delorme, E. M., McGee Jr., R., and McGee, R. Regulation of voltage-dependent Ca2+ channels of neuronal cells by chronic changes in membrane potential. *Brain Research*, 397(1):189–92, Nov. 1986.

Demarque, M. and Spitzer, N. C. Activity-dependent expression of Lmx1b regulates specification of serotonergic neurons modulating swimming behavior. *Neuron*, 67: 321–334, 2010.

Demarse, T. B., Wagenaar, D. A., Blau, A. W., and Potter, S. M. The neurally controlled animat: biological brains acting with simulated bodies. *Autonomous Robots*, 11:305–310, 2001.

Desai, N. S., Rutherford, L. C., and Turrigiano, G. G. Plasticity in the intrinsic excitability of cortical pyramidal neurons. *Nature Neuroscience*, 2:515–520, 1999a.

Desai, N. S., Rutherford, L. C., and Turrigiano, G. G. BDNF regulates the intrinsic excitability of cortical neurons. *Learning and Memory*, 6(3):284–91, 1999b.

Desai, N. S., Cudmore, R. H., Nelson, S., and Turrigiano, G. G. Critical periods for experience-dependent synaptic scaling in visual cortex. *Nature Neuroscience*, 5(8): 783–789, 2002.

Destexhe, A. and Contreras, D. Neuronal computations with stochastic network states. *Science*, 314(5796):85–90, Oct. 2006.

Diamond, J. S. and Jahr, C. E. Asynchronous release of synaptic vesicles determines the time course of the AMPA receptor-mediated EPSC. *Neuron*, 15(5):1097–107, Nov. 1995.

DiAntonio, A., Petersen, S. A., Heckmann, M., and Goodman, C. S. Glutamate receptor expression regulates quantal size and quantal content at the Drosophila neuromuscular junction. *The Journal of Neuroscience*, 19:3023–3032, 1999.

Dickman, D. K. and Davis, G. W. The schizophrenia susceptibility gene dysbindin controls synaptic homeostasis. *Science*, 326(5956):1127–30, Nov. 2009.

Dickman, D. K., Tong, A., and Davis, G. W. Snapin is critical for presynaptic homeostatic plasticity. *The Journal of Neuroscience*, 32:8716–8724, 2012.

Driscoll, H. E., Muraro, N. I., He, M., and Baines, R. a. Pumilio-2 regulates translation of Nav1.6 to mediate homeostasis of membrane excitability. *The Journal of Neuroscience*, 33:9644–54, 2013.

Dulcis, D. and Spitzer, N. C. Illumination controls differentiation of dopamine neurons regulating behaviour. *Nature*, 456:195–201, 2008.

Dulcis, D., Jamshidi, P., Leutgeb, S., and Spitzer, N. C. Neurotransmitter switching in the adult brain regulates behavior. *Science*, 340:449–53, 2013.

Echegoyen, J., Neu, A., Graber, K. D., and Soltesz, I. Homeostatic plasticity studied using in vivo hippocampal activity-blockade: synaptic scaling, intrinsic plasticity and age-dependence. *PLoS ONE*, 2(8):e700, Jan. 2007.

Etheredge, J. A., Murchison, D., Abbott, L. C., and Griffith, W. H. Functional compensation by other voltage-gated Ca2+ channels in mouse basal forebrain neurons with CaV2.1 mutations. *Brain Research*, 1140:105–119, 2007.

Fan, Y., Fricker, D., Brager, D. H., Chen, X., Lu, H.-C., Chitwood, R. A., and Johnston, D. Activity-dependent decrease of excitability in rat hippocampal neurons through increases in I(h). *Nature Neuroscience*, 8:1542–1551, 2005.

Feller, M. Spontaneous Correlated Activity in Developing Neural Circuits. *Neuron*, 22:653–656, 1999.

Fenno, L., Yizhar, O., and Deisseroth, K. The development and application of optogenetics. *Annual Review of Neuroscience*, 34:389–412, Jan. 2011.

Follesa, P. and Ticku, M. K. NMDA receptor upregulation: molecular studies in cultured mouse cortical neurons after chronic antagonist exposure. *The Journal of Neuroscience*, 16(7):2172–8, Apr. 1996.

Frank, C. A., Kennedy, M. J., Goold, C. P., Marek, K. W., and Davis, G. W. Mechanisms underlying the rapid induction and sustained expression of synaptic homeostasis. *Neuron*, 52(4):663–77, 2006.

Frank, C. A., Pielage, J., and Davis, G. W. A presynaptic homeostatic signaling system composed of the Eph receptor, Ephexin, Cdc42, and CaV2.1 calcium channels. *Neuron*, 61:556–569, 2009.

Franklin, J. L., Fickbohm, D. J., and Willard, a. L. Long-term regulation of neuronal calcium currents by prolonged changes of membrane potential. *The Journal of Neuroscience*, 12(5):1726–35, May 1992.

Frick, A. and Johnston, D. Plasticity of dendritic excitability. *Journal of neurobiology*, 64(1):100–15, July 2005.

Furshpan, E. and Potter, D. Seizure-like activity and cellular damage in rat hippocampal neurons in cell culture. *Neuron*, 3:199–207, 1989.

Fusi, S., Drew, P. J., and Abbott, L. F. Cascade models of synaptically stored memories. *Neuron*, 45(4):599–611, 2005.

Gallo, V. and Russell, J. T. Excitatory amino acid receptors in glia: different subtypes for distinct functions? *Journal of Neuroscience Research*, 42:1–8, 1995.

Garcia-Bereguiain, M. A., Gonzalez-Islas, C., Lindsly, C., Butler, E., Hill, A. W., and Wenner, P. In vivo synaptic scaling is mediated by GluA2-lacking AMPA receptors in the embryonic spinal cord. *The Journal of Neuroscience*, 33(16):6791–9, Apr. 2013.

Gibson, J. R., Bartley, A. F., and Huber, K. M. Role for the subthreshold currents I_{Leak} and I_{H} in the homeostatic control of excitability in neocortical somatostatin-positive inhibitory neurons. *Journal of Neurophysiology*, 96:420–432, 2006.

Goel, A. and Lee, H. Persistence of experience-induced homeostatic synaptic plasticity through adulthood in superficial layers of mouse visual cortex. *The Journal of Neuroscience*, 27(25):6692, 2007.

Goel, A., Jiang, B., Xu, L. W., Song, L., Kirkwood, A., and Lee, H.-K. Cross-modal regulation of synaptic AMPA receptors in primary sensory cortices by visual experience. *Nature Neuroscience*, 9:1001–1003, 2006.

Goel, A., Xu, L. W., Snyder, K. P., Song, L., Goenaga-Vazquez, Y., Megill, A., Takamiya, K., Huganir, R. L., and Lee, H. K. Phosphorylation of ampa receptors is required for sensory deprivation-induced homeostatic synaptic plasticity. *PLoS ONE*, 6, 2011.

Goldberg, J., Holthoff, K., and Yuste, R. A problem with Hebb and local spikes. *Trends in Neurosciences*, 25(9):433–5, Sept. 2002.

Gómez-Lira, G., Lamas, M., Romo-Parra, H., and Gutiérrez, R. Programmed and induced phenotype of the hippocampal granule cells. *The Journal of Neuroscience*, 25:6939–6946, 2005.

Gonzalez-Islas, C. and Wenner, P. Spontaneous network activity in the embryonic spinal cord regulates AMPAergic and GABAergic synaptic strength. *Neuron*, 49 (4):563–75, 2006.

Gonzalez-Islas, C., Chub, N., Garcia-Bereguiain, M. A., and Wenner, P. GABAergic synaptic scaling in embryonic motoneurons is mediated by a shift in the chloride reversal potential. *The Journal of Neuroscience*, 30:13016–13020, 2010.

Gonzalez-Islas, C., Garcia-Bereguiain, M. A., and Wenner, P. Tonic and transient endocannabinoid regulation of AMPAergic miniature postsynaptic currents and homeostatic plasticity in embryonic motor networks. *The Journal of Neuroscience*, 32:13597–13607, 2012.

Goold, C. and Nicoll, R. Single-cell optogenetic excitation drives homeostatic synaptic depression. *Neuron*, 68(3):512–528, 2010.

Govindarajan, A., Kelleher, R. J., and Tonegawa, S. A clustered plasticity model of long-term memory engrams. *Nature Reviews Neuroscience*, 7:575–583, 2006.

Gross, G. W. Simultaneous single unit recording in vitro with a photoetched laser deinsulated gold multimicroelectrode surface. *IEEE Transactions on Biomedical Engineering*, 26:273–279, 1979.

Gross, G. W. and Kowalski, J. M. Origins of activity patterns in self-organizing neuronal networks in vitro. *Journal of Intelligent Material Systems and Structures*, 10:558–564, 1999.

Gross, G. W. and Schwalm, F. U. A closed flow chamber for long-term multichannel recording and optical monitoring. *Journal of Neuroscience Methods*, 52:73–85, 1994.

Gross, G. W., Rieske, E., Kreutzberg, G. W., and Meyer, A. A new fixed-array multi-microelectrode system designed for long-term monitoring of extracellular single unit neuronal activity in vitro. *Neuroscience Letters*, 6:101–105, 1977.

Groth, R. D., Lindskog, M., Thiagarajan, T. C., Li, L., and Tsien, R. W. Beta Ca2+/CaM-dependent kinase type II triggers upregulation of GluA1 to coordinate adaptation to synaptic inactivity in hippocampal neurons. *Proceedings of the National Academy of Sciences of the United States of America*, 108:828–833, 2011.

Grubb, M. S. and Burrone, J. Activity-dependent relocation of the axon initial segment fine-tunes neuronal excitability. *Nature*, 465(7301):1070–4, June 2010.

Guo, Y., Huang, S., de Pasquale, R., McGehrin, K., Lee, H.-K., Zhao, K., and Kirkwood, A. Dark exposure extends the integration window for spike-timing-dependent plasticity. *The Journal of Neuroscience*, 32:15027–15035, 2012.

Hales, C. M., Rolston, J. D., and Potter, S. M. How to culture, record and stimulate neuronal networks on micro-electrode arrays (MEAs). *Journal of Visualized Experiments*, (39):1–7, May 2010.

Hales, C. M., Zeller-Townson, R., Newman, J. P., Shoemaker, J. T., Killian, N. J., and Potter, S. M. Stimulus-evoked high frequency oscillations are present in neuronal networks on microelectrode arrays. *Frontiers in Neural Circuits*, 6(May):29, Jan. 2012.

Hartman, K. N., Pal, S. K., Burrone, J., and Murthy, V. N. Activity-dependent regulation of inhibitory synaptic transmission in hippocampal neurons. *Nature Neuroscience*, 9(5):642–9, 2006.

Hartmann, K., Bruehl, C., Golovko, T., and Draguhn, A. Fast homeostatic plasticity of inhibition via activity-dependent vesicular filling. *PLoS ONE*, 3, 2008.

He, K., Petrus, E., Gammon, N., and Lee, H.-K. Distinct sensory requirements for unimodal and cross-modal homeostatic synaptic plasticity. *The Journal of Neuroscience*, 32(25):8469–74, June 2012.

Hengen, K. B., Lambo, M. E., Van Hooser, S. D., Katz, D. B., and Turrigiano, G. G. Firing rate homeostasis in visual cortex of freely behaving rodents. *Neuron*, 80(2): 335–42, Oct. 2013.

Hires, S. A., Zhu, Y., and Tsien, R. Y. Optical measurement of synaptic glutamate spillover and reuptake by linker optimized glutamate-sensitive fluorescent reporters. *Proceedings of the National Academy of Sciences of the United States of America*, 105:4411–4416, 2008.

Hong, S. and Lnenicka, G. Activity-dependent reduction in voltage-dependent calcium current in a crayfish motoneuron. *The Journal of Neuroscience*, 15(5 Pt 1): 3539–47, May 1995.

Hou, Q., Zhang, D., Jarzylo, L., Huganir, R. L., and Man, H.-Y. Homeostatic regulation of AMPA receptor expression at single hippocampal synapses. *Proceedings of the National Academy of Sciences of the United States of America*, 105(2):775–80, Jan. 2008.

Hou, Q., Gilbert, J., and Man, H.-Y. Homeostatic regulation of AMPA receptor trafficking and degradation by light-controlled single-synaptic activation. *Neuron*, 72(5):806–18, Dec. 2011.

Huang, S., Treviño, M., He, K., Ardiles, A., Pasquale, R. D., Guo, Y., Palacios, A., Huganir, R., and Kirkwood, A. Pull-push neuromodulation of LTP and LTD enables bidirectional experience-induced synaptic scaling in visual cortex. *Neuron*, 73(3):497–510, Feb. 2012.

Ibata, K., Sun, Q., and Turrigiano, G. G. Rapid synaptic scaling induced by changes in postsynaptic firing. *Neuron*, 57(6):819–826, 2008.

Jakawich, S. K., Nasser, H. B., Strong, M. J., McCartney, A. J., Perez, A. S., Rakesh, N., Carruthers, C. J. L., and Sutton, M. A. Local presynaptic activity gates homeostatic changes in presynaptic function driven by dendritic BDNF synthesis. *Neuron*, 68(6):1143–58, Dec. 2010.

Janssens, N. and Lesage, A. S. J. Glutamate receptor subunit expression in primary neuronal and secondary glial cultures. *Journal of Neurochemistry*, 77(6):1457–74, June 2001.

Jimbo, Y., Robinson, H., and Kawana, A. Simultaneous measurement of intracellular calcium and electrical activity from patterned neural networks in culture. *IEEE Transactions on Biomedical Engineering*, 40(8):804–10, Aug. 1993.

Jimbo, Y., Tateno, T., and Robinson, H. P. Simultaneous induction of pathway-specific potentiation and depression in networks of cortical neurons. *Biophysical Journal*, 76:670–678, 1999.

Ju, W., Morishita, W., Tsui, J., and Gaietta, G. Activity-dependent regulation of dendritic synthesis and trafficking of AMPA receptors. *Nature Neuroscience*, 7(3): 244–253, 2004.

Kamioka, H., Maeda, E., Jimbo, Y., Robinson, H., and Kawana, A. Spontaneous periodic synchronized bursting during formation of mature patterns of connections in cortical cultures. *Neuroscience Letters*, 206(2-3):109–112, 1996.

Karmarkar, U. R. and Buonomano, D. V. Different forms of homeostatic plasticity are engaged with distinct temporal profiles. *European Journal of Neuroscience*, 23: 1575–1584, 2006.

Kastanenka, K. V. and Landmesser, L. T. In vivo activation of channelrhodopsin-2 reveals that normal patterns of spontaneous activity are required for motoneuron guidance and maintenance of guidance molecules. *The Journal of Neuroscience*, 30 (31):10575–10585, Aug. 2010.

Keck, T., Keller, G. B., Jacobsen, R. I., Eysel, U. T., Bonhoeffer, T., and Hübener, M. Synaptic scaling and homeostatic plasticity in the mouse visual cortex invivo. *Neuron*, 80(2):327–34, Oct. 2013.

Khazipov, R. and Luhmann, H. J. Early patterns of electrical activity in the developing cerebral cortex of humans and rodents. *Trends in Neurosciences*, 29(7):414–8, 2006.

Khorkova, O. and Golowasch, J. Neuromodulators, not activity, control coordinated expression of ionic currents. *The Journal of Neuroscience*, 27:8709–8718, 2007.

Kilman, V., van Rossum, M. C. W., and Turrigiano, G. G. Activity deprivation reduces miniature IPSC amplitude by decreasing the number of postsynaptic $GABA_A$ receptors clustered at neocortical synapses. *The Journal of Neuroscience*, 22(4): 1328, 2002.

Kim, J. and Alger, B. Reduction in endocannabinoid tone is a homeostatic mechanism for specific inhibitory synapses. *Nature Neuroscience*, 13(5):592–600, 2010.

Kim, J. and Tsien, R. Synapse-specific adaptations to inactivity in hippocampal circuits achieve homeostatic gain control while dampening network reverberation. *Neuron*, 58(6):925–937, 2008.

Kim, S. H. and Ryan, T. A. CDK5 Serves as a Major Control Point in Neurotransmitter Release. *Neuron*, 67:797–809, 2010.

Kim, S. H. and Ryan, T. a. Balance of calcineurin Aα and CDK5 activities sets release probability at nerve terminals. *The Journal of Neuroscience*, 33:8937–50, 2013.

Kirkwood, A., Rioult, M. C., and Bear, M. F. Experience-dependent modification of synaptic plasticity in visual cortex. *Nature*, 381:526–528, 1996.

Kleckner, N. W. and Dingledine, R. Regulation of hippocampal NMDA receptors by magnesium and glycine during development. *Molecular Brain Research*, 11: 151–159, 1991.

Kleinlogel, S., Feldbauer, K., Dempski, R. E., Fotis, H., Wood, P. G., Bamann, C., and Bamberg, E. Ultra light-sensitive and fast neuronal activation with the Ca^{2+}-permeable channelrhodopsin CatCh. *Nature Neuroscience*, 14:513–518, 2011.

Knogler, L. D., Liao, M., and Drapeau, P. Synaptic scaling and the development of a motor network. *The Journal of Neuroscience*, 30(26):8871–81, June 2010.

Knöpfel, T. Genetically encoded optical indicators for the analysis of neuronal circuits. *Nature Reviews Neuroscience*, 13(10):687–700, Oct. 2012.

Kovács, I., Simon, A., Szárics, E., Barabás, P., Héja, L., Nyikos, L., and Kardos, J. Cyclothiazide binding to functionally active AMPA receptor reveals genuine allosteric interaction with agonist binding sites. *Neurochemistry International*, 44: 271–280, 2004.

Krook-Magnuson, E., Armstrong, C., Oijala, M., and Soltesz, I. On-demand optogenetic control of spontaneous seizures in temporal lobe epilepsy. *Nature Communications*, 4:1376, 2013.

Landmesser, L. T. and O'Donovan, M. J. Activation patterns of embryonic chick hind limb muscles recorded in ovo and in an isolated spinal cord preparation. *The Journal of Physiology*, 347:189–204, 1984.

Larkum, M. E. and Nevian, T. Synaptic clustering by dendritic signalling mechanisms. *Current Opinion in Neurobiology*, 18:321–331, 2008.

Lau, C. G. and Murthy, V. N. Activity-Dependent Regulation of Inhibition via GAD67. *The Journal of Neuroscience*, 32:8521–8531, 2012.

Lazarevic, V., Schöne, C., Heine, M., Gundelfinger, E. D., and Fejtova, A. Extensive remodeling of the presynaptic cytomatrix upon homeostatic adaptation to network activity silencing. *The Journal of Neuroscience*, 31:10189–10200, 2011.

Lee, H. K. Ca-permeable AMPA receptors in homeostatic synaptic plasticity. *Front Mol Neurosci*, 5:17, 2012.

Lee, K. F. H., Soares, C., and Béïque, J.-C. Tuning into diversity of homeostatic synaptic plasticity. *Neuropharmacology*, 78:31–7, Mar. 2014.

Lee, K. J., Park, I. S., Kim, H., Greenough, W. T., Pak, D. T. S., and Rhyu, I. J. Motor skill training induces coordinated strengthening and weakening between neighboring synapses. *The Journal of Neuroscience*, 33(23):9794–9, June 2013a.

Lee, K. J., Queenan, B. N., Rozeboom, A. M., Bellmore, R., Lim, S. T., Vicini, S., and Pak, D. T. S. Mossy fiber-CA3 synapses mediate homeostatic plasticity in mature hippocampal neurons. *Neuron*, 77(1):99–114, Jan. 2013b.

Lee, S.-H., Govindaiah, G., and Cox, C. L. Selective excitatory actions of DNQX and CNQX in rat thalamic neurons. *Journal of neurophysiology*, 103:1728–1734, 2010.

Leifer, A. M., Fang-Yen, C., Gershow, M., Alkema, M. J., and Samuel, A. D. T. Optogenetic manipulation of neural activity in freely moving Caenorhabditis elegans. *Nature Methods*, 8:147–152, 2011.

LeMasson, G., Marder, E., and Abbott, L. F. Activity-dependent regulation of conductances in model neurons. *Science*, 259(5103):1915–7, Mar. 1993.

Leslie, K. R., Nelson, S. B., and Turrigiano, G. G. Postsynaptic depolarization scales quantal amplitude in cortical pyramidal neurons. *The Journal of Neuroscience*, 21 (19):RC170, Oct. 2001.

Li, D., Hérault, K., Isacoff, E. Y., Oheim, M., and Ropert, N. Optogenetic activation of LiGluR-expressing astrocytes evokes anion channel-mediated glutamate release. *The Journal of Physiology*, 590:855–73, 2012.

Li, X., Gutierrez, D. V., Hanson, M. G., Han, J., Mark, M. D., Chiel, H., Hegemann, P., Landmesser, L. T., and Herlitze, S. Fast noninvasive activation and inhibition of neural and network activity by vertebrate rhodopsin and green algae channel-rhodopsin. *Proceedings of the National Academy of Sciences of the United States of America*, 102(49):17816–21, Dec. 2005.

Lin, J. Y., Sann, S. B., Zhou, K., Nabavi, S., Proulx, C. D., Malinow, R., Jin, Y., and Tsien, R. Y. Optogenetic inhibition of synaptic release with chromophore-assisted light inactivation (CALI). *Neuron*, 79(2):241–53, July 2013.

Linden, M. M. L., Heynen, A. J. A., Haslinger, R. R. H., and Bear, M. M. F. Thalamic activity that drives visual cortical plasticity. *Nature Neuroscience*, 12(4):390–392, Apr. 2009.

Lindskog, M. and Li, L. Postsynaptic GluA1 enables acute retrograde enhancement of presynaptic function to coordinate adaptation to synaptic inactivity. *Proceedings of the National Academy of Sciences of the United States of America*, 107(50): 21806–21811, 2010.

Lindsly, C., Gonzalez-Islas, C., and Wenner, P. Activity blockade and $GABA_A$ receptor blockade produce synaptic scaling through chloride accumulation in embryonic spinal motoneurons and interneurons. *PLoS ONE*, 9(4):e94559, Jan. 2014.

Linsdell, P. and Moody, W. J. Na+ channel mis-expression accelerates K+ channel development in embryonic Xenopus laevis skeletal muscle. *The Journal of Physiology*, 480(3):405–410, Nov. 1994.

Lissin, D. V., Gomperts, S. N., Carroll, R. C., Christine, C. W., Kalman, D., Kitamura, M., Hardy, S., Nicoll, R. A., Malenka, R. C., and von Zastrow, M. Activity

differentially regulates the surface expression of synaptic AMPA and NMDA glutamate receptors. *Proceedings of the National Academy of Sciences of the United States of America*, 95(12):7097–102, June 1998.

Liu, G. and Tsien, R. Properties of synaptic transmission at single hippocampal synaptic boutons. *Nature*, 375:404–408, 1995.

Liu, L., Wong, T. P., Pozza, M. F., Lingenhoehl, K., Wang, Y., Sheng, M., Auberson, Y. P., and Wang, Y. T. Role of NMDA receptor subtypes in governing the direction of hippocampal synaptic plasticity. *Science*, 304:1021–1024, 2004.

Liu, M.-G., Chen, X.-F., He, T., Li, Z., and Chen, J. Use of multi-electrode array recordings in studies of network synaptic plasticity in both time and space. *Neuroscience Bulletin*, 28(4):409–22, Aug. 2012.

Liu, Z., Golowasch, J., Marder, E., and Abbott, L. A model neuron with activity-dependent conductances regulated by multiple calcium sensors. *The Journal of Neuroscience*, 18(7):2309–20, Apr. 1998.

London, M. and Häusser, M. Dendritic computation. *Annual Review of Neuroscience*, 28:503–532, 2005.

Lu, W., Shi, Y., Jackson, A. C., Bjorgan, K., During, M. J., Sprengel, R., Seeburg, P. H., and Nicoll, R. A. Subunit composition of synaptic AMPA receptors revealed by a single-cell genetic approach. *Neuron*, 62:254–268, 2009.

Maccaferri, G. and Dingledine, R. Complex effects of CNQX on CA1 interneurons of the developing rat hippocampus. *Neuropharmacology*, 43:523–529, 2002.

MacLean, J. N., Zhang, Y., Johnson, B. R., and Harris-Warrick, R. M. Activity-independent homeostasis in rhythmically active neurons. *Neuron*, 37:109–120, 2003.

Madhavan, R. *Role of spontaneous bursts in functional plasticity and spatiotemporal dynamics of dissociated cortical cultures*. PhD thesis, Georgia Institute of Technology, 2007.

Madhavan, R., Chao, Z. C., and Potter, S. M. Plasticity of recurring spatiotemporal activity patterns in cortical networks. *Physical Biology*, 4(3):181–93, Sept. 2007.

Maffei, A. and Turrigiano, G. G. Multiple modes of network homeostasis in visual cortical layer 2/3. *The Journal of Neuroscience*, 28(17):4377–84, 2008.

Magee, J. C. Dendritic integration of excitatory synaptic input. *Nature Reviews Neuroscience*, 1:181–190, 2000.

Makino, H. and Malinow, R. Compartmentalized versus global synaptic plasticity on dendrites controlled by experience. *Neuron*, 72(6):1001–11, Dec. 2011.

Man, H.-Y. GluA2-lacking, calcium-permeable AMPA receptors–inducers of plasticity? *Current Opinion in Neurobiology*, 21:291–298, 2011.

Marder, E. and Goaillard, J.-M. Variability, compensation and homeostasis in neuron and network function. *Nature Reviews Neuroscience*, 7(7):563–74, July 2006.

Marder, E. and Prinz, A. a. Modeling stability in neuron and network function: the role of activity in homeostasis. *BioEssays*, 24(12):1145–54, 2002.

Martinoia, S., Bonzano, L., Chiappalone, M., and Tedesco, M. Electrophysiological activity modulation by chemical stimulation in networks of cortical neurons coupled to microelectrode arrays: A biosensor for neuropharmacological applications. *Sensors and Actuators B: Chemical*, 108(1-2):589–596, July 2005.

Marvin, J. S., Borghuis, B. G., Tian, L., Cichon, J., Harnett, M. T., Akerboom, J., Gordus, A., Renninger, S. L., Chen, T.-W., Bargmann, C. I., Orger, M. B., Schreiter, E. R., Demb, J. B., Gan, W.-B., Hires, S. A., and Looger, L. L. An optimized fluorescent probe for visualizing glutamate neurotransmission. *Nature Methods*, 10(2):162–70, Feb. 2013.

Mateos, J. M., Lüthi, A., Savic, N., Stierli, B., Streit, P., Gähwiler, B. H., and McKinney, R. A. Synaptic modifications at the CA3-CA1 synapse after chronic AMPA receptor blockade in rat hippocampal slices. *The Journal of Physiology*, 581 (Pt 1):129–38, May 2007.

Matsuzaki, M., Honkura, N., Ellis-Davies, G., and Kasai, H. Structural basis of long-term potentiation in single dendritic spines. *Nature*, 429, 2004.

McBain, C. J., Eaton, J. V., Brown, T., and Dingledine, R. CNQX increases spontaneous inhibitory input to CA3 pyramidal neurones in neonatal rat hippocampal slices. *Brain Research*, 592:255–260, 1992.

McCormick, D. a. and von Krosigk, M. Corticothalamic activation modulates thalamic firing through glutamate "metabotropic" receptors. *Proceedings of the National Academy of Sciences of the United States of America*, 89(7):2774–8, Apr. 1992.

McDonald, J., Silverstein, F., and Johnston, M. MK-801 pretreatment enhances N-methyl-D-aspartate-mediated brain injury and increases brain N-methyl-D-aspartate recognition site binding in rats. *Neuroscience*, 38(1):103–113, 1990.

Mee, C. J., Pym, E. C. G., Moffat, K. G., and Baines, R. A. Regulation of neuronal excitability through pumilio-dependent control of a sodium channel gene. *The Journal of Neuroscience*, 24:8695–8703, 2004.

Mennerick, S. and Zorumski, C. F. Presynaptic influence on the time course of fast excitatory synaptic currents in cultured hippocampal cells. *The Journal of Neuroscience*, 15(4):3178–92, Apr. 1995.

Menuz, K., Stroud, R. M., Nicoll, R. A., and Hays, F. A. TARP auxiliary subunits switch AMPA receptor antagonists into partial agonists. *Science*, 318(5851):815–7, Nov. 2007.

Miesenböck, G. Optogenetic control of cells and circuits. *Annual Review of Cell and Developmental biology*, 27:731–58, Jan. 2011.

Miesenböck, G. and Kevrekidis, I. G. Optical imaging and control of genetically designated neurons in functioning circuits. *Annual Review of Neuroscience*, 28: 533–63, Jan. 2005.

Miller, K. D. and MacKay, D. J. C. The Role of Constraints in Hebbian Learning. *Neural Computation*, 6(1):100–126, Jan. 1994.

Minerbi, A., Kahana, R., Goldfeld, L., Kaufman, M., Marom, S., and Ziv, N. E. Long-term relationships between synaptic tenacity, synaptic remodeling, and network activity. *PLoS Biology*, 7(6):e1000136, June 2009.

Misonou, H., Mohapatra, D. P., Park, E. W., Leung, V., Zhen, D., Misonou, K., Anderson, A. E., and Trimmer, J. S. Regulation of ion channel localization and phosphorylation by neuronal activity. *Nature Neuroscience*, 7:711–718, 2004.

Moulder, K. L., Meeks, J. P., Shute, A. A., Hamilton, C. K., De Erausquin, G., and Mennerick, S. Plastic elimination of functional glutamate release sites by depolarization. *Neuron*, 42:423–435, 2004.

Moulder, K. L., Jiang, X., Taylor, A. A., Olney, J. W., and Mennerick, S. Physiological activity depresses synaptic function through an effect on vesicle priming. *The Journal of Neuroscience*, 26:6618–6626, 2006.

Mozzachiodi, R. and Byrne, J. H. More than synaptic plasticity: role of nonsynaptic plasticity in learning and memory. *Trends in Neurosciences*, 33(1):17–26, Jan. 2010.

Müller, M. and Davis, G. W. Transsynaptic control of presynaptic Ca2+ influx achieves homeostatic potentiation of neurotransmitter release. *Current Biology*, 22:1102–1108, 2012.

Müller, M., Liu, K. S. Y., Sigrist, S. J., and Davis, G. W. RIM controls homeostatic plasticity through modulation of the readily-releasable vesicle pool. *The Journal of Neuroscience*, 32:16574–85, 2012.

Murphy, T. H., Blatter, L. A., Wier, W. G., and Baraban, J. M. Spontaneous Synchronous Synaptic Calcium Transients in Cultured Cortical Neurons. *The Journal of Neuroscience*, 12(2):4834–4845, 1992.

Murthy, V. N., Schikorski, T., Stevens, C. F., and Zhu, Y. Inactivity Produces increases in Neurotransmitter Release and Synapse Size. *Neuron*, 32:673–682, 2001.

Nagel, G., Szellas, T., Huhn, W., Kateriya, S., Adeishvili, N., Berthold, P., Ollig, D., Hegemann, P., and Bamberg, E. Channelrhodopsin-2, a directly light-gated cation-selective membrane channel. *Proceedings of the National Academy of Sciences of the United States of America*, 100(24):13940–5, Nov. 2003.

Nagel, G., Brauner, M., Liewald, J. F., Adeishvili, N., Bamberg, E., and Gottschalk, A. Light activation of channelrhodopsin-2 in excitable cells of Caenorhabditis elegans triggers rapid behavioral responses. *Current Biology*, 15:2279–2284, 2005.

Nakayama, K., Kiyosue, K., and Taguchi, T. Diminished neuronal activity increases neuron-neuron connectivity underlying silent synapse formation and the rapid conversion of silent to functional synapses. *The Journal of Neuroscience*, 25(16):4040–51, Apr. 2005.

Nataraj, K., Le Roux, N., Nahmani, M., Lefort, S., and Turrigiano, G. G. Visual deprivation suppresses L5 Pyramidal neuron excitability by preventing the induction of intrinsic plasticity. *Neuron*, 68:750–762, 2010.

Nelson, A. B., Krispel, C. M., Sekirnjak, C., and du Lac, S. Long-lasting increases in intrinsic excitability triggered by inhibition. *Neuron*, 40(3):609–20, Oct. 2003.

Newman, J. P. *Optogenetic feedback control of neural activity*. PhD thesis, Georgia Institute of Technology, 2013.

Newman, J. P., Zeller-Townson, R., Fong, M.-f., Arcot Desai, S., Gross, R. E., and Potter, S. M. Closed-Loop, Multichannel Experimentation Using the Open-Source NeuroRighter Electrophysiology Platform. *Frontiers in Neural Circuits*, 6 (January):98, Jan. 2013.

Newman, J. P., Fong, M.-f., Millard, D. C., Shephard, C. J., Stanley, G. B., and Potter, S. M. Optogenetic feedback control of neuronal firing. Under review.

O'Brien, R., Kamboj, S., Ehlers, M., Rosen, K., Fischbach, G., and Huganir, R. Activity-dependent modulation of synaptic AMPA receptor accumulation. *Neuron*, 21(5):1067–1078, 1998.

O'Connor, D. H., Hires, S. A., Guo, Z. V., Li, N., Yu, J., Sun, Q.-Q., Huber, D., and Svoboda, K. Neural coding during active somatosensation revealed using illusory touch. *Nature Neuroscience*, 16(6):958–965, June 2013.

Oja, E. A Simplified Neuron Model as a Principle Component Analyzer. *Journal of Mathematical Biology*, 15(3):267–273, 1982.

Okumoto, S., Looger, L. L., Micheva, K. D., Reimer, R. J., Smith, S. J., and Frommer, W. B. Detection of glutamate release from neurons by genetically encoded surface-displayed FRET nanosensors. *Proceedings of the National Academy of Sciences of the United States of America*, 102:8740–8745, 2005.

O'Leary, T., van Rossum, M. C. W., and Wyllie, D. J. A. Homeostasis of intrinsic excitability in hippocampal neurones: dynamics and mechanism of the response to chronic depolarization. *The Journal of Physiology*, 588:157–170, 2010.

Opitz, T., De Lima, A. D., and Voigt, T. Spontaneous development of synchronous oscillatory activity during maturation of cortical networks in vitro. *Journal of Neurophysiology*, 88(5):2196–206, Nov. 2002.

Panchin, Y. V., Arshavsky, Y. I., Selverston, A., and Cleland, T. A. Lobster stomatogastric neurons in primary culture. I. Basic characteristics. *Journal of Neurophysiology*, 69:1976–1992, 1993.

Paradis, S., Sweeney, S. T., and Davis, G. W. Homeostatic control of presynaptic release is triggered by postsynaptic membrane depolarization. *Neuron*, 30(3):737–49, June 2001.

Partin, K., Patneau, D., Winters, C., Mayer, M., and Buonanno, A. Selective modulation of desensitization at AMPA versus kainate receptors by cyclothiazide and concanavalin A. *Neuron*, 11:1069–1082, 1993.

Patneau, D. K., Wright, P. W., Winters, C., Mayer, M. L., and Gallo, V. Glial cells of the oligodendrocyte lineage express both kainate- and AMPA-preferring subtypes of glutamate receptor. *Neuron*, 12:357–371, 1994.

Paz, J. T., Davidson, T. J., Frechette, E. S., Delord, B., Parada, I., Peng, K., Deisseroth, K., and Huguenard, J. R. Closed-loop optogenetic control of thalamus as a tool for interrupting seizures after cortical injury. *Nature Neuroscience*, 16(1): 64–70, Jan. 2013.

Peng, Y.-R., Zeng, S.-Y., Song, H.-L., Li, M.-Y., Yamada, M. K., and Yu, X. Postsynaptic spiking homeostatically induces cell-autonomous regulation of inhibitory inputs via retrograde signaling. *The Journal of Neuroscience*, 30(48):16220–31, Dec. 2010.

Petersen, S. A., Fetter, R. D., Noordermeer, J. N., Goodman, C. S., and DiAntonio, A. Genetic analysis of glutamate receptors in drosophila reveals a retrograde signal regulating presynaptic transmitter release. *Neuron*, 19:1237–1248, 1997.

Petrus, E., Anguh, T. T., Pho, H., Lee, A., Gammon, N., and Lee, H.-K. Developmental switch in the polarity of experience-dependent synaptic changes in layer 6 of mouse visual cortex. *Journal of Neurophysiology*, 106(5):2499–505, Nov. 2011.

Philpot, B. D., Espinosa, J. S., and Bear, M. F. Evidence for altered NMDA receptor function as a basis for metaplasticity in visual cortex. *The Journal of Neuroscience*, 23:5583–5588, 2003.

Pine, J. Recording action potentials from cultured neurons with extracellular microcircuit electrodes. *Journal of Neuroscience Methods*, 2:19–31, 1980.

Plomp, J. J., van Kempen, G. T., and Molenaar, P. C. Adaptation of quantal content to decreased postsynaptic sensitivity at single endplates in alpha-bungarotoxin-treated rats. *The Journal of Physiology*, 458:487–499, 1992.

Potter, S. M. *MEA in hand.* Photograph, 1998.

Potter, S. M. and Demarse, T. B. A new approach to neural cell culture for long-term studies. *Journal of Neuroscience Methods*, 110(1-2):17–24, Sept. 2001.

Potter, S. M., Wagenaar, D. A., and Demarse, T. B. Closing the loop: stimulation feedback systems for embodied MEA cultures. In Taketani, M. and Baudry, M., editors, *Advances in network electrophysiology using multi-electrode arrays*, volume 78, chapter 9, pages 215–242. Springer, 2006.

Prinz, A. A., Bucher, D., and Marder, E. Similar network activity from disparate circuit parameters. *Nature Neuroscience*, 7(12):1345–52, 2004.

Queenan, B. N., Lee, K. J., and Pak, D. T. S. Wherefore art thou, homeo(stasis)? Functional diversity in homeostatic synaptic plasticity. *Neural Plasticity*, 2012: 718203, Jan. 2012.

Quinlan, E., Philpot, B., Huganir, R., and Bear, M. Rapid, experience-dependent expression of synaptic NMDA receptors in visual cortex in vivo. *Nature Neuroscience*, 2(4):352–357, 1999.

Quiroga, Q., Nadasdy, Z., and Ben-Shaul, Y. Unsupervised spike detection and sorting with wavelets and superparamagnetic clustering. *Neural Computation*, 1687: 1661–1687, 2004.

Rabinowitch, I. and Segev, I. Two opposing plasticity mechanisms pulling a single synapse. *Trends in Neurosciences*, 31(8):377–83, 2008.

Ramakers, G., Corner, M. A., and Habets, A. Development in the absence of spontaneous bioelectric activity results in increased stereotyped burst firing in cultures of dissociated cerebral cortex. *Experimental Brain Research*, 79(1):157–66, 1990.

Rammes, G., Parsons, C., Müller, W., and Swandulla, D. Modulation of fast excitatory synaptic transmission by cyclothiazide and GYKI 52466 in the rat hippocampus. *Neuroscience Letters*, 175:21–24, 1994.

Rannals, M. D. and Kapur, J. Homeostatic strengthening of inhibitory synapses is mediated by the accumulation of GABA(A) receptors. *The Journal of Neuroscience*, 31(48):17701–12, Nov. 2011.

Rao, A. and Craig, A. M. Activity regulates the synaptic localization of the NMDA receptor in hippocampal neurons. *Neuron*, 19(4):801–12, Oct. 1997.

Riccio, R. V. and Matthews, M. a. The postnatal development of the rat primary visual cortex during optic nerve impulse blockade by intraocular tetrodotoxin: a quantitative electron microscopic analysis. *Brain Research*, 352(1):55–68, May 1985a.

Riccio, R. V. and Matthews, M. a. Effects of intraocular tetrodotoxin on dendritic spines in the developing rat visual cortex: a Golgi analysis. *Brain Research*, 351 (2):173–82, Apr. 1985b.

Rolston, J., Gross, R., and Potter, S. A low-cost multielectrode system for data acquisition enabling real-time closed-loop processing with rapid recovery from stimulation artifacts. *Frontiers in Neuroengineering*, 2(July):1–17, 2009.

Royer, S. and Paré, D. Conservation of total synaptic weight through balanced synaptic depression and potentiation. *Nature*, 422:518–522, 2003.

Rumsey, C. C. and Abbott, L. F. Equalization of synaptic efficacy by activity- and timing-dependent synaptic plasticity. *Journal of Neurophysiology*, 91(5):2273–80, May 2004.

Rutherford, L. C., Nelson, S. B., and Turrigiano, G. G. BDNF has opposite effects on the quantal amplitude of pyramidal neuron and interneuron excitatory synapses. *Neuron*, 21:521–530, 1998.

Schoenenberger, P., Schärer, Y.-P. Z., and Oertner, T. G. Channelrhodopsin as a tool to investigate synaptic transmission and plasticity. *Experimental Physiology*, 96:34–39, 2011.

Schulz, D. J., Goaillard, J.-M., and Marder, E. Variable channel expression in identified single and electrically coupled neurons in different animals. *Nature Neuroscience*, 9:356–362, 2006.

Shatz, C. and Stryker, M. Prenatal Tetrodotoxin Infusion Blocks Segregation of Retinogeniculate Afferents. *Science*, 242(4875):87–89, 1988.

Shepherd, G. M. *The Synaptic Organization of the Brain*, volume 5th ed. Oxford University Press, 2004.

Shepherd, J. D., Rumbaugh, G., Wu, J., Chowdhury, S., Plath, N., Kuhl, D., Huganir, R. L., and Worley, P. F. Arc/Arg3.1 mediates homeostatic synaptic scaling of AMPA receptors. *Neuron*, 52(3):475–84, 2006.

Shin, M. and Chetkovich, D. M. Activity-dependent regulation of h channel distribution in hippocampal CA1 pyramidal neurons. *Journal of Biological Chemistry*, 282:33168–33180, 2007.

Siegel, M., Marder, E., and Abbott, L. F. Activity-dependent current distributions in model neurons. *Proceedings of the National Academy of Sciences of the United States of America*, 91(24):11308–12, Nov. 1994.

Spitzer, N. Electrical activity in early neuronal development. *Nature*, 444(7120): 707–712, 2006.

Spitzer, N. C. Activity-dependent neurotransmitter respecification. *Nature Reviews Neuroscience*, 13(2):94–106, Feb. 2012.

Spruston, N. Pyramidal neurons: dendritic structure and synaptic integration. *Nature Reviews Neuroscience*, 9:206–221, 2008.

Steinert, J. R., Robinson, S. W., Tong, H., Haustein, M. D., Kopp-Scheinpflug, C., and Forsythe, I. D. Nitric oxide is an activity-dependent regulator of target neuron intrinsic excitability. *Neuron*, 71(2):291–305, July 2011.

Steinmetz, C. C. and Turrigiano, G. G. Tumor necrosis factor-α signaling maintains the ability of cortical synapses to express synaptic scaling. *The Journal of Neuroscience*, 30(44):14685–90, Nov. 2010.

Stellwagen, D. and Malenka, R. Synaptic scaling mediated by glial TNF-alpha. *Nature*, 440(7087):1054–1059, 2006.

Stewart, B. A., Schuster, C. M., Goodman, C. S., and Atwood, H. L. Homeostasis of synaptic transmission in Drosophila with genetically altered nerve terminal morphology. *The Journal of Neuroscience*, 16:3877–3886, 1996.

Stirman, J. N., Crane, M. M., Husson, S. J., Wabnig, S., Schultheis, C., Gottschalk, A., and Lu, H. Real-time multimodal optical control of neurons and muscles in freely behaving Caenorhabditis elegans. *Nature Methods*, 8(2):153–8, Feb. 2011.

Sun, Q. and Turrigiano, G. G. PSD-95 and PSD-93 play critical but distinct roles in synaptic scaling up and down. *The Journal of Neuroscience*, 31:6800–6808, 2011.

Sutton, M. A., Ito, H. T., Cressy, P., Kempf, C., Woo, J. C., and Schuman, E. M. Miniature neurotransmission stabilizes synaptic function via tonic suppression of local dendritic protein synthesis. *Cell*, 125(4):785–99, May 2006.

Swanwick, C. C., Murthy, N. R., and Kapur, J. Activity-dependent scaling of GABAergic synapse strength is regulated by brain-derived neurotrophic factor. *Molecular and cellular neurosciences*, 31(3):481–92, Mar. 2006.

Szobota, S., Gorostiza, P., Del Bene, F., Wyart, C., Fortin, D. L., Kolstad, K. D., Tulyathan, O., Volgraf, M., Numano, R., Aaron, H. L., Scott, E. K., Kramer, R. H., Flannery, J., Baier, H., Trauner, D., and Isacoff, E. Y. Remote control of neuronal activity with a light-gated glutamate receptor. *Neuron*, 54(4):535–45, May 2007.

Taketani, M. and Baudry, M. *Advances in network electrophysiology using multi-electrode arrays.* Springer, 2006.

Tang, Y. P., Shimizu, E., Dube, G. R., Rampon, C., Kerchner, G. A., Zhuo, M., Liu, G., and Tsien, J. Z. Genetic enhancement of learning and memory in mice. *Nature*, 401:63–69, 1999.

Tatavarty, V., Sun, Q., and Turrigiano, G. G. How to scale down postsynaptic strength. *The Journal of Neuroscience*, 33:13179–89, 2013.

Temporal, S., Desai, M., Khorkova, O., Varghese, G., Dai, A., Schulz, D. J., and Golowasch, J. Neuromodulation independently determines correlated channel expression and conductance levels in motor neurons of the stomatogastric ganglion. *Journal of Neurophysiology*, 107:718–727, 2012.

Thiagarajan, T., Lindskog, M., and Tsien, R. Adaptation to synaptic inactivity in hippocampal neurons. *Neuron*, 47(5):725–737, Sept. 2005.

Thiagarajan, T. C., Piedras-Renteria, E. S., and Tsien, R. W. alpha- and beta-CaMKII. Inverse regulation by neuronal activity and opposing effects on synaptic strength. *Neuron*, 36:1103–1114, 2002.

Thoby-Brisson, M. and Simmers, J. Neuromodulatory inputs maintain expression of a lobster motor pattern-generating network in a modulation-dependent state: evidence from long-term decentralization in vitro. *The Journal of Neuroscience*, 18 (6):2212–2225, Mar. 1998.

Thomas, C. A., Springer, P. A., Loeb, G. E., Berwald-Netter, Y., and Okun, L. M. A miniature microelectrode array to monitor the bioelectric activity of cultured cells. *Experimental cell research*, 74:61–66, 1972.

Turrigiano, G. G. The self-tuning neuron: synaptic scaling of excitatory synapses. *Cell*, 135(3):422–35, 2008.

Turrigiano, G. G. Too many cooks? Intrinsic and synaptic homeostatic mechanisms in cortical circuit refinement. *Annual Review of Neuroscience*, 34:87–101, 2011.

Turrigiano, G. G. Homeostatic synaptic plasticity: local and global mechanisms for stabilizing neuronal function. *Cold Spring Harbor Perspectives in Biology*, pages 1–17, Nov. 2012.

Turrigiano, G. G. and Marder, E. Modulation of identified stomatogastric ganglion neurons in primary cell culture. *Journal of Neurophysiology*, 69:1993–2002, 1993.

Turrigiano, G. G. and Nelson, S. B. Hebb and homeostasis in neuronal plasticity. *Current Opinion in Neurobiology*, 10(3):358–64, June 2000.

Turrigiano, G. G. and Nelson, S. B. Homeostatic plasticity in the developing nervous system. *Nature Reviews Neuroscience*, 5(2):97–107, 2004.

Turrigiano, G. G., Abbott, L., and Marder, E. Changes in the intrinsic activity-dependent properties of cultured neurons. *Science*, 264(5161):974, 1994.

Turrigiano, G. G., LeMasson, G., and Marder, E. Selective regulation of current densities underlies spontaneous changes in the activity of cultured neurons. *The Journal of Neuroscience*, 15(5):3640–3652, 1995.

Turrigiano, G. G., Leslie, K. R., Desai, N. S., Rutherford, L. C., and Nelson, S. B. Activity-dependent scaling of quantal amplitude in neocortical neurons. *Nature*, 391(February):892–895, 1998.

Van den Pol, A., Obrietan, K., and Belousov, A. Glutamate hyperexcitability and seizure-like activity throughout the brain and spinal cord upon relief from chronic glutamate receptor blockade in culture. *Neuroscience*, 74(3):653–74, Oct. 1996.

Van Pelt, J., Corner, M. A., Wolters, P., Rutten, W., and Ramakers, G. Longterm stability and developmental changes in spontaneous network burst firing patterns in dissociated rat cerebral cortex cell cultures on multielectrode arrays. *Neuroscience Letters*, 361(1-3):86–89, 2004.

van Welie, I., van Hooft, J. A., and Wadman, W. J. Homeostatic scaling of neuronal excitability by synaptic modulation of somatic hyperpolarization-activated I_h channels. *Proceedings of the National Academy of Sciences of the United States of America*, 101(14):5123–5128, 2004.

Vitureira, N. and Goda, Y. Cell biology in neuroscience: the interplay between Hebbian and homeostatic synaptic plasticity. *The Journal of Cell Biology*, 203(2): 175–86, Oct. 2013.

Vitureira, N., Letellier, M., and Goda, Y. Homeostatic synaptic plasticity: from single synapses to neural circuits. *Current Opinion in Neurobiology*, 22(3):516–21, June 2012.

Vlachos, A., Becker, D., Jedlicka, P., Winkels, R., Roeper, J., and Deller, T. Entorhinal denervation induces homeostatic synaptic scaling of excitatory postsynapses of dentate granule cells in mouse organotypic slice cultures. *PLoS ONE*, 7(3):e32883, Jan. 2012.

Volgraf, M., Gorostiza, P., Numano, R., Kramer, R. H., Isacoff, E. Y., and Trauner, D. Allosteric control of an ionotropic glutamate receptor with an optical switch. *Nature Chemical Biology*, 2:47–52, 2006.

Wagenaar, D. A. *Development and Control of Epileptiform Bursting in Dissociated Cortical Cultures*. PhD thesis, California Institute of Technology, 2006.

Wagenaar, D. A., Demarse, T. B., and Potter, S. M. MeaBench: A toolset for multi-electrode data acquisition and on-line analysis. In *2nd International IEEE EMBS Conference on Neural Engineering*, volume 2005, pages 518–521, 2005a.

Wagenaar, D. A., Madhavan, R., Pine, J., and Potter, S. M. Controlling bursting in cortical cultures with closed-loop multi-electrode stimulation. *The Journal of Neuroscience*, 25(3):680–8, 2005b.

Wagenaar, D. A., Nadasdy, Z., and Potter, S. M. Persistent dynamic attractors in activity patterns of cultured neuronal networks. *Physical Review E*, 73(5):51907, 2006a.

Wagenaar, D. A., Pine, J., and Potter, S. M. An extremely rich repertoire of bursting patterns during the development of cortical cultures. *BMC neuroscience*, 7:11, 2006b.

Wallach, A. and Marom, S. Interactions between network synchrony and the dynamics of neuronal threshold. *Journal of Neurophysiology*, 107(11):2926–36, June 2012.

Wallach, A., Eytan, D., Gal, A., Zrenner, C., and Marom, S. Neuronal Response Clamp. *Frontiers in Neuroengineering*, 4(April):1–10, 2011.

Wang, H.-L., Zhang, Z., Hintze, M., and Chen, L. Decrease in calcium concentration triggers neuronal retinoic acid synthesis during homeostatic synaptic plasticity. *The Journal of Neuroscience*, 31(49):17764–71, Dec. 2011.

Wenner, P. Mechanisms of GABAergic homeostatic plasticity. *Neural Plasticity*, 2011: 489470, Jan. 2011.

Weyhersmüller, A., Hallermann, S., Wagner, N., and Eilers, J. Rapid active zone remodeling during synaptic plasticity. *The Journal of Neuroscience*, 31:6041–6052, 2011.

Wierenga, C. J., Ibata, K., and Turrigiano, G. G. Postsynaptic expression of homeostatic plasticity at neocortical synapses. *The Journal of Neuroscience*, 25(11):2895, 2005.

Wilhelm, J., Rich, M., and Wenner, P. Compensatory changes in cellular excitability, not synaptic scaling, contribute to homeostatic recovery of embryonic network activity. *Proceedings of the National Academy of Sciences of the United States of America*, 106(16):6760, 2009.

Wilhelm, J. C. and Wenner, P. GABA$_A$ transmission is a critical step in the process of triggering homeostatic increases in quantal amplitude. *Proceedings of the National Academy of Sciences of the United States of America*, 105(32):11412–7, Aug. 2008.

Williams, K., Dichter, M. A., and Molinoff, P. B. Up-regulation of N-methyl-D-aspartate receptors on cultured cortical neurons after exposure to antagonists. *Molecular Pharmacology*, 42:147–151, 1992.

Wilson, N., Kang, J., Hueske, E., Leung, T., Varoqui, H., Murnick, J., Erickson, J., and Liu, G. Presynaptic regulation of quantal size by the vesicular glutamate transporter VGLUT1. *The Journal of Neuroscience*, 25(26):6221, 2005.

Winnubst, J. and Lohmann, C. Synaptic clustering during development and learning: the why, when, and how. *Frontiers in Molecular Neuroscience*, 5, 2012.

Wöhrl, R., von Haebler, D., and Heinemann, U. Low-frequency stimulation of the direct cortical input to area CA1 induces homosynaptic LTD and heterosynaptic LTP in the rat hippocampal-entorhinal cortex slice preparation. *European Journal of Neuroscience*, 25(1):251–8, Jan. 2007.

Xie, A. X., Sun, M.-Y., Murphy, T., Lauderdale, K., Tiglao, E., and Fiacco, T. a. Bidirectional scaling of astrocytic metabotropic glutamate receptor signaling following long-term changes in neuronal firing rates. *PLoS ONE*, 7(11):e49637, Jan. 2012.

Yamada, K. A. and Tang, C. M. Benzothiadiazides inhibit rapid glutamate receptor desensitization and enhance glutamatergic synaptic currents. *The Journal of Neuroscience*, 13:3904–3915, 1993.

Yuste, R. and Tank, D. W. Dendritic integration in mammalian neurons, a century after Cajal. *Neuron*, 16:701–716, 1996.

Zhang, W. and Linden, D. J. The other side of the engram: experience-driven changes in neuronal intrinsic excitability. *Nature Reviews Neuroscience*, 4(11):885–900, Nov. 2003.

Zhang, Y. and Oertner, T. Optical induction of synaptic plasticity using a light-sensitive channel. *Nature Methods*, 4(2):139–142, 2007.

Zhao, C., Dreosti, E., and Lagnado, L. Homeostatic synaptic plasticity through changes in presynaptic calcium influx. *The Journal of Neuroscience*, 31:7492–7496, 2011.

Zorumski, C. F., Yamada, K. A., Price, M. T., and Olney, J. W. A benzodiazepine recognition site associated with the non-NMDA glutamate receptor. *Neuron*, 10: 61–67, 1993.